New Catalytic Properties of Chiral-at-Metal Complexes and a Cyclometalated Ru Complex

A DISSERTATION

In

Chemistry

Presented to the Faculties of Philipps-Universität Marburg in Partial Fulfillment

of the Requirements for the Degree of Doctor of Science

(Dr. rer. nat.)

Jie Qin

Shandong, P. R. China

Marburg/Lahn 2019

Die vorliegende Dissertation entstand in der Zeit von August 2015 bis January 2019 am Fachbereich Chemie der Philipps-Universität Marburg unter der Betreuung von Herrn Prof. Dr. Eric Meggers.

Vom Fachbereich Chemie der Philipps-Universität Marburg (Hochschulkennziffer: 1180) als Dissertation am _____ angenommen.

Erstgutachter:	Prof. Dr. Eric Meggers
Zweitgutachter:	Prof. Dr. Armin Geyer
weitere Mitglieder Prüfungskommission:	Prof. Dr. Andreas Seubert

Tag der mündlichen Prüfung: _____

Acknowledgements

First of all, I would like to express my sincere appreciation to my advisor Prof. Eric Meggers. Thanks a lot for offering me the opportunity to do my doctoral study in this group. I have learned so much from his knowledge of chemistry and dedication to scientific research. All of these are very important for my future career.

Next, I am very thankful to Prof. Armin Geyer and Prof. Andreas Seubert for reviewing my thesis and being the committee members of my defense.

In addition, I would like to thank all of the past and current members of the Meggers group for their help, support, and accompany. Thanks a lot to Dr. Lilu Zhang for helping me to revise my thesis. Thanks a lot to Zijun Zhou, Dr. Vladimir Larionov, Tianjiao Cui and Marcel Hemming for their cooperation and help on my research and publications. Thanks a lot to Philipp Steinlandt for translating the abstract into the German version. Thanks a lot to Ina Pinnschmidt and Dr. Sabrina Höbenreich for their kind help. Thanks a lot to all of the past group members Dr. Xiao Zhang, Dr. Qi Zhang, Dr. Shipeng Luo, Dr. Xiaoqiang Huang, Dr. Jiajia Ma, Dr. Yu Zheng, Dr. Chuanyong Wang, Dr. Xiaodong Shen, Dr. Haohua Huo, Dr. Wei Zuo, Dr. Thomas Cruchter, Thomas Mietke, Dr. Nathalie Nett and Dr. Sabine Duewel for their help and support. Furthermore, thanks a lot to the current group members Yuqi Tan, Yubiao Hong, Chenhao Zhang, Yvonne Grell, Erik Winterling, Xiang Shen, Dr. Guanghui Wang, Dr. Lucie Jarrige, Lifang Zhao, Xingwen Zheng, Xin Nie, Yuanze Tang and Jiahui Lin for their help and accompany.

Moreover, I would like to thank all of the technical staffs in the department for their help and cooperation. Thanks a lot to Dr. Klaus Harms, Radostan Riedel and Michael Marsch for the measurement and analysis of the single crystals. Thanks a lot to Dr. Xiulan Xie for the NMR service.

At last, I really appreciate my families for their support and encouragement.

Best wishes to all of you.

Publications and Poster Presentations

Publications:

1. J. Qin, Z. Zhou, T. Cui, M. Hemming, E. Meggers, Enantioselective intramolecular C-H amination of aliphatic azides by dual ruthenium and phosphine catalysis, *Chem. Sci.* **2019**, *10*, 3202-3207.
2. J. Qin,[#] V. A. Larionov,[#] K. Harms, E. Meggers, Kinetic resolution of epoxides with CO_2 catalyzed by a chiral-at-iridium complex, *ChemSusChem* **2019**, *12*, 320-325. ([#]Equal contribution)
3. Z. Zhou,[#] S. Chen,[#] J. Qin,[#] X. Nie, X. Zheng, K. Harms, R. Riedel, K. N. Houk, E. Meggers, Catalytic enantioselective intramolecular C(sp^3)-H amination of 2-azidoacetamides, *Angew. Chem. Int. Ed.* **2019**, 58, 1088-1093. ([#]Equal contribution)
4. T. Cui, J. Qin, K. Harms, E. Meggers, Chiral-at-ruthenium catalyst with sterically demanding furo[3,2-b]pyridine ligands, *Eur. J. Inorg. Chem.* **2019**, 195-198.
5. X. Zhang, J. Qin, X. Huang, E. Meggers, Sequential asymmetric hydrogenation and photoredox chemistry with a single catalyst, *Org. Chem. Front.* **2018**, *5*, 166-170.
6. X. Zhang, J. Qin, X. Huang, E. Meggers, One-pot sequential photoredox and asymmetric transfer hydrogenation with a single catalyst, *Eur. J. Org. Chem.* **2018**, 571-577.
7. C. Wang, J. Qin, X. Shen, R. Riedel, K. Harms, E. Meggers, Asymmetric radical-radical cross-coupling through visible-light-activated iridium catalysis, *Angew. Chem. Int. Ed.* **2016**, *55*, 685-688.

Poster Presentation:

"ORCHEM 2018", Poster: Enantioselective Intramolecular C-H Amination of Aliphatic Azides by Combining Ru Catalysis with the Staudinger Reaction, 10^{th}-12^{th} September **2018**, Berlin, Germany.

Abstract

Asymmetric transition-metal catalysis constitutes one of the most powerful strategies to construct non-racemic chiral molecules. This thesis deals with enantioselelctive catalysis of chiral-at-metal iridium and ruthenium complexes as well as a chiral mono-cyclometalated ruthenium complex.

1) Kinetic resolution of racemic epoxides with CO_2 catalyzed by a chiral-at-metal bis-cyclometalated iridium complex was accomplished, and s-factors between 6.4 and 16.6 were obtained for overall 21 monosubstituted epoxides containing diverse functional side chains. Notably, all reactions were performed at room temperature, and no copolymerization side reaction which occurred often in other catalytic systems was observed (Chapter 3.1).

2) Enantioselective intramolecular benzylic C-H amination of primary aliphatic azides was achieved by using a chiral-at-metal bis(pyridyl-NHC) ruthenium complex in combination with tris(*p*-fluorophenyl)phosphine (both 1 mol%) to provide a vatiety of chiral α-aryl pyrrolidines with enantioselectivities of up to 99% ee. In this unique case, the phosphine serves as a crucial nitrene transfer co-catalyst and activates the organic azide through the formation of an intermediate iminophosphorane. This methodology offers direct access to non-racemic α-aryl pyrrolidines which are very important structural motifs in many bioactive compounds. (Chapter 3.2).

3) A chiral cyclometalated ruthenium catalyst enabled direct enantioselective and highly diastereoselective oxidative homocoupling of 2-acyl imidazoles in the presence of one equivalent $BrCCl_3$ to provide chiral symmetric 1,4-dicarbonyl compounds in 38-75% yield with 57-95% ee. Only one diastereomer was obtained for all the investigated substrates. Mechanistic experiments support a unique ruthenium catalyzed two-steps mechanism. The first step is a ruthenium catalyzed bromination of 2-acyl imidazole generating a brominated intermediate, followed by a ruthenium catalyzed stereo-controlled radical-enolate reaction providing the final product (Chapter 3.3).

Zusammenfassung

Die asymmetrische Übergangsmetallkatalyse stellt eine der effektivsten Methoden zum Aufbau chiraler Moleküle dar. In dieser Arbeit wird sowohl die enantioselektive Katalyse mit chiral-at-metal Iridium- und Rutheniumkomplexen als auch mit chiralen mono-cyclometallierten Rutheniumkomplexen thematisiert.

1) Eine kinetische Racematspaltung von racemischen Epoxiden mit CO_2 katalysiert durch einen chiral-at-metal, bis-cyclometallierten Iridiumkomplex konnte erfolgreich durchgeführt werden, wobei s-Faktoren von 6.4 bis 16.6 für insgesamt 21 monosubstituierte Epoxide mit verschieden funktionalisierten Seitenketten erreicht werden konnten. Bemerkenswerterweise konnten alle Reaktionen bei Raumtemperatur durchgeführt werden. Hierbei wurde keine Copolymerisation als Nebenreaktion beobachtet, welche in anderen katalytischen Systemen häufig auftrat. (Kapitel 3.1).

2) Die enantioselektive, intramolekulare, benzylische C-H-Aminierung von primären, aliphatischen Aziden wurde durch die Verwendung eines chiral-at-metal, bis(pyridyl-NHC)-Rutheniumkomplexes in Kombination mit Tris(*p*-fluorophenyl)phosphin (beide 1 mol%) erfolgreich angewandt, um eine Vielzahl chiraler α-Arylpyrrolidine mit bis zu 99% *ee* zu synthetisieren. In diesem einzigartigen Fall dient das Phosphin als entscheidender Nitren-Transfer-Cokatalysator, der das organische Azid durch Bildung eines intermediären Iminophosphorans aktiviert. Diese Methode bietet somit einen direkten, synthetischen Zugang zu chiralen α-Arylpyrrolidinen, die ein wichtiges Strukturmotiv in vielen bioaktiven Wirkstoffen sind (Kapitel 3.2).

3) Ein chiraler, cyclometallierter Ruthenium-Katalysator ermöglichte die direkte, enantioselektive und hochgradig diastereoselektive, oxidative Homokupplung von 2-Acylimidazolen in Anwesenheit eines Äquivalents $BrCCl_3$, um chirale 1,4-Dicarbonylverbindungen mit einer Ausbeute von 38-75% und 57-95% *ee* zu erhalten. Bemerkenswerterweise wurde nur ein Diastereomer für alle untersuchten Substrate erhalten. Mechanistische Untersuchungen unterstützen einen einzigartigen Ruthenium-katalysierten Zwei-Stufen-Mechanismus. Der erste Schritt hierbei ist eine Ruthenium-katalysierte Bromierung der 2-Acylimidazole, welche das bromierte Produkt generiert, gefolgt von der Ruthenium-katalysierten, stereokontrollierten Radikal-Enolat Reaktion, die daraufhin zum finalen Produkt führt (Kapitel 3.3).

Table of Contents

Chapter 1: Theoretical Part

1.1 Introduction

The importance of molecular chirality has been demonstrated for a long time. It is an essential objective for chemists to discover efficient methods for constructing non-racemic molecules.[1] To date, different kinds of strategies have been developed to achieve this goal. Asymmetric catalysis represents one of the most economic methods to synthesize enantiopure compounds, which involves three main branches: transition-metal catalysis, organocatalysis and enzyme catalysis. The reactivity of transition metals can be easily tuned by the ligands around the metal center, thus making transition-metal catalysis a powerful and flexible tool to synthesize organic molecules. In 2001, the Nobel Prize in Chemistry was awarded to Knowles, Noyori, and Sharpless for their contributions to the asymmetric hydrogenation and oxidation,[2] thereby recognizing the prominent role of asymmetric transition-metal catalysis.

The work of this thesis is focused on asymmetric transition-metal catalysis including three sections: kinetic resolution of epoxides with CO_2 catalyzed by a chiral-at-iridium complex, enantioselective intramolecular C-H amination of aliphatic azides by dual ruthenium and phosphine catalysis, and a ruthenium catalyzed asymmetric oxidative homocoupling of 2-acyl imidazoles. In the following, the theoretical part will introduce the background for these three topics.

1.2 Kinetic Resolution of Epoxides with CO_2

The reaction of epoxides with CO_2 to form cyclic carbonates has attracted much attention since CO_2 constitutes a sustainable C_1 feedstock.[3] The reaction is highly atom economical, and the resulting cyclic carbonates are important synthetic building blocks.[4] Although many efficient catalysts are known for the racemic reactions,[5] the kinetic resolution of racemic epoxides with CO_2 poses significant challenges.[6] The selectivity factor s, which is defined as the ratio of the rate constants (k_R and k_S) for the reaction with the two individual enantiomers ($s = k_R/k_S$), is typically quite low ($s < 10$). The existing catalytic systems for the kinetic resolution normally consist of a chiral Lewis acid for activation of the epoxide in combination with a reversible nucleophile as co-catalyst for the epoxide ring opening (Figure 1).[5] The enantiodifferentiation either already occurs during the

formation of the Lewis acid-substrate complex **I** or in the subsequent reaction of the formation of the ring-opened alkoxide intermediate **II** upon the addition of nucleophile.

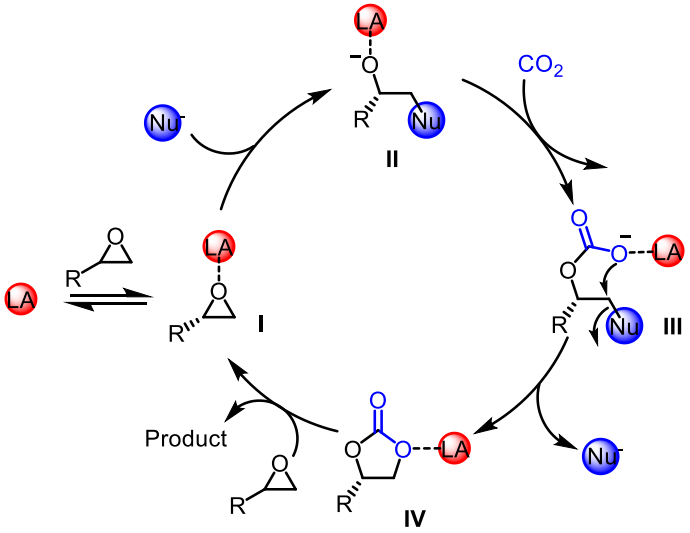

Figure 1. General mechanism of a binary catalytic system for the kinetic resolution of epoxides with CO_2.

1.2.1 Metal Catalysts for the Kinetic Resolution of Epoxides with CO_2

The earliest study dates back to 1993.[7] Vogt and co-workers reported the kinetic resolution of epoxides with CO_2 by chiral titanium or vanadium-binol complexes, providing s-factors only up to 2.6 (Scheme 1).

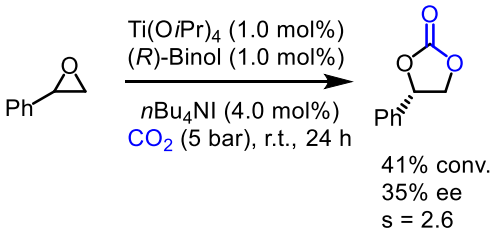

Scheme 1. Kinetic resolution of styrene epoxide with CO_2 catalyzed by Ti(O*i*Pr)$_4$/binol.

In the following several years, chiral cobalt Schiff base complexes have been the most studied catalysts and showed the most successful results, which were firstly introduced by Lu and co-workers in 2004.[9] In presence of 0.1 mol% **Co^{III}(salen)1** in combination with *n*-butylammonium chloride (*n*Bu$_4$NCl) as co-catalyst, s-factors of up to 9.0 at 40% conversion were obtained for propylene carbonate (Figure 2a). In their study, the nature of the co-catalyst had great influence on the s-factor.

For example, the use of nBu$_4$NCl was more beneficial for improving enantiomeric excess of the product compared with nBu$_4$NBr and nBu$_4$NI. The same year, Nguyen and co-workers reported a similar catalyst **Co^{III}(salen)2** (0.1 mol%) together with (*R*)-(+)-4-dimethylaminopyridinyl (pentaphenylcyclopentadienyl)iron (DMAP*) as co-catalyst, but s-factors of only 5.6 at very low conversion of 8% were obtained (Figure 2a).[8] Further improvement was achieved by Berkessel and co-workers, with s-factor reaching up to 18.7 by replacing the counterion of the Co^{III}(salen) complex with trifluoroacetyl (**Co^{III}(salen)3**) and employing bis-(triphenylphosphoranylidene)ammonium fluoride (PPNF) as co-catalyst, but the reaction was reacted at -40 ℃ for 5 days (Figure 2a).[10]

Encouraged by these results, a number of modified chiral cobalt Schiff base catalysts were developed.[11,12] Jing and co-workers made great contributions to this field.[11] For example, they employed a polymer based catalyst **Co^{III}(salen)4** together with *n*-butylammonium fluorine (nBu$_4$NF) as co-catalyst and obtained a good s-factor of 10.2 for propylene carbonate (Figure 2b).[11c] This catalyst could be recovered and reused for more than ten times without loss of activity and enantioselectivity. In 2012, Lu and co-workers reported the most effective catalyst **Co^{III}(salen)5**. With this particular catalyst and 200 equivalents of co-catalyst bis-(triphenylphosphoranyliden)ammonium 2,4-dinitrophenoxide (PPN-DNP) (for the purpose of suppressing copolymerization side reaction), the reaction provided an impressive kinetic resolution with an s-factor of 75.8 at -25 ℃ but at a very low conversion of 10% for propylene oxide (Figure 2b).[13]

Besides Co^{III}(salen) complexes, a series of ketoiminatocobalt(II) complexes developed by Yamada and co-workers also displayed good activities for this transformation.[14] For example, **Co^{II}(salen)6** could catalyze the kinetic resolution of *N*-(2,3-epoxypropyl)diphenylamine with CO_2 providing s-factors of up to 43.5 (Figure 2c).[14b] Unfortunately, this system suffered the copolymerization as side reaction for most of the investigated substrates. And the s-factor was sensitive to the nature of the epoxide. For example, the s-factor dramatically dropped to 2.2 for the substrate glycidyl phenyl ether.

There are some problems associated with the kinetic resolution of epoxides with CO_2 in spite of the encouraging results based on chiral cobalt Schiff base catalysts: the substrate was mainly focused on propylene epoxide, and the reaction had poor substrate tolerance. For example, although for propylene epoxide substrate **Co^{III}(salen)4** provided an s-fator of 10.2, no kinetic resolution could be obtained (46% conversion with 0% ee) once the substrate was changed to glycidyl phenyl ether.[11c]

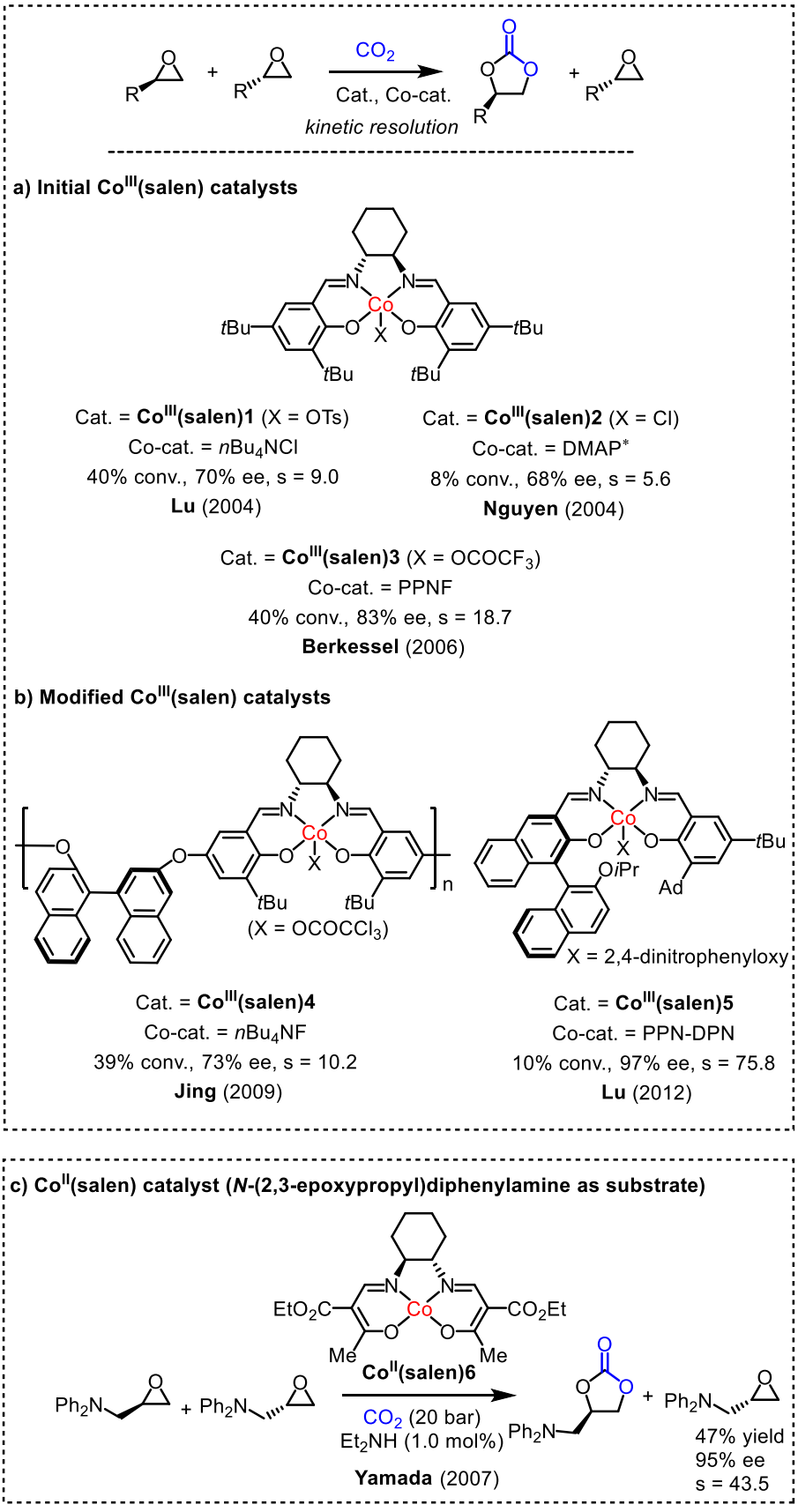

Figure 2. Kinetic resolution of epoxides with CO_2 catalyzed by chiral cobalt Schiff base catalysts.

In addition to chiral cobalt Schiff base catalysts, a number of other salen-metal complexes were also explored for this transformation. In 2013, Jiang and co-workers reported a Ni(salen) complex incorporated within a MOF giving very modest s-factors of up to 3.2 for the kinetic resolution of propylene epoxide with CO_2.[15b] Two years later, North and co-workers demonstrated that both complexes **Al(salen)** and **Cr(salen)** could be employed as catalysts for the kinetic resolution of *N*-(2,3-epoxypropyl)diphenylamine with CO_2 providing s-factors of up to 15.4 (Figure 3).[15c] Unfortunately, these salen-metal catalysts are also very sensitive to the nature of the epoxide. For example, the s-factor decreased to less than 5 when glycidyl phenyl ether was used as substrate.

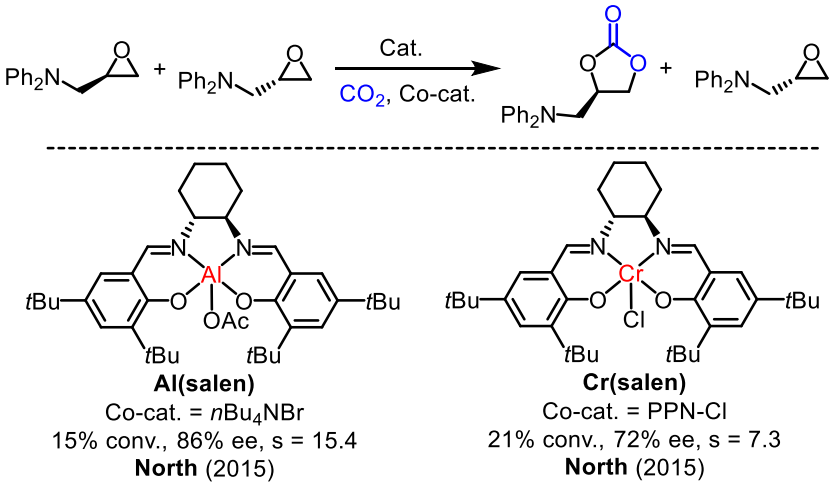

Figure 3. Kinetic resolution of *N*-(2,3-epoxypropyl)diphenylamine with CO_2 catalyzed by **Al(salen)** and **Cr(salen)**.

1.2.2 Organocatalysts for the Kinetic Resolution of Epoxides with CO_2

Organocatalysts have recently also been investigated for the kinetic resolution of epoxides with CO_2.[16] In 2016, Shirakawa and co-workers designed a bifunctional quaternary phosphonium bromine catalyst for the kinetic resolution reaction (the upper reaction in Figure 4),[16a] and the co-catalyst was not needed in this system. However, only two substrates with very low s-factors (less than 1.5) were presented. One year later, Ema and co-workers developed a series of chiral macrocyclic organocatalysts,[16b] which performed well for the kinetic resolution of disubstituted epoxides with CO_2 providing s-factors of up to 13.0 (the bottom reaction in Figure 4). But for monosubstituted epoxides, the s-factors dropped to below 4.5.

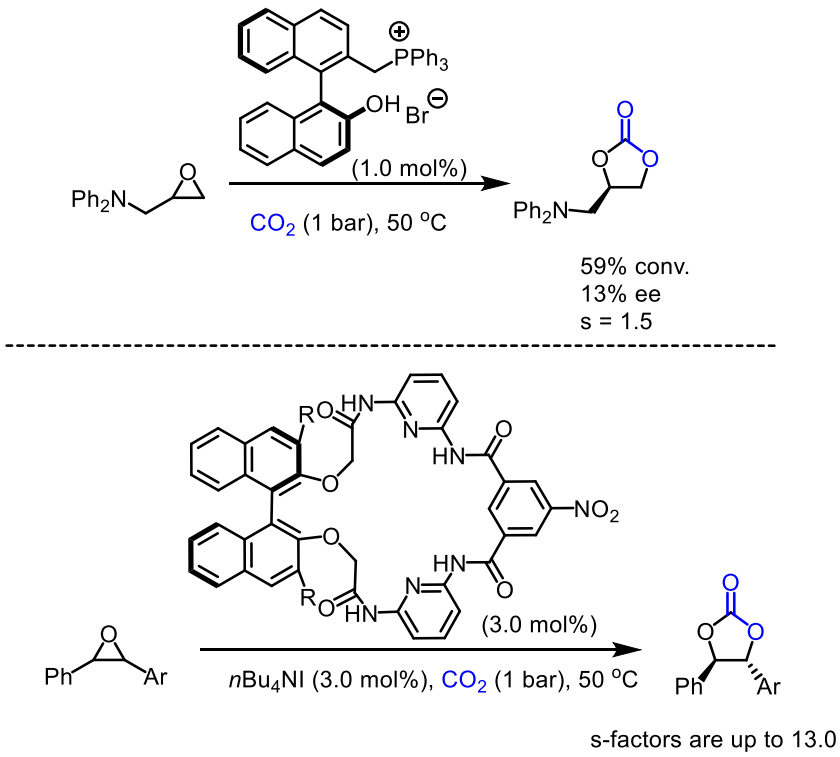

Figure 4. Kinetic resolution of epoxides with CO_2 catalyzed by organocatalysts.

1.3 Enantioselective C(sp^3)-H Aminations through Metal-Imido Intermediates

C-H amination represents an attractive strategy to activate C-H bonds and construct C-N bonds.[17] This method offers a way to synthesize nitrogen-containing molecules which constitute a prominent structural motif in many bioactive compounds.[18] One important mechanism of C-H amination is the socalled 'C-H insertion catalysis' which proceeds through a metal-imido intermediate.[17f] Generally, the catalytic process involves the formation of a metal-imido species through reaction between the metal catalyst and a suitable aminating reagent (such as amine, amide, imidoiodinane, organic azide and so on), followed by a C-H insertion to afford the target product (Figure 5). There are two mechanisms for the C-H insertion step: one is the direct C-H insertion (in a concerted way); another goes through a stepwise radical mechanism with H-atom abstraction, followed by radical recombination. Which mechanism is employed mainly relates to the nature of the catalyst. However, enantioselective C(sp^3)-H aminations through the metal-imido intermediate are still underdeveloped. In the following, enantioselective inter- or intramolecular C(sp^3)-H aminations via nitrene insertion catalyzed by transition-metal complexes and enzymes will be reviewed.

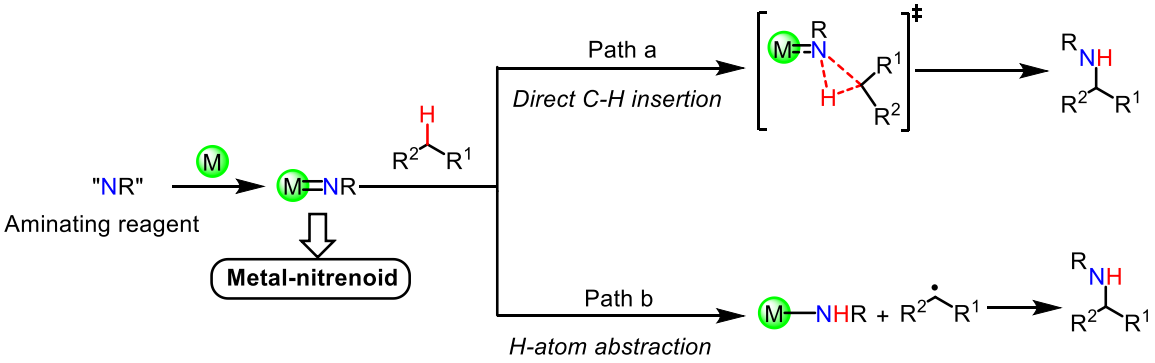

Figure 5. General process of C-H amination through metal-imido intermediate.

1.3.1 Catalytic Enantioselective Intramolecular C(sp^3)-H Amination

In 2002, Che and co-workers reported the first metalloporphyrin-catalyzed enantioselective intramolecular benzylic C-H amination.[19] In the presence of 1.5 mol% chiral ruthenium porphyrin and $PhI(OAc)_2$ as the oxidant, sulfamate esters could be transformed to cyclic sulfamidates with up to 87% ee (the upper reaction in Figure 6). Low reaction temperature was required for obtaining good enantioselectivity, but which sacrificed the reaction yield (less than 40% yields in some cases). Later in 2008, Blakey and co-workers developed a ruthenium pybox complex to catalyze the C-H amination of sulfamate esters in the presence of $PhI(O_2CtBu)_2$, offering moderate to good ees (75-92%) in good yields (the middle reaction in Figure 6).[20] Substrates investigated in this study are broader than Che's report, which contain aromatic groups, one allylic group and even one alkyl group but with very poor yield of 14%. In the same year, Du Bois and co-workers reported the enantioselective intramolecular benzylic or allylic C-H amination of sulfamate esters by using the chiral dirhodium(II) complex **Rh_2(*S*-nap)$_4$** as catalyst and PhIO as the oxidant (the bottom reaction in Figure 6).[21] This catalytic system displayed unprecedented performance especially for sulfamate esters containing aromatic groups, and enantioselectivities of up to 99% ee could be obtained in up to 98% yield. For homoallyl sulfamate ester substrate, C-H amination product is favored and no aziridination product formed when employing **Rh_2(*S*-nap)$_4$** as the catalyst.

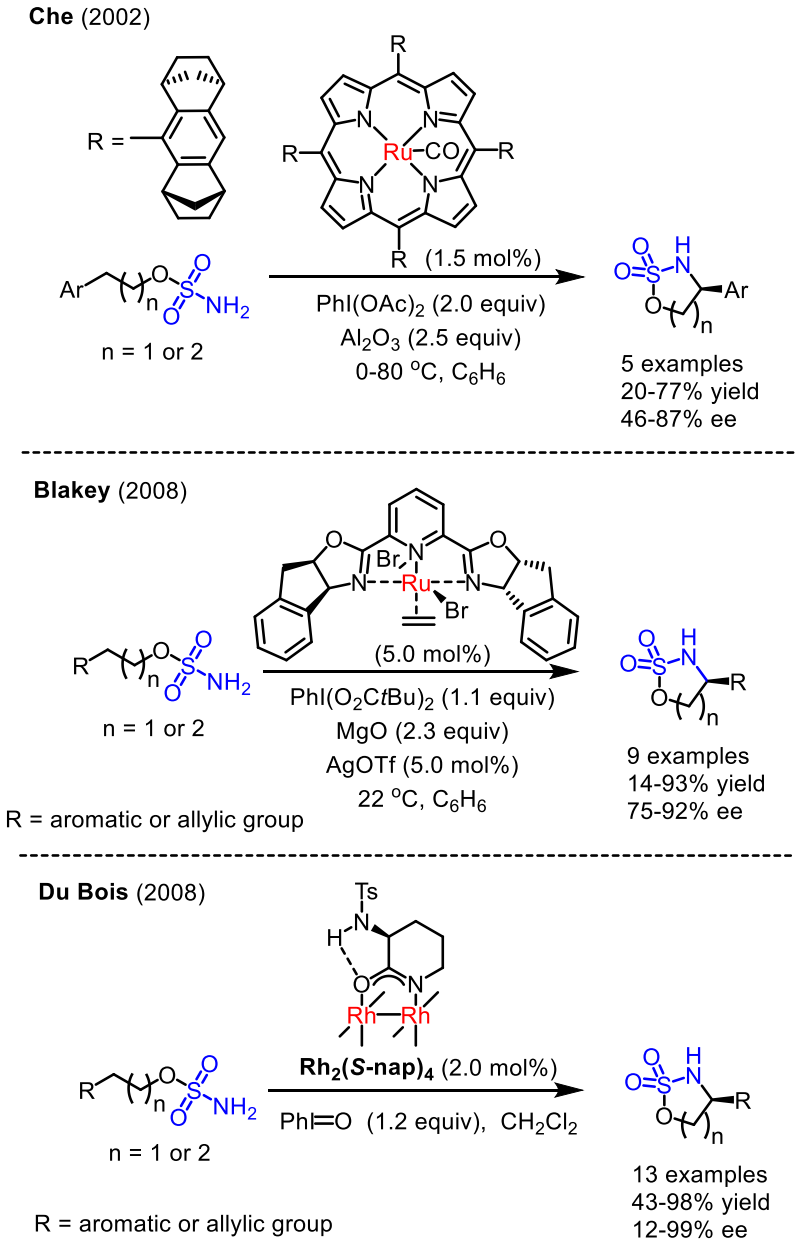

Figure 6. Transition-metal catalyzed enantioselective intramolecular C-H amination of sulfamate esters in the presence of stoichiometric amount of oxidant.

The possible mechanism of above examples might be as follows: the sulfamate ester firstly reacted with the oxidant to form an iminoiodane species (PhI=NR), which then reacted with the metal catalyst affording the metal-imido intermediate, followed by intramolecular C-H insertion to afford the product. Stoichiometric amount of oxidant such as $PhI(OAc)_2$ is required in the above systems, which is definitely a disadvantage. An obvious way forward is to choose organic azides as starting materials because no additional oxidant is required, and the only by-product is dinitrogen. In 2011, Katsuki and

co-workers reported that iridium(III)-salen complexes served as efficient catalysts for asymmetric intramolecular C-H aminations of benzenesulfonyl azides providing high enantioselectivities of up to 93% ee (the upper reaction in Figure 7).[22] This is the first example of a highly enantioselective intramolecular C-H amination starting with organic azides. Most recently, Zhang and co-workers reported the enantioselective 1,6-C-H amination of sulfamoyl azides by a chiral Co(II)-porphyrin complex (the bottom reaction in Figure 7).[23] A series of the six-membered cyclic sulfamides were obtained in high yields (up to 95%) with excellent enantioselectivities (up to 98% ee). The substrate scope of this system was very broad, consisting of benzylic, allylic and propargylic C-H bonds, also electron-deficient C-H bonds, and even non-activated C-H bonds. Mechanistic studies supported that this reaction went through a stepwise radical mechanism.

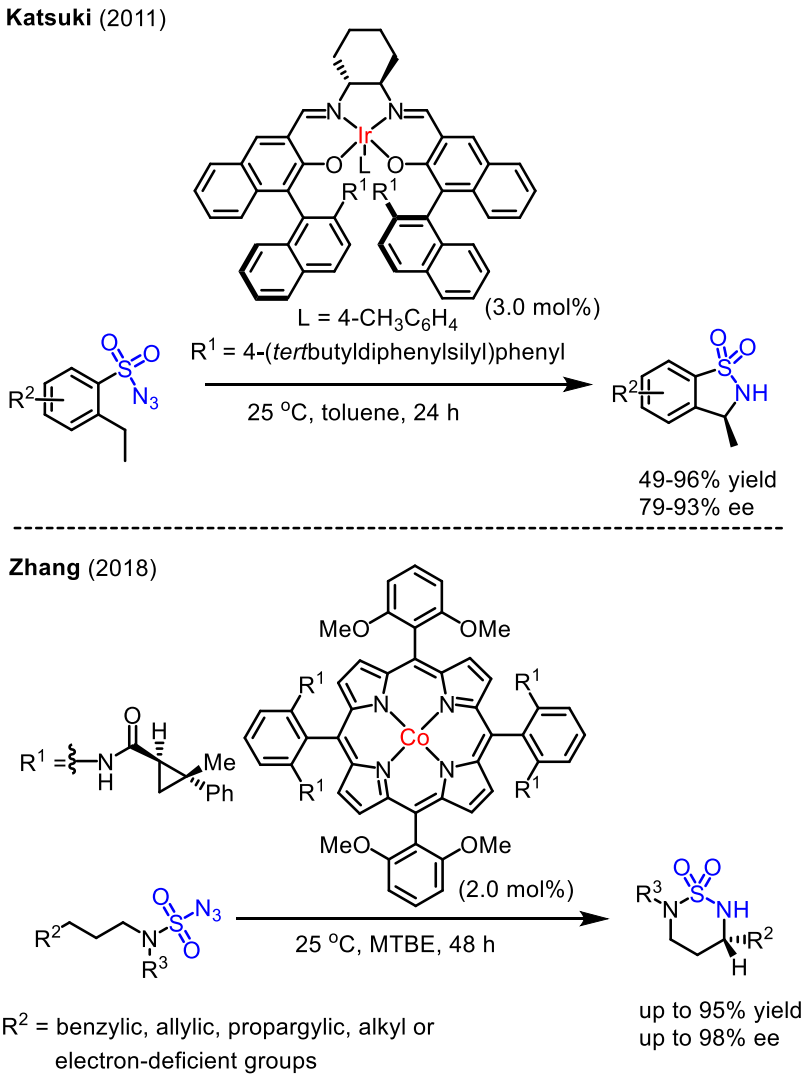

Figure 7. Transition-metal catalyzed enantioselective intramolecular C-H amination of sulfonyl azides.

To avoid using an oxidant, *N*-tosyloxycarbamate was also chosen as the starting compound for intramolecular C-H amination reported by Davies and co-workers in 2006 (Scheme 2).[24] C-H amination of *N*-tosyloxycarbamate was achieved by the dirhodium(II) complex **Rh_2(*S*-TCPTAD)$_4$** providing enantioselectivities of up to 82% ee. In this case, a tosylate group served as the leaving group.

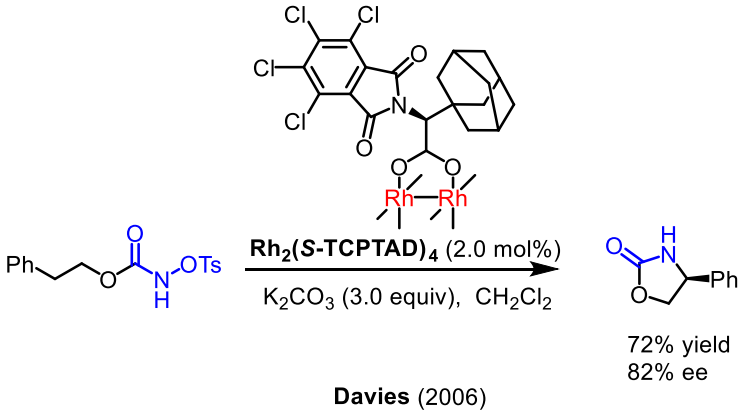

Scheme 2. Enantioselective intramolecular C-H amination of *N*-tosyloxycarbamate catalyzed by **Rh_2(*S*-TCPTAD)$_4$**.

In addition to transition-metal catalysts, enzymes have also been investigated for enantioselective intramolecular C-H amination.[25] The first highly active enzyme catalysts was reported by Arnold and co-workers in 2013.[25a] Serine-ligated P450s (called **P411s**) were employed to catalyze the enantioselective C-H amination of sulfamoyl azides, which displayed moderate reactivity with enantioselectivities of up to 89% ee (the upper reaction in Figure 8). One year later, Fasan and co-workers reported an alternative enzyme system, a cysteine-ligated P450s catalyzed intramolecular C(sp^3)-H amination of arylsulfonyl azide providing enantioselectivities of up to 91% ee (the middle reaction in Figure 8).[25b] The catalytic activities of the above two examples originated from the iron porphyrin moieties of the enzymes, which reacted with the organic azides to form iron(IV)-imido intermediates. In 2017, Hartwig and co-workers reported that P450s derived from a thermophilic organism and containing an iridium porphyrin cofactor (**Ir(Me)-PIX**) could catalyze enantioselective intramolecular C-H amination of sulfonyl azides with up to 98% yield and 90% ee (the bottom reaction in Figure 8).[25c] This system offered not only better chemoselectivity (C-H amination product

vs reduction of the azide) but also broader substrate scope compared with the above two reports which employed iron porphyrins containing enzymes as catalysts.

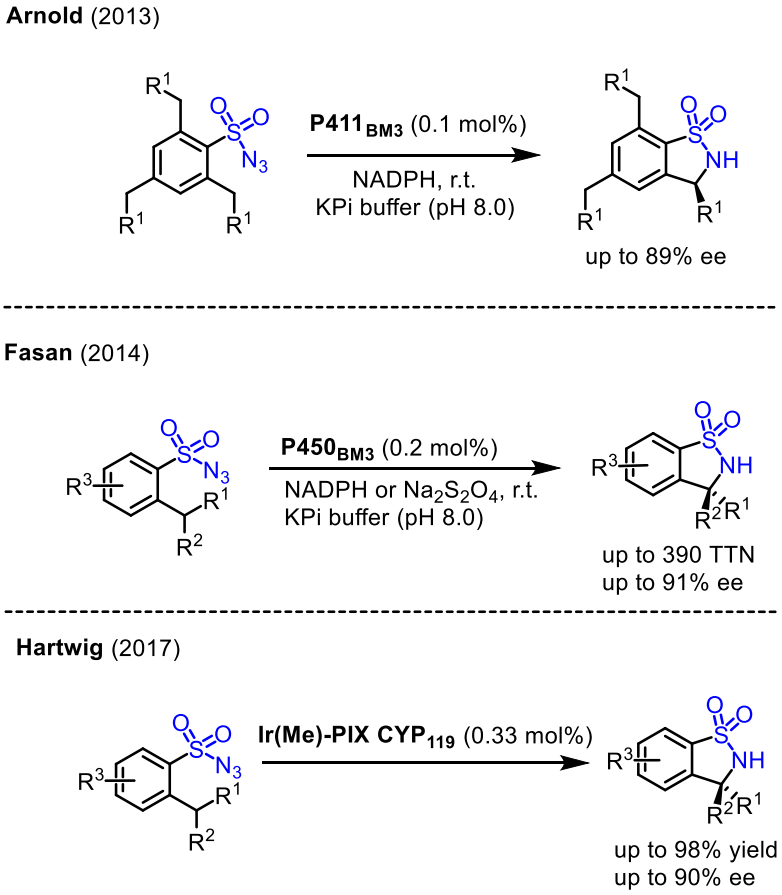

Figure 8. Enantioselective intramolecular C-H amination of sulfonyl azides catalyzed by enzymes.

Due to the high energy barrier for C-H activation especially for the C(sp^3)-H bond, electron-deficient organic azides (such as sulfonyl azides) are generally used as substrates for the C-H amination. Enantioselective intramolecular C(sp^3)-H aminations of aliphatic azides is only a recent accomplishment, which will be of great significance, because it enables to directly synthesize saturated chiral N-heterocyclic compounds. In 2017, de Bruin and co-workers reported the only example of a catalytic enantioselective C(sp^3)-H amination of (4-azidobutyl)benzene by using a chiral cobalt(II) porphyrin as catalyst affording 46% ee in 22% yield (Scheme 3).[26] Unfortunately, the enantioselectivity was low.

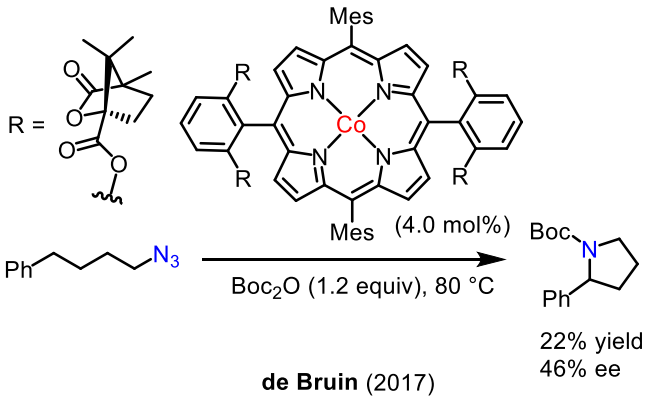

Scheme 3. Enantioselective intramolecular C-H amination of (4-azidobutyl)benzene catalyzed by a chiral cobalt(II) porphyrin.

1.3.2 Catalytic Enantioselective Intermolecular C(sp^3)-H Amination

Intermolecular C(sp^3)-H aminations are more challenging than intramolecular versions although the intermolecular C(sp^3)-H amination was reported earlier. Asymmetric intermolecular benzylic C-H amination of indane catalyzed by a chiral dirhodium(II) complex was demonstrated by the Müller group in 1997, but it provided very low enantioselectivity of only 31% ee (the upper reaction in Figure 9).[27a] In 1999, Che and co-workers reported that chiral ruthenium and manganese porphyrins could catalyze the enantioselective C-H amination of ethylbenzene and ethylnaphthalenes leading to 58% ee in moderate to good yields (the middle reaction in Figure 9).[27b] Two years later, Katsuki and co-workers reported that a Mn(salen) complex acted as the catalyst for enantioselective C-H aminations resulting in up to 89% ee at -40 ℃ (the bottom reaction in Figure 9).[27c] Not only benzylic C-H, but also allylic C-H bond could be aminated in their catalytic system. Moreover, allylic C-H amination occurred in preference to aziridination with respect to cycloalkenes.

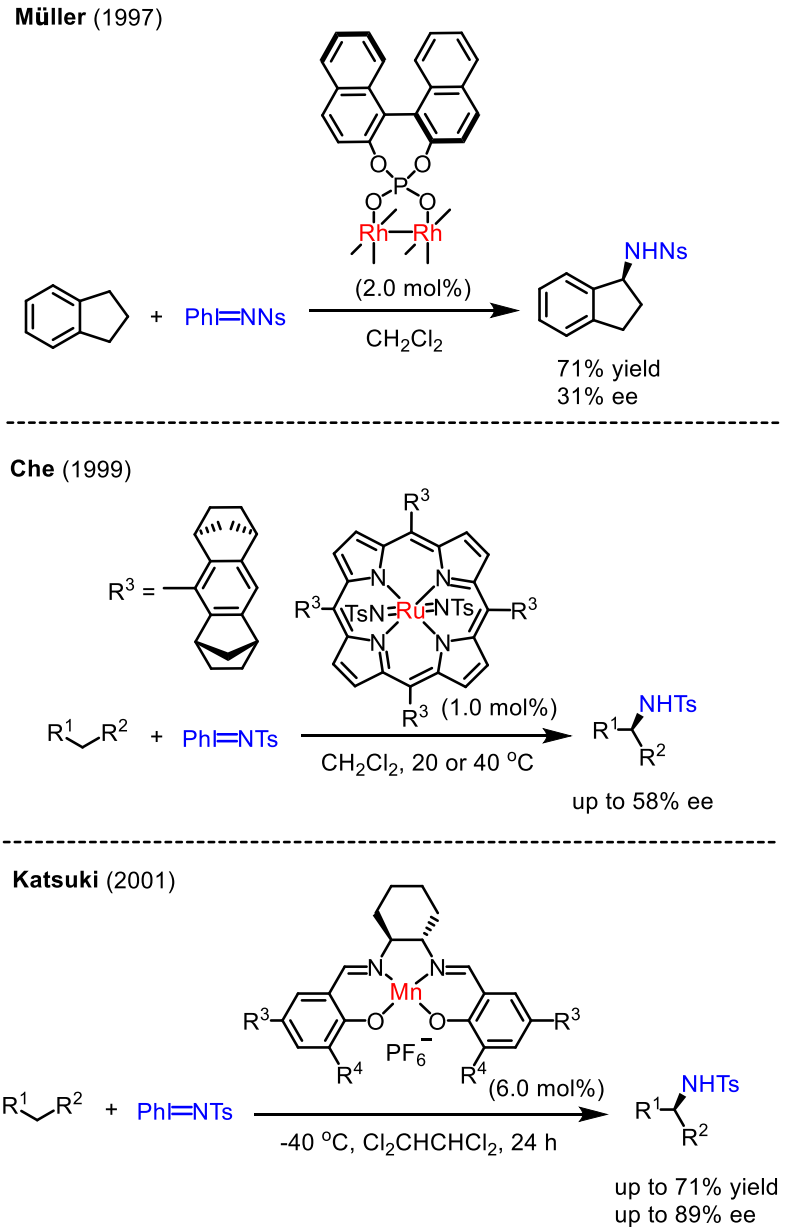

Figure 9. Transition-metal catalyzed enantioselective intermolecular C-H amination with [*N*-(*p*-toluenesulfonyl)imino] phenyliodinane (PhINTs) as the aminating reagent.

[*N*-(*p*-toluenesulfonyl)imino]phenyliodinane (PhINTs) was selected as the aminating reagent in all the above examples. As introduced in Chaper 1.3.1, organic azides constitute atom-efficient aminating reagents. In 2003, Katsuki and co-workers demonstrated that intermolecular allylic C-H amination could be realized by using a Ru(salen) complex as the catalyst and tosyl azide (TsN_3) as the aminating reagent, which provided a good enantioselectivity of 80% ee but in a poor yield of 17% (the upper reaction in Figure 10).[28a] Ten years later, the same group reported an improved Ru(salen)

catalyst together with 2-(trimethylsilyl)ethanesulfonyl azide (SES) as the aminating reagent could highly enantio- and regioselective aminate benzylic and allylic C-H bonds with up to 99% ee in up to 98% yield (the bottom reaction in Figure 10).[28b]

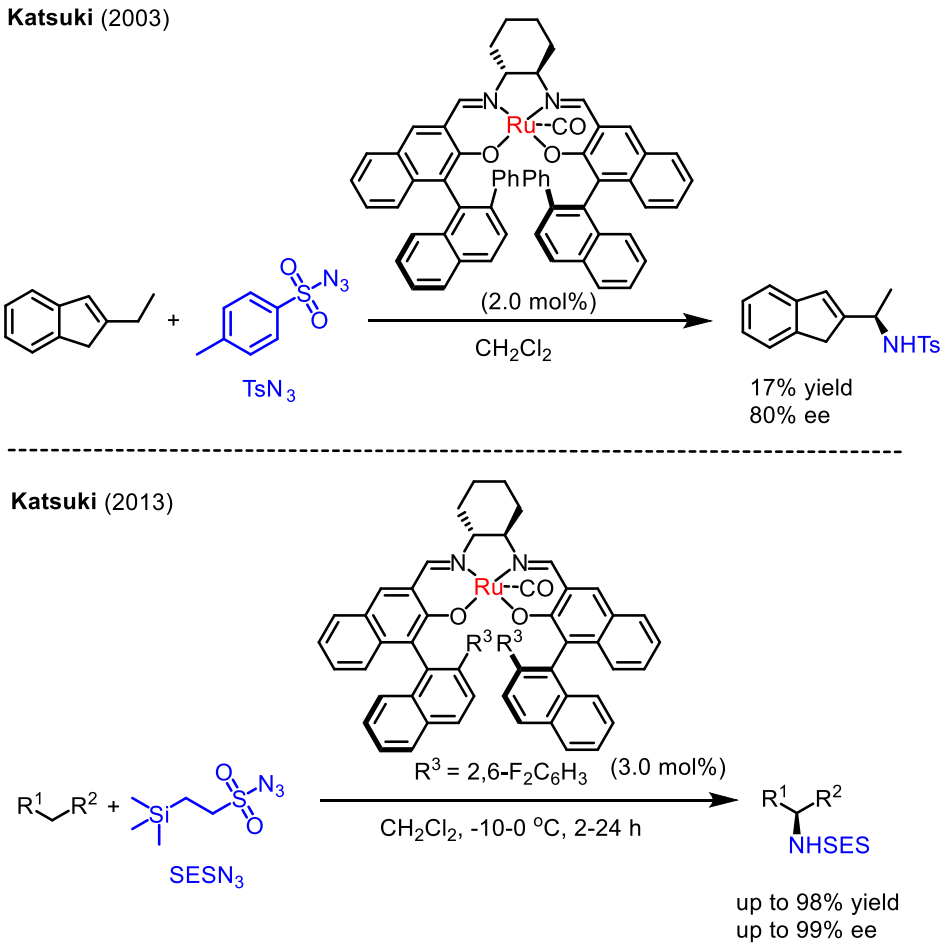

Figure 10. Transition-metal catalyzed enantioselective intermolecular C-H amination with electron-deficient organic azides as the aminating reagents.

In 2017, Arnold and co-workers reported an iron-containing enzymatic catalyst based on a cytochrome P450 monooxygenase for the highly enantioselective intermolecular benzylic C-H amination by using tosyl azide as the aminating reagent (Scheme 4).[29] The turnover number (TON) of this biocatalyst could reach up to 1300 with very good enantioselectivities of up to >99% ee. This methodolody could be used for the synthesis of a variety of chiral benzylic amines.

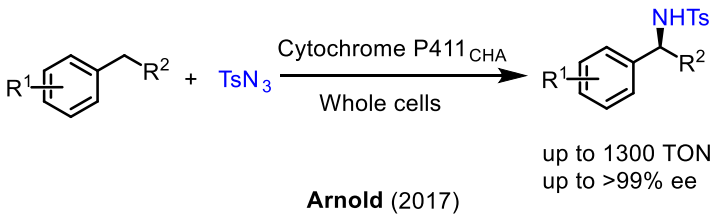

Scheme 4. Enantioselective intermolecular benzylic C-H amination catalyzed by an engineered iron-haeme enzyme.

1.4 Asymmetric Oxidative Coupling of Carbonyl Compounds

An oxidative coupling of two carbonyl compounds offers a direct and efficient way to construct molecules contain 1,4-dicarbonyl moieties,[30] which are important synthetic intermediates. Actually, indirect methods for the oxidative coupling of two carbonyl compounds have been reported a long time ago (Figure 11a).[30b] Normally, the first step is to transform the carbonyl compounds to electron-rich enolates or related carbonyl derivatives (like enol silanes and enamines), then undergo the coupling reaction in the presence of an oxidant. According to this general scheme, different kinds of methods have been developed for the indirect oxidative coupling of carbonyl compounds including coupling of lithium metal enolates, intramolecular oxidative coupling of silyl bis-enol ethers, and enamine catalysis.

There are three kinds of mechanisms[30] for the enolate coupling: radical-radical coupling, radical-enolate reaction, and S_N2 reaction (Figure 11b). How to control stereoselectivity (diastereo- and enantioselectivity) of these coupling reactions has been a difficult task. Most enantioselective oxidative couplings mainly relied on the use of stoichiometric chiral reagents or substrates containing a chiral auxiliary, catalytic asymmetric versions have been very limited.

Ideally, chiral 1,4-dicarbonyl compounds could directly form by oxidative coupling of two nucleophilic carbonyls (Figure 11c), although this is very challenging and until recently only one example is reported.[31] In the following, enantioselective oxidative couplings of two carbonyl compounds will be discussed.

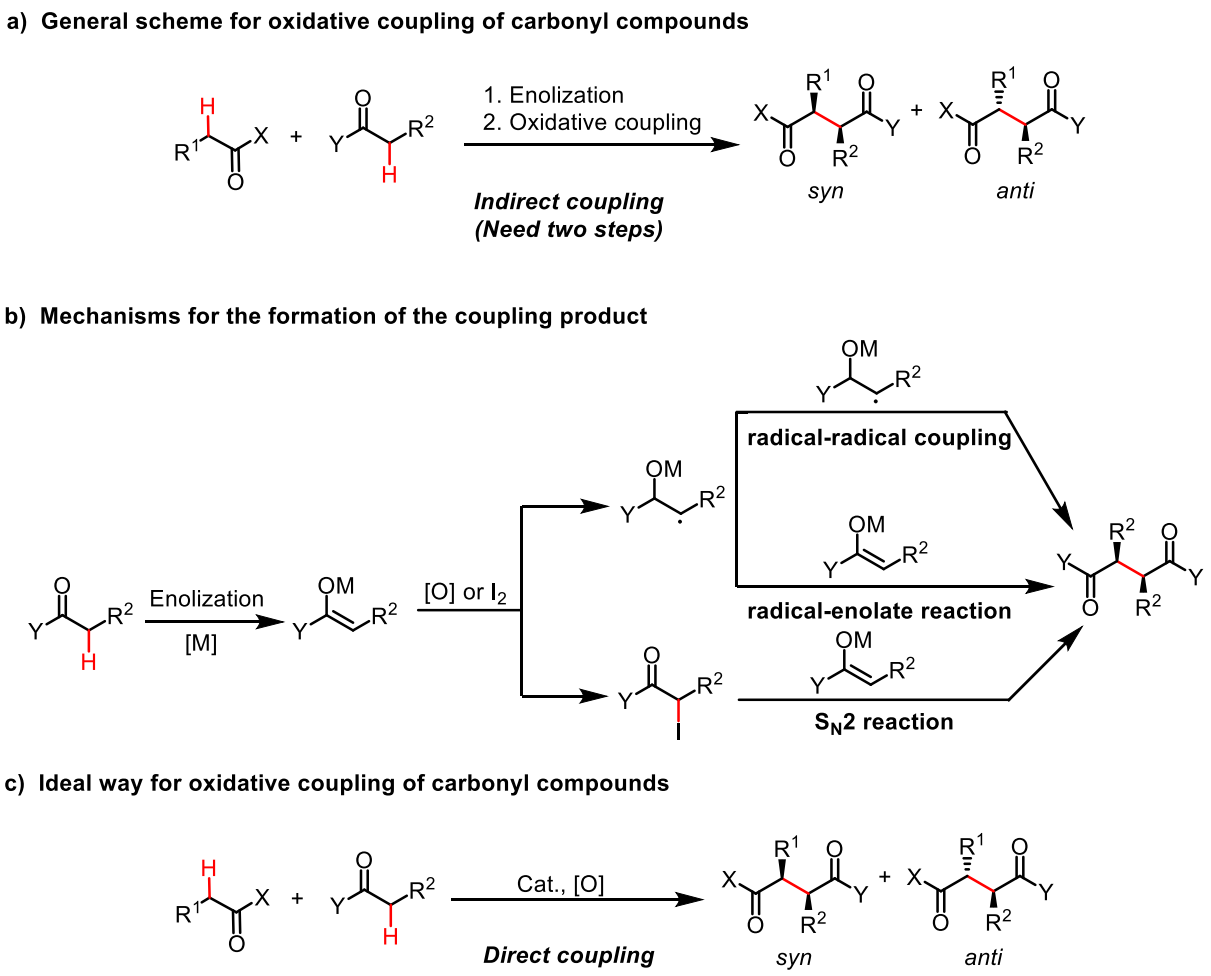

Figure 11. a) General scheme for oxidative coupling of carbonyl compounds; b) Mechanisms for the formation of the coupling product; c) Ideal way for oxidative coupling of carbonyl compounds.

1.4.1 Indirect Asymmetric Oxidative Coupling of Carbonyl Compounds

The most popular strategy of oxidative coupling starts with lithium metal enolates, and early examples of enantioselective oxidative coupling mainly relied on the use of substrates containing chiral auxiliaries.[32] For example in 1993, Porter and co-workers reported the enolization of optically pure butyryloxazolidine by using LDA as the base, then enantioselective oxidative homocoupling occurred in the presence of $CuCl_2$. Almost only *syn*-product was obtained (50% yield with 97% ee) (Figure 12a).[32a] Based on this result, different kinds of chiral auxiliaries have been investigated for the asymmetric oxidative coupling (Figure 12b). Both the diastereoselectivity and enantioselectivity depend on the chiral auxiliaries and reaction conditions. Importantly, this methodology has been successfully applied for the synthesis of natural products. For example, the synthesis of (-)-hinokinin

was reported by Kise and co-workers (Figure 12c).[32f]

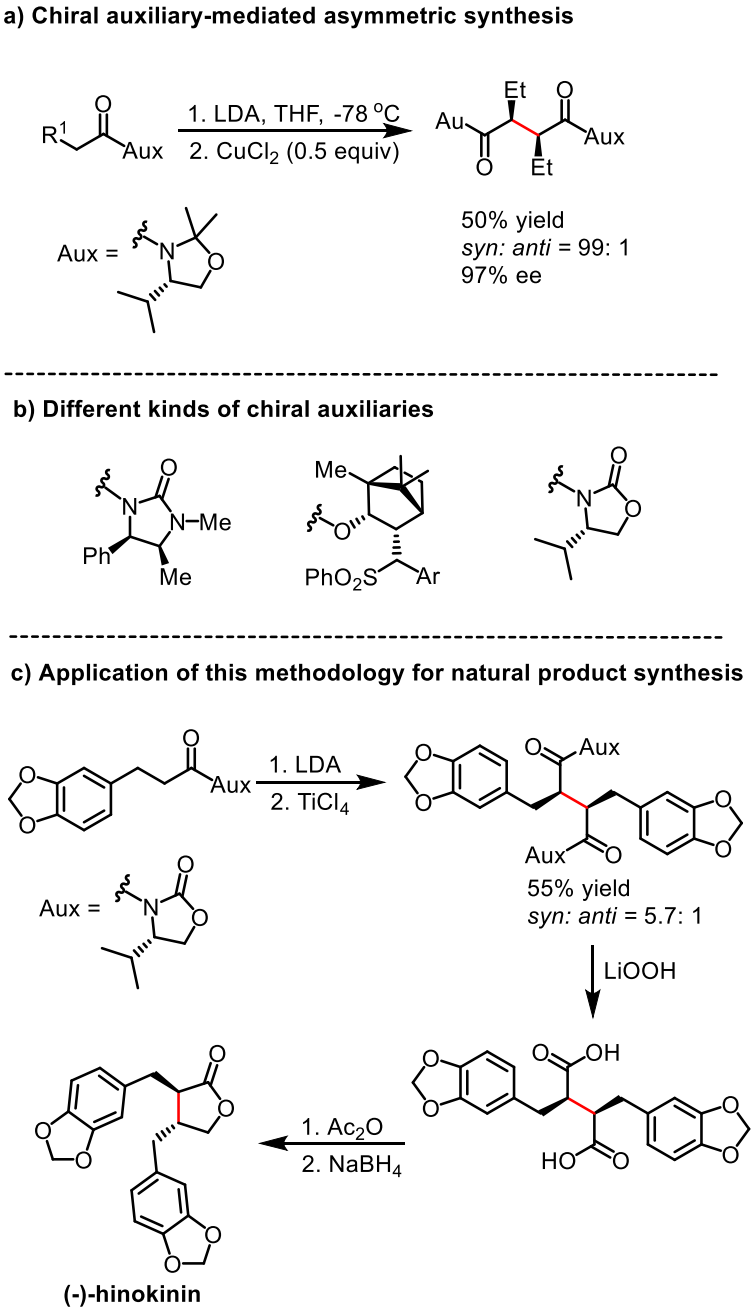

Figure 12. Chiral auxiliary-mediated asymmetric oxidative enolate coupling.

In 2001, Schäfer and co-workers reported the enantioselective oxidative homocoupling by using a stoichiometric chiral ligand as additive, instead of chiral auxiliary, and homocoupling of 3-(2-phenylacetyl)oxazolidin-2-one was achieved with up to 76% ee (Scheme 5).[33] Unfortunately, the *anti*-product (*mesometic* product) rather the *syn*-product was obtained as the major diastereomer.

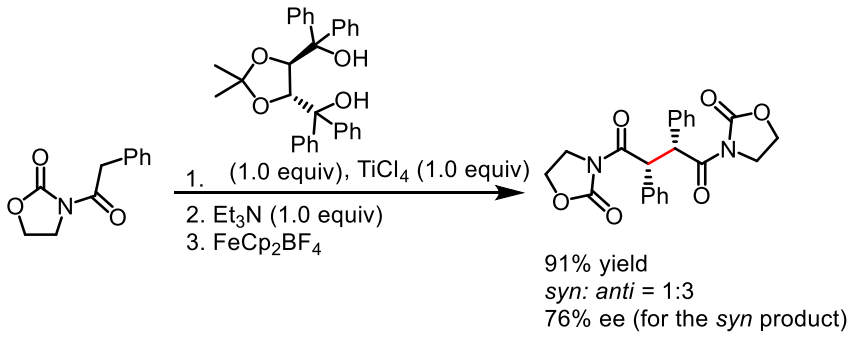

Scheme 5. Asymmetric oxidative enolate coupling in the presence of stoichiometric amounts of chiral ligand.

Besides going through lithium enolates, a related oxidative enolate coupling reported by Thomson and co-workers proceeded via silyl bis-enol ethers (Scheme 6).[34] This strategy allowed for the convergent and stereoselectively assembly of polycyclic molecules through cross-coupling of chiral substrates.

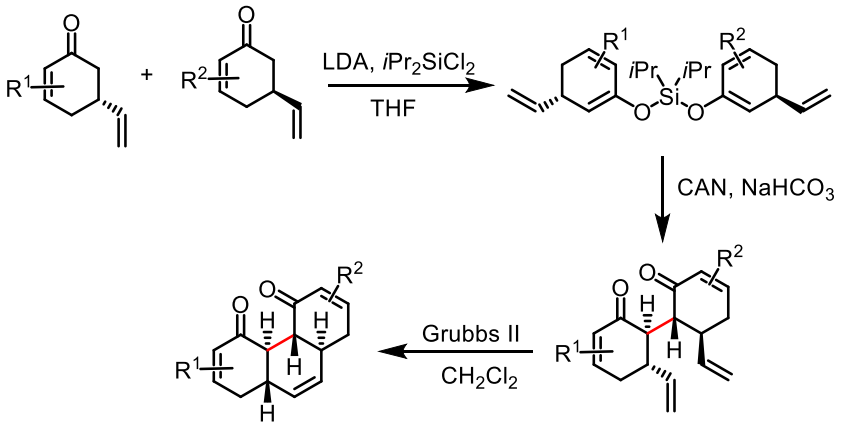

Scheme 6. Oxidative enolate cross-coupling via silyl bis-enol ethers.

All the examples described above required using of chiral substrates or stoichiometric amount of chiral ligands to achieve enantioselective transformations. The first report of catalytic enantioselective oxidative enolate coupling was disclosed by MacMillan and co-workers in 2007 through enamine catalysis (Scheme 7).[35] The enamine generated by reaction of the aldehyde substrate and the chiral imidazolidinone catalyst underwent oxidative bond formation with enol silane in the presence of ceric ammonium nitrate (CAN), providing the coupling products in high yields (55-92%) with excellent

enantioselectivities (86-96% ee).

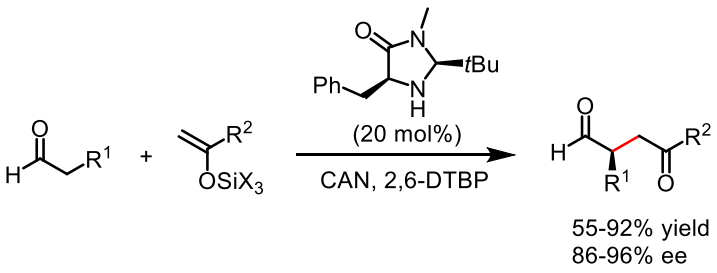

Scheme 7. Catalytic enantioselective enolate oxidative coupling via enamine catalysis.

1.4.2 Direct Asymmetric Oxidative Coupling of Carbonyl Compounds

The only example of direct asymmetric oxidative coupling of two carbonyl compounds was reported very recently by Jørgensen and coworkers (Scheme 8).[31] The homocoupling of α-branched aldehydes with good yields and moderate to excellent enantioselectivities was achieved in the presence of 40 mol% chiral amine catalyst and Ag_2CO_3 as the oxidant. Diastereoselectivities and enantioselectivities were sensitive to the nature of the substrates. Electron-poor aromatic aldehydes performed better than electron-rich substrates. Mechanism studies indicated that the homocoupling proceeds through a radical cation intermediate.

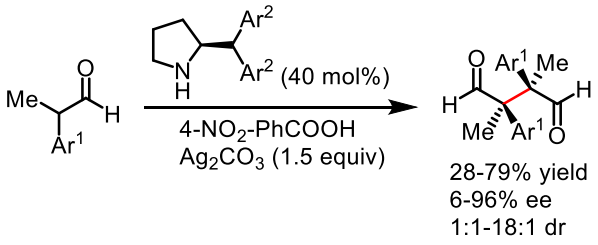

Scheme 8. Direct enantioselective oxidative homocoupling of aldehydes.

1.5 Conclusions

(1) The reported catalysts for the kinetic resolution of epoxides with CO_2 are mainly Schiff base metal complexes. Almost all the reported systems display poor substrate tolerance, and no general catalytic system for a variety of different epoxide substrates exists. Another problem is the reaction suffers from

copolymerization side reaction especially when cobalt Schiff base used as catalysts. Development of new updated catalysts is therefore of great interest.

(2) Both transition metal complexes and enzymes can catalyze enantioselective C(sp^3)-H aminations through metal-imido intermediates with excellent enantioselectivities using organic azides with electron-withdrawing groups like sulfonyl azides as the aminating reagents. However, enantioselective C-H aminations of primary aliphatic organic azides are apparently much more difficult and only one example was recently disclosed but with low enantioselectivity of only 46% ee. Therefore, the development of new catalytic systems for highly enantioselective C-H aminations of primary aliphatic organic azides is of high interest.

(3) As one of the most efficient ways to construct 1,4-carbonyl moieties, oxidative coupling of carbonyl compounds has been achieved by different kinds of indirect strategies, such as the oxidative coupling of lithium enolates. These indirect strategies go through a two-steps procedure: the first step is the enolization, the second step is an oxidative coupling of the formed enolate. However, the direct enantioselective oxidative coupling of carbonyl compounds which provides a more direct access to chiral 1,4-carbonyl molecules has been much less addressed. It will be of great interest to explore new catalytic systems for the direct asymmetric coupling of carbonyl compounds.

References

1 P. J. Walsh, M. C. Kozlowski, *Fundamentals of asymmetric catalysis*, University Science Books: Sausalito, California, **2009**.

2 (*a*) W. S. Knowles, *Angew. Chem. Int. Ed.* **2002**, *41*, 1998; (*b*) R. Noyori, *Angew. Chem. Int. Ed.* **2002**, *41*, 2008; (*c*) K. B. Sharoless, *Angew. Chem. Int. Ed.* **2002**, *41*, 2024.

3 J. Artz, T. E. Müller, K. Thenert, J. Kleinekorte, R. Meys, A. Sternberg, A. Bardow, W. Leitner, *Chem. Rev.* **2018**, *118*, 434.

4 For reviews on the application of organic cyclic carbonates, see: (*a*) A. A. Shaikh, S. Sivaram, *Chem. Rev.* **1996**, *96*, 951; (*b*) J. H. Clements, *Ind. Eng. Chem. Res.* **2003**, *42*, 663; (*c*) B. Schäffner, F. Schäffner, S. P. Verevkin, A. Börner, *Chem. Rev.* **2010**, *110*, 4554.

5 For reviews on the synthesis of organic cyclic carbonates from CO_2, see: (*a*) M. North, R. Pasquale, C. Young, *Green Chem.* **2010**, *12*, 1514; (*b*) A. Decortes, A. M. Castilla, A. W. Kleij, *Angew. Chem. Int. Ed.* **2010**, *49*, 9822; (*c*) X.-B. Lu, D. J. Darensbourg, *Chem. Soc. Rev.* **2012**, *41*, 1462; (*d*) C. Maeda, Y. Miyazaki, T. Ema, *Catal. Sci. Technol.* **2014**, *4*, 1482; (*e*) C. Martín, G. Fiorani, A. W. Kleij, *ACS Catal.* **2015**, *5*, 1353; (*f*) M. Cokoja, M. E. Wilhelm, M. H. Anthofer, W. A. Herrmann, F. E. Kuhn, *ChemSusChem* **2015**, *8*, 2436; (*g*) J. W. Comerford, I. D. V. Ingram, M. North, X. Wu, *Green Chem.* **2015**, *17*, 1966; (*h*) X.-D. Lang, L.-N. He, *Chem. Rec.* **2016**, *16*, 1337; (*i*) H. Büttner, L. Longwitz, J. Steinbauer, C. Wulf, T. Werner, *Topics in Current Chem.* **2017**, *3*, 375; (*j*) R. R. Shaikh, S. Pornpraprom, V. D'Elia, *ACS Catal.* **2018**, *8*, 419.

6 For reviews on asymmetric couplings of racemic epoxides with CO_2, see: (*a*) N. Kielland, C. J. Whiteoak, A. W. Kleij, *Adv. Synth. Catal.* **2013**, *355*, 2115; (*b*) X. Wu , J. A. Castro-Osma, M. North, *Symmetry* **2016**, *8*, 4.

7 M. Brunner, L. Mußmann, D. Vogt, *Synlett* **1993**, 893.

8 X.-B. Lu, B. Liang, Y.-J. Zhang, Y.-Z. Tian, Y.-M. Wang, C.-X. Bai, H. Wang, R. Zhang, *J. Am. Chem. Soc.* **2004**, *126*, 3732.

9 R. L. Paddock, S. T. Nguyen, *Chem. Commun.* **2004**, 1622.

10 A. Berkessel, M. Brandenburg, *Org. Lett.* **2006**, *8*, 4401.

11 (*a*) T. Chang, H. Jing, L. Jin, W. Qiu, *J. Mol. Catal. A: Chem.* **2007**, *264*, 241; (*b*) L. Jin, Y. Huang, H. Jing, T. Chang, P. Yan, *Tetrahedron: Asymmetry* **2008**, *19*, 1947; (*c*) P. Yan, H. Jing,

Adv. Synth. Catal. **2009**, *351*, 1325; (*d*) T. Chang, L. Jin, H. Jing, *ChemCatChem* **2009**, *1*, 379; (*e*) S. Zhang, Y. Song, H. Jing, P. Yan, Q. Cai, *Chin. J. Catal.* **2009**, *30*, 1255; (*f*) S. Zhang, Y. Huang, H. Jing, W. Yao, P. Yan, *Green Chem.* **2009**, *11*, 935; (*g*) Y. Song, Q. Jin, S. Zhang, H. Jing, Q. Zhu, *Sci. China Chem.* **2011**, *7*, 1044; (*h*) S. Duan, X. Jing, D. Li, H. Jing, *J. Mol. Catal. A: Chem.* **2016**, *411*, 34.

12 (*a*) S.-W. Chen, R. B. Kawthekar, G.-J. Kim, *Tetrahedron Lett.* **2007**, *48*, 297; (*b*) R. B. Kawthekar, G.-J. Kim, *Bull. Korean Chem. Soc.* **2008**, *29*, 313; (*c*) D. Y. Jang, H. G. Jang, G. R. Kim, G.-J. Kim, *Catal. Today* **2012**, *185*, 306; (*d*) T. Roy, R. I. Kureshy, N. H. Khan, S. H. R. Abdi, H. C. Bajaj, *Catal. Sci. Technol.* **2013**, *3*, 2661; (*e*) V. A. Larionov, E. P. Markelova, A. F. Smol'yakov, T. F. Savel'yeva, V. I. Maleev, Y. N. Belokon, *RSC Adv.* **2015**, *5*, 72764.

13 W.-M. Ren, G.-P. Wu, F. Lin, J.-Y. Jiang, C. Liu, Y. Luo, X.-B. Lu, *Chem. Sci.* **2012**, *3*, 2094.

14 (*a*) H. Tanaka, Y. Kitaichi, M. Sato, T. Ikeno, T. Yamada, *Chem. Lett.* **2004**, *33*, 676; (*b*) W. Yamada, Y. Kitaichi, H. Tanaka, T. Kojima, M. Sato, T. Ikeno, T. Yamada, *Bull. Chem. Soc. Jpn.* **2007**, *80*, 1391.

15 (*a*) M. Aresta, A. Dibenedetto, L. Gianfrate, C. Pastore, *Appl. Catal. A* **2003**, *255*, 5; (*b*) Y. Ren, X. Cheng, S. Yang, C. Qi, H. Jiang, Q. Mao, *Dalton Trans.* **2013**, *42*, 9930; (*c*) M. North, S. C. Z. Quek, N. E. Pridmore, A. C. Whitwood, X. Wu, *ACS Catal.* **2015**, *5*, 3398.

16 (*a*) S. Liu, N. Suematsu, K. Maruoka, S. Shirakawa, *Green Chem.* **2016**, *18*, 4611; (*b*) T. Ema, M. Yokoyama, S. Watanabe, S. Sasaki, H. Ota, K. Takaishi, *Org. Lett.* **2017**, *19*, 4070.

17 For reviews on catalytic C-H aminations, see: (*a*) C.-M. Che, V. K.-Y. Lo, C.-Y. Zhou, J.-S. Huang, *Chem. Soc. Rev.* **2011**, *40*, 1950; (*b*) F. Collet, C. Lescot, P. Dauban, *Chem. Soc. Rev.* **2011**, *40*, 1926; (*c*) B. J. Stokes, T. G. Driver, *Eur. J. Org. Chem.* **2011**, 4071; (*d*) J. L. Jeffrey, R. Sarpong, *Chem. Sci.* **2013**, *4*, 4092; (*e*) D. Hazelard, P.-A. Nocquet, P. Compain, *Org. Chem. Front.* **2017**, *4*, 2500; (*f*) Y. Park, Y. Kim, S. Chang, *Chem. Rev.* **2017**, *117*, 9247.

18 R. D. Taylor, M. MacCoss, A. D. G. Lawson, *J. Med. Chem.* **2014**, *57*, 5845.

19 J.-L. Liang, S.-X. Yuan, J.-S. Huang, W.-Y. Yu, C.-M. Che, *Angew. Chem. Int. Ed.* **2002,** *41*, 3465.

20 E. Milczek, N. Boudet, S. Blakey, *Angew. Chem. Int. Ed.* **2008,** *47*, 6825.

21 D. N. Zalatan, J. Du Bois, *J. Am. Chem. Soc.* **2008**, *130*, 9220.

22 M. Ichinose, H. Suematsu, Y. Yasutomi, Y. Nishioka, T. Uchida, T. Katsuki, *Angew. Chem. Int. Ed.* **2011**, *50*, 9884.

23 C. Li, K. Lang, H. Lu, Y. Hu, X. Cui, L. Wojtas, X. P. Zhang, *Angew. Chem. Int. Ed.* **2018**, *57*, 16837.

24 R. P. Reddy, H. M. L. Davies, *Org. Lett.* **2006**, *8*, 5013.

25 For enzymes catalyzed enantioselective intramolecular C(sp^3)-H amination of sulfonyl azides, see: (*a*) J. A. McIntosh, P. S. Coelho, C. C. Farwell, Z. J. Wang, J. C. Lewis, T. R. Brown, F. H. Arnold, *Angew. Chem. Int. Ed.* **2013**, *52*, 9309; (*b*) R. Singh, M. Bordeaux, R. Fasan, *ACS Catal.* **2014**, *4*, 546; (*c*) P. Dydio, H. M. Key, H. Hayashi, D. S. Clark, J. F. Hartwig, *J. Am. Chem. Soc.* **2017**, *139*, 1750.

26 P. F. Kuijpers, M. J. Tiekink, W. B. Breukelaar, D. L. J. Broere, N. P. van Leest, J. I. van der Vlugt, J. N. H. Reek, B. de Bruin, *Chem. Eur. J.* **2017**, *23*, 7945.

27 For early studies of enantioselective intermolecular C(sp^3)-H amination with PhI=NTs as aminating reagent, see: (*a*) I. Nägeli, C. Baud, G. Bernardineli, Y. Jacquier, M. Moran, P. Müller, *Helv. Chim. Acta* **1997**, *80*, 1087; (*b*) Zhou, X.-G.; Yu, X.-Q.; Huang, J.-S.; Che, C.-M. *Chem. Commun*. **1999**, 2377; (*c*) Y. Kohmura, T. Katsuki, *Tetrahedron Lett.* **2001**, *42*, 3339.

28 (*a*) K. Omura, M. Murakami, T. Uchida, R. Irie, T. Katsuki, *Chem. Lett.* **2003**, *32*, 354; (*b*) Y. Nishioka, T. Uchida, T. Katsuki, *Angew. Chem. Int. Ed.* **2013**, *52*, 1739.

29 A. K. Prier, R. K. Zhang, A. R. Buller, S. Brinkmann-Chen, F. H. Arnold, *Nat. Chem.* **2017**, *9*, 629.

30 For reviews of oxidative coupling of carbonyl compounds, see: (*a*) A. G. Csákÿ, J. Plumet, *Chem. Soc. Rev.* **2001**, *30*, 313; (*b*) F. Guo, M. D. Clift, R. J. Thomson, *Eur. J. Org. Chem.* **2012**, 4881.

31 L. Næsborg, L. A. Leth, G. J. Reyes-Rodríguez, T. A. Palazzo, V. Corti, K. A. Jørgensen, *Chem. Eur. J.* **2018**, *24*, 14844.

32 For chiral auxiliary-mediated asymmetric oxidative enolate coupling, see: (*a*) N. A. Porter, Q. Su, J. J. Harp, I. J. Rosenstein, A. T. McPhail, *Tetrahedron Lett.* **1993**, *34*, 4457; (*b*) Y. Matsumura, M. Nishimura, H. Hiu, M. Watanabe, N. Kise, *J. Org. Chem.* **1996**, *61*, 2809; (*c*) N. A. Porter, Q. Su, J. J. Harp, I. J. Rosenstein, A. T. McPhail, *Tetrahedron Lett.* **1993**, *34*, 4457; (*d*) T. Langer, M. Illich, G. Helmchen, *Tetrahedron Lett.* **1995**, *36*, 4409; (*e*) T. Langer, M. Illich, G. Helmchen, *Synlett* **1996**, 1137; (*f*) N. Kise, T. Ueda, K. Kumada, Y. Terao, N. Ueda, *J. Org. Chem.* **2000**, *65*, 464.

33 P. Q. Nguyen, H. J. Schäfer, *Org. Lett.* **2001**, *3*, 2993.

34 E. E. Robinson, R. J. Thomson, *J. Am. Chem. Soc.* **2018**, *140*, 1956.

35 H.-Y. Jang, J.-B. Hong, D. W. C. MacMillan, *J. Am. Chem. Soc.* **2007**, *129*, 7004.

Chapter 2: Aim of the Work

As one of the most important strategies to synthesizing non-racemic compounds, asymmetric catalysis by chiral transition metal catalysts has been extensively studied in the past several decades.[1] Typically, the chiral transition metal catalyst contains at least one chiral ligand which is the origin of the chirality during the catalytic transformation. A variety of chiral ligands, such as heteroatom (phosphorus, nitrogen, oxygen, sulfur)-containing ligands, carbene ligands, cyclometalated ligands, and cyclopentadienyl ligands, have been successfully developed and applied in asymmetric catalysis. In a different and more or less neglected strategy, the chiral transition metal complex includes only achiral ligands, in which the origin of the chirality is solely from the stereogenic metal center generated upon the asymmetric coordination of the achiral ligands around the central metal (Figure 13).[2] Compared with transition metal catalysts with chiral ligands, those with only achiral ligands are much less studied and only a recent development especially by the Meggers group. “Chiral-at-metal” will be used as a term throughout the thesis to describe such complexes, referring to chiral metal complexes with only achiral ligands in which the chirality is the exclusive result of a stereogenic metal center. Over the last 5 years, the Meggers group developed a series of chiral-at-metal complexes (include iridium, rhodium, and ruthenium) which possess metal-centered Λ- (left-handed propeller) or Δ-configuration (righthanded propeller) derived from the propeller-type arrangement of the two bidentate achiral ligands (Figure 13).[3-5] Importantly, this novel class of chiral-at-metal complexes has been demonstrated as efficient catalysts for a variety of transformations (like Michael additions, Friedel-Crafts reactions, cycloadditions, asymmetric transfer hydrogenation, light-activated asymmetric transformations, alkynylation of trifluoromethyl ketones and so on) with very high enantioselectivities.[2]

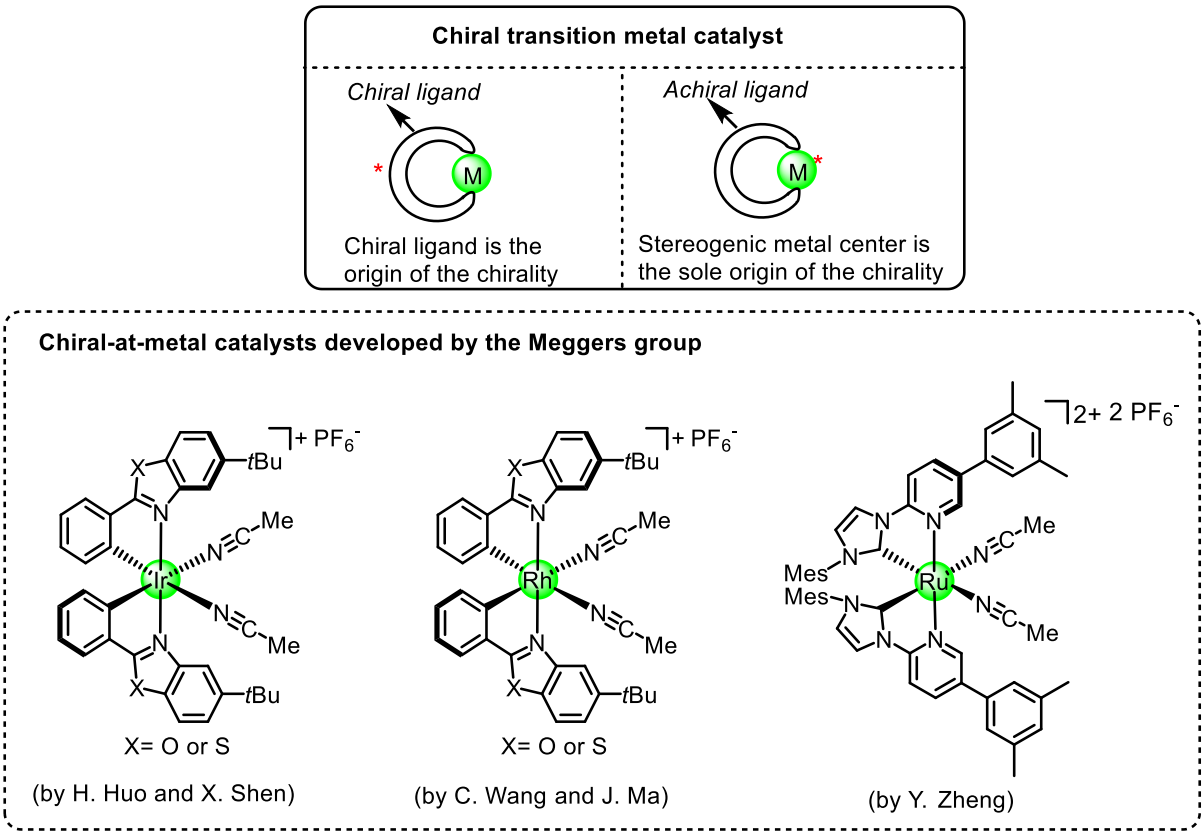

Figure 13. Chiral transition metal catalysts with chiral or achiral ligand and representative chiral-at-metal catalysts developed by the Meggers group.

Aim 1: Expanding the catalytic properties of chiral-at-metal iridium catalysts

As mentioned above, the chiral-at-metal iridium and rhodium complexes developed by the Meggers group have been used as powerful Lewis acids for a variety of transformations. To get high enantioselectivity, the substrates employed in the catalytic reactions such as 2-acyl imidazole usually contain an auxiliary moiety for two-point binding.[2b] There are notable exceptions, like an iridium-catalyzed enantioselective transfer hydrogenation of arylketones.[6] In this respect, one can wonder if there are other types of enantioselective transformations that can be catalyzed by the chiral-at-metal Lewis acid catalysts without utilizing a bidentate coordination of the substrate. Thus, the author of this thesis is interested in investigating new catalytic properties of chiral-at-iridium Lewis acids using different coordination modes (Figure 14).

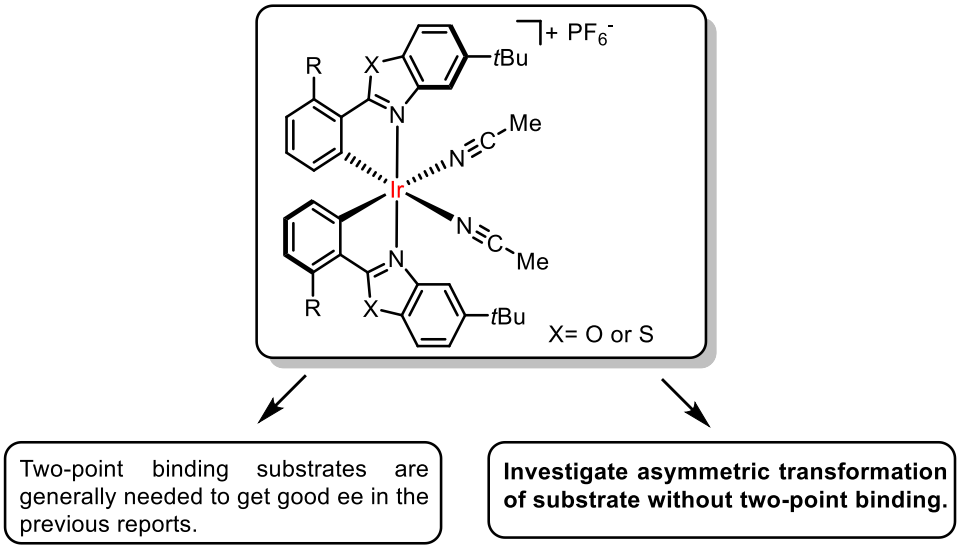

Figure 14. Aim1: Expand the catalytic properties of chiral-at-metal iridium catalysts.

Aim 2: Expanding the catalytic properties of chiral-at-metal ruthenium catalyst

In 2017, former group member Yu Zheng synthesized a novel chiral-at-ruthenium complex coordinated by two *N*-(2-pyridyl)-substituted *N*-heterocyclic carbene (PyNHC) bidentate ligands in addition to two acetonitrile ligands in a C_2-symmetric fashion.[5] This ruthenium complex displayed high activity (up to 99% yield) and enantioselectivity (up to >99% ee) for the asymmetric alkynylation of trifluoromethyl ketones. It is well known that a variety of reactive intermediates can be generated through ruthenium complexes (like ruthenium-oxo, ruthenium-imido, ruthenium-hydride and so on). Further investigation of the catalytic properties of this type of chiral-at-ruthenium catalysts will be of high interest for our group, which is thus my aim of work (Figure 15).

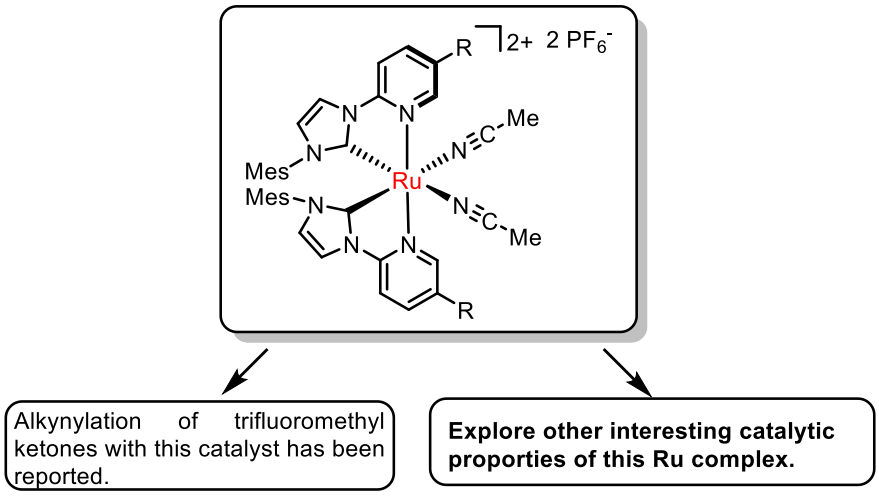

Figure 15. Aim 2: Expand the catalytic properties of chiral-at-metal ruthenium catalysts.

Aim 3: Expanding the catalytic properties of chiral cyclometalated ruthenium catalysts

The success of bis-cyclometalated chiral-at-metal iridium and rhodium complexes in asymmetric catalysis encouraged us to further investigate the catalytic property of other chiral cyclometalated transition metal complex, like ruthenium which is less reported.[7] Cyclometalated ruthenium complexes are relatively electron-rich, which may be potentially good reducing agents. But asymmetric redox reactions catalyzed by cyclometalated ruthenium complexes are rare. Thus in this part, investigating the catalytic properties of chiral cyclometalated ruthenium complexes especially for redox reactions will be my aim of work (Figure 16).

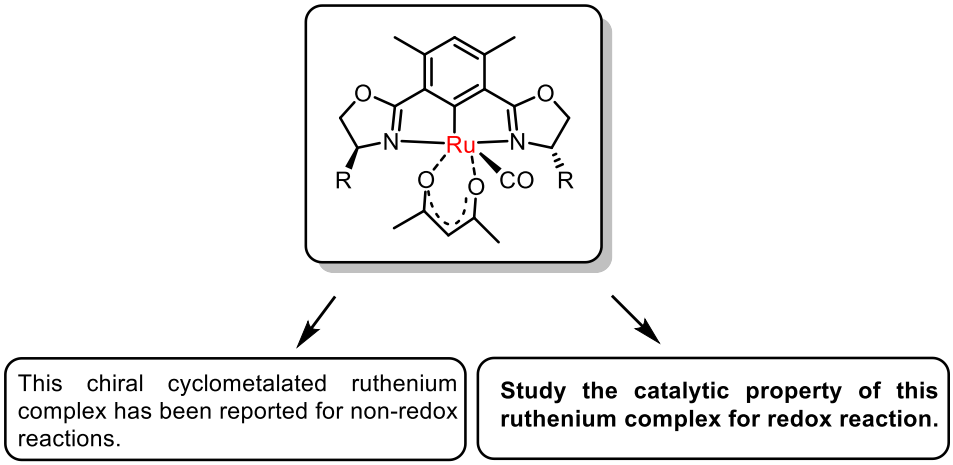

Figure 16. Aim 3: Expand the catalytic properties of chiral cyclometalated ruthenium catalysts.

References

1 V. Bhat, E. R. Welin, X. Guo, B. M. Stoltz, *Chem. Rev.* **2017**, *117*, 4528.

2 (*a*) L. Zhang, E. Meggers, *Chem. Asian J.* **2017**, *12*, 2335; (*b*) L. Zhang, E. Meggers, *Acc. Chem. Res.* **2017**, *50*, 320; (*c*) T. Cruchter, V. A. Larionov, *Coord. Chem. Rev.*, **2018**, *376*, 95.

3 For the first report of chiral-at-iridium catalysis from the Meggers group, see: H. Huo, C. Fu, K. Harms, E. Meggers, *J. Am. Chem. Soc.* **2014**, *136*, 2990.

4 For the first report of chiral-at-rhodium catalysis from the Meggers group, see: C. Wang, L.-A. Chen, H. Huo, X. Shen, K. Harms, L. Gong, E. Meggers, *Chem. Sci.* **2015**, *6*, 1094.

5 For the first report of chiral-at-ruthenium catalysis from the Meggers group, see: Y. Zheng, Y. Tan, K. Harms, M. Marsch, R. Riedel, L. Zhang, E. Meggers, *J. Am. Chem. Soc.* **2017**, *139*, 4322.

6 C. Tian, L. Gong, E. Meggers, *Chem. Commun.* **2016**, *52*, 4207.

7 For chiral cyclometalated ruthenium complexes in asymmetric catalysis, see: (*a*) J. Ito, S. Ujiie, H. Nishiyama, *Chem. Commun.* **2008**, 1923; (*b*) J. Ito, R. Asai, H. Nishiyama, *Org. Lett.* **2010**, *12*, 3860; (*c*) S. Ubukata, J. Ito, R. Oguri, H. Nishiyama, *J. Org. Chem.* **2016**, *81*, 3347; (*d*) S. Chanthamath, S. Iwasa, *Acc. Chem. Res.* **2016**, *49*, 2080.

Chapter 3: Results and Discussion

3.1 Kinetic Resolution of Epoxides with CO_2 Catalyzed by a Chiral-at-Iridium Complex

3.1.1 Project Design and Research Background

The Meggers group recently introduced chiral-at-metal bis-cyclometalated iridium(III)[1] and rhodium(III)[2] complexes as a novel class of Lewis acids. These complexes contain only achiral ligands with the metal serving as the formal stereocenter (chiral-at-metal complex), which represent a new type of catalysts for many transformations providing excellent enantioselectivities with high activities.[3] For example, both the chiral-at-metal iridium complexes Λ/Δ-**IrO** and the rhodium complex Λ/Δ-**RhO** could catalyze the Friedel-Crafts alkylation of α,β-unsaturated 2-acyl imidazoles with high yields and enantioselectivities (Figure 17a).[4] In most of the previous studies, substrates with two-point binding like 2-acyl imidazoles are necessary to obtain good asymmetric induction.[3] There are also exceptions. For example, Λ/Δ-**IrS** has been demonstrated as an excellent catalyst for asymmetric transfer hydrogenations of ketones providing high enantioselectivities of up to 99% ee at low catalyst loadings down to 0.002 mol% in the presence of pyrazole co-ligand (Figure 17b).[5] In this case, only simple ketones are used as substrates, and an iridium-hydride is proposed to be the key intermediate. It will be of high interest for our group to develop other asymmetric transformations without the need for two-point binding substrates. With this expectation, my co-worker Dr. Vladimir Larionov found that a modified chiral-at-iridium complex Λ-**IrO(Carb)** could serve as the catalyst for the kinetic resolution of epoxides with CO_2 to afford cyclic carbonate with a moderate conversion of 23% and enantioselectivity of 71% ee (Figure 17c). This reflects an s-factor of 7.3.

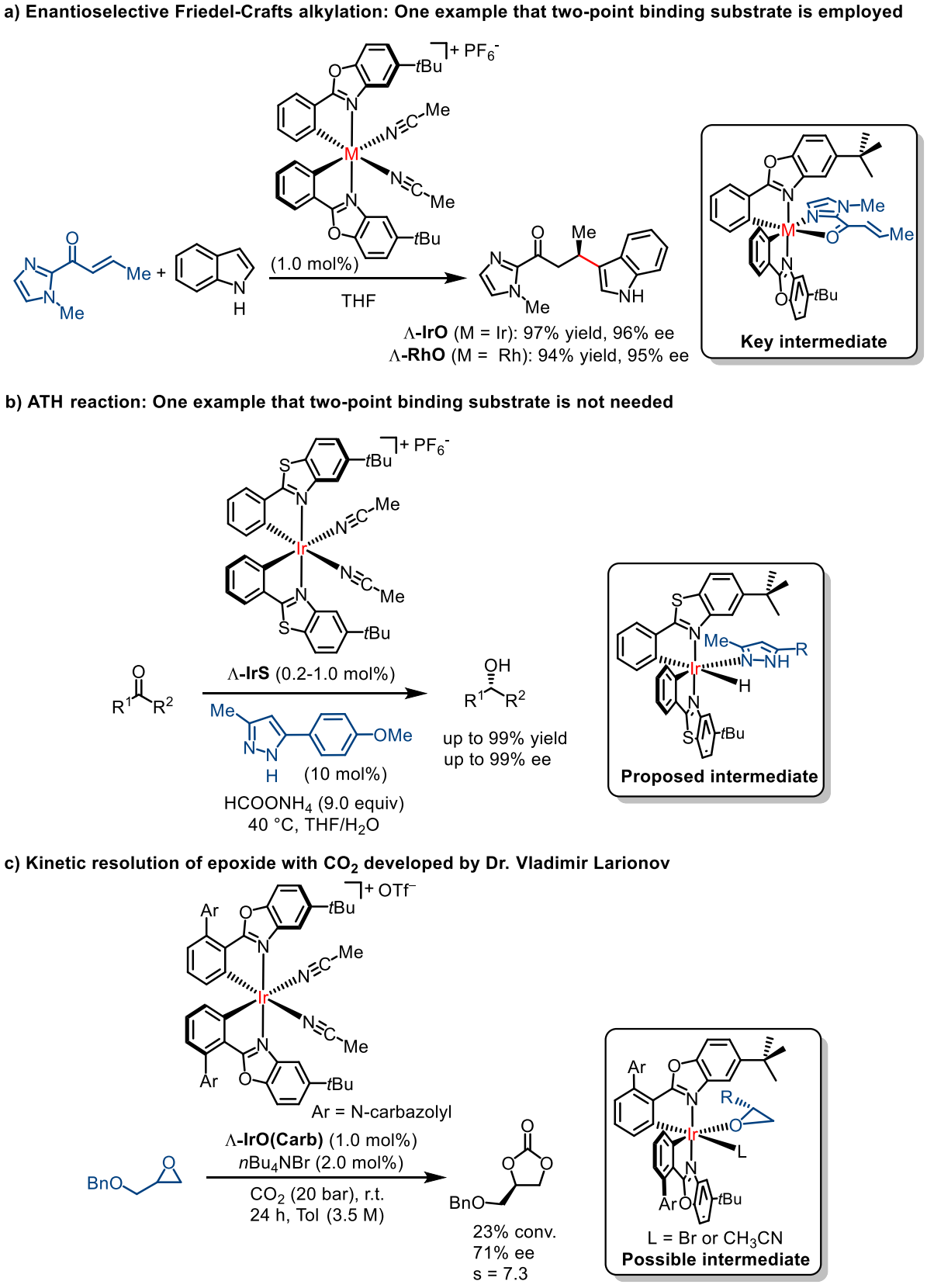

Figure 17. a) Enantioselective Friedel-Crafts alkylation of substrate with two-point binding; b) ATH reaction of substrate with one-point binding; c) Kinetic resolution of epoxide with CO_2.

As described in Chapter 1.2, the kinetic resolution of epoxides with CO_2 is of great interest because it features a perfect atom economy. Moreover, chiral cyclic carbonates are important synthetic intermediates.[6] However, the kinetic resolution of epoxides with CO_2 is still underdeveloped to date.[7] Low s-factors (s < 10) are typical in most of the reported catalytic systems. Another problem is the poor substrate tolerance. Almost all the reported catalytic systems are very sensitive to the nature of the substrate.

In theory, there is a real possibility to get good s-factors for this kinetic resolution reaction with the chiral-at-metal iridium or rhodium catalysts if the coordination of the epoxide and later ring opening occur around the metal center. The primary s-factor of 7.3 obtained by Dr. Vladimir Larionov is comparable with other reported Lewis acid catalysts.[8-12] Encouragingly, the author of this thesis decided to further investigate this kinetic resolution reaction with the chiral-at-metal complexes as catalysts to improve the s-factor.

3.1.2 Initial Experiments and Optimization of Reaction Conditions

The investigation was started by testing a number of bis-cyclometalated chiral-at-iridium and chiral-at-rhodium Lewis acid complexes for the kinetic resolution of racemic glycidyl benzyl ether (**4a**) with CO_2. All reactions shown in Table 1 were performed at 25 °C with CO_2 pressure of 20 bar in the presence of 1 mol% chiral Lewis acid catalyst. Using the benzoxazole rhodium catalyst Λ-**RhO** together with *n*Bu_4NBr as the co-catalyst provided the cyclic carbonate **5a** with 8% conversion and 47% ee, which relates to an s-factor of 2.9 (entry 1). The related benzothiazole rhodium catalyst Λ-**RhS** displayed a higher catalytic activity with 26% conversion after 24 hours but an unchanged s-factor (entry 2). The analogous iridium complexes Λ-**IrO** and Λ-**IrS** provided better results (entries 3 and 4). Especially Λ-**IrO** provided an s-factor of 6.0 (entry 3). A further slight improvement was achieved with the iridium catalyts Λ-**IrO(Carb)** functionalized with two carbazole moieties which provided an s-factor of 6.3 (entry 5). The role of the carbazole moiety is unclear. However, our group[13a] and independently the Kang group[13b] found that for related bis-cyclometalated catalysts the functionalization of the phenyl moiety at this position with an aryl moiety can sometimes have a positive effect on the stereocontrol.

Catalyst Λ-**IrO(Carb)** was used to optimize the reaction conditions next. First the co-catalyst was optimized (entries 6-12), and it was found that bromide was optimal as a nucleophile in combination with tetraethylammonium cation to provide an s-factor of 7.6 (entry 11). This was different from the result of the Co^{III}(salen) complex system which provided better s-factor with co-catalyst bearing bulky cation.[8b] With respect to the amount of the nucleophilic co-catalyst Et_4NBr (entries 13-16), the highest s-factor of 8.7 (entry 15) was observed at a catalyst loading of 1.5 mol%. It should be noted here that there is totally no catalytic activity in the presence of 1.0 mol% co-catalyst (entry 16). Under solvent-free conditions the s-factor decreased to 5.4 (entry 17), but testing some other solvents (entries 18-21) revealed that 1,4-dioxane was the solvent of choice providing an s-factor of 10.8 (entry 21). It is noteworthy that doubling the loadings of catalyst and co-catalyst leads to a higher conversion but also decreases the enantiomeric excess of the cyclic carbonate and reduces the s-factor (entry 22). Finally, control experiments verified that neither the Lewis acids nor Et_4NBr alone can catalyze this transformation (entries 23 and 24). Notably, selectivities for the cyclic carbonate product were perfect in all cases, and no copolymerization side reaction was observed, which is often encountered for the chiral cobalt Schiff base catalysts.[8b,9]

Table 1 Initial experiments of kinetic resolution of glycidyl phenyl ether (**4a**) with CO_2[a]

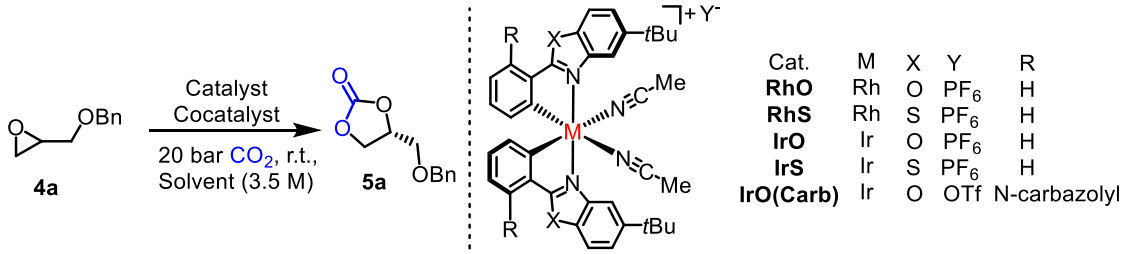

Cat.	M	X	Y	R
RhO	Rh	O	PF_6	H
RhS	Rh	S	PF_6	H
IrO	Ir	O	PF_6	H
IrS	Ir	S	PF_6	H
IrO(Carb)	Ir	O	OTf	N-carbazolyl

entry	cat. (mol%)	co-cat. (mol%)	solvent	conv. (%)[b]	ee (%)[c]	s[d]
1	Λ-**RhO** (1.0)	nBu$_4$NBr (2.0)	Tol	8	47	2.9
2	Λ-**RhS** (1.0)	nBu$_4$NBr (2.0)	Tol	26	43	2.9
3	Λ-**IrO** (1.0)	nBu$_4$NBr (2.0)	Tol	16	68	6.0
4	Λ-**IrS** (1.0)	nBu$_4$NBr (2.0)	Tol	20	50	3.4
5	Λ-**IrO(Carb)** (1.0)	nBu$_4$NBr (2.0)	Tol	14	70	6.3
6	Λ-**IrO(Carb)** (1.0)	nBu$_4$NI (2.0)	Tol	26	43	2.9
7	Λ-**IrO(Carb)** (1.0)	nBu$_4$NCl (2.0)	Tol	8	70	6.0
8	Λ-**IrO(Carb)** (1.0)	nBu$_4$NDNP (2.0)[e]	Tol	2	-	-
9	Λ-**IrO(Carb)** (1.0)	nBu$_4$NOBz (2.0)	Tol	2	-	-
10	Λ-**IrO(Carb)** (1.0)	nOctyl$_4$NBr (2.0)	Tol	13	63	4.9
11	Λ-**IrO(Carb)** (1.0)	Et$_4$NBr (2.0)	Tol	15	74	7.6
12	Λ-**IrO(Carb)** (1.0)	Me$_4$NBr (2.0)	Tol	trace	-	-
13	Λ-**IrO(Carb)** (1.0)	Et$_4$NBr (4.0)	Tol	18	73	7.5
14	Λ-**IrO(Carb)** (1.0)	Et$_4$NBr (8.0)	Tol	22	65	5.6
15	Λ-**IrO(Carb)** (1.0)	Et$_4$NBr (1.5)	Tol	14	77	8.7
16	Λ-**IrO(Carb)** (1.0)	Et$_4$NBr (1.0)	Tol	trace	-	-
17	Λ-**IrO(Carb)** (1.0)	Et$_4$NBr (1.5)	no solvent	21	64	5.4
18	Λ-**IrO(Carb)** (1.0)	Et$_4$NBr (1.5)	DCE	9	63	4.7
19	Λ-**IrO(Carb)** (1.0)	Et$_4$NBr (1.5)	THF	14	71	6.6
20	Λ-**IrO(Carb)** (1.0)	Et$_4$NBr (1.5)	nBu$_2$O	13	77	8.6
21[f]	Λ-**IrO(Carb)** (1.0)	Et$_4$NBr (1.5)	1,4-dioxane	14	81	10.8
22[f]	Λ-**IrO(Carb)** (2.0)	Et$_4$NBr (3.0)	1,4-dioxane	28	71	7.5
23[f]	Λ-**IrO(Carb)** (1.0)	no cocat.	1,4-dioxane	0	-	-
24[f]	no cat.	Et$_4$NBr (1.5)	1,4-dioxane	<1	-	-

[a]Reaction conditions: **4a** (32.8 mg, 0.2 mmol), catalyst and co-catalyst in the indicated solvent (57 μL) were stirred at 25 ℃ at 20 bar CO_2 for 24 h. [b]Determined by ^{1}H NMR. No other products formed. [c]Determined by HPLC on chiral stationary phase. [d]Calculated as (ln[1 - c(1 + ee)])/(ln[1 - c(1 - ee)]) where c is the conversion and ee is the enantiomeric excess of the cyclic carbonate product. [e]DNP = 2,4-dinitrophenoxide. [f]Reaction time was 30 h.

3.1.3 Substrate Scope

Using the optimized conditions with the chiral Lewis acid Λ-**IrO(Carb)** at 1 mol% and the co-catalyst Et_4NBr at 1.5 mol% in 1,4-dioxane at room temperature with 20 bar CO_2, the substrate scope was next investigated starting with a variety of glycidyl ethers (Figure 18). Glycidyl phenylether gave the carbonate **5b** with 20% conversion and 82% ee (s = 12.3). A comparable s-factor of 10.7 at a conversion of 43% was obtained with Lu's binol-functionalized Co(salen) complex.[8b] Methyl groups in *para*- and *meta*-position did not affect the outcome (**5c** and **5d**) but a methyl group in *ortho*-position of the phenyl moiety somewhat decreased the conversion (**5e**). Glycidyl phenylethers with electron donating and electron accepting groups in the phenyl moiety were well tolerated (cyclic carbonates **5f**-**h**) with s-factors of 10.1-11.5. Glycidyl (2-naphthyl)ether afforded the carbonate **5i** with 22% conversion and 80% ee (s = 11.2). A variety of other glycidyl ethers provided the cyclic carbonates **5j**-**m** with s = 7.5-11.8. For glycidyl ethers, our chiral-at-metal catalyst provided much higher s-factors compared with most of other catalytic systems.[9b,10f,12c] To further evaluate effect of the nature of epoxide side chain on the s-factor, substrates **4n**-**t** were tested. Replacing the ether side chain with an ester group gave the carbonate **5n** with 15% conversion and 74% ee (s = 7.6), for which only a s-factor of 2.1 was obtained with the ketoiminatocobalt(II) catalytic system.[9b] A phenylethyl side chain led to a decreased conversion with an s-factor of 9.0 (**5o**), while a butyl side chain provided carbonate **5p** with an s-factor of 8.5, and an ethyl side chain provided the carbonate **5q** with an s-factor of 6.4. For substrate **4q**, Lu's catalyst is superior, providing cyclic carbonate **5q** with an s-factor of 31.5.[8b] To our delight, a benzyl substituent afforded the carbonate **5r** with 21% conversion and 86% ee, which reflected an s-factor of 16.6 and a *p*-methoxybenzyl substituent the cyclic carbonate **5s** with 80% ee at 40% conversion (s = 15.3). A chloromethyl group gave a better conversion of 40% but a decreased s-factor of 8.9 (cyclic carbonate **5t**). For this chloromethyl cyclic carbonate **5t** most studies reported moderate to low s-factors below 6.0, except for Lu's system which provided an s-factor of 13.2 at a conversion of 41%.[8b] An epoxide with a quartenary carbon center **4u** did not show any reactivity. Finally, styrene oxide **4v** afforded the cyclic carbonate **5v** with an s-factor of 7.3, compared to an s-factor of 5.4 in Lu's catalytic system.[8b] It should be noted that no detectable signal of polycarbonate side product was observed in the ^1H NMR spectrums for all presented substrates. This is consistent with determined mass balances of >99% for several reactions (for **4b**, **4g** and **4i**).

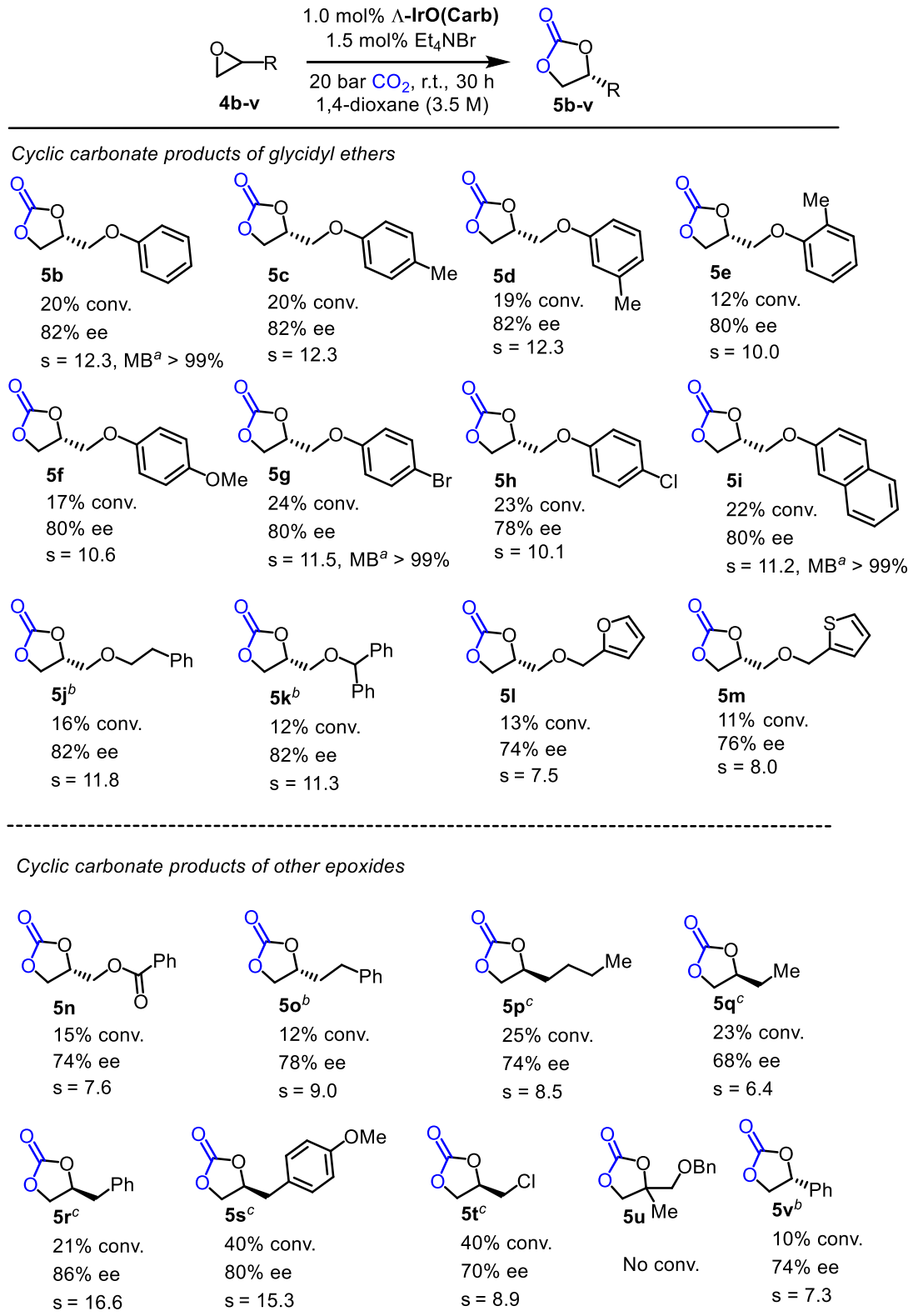

Figure 18. Asymmetric coupling of various epoxides with CO_2. [a]MB = mass balance. [b]Reaction time was 70 h. [c]2 mol% nBu$_4$NBr, 1 mol% Δ-**IrO(Carb)** and 45 h were used instead.

To give a better indication of the performance of the chiral-at-iridium catalyst for this kinetic resolution of epoxides, s-factors of selected substrates (**4b**-**d**, **4g**) were determined at higher conversions (around 40%), resulting in slightly reduced s-factors (Table 2). For an example, the s-factor of glycidyl phenylether **4b** decreased from 12.3 (at 20% conversion) to 10.5 (at 41% conversion).

Table 2. Catalytic results of selected epoxides at high conversions[a]

entry	epoxides	conversion (%)[b]	ee (%)[c]	s[d]
1	**4b**	41	73	10.5
2	**4c**	40	73	10.3
3	**4d**	39	74	10.6
4	**4g**	45	70	10.0

[a]Reaction conditions: Epoxides (0.3 mmol), *n*Bu_4NBr (1.9 mg, 0.006 mmol, 2 mol%), Δ-**IrO(Carb)** (3.8 mg, 0.003 mmol, 1 mol%) in 1,4-dioxane (86 μL, 3.5 M) were stirred at room temperature at 20 bar CO_2 for 50 h. [b]Determined by ^{1}H NMR. Selectivity for the cyclic carbonate product were all >99%. [c]Determined by HPLC on chiral stationary phase. [d]Calculated as (ln[1 - *c*(1 + ee)])/(ln[1 - *c*(1 - ee)]) where *c* is the conversion and ee is the enantiomeric excess of the cyclic carbonate product.

3.1.4 Additional Experiments

Next, a few mechanistic experiments were performed. To verify that there is a stereochemical match and mismatch between the metal-centered configuration of the iridium catalyst and the stereochemistry of the chiral epoxide, the enantiomerically pure (*S*)-glycidyl phenyl ether (>99% ee) was used as substrate in the CO_2-coupling reaction catalyzed by the individual enantiomeric catalysts Λ-**IrO(Carb)** and Δ-**IrO(Carb)** (Figure 19a). As a result, after 20 hours at room temperature a conversion of 20% was observed for catalyst Λ-**IrO(Carb)**, while under the same conditions Δ-**IrO(Carb)** only provided a conversion of 2%, thus demonstrating a strong preference of (*S*)-**4b** for Λ-**IrO(Carb)** over Δ-**IrO(Carb)**. Furthermore, the cyclic carbonate product (*R*)-**5b** was formed under complete retention of the configuration, which is in accordance to the established mechanism.[14] Figure 19b features the correlation between conversion and enantiomeric excess of the formed cyclic carbonate. As expected, with a progress in conversion the enantiomeric excess declines. However, it is surprising that the s-factor also decreases gradually with increasing conversion. The explanation for this unusal effect is unclear at this stage, but it is possible that the formed

cyclic carbonate interferes with the catalysis of just increases the overall polarity of the solvent. Finally, the direct reaction of nBu$_4$NBr with the catalyst was investigated (Figure 19c). An immediate color change from yellow to orange was observed when mixing the catalyst Λ-**IrO(Carb)** with one equivalent of nBu$_4$NBr with a disappearance of an acetonitrile signal, which indicates that the bromide replaced one acetonitrile ligand by directly coordinating to the iridium and providing a neutral complex. This explains why a slight excess of co-catalyst over the iridium complex is necessary for observing catalytic activity.

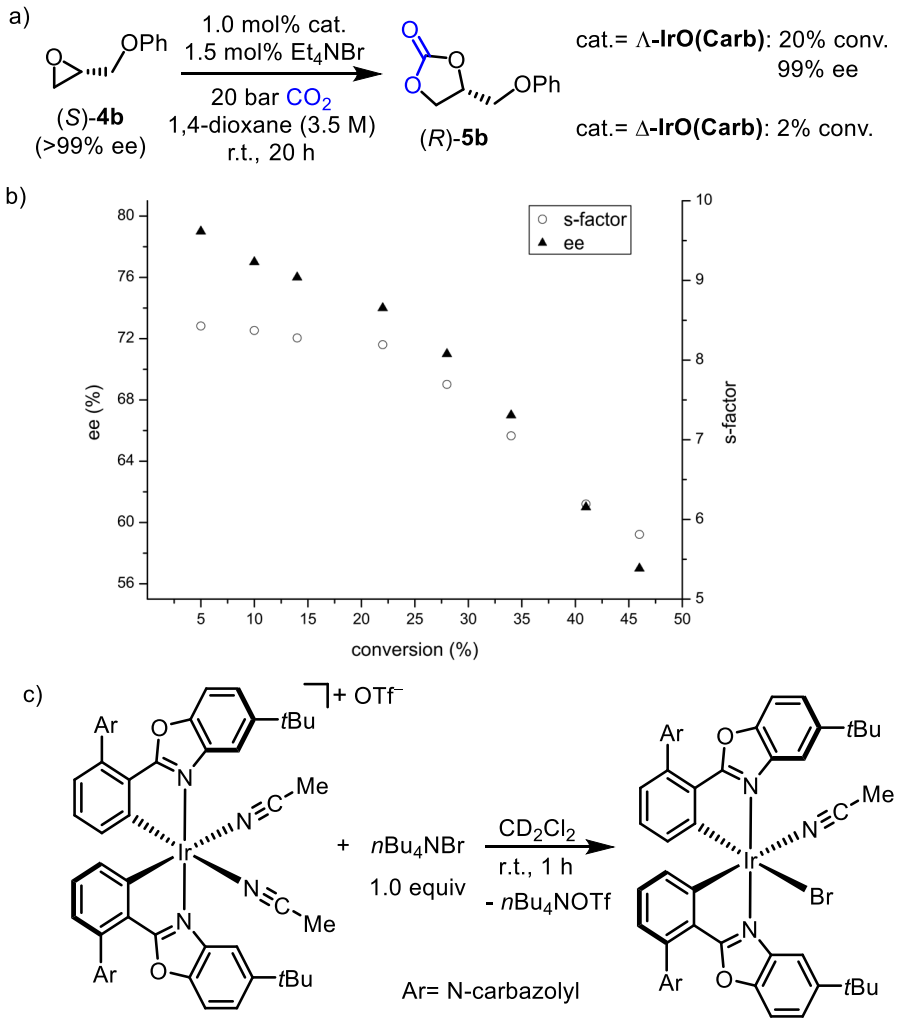

Figure 19. Additional experiments. a) Investigation of match and mismatch of chiral catalyst and epoxide substrate. b) Dependence of enantioselectivity and s-factor on the conversion. Reaction conditions: glycidyl ether **4b** (0.2 mmol) with Λ-**IrO(Carb)** (2.0 mol%), Et$_4$NBr (3.0 mol%) in 1,4-dioxane (57 µL) at room temperature under 20 bar CO_2. c) Stoichiometric reaction of Λ-**IrO(Carb)** with nBu$_4$NBr.

Based on previous reports[7] and our mechanistic experiments, the catalytic cycle shown in Figure 20 is proposed. The catalyst Λ-**IrO(Carb)** first reacts with one equivalent nBu$_4$NBr to replace one MeCN ligand with bromide and to form the neutral iridium complex **I**. Replacement of the second MeCN ligand with the epoxide substrate then leads to complex **II**. The observed enantiodifferentiation either already occurs during the formation of this iridium-substrate complex **II** or the subsequent reaction with bromide to form the ring-opened alkoxide intermediate **III**. The nucleophilic alkoxide then reacts with CO_2 to form the short-lived carbonate intermediate **IV** which undergoes a ring-closing intramolecular S_N2 reaction to generate the catalyst bound cyclic carbonate product. Dissociation of the product and new coordination of substrate finally initiates a new catalytic cycle.

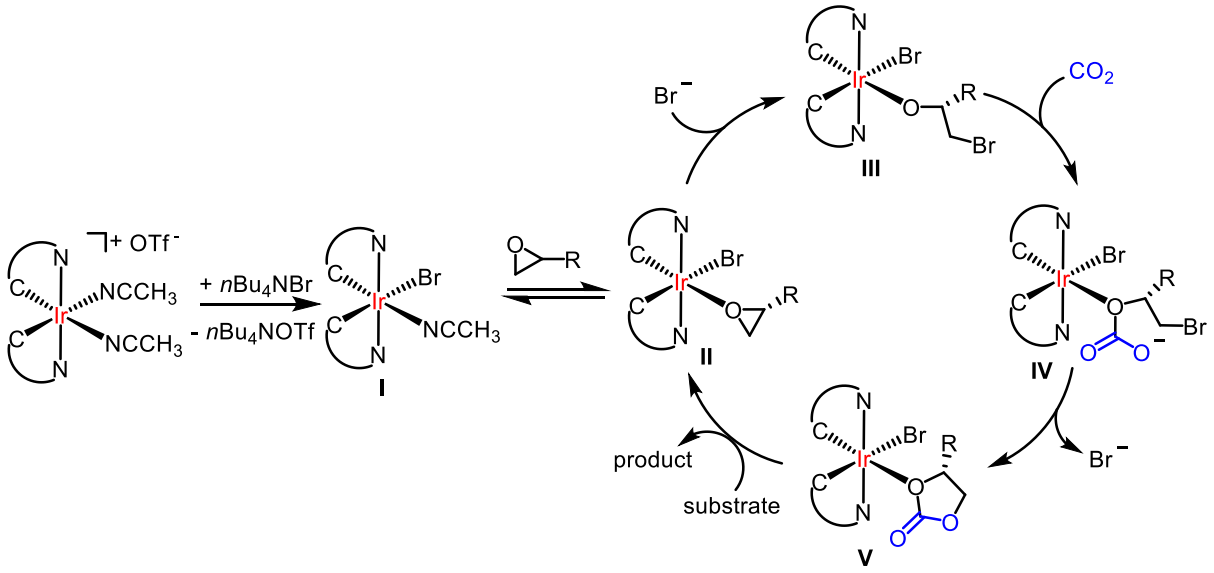

Figure 20. Proposed mechanism for the kinetic resolution of epoxides with CO_2.

3.1.5 Conclusions

In summary, bis-cyclometalated iridium complexes are demonstrated to be a new and promising class of chiral catalysts for the kinetic resolution of racemic epoxides with CO_2. Significant s-factors of up to 16.6 are achieved for a variety of monosubstituted epoxides including epoxides with aliphatic side chains, glycidyl ethers, styrene epoxide, and a glycidyl ester. It is noteworthy that all reactions were performed at room temperature and no polymerization side reaction was detected.

References

1 For the first report on chiral-at-iridium Lewis acid catalysis from the Meggers group, see: H. Huo, C. Fu, K. Harms, E. Meggers, *J. Am. Chem. Soc.* **2014**, *136*, 2990.

2 For the first report on chiral-at-rhodium Lewis acid catalysis from the Meggers group, see: C. Wang, L.-A. Chen, H. Huo, X. Shen, K. Harms, L. Gong, E. Meggers, *Chem. Sci.* **2015**, *6*, 1094.

3 For reviews on reactive chiral-at-metal catalysts, see: (*a*) L. Zhang, E. Meggers, *Acc. Chem. Res.* **2017**, *50*, 320. (*b*) L. Zhang, E. Meggers, *Chem. Asian J.* **2017**, *12*, 2335; (*c*) T. Cruchter, V. A. Larionov, *Coord. Chem. Rev.* **2018**, *376*, 95.

4 X. Shen, H. Huo, C. Wang, B. Zhang, K. Harms, E. Meggers, *Chem. Eur. J.* **2015**, *21*, 9720.

5 C. Tian, L. Gong, E. Meggers, *Chem. Commun.* **2016**, *52*, 4207.

6 (*a*) C. E. Song, S. G. Lee, *Chem. Rev.* **2002**, *102*, 3495; (*b*) B. Schäffner, F. Schäffner, S. P. Verevkin, A. Börner, *Chem. Rev.* **2010**, *110*, 4554.

7 For reviews on asymmetric couplings of racemic epoxides with CO_2, see: (*a*) N. Kielland, C. J. Whiteoak, A. W. Kleij, *Adv. Synth. Catal.* **2013**, *355*, 2115; (*b*) X. Wu , J. A. Castro-Osma, M. North, *Symmetry* **2016**, *8*, 4.

8 (*a*) X.-B. Lu, B. Liang, Y.-J. Zhang, Y.-Z. Tian, Y.-M. Wang, C.-X. Bai, H. Wang, R. Zhang, *J. Am. Chem. Soc.* **2004**, *126*, 3732; (*b*) W.-M. Ren, G.-P. Wu, F. Lin, J.-Y. Jiang, C. Liu, Y. Luo, X.-B. Lu, *Chem. Sci.* **2012**, *3*, 2094.

9 (*a*) H. Tanaka, Y. Kitaichi, M. Sato, T. Ikeno, T. Yamada, *Chem. Lett.* **2004**, *33*, 676; (*b*) W. Yamada, Y. Kitaichi, H. Tanaka, T. Kojima, M. Sato, T. Ikeno, T. Yamada, *Bull. Chem. Soc. Jpn.* **2007**, *80*, 1391.

10 (*a*) T. Chang, H. Jing, L. Jin, W. Qiu, *J. Mol. Catal. A: Chem.* **2007**, *264*, 241; (*b*) L. Jin, Y. Huang, H. Jing, T. Chang, P. Yan, *Tetrahedron: Asymmetry* **2008**, *19*, 1947; (*c*) P. Yan, H. Jing, *Adv. Synth. Catal.* **2009**, *351*, 1325; (*d*) T. Chang, L. Jin, H. Jing, *ChemCatChem* **2009**, *1*, 379; (*e*) S. Zhang, Y. Song, H. Jing, P. Yan, Q. Cai, *Chin. J. Catal.* **2009**, *30*, 1255; (*f*) S. Zhang, Y. Huang, H. Jing, W. Yao, P. Yan, *Green Chem.* **2009**, *11*, 935; (*g*) Y. Song, Q. Jin, S. Zhang, H. Jing, Q. Zhu, *Sci. China Chem.* **2011**, *7*, 1044; (*h*) S. Duan, X. Jing, D. Li, H. Jing, *J. Mol. Catal. A: Chem.* **2016**, *411*, 34.

11 (*a*) R. L. Paddock, S. T. Nguyen, *Chem. Commun.* **2004**, 1622; (*b*) A. Berkessel, M. Brandenburg, *Org. Lett.* **2006**, *8*, 4401; (*c*) S.-W. Chen, R. B. Kawthekar, G.-J. Kim, *Tetrahedron Lett.* **2007**, *48*, 297; (*d*) R. B. Kawthekar, G.-J. Kim, *Bull. Korean Chem. Soc.* **2008**, *29*, 313; (*e*) D. Y. Jang, H. G. Jang, G. R. Kim, G.-J. Kim, *Catal. Today* **2012**, *185*, 306; (*f*) T. Roy, R. I. Kureshy, N. H. Khan, S. H. R. Abdi, H. C. Bajaj, *Catal. Sci. Technol.* **2013**, *3*, 2661; (*g*) V. A. Larionov, E. P. Markelova, A. F. Smol'yakov, T. F. Savel'yeva, V. I. Maleev, Y. N. Belokon, *RSC Adv.* **2015**, *5*, 72764.

12 (*a*) M. Aresta, A. Dibenedetto, L. Gianfrate, C. Pastore, *Appl. Catal. A* **2003**, *255*, 5; (*b*) Y. Ren, X. Cheng, S. Yang, C. Qi, H. Jiang, Q. Mao, *Dalton Trans.* **2013**, *42*, 9930; (*c*) M. North, S. C. Z. Quek, N. E. Pridmore, A. C. Whitwood, X. Wu, *ACS Catal.* **2015**, *5*, 3398.

13 (*a*) J. Ma, A. R. Rosales, X. Huang, K. Harms, R. Riedel, O. Wiest, E. Meggers, *J. Am. Chem. Soc.* **2017**, *139*, 17245; (*b*) K. Li, Q. Wan, Q. Kang, *Org. Lett.* **2017**, *19*, 3299.

14 (*a*) C. J. Whiteoak, E. Martin, M. M. Belmonte, J. Benet-Buchholz, A. W. Kleij, *Adv. Synth. Catal.* **2012**, *354*, 469; (*b*) C. Beattie, M. North, P. Villuendas, C. Young, *J. Org. Chem.* **2013**, *78*, 419; (*c*) J. Qin, P. Wang, Q. Li, Y. Zhang, D. Yuan, Y. Yao, *Chem. Commun.* **2014**, *50*, 10952; (*d*) W.-M. Ren, Y. Liu, X.-B. Lu, *J. Org. Chem.* **2014**, *79*, 9771.

3.2 Enantioselective Intramolecular C-H Amination of Aliphatic Azides by Dual Ruthenium and Phosphine Catalysis

3.2.1 Project Design and Research Background

As discussed in Chapter 3.1, the Meggers group developed the bis-cyclometalated iridium(III) and rhodium(III) complexes as a novel class of chiral Lewis acids, which showed excellent asymmetric induction for a variety of transformations.[1] Most recently, former group member Yu Zheng synthesized a new class of chiral-at-metal ruthenium catalysts[2] which displayed high activity (up to 99% yield) and enantioselectivity (up to 99% ee) for the alkynylation of trifluoromethyl ketones (Scheme 9). Ruthenium complexes are well known to exhibit diverse reactivities, especially generating a variety of highly reactive ruthenium-bound intermediates. The author of this thesis holds a great interest in investigating new catalytic properties of this class of chiral-at-metal ruthenium catalysts.

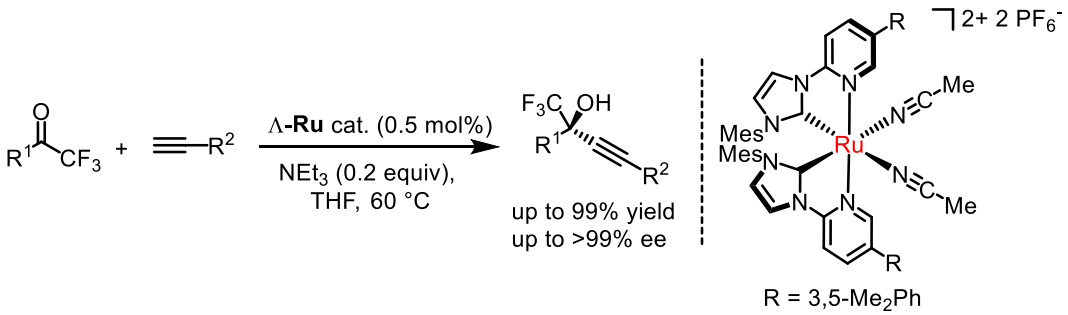

Scheme 9. Enantioselective alkynylation of trifluoromethyl ketones catalyzed by chiral-at-metal ruthenium complex.

At the onset of the study, the author of this thesis focused on transformations involving ruthenium imido intermediates which have been well demonstrated in the literature.[3] A number of interesting transformations like aziridination and C-H amination had been realized through the reactive ruthenium imido intermediate (Figure 21).[4] In particular, C-H amination represents one of the most effective methodologies to construct nitrogen-containing molecules.[5] Organic azide was chosen as the testing substrate because it has been well reported to react with ruthenium complexes forming ruthenium imido intermediates.[3] Furthermore, organic azides are attractive functionalities for C-H amination because no additional oxidant is required and molecular nitrogen is the only by-product.[6]

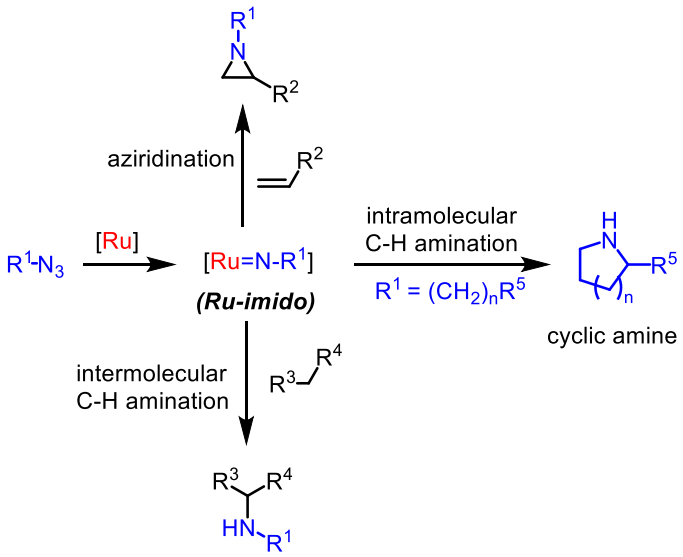

Figure 21. Transformations via the ruthenium imido intermediate.

With the above idea in mind, the literature of C-H aminations of organic azides was reviewed carefully. As introduced in Chapter 1.3, the amination of saturated C(sp^3)-H bonds with aryl, sulfonyl, acyl and phosphoryl azides has been well established,[7] but the use of non-activated, aliphatic azides is only a recent accomplishment.[8,12,15-18] In addition to their lower reactivity, a major pitfall for C(sp^3)-H aminations of primary aliphatic azides constitutes a competing unproductive 1,2-hydride shift of the intermediate alkyl nitrenoid intermediate leading to the irreversible formation of undesirable imines (Figure 22a).[9,10] Betley and co-workers introduced an elegant dipyrrinato-iron(II)-catalyzed ring-closing C(sp^3)-H amination of aliphatic azides but the reported turnover numbers were modest with TON < 10 (Figure 22b).[11,12] This protocol[13] offers a direct access to saturated cyclic amines.[14] Subsequently reported MOF-functionalized Fe(II)-β-diketiminate,[15] iron(III)-coordinated redox-active pyridine-aminophenol,[16] and cobalt(II) porphyrin[17] catalysts by Lin, van der Vlugt, and de Bruin, respectively, provided improved catalytic performances for this challenging transformation. Finally, Che and co-workers very recently reported an *N*-heterocyclic carbene iron(III) porphyrin complex exhibiting high activity for this transformation under microwave conditions.[18] However, cyclic amines like pyrrolidines as part of bioactive compounds are typically chiral but only a single example of a catalytic enantioselective reaction has been reported using a chiral cobalt(II) porphyrin achieving low yields and very low enantiomeric excess (Figure 22c).[17,19] Apparently, it is difficult to get both high enantioselectivity and good catalytic turnover number.

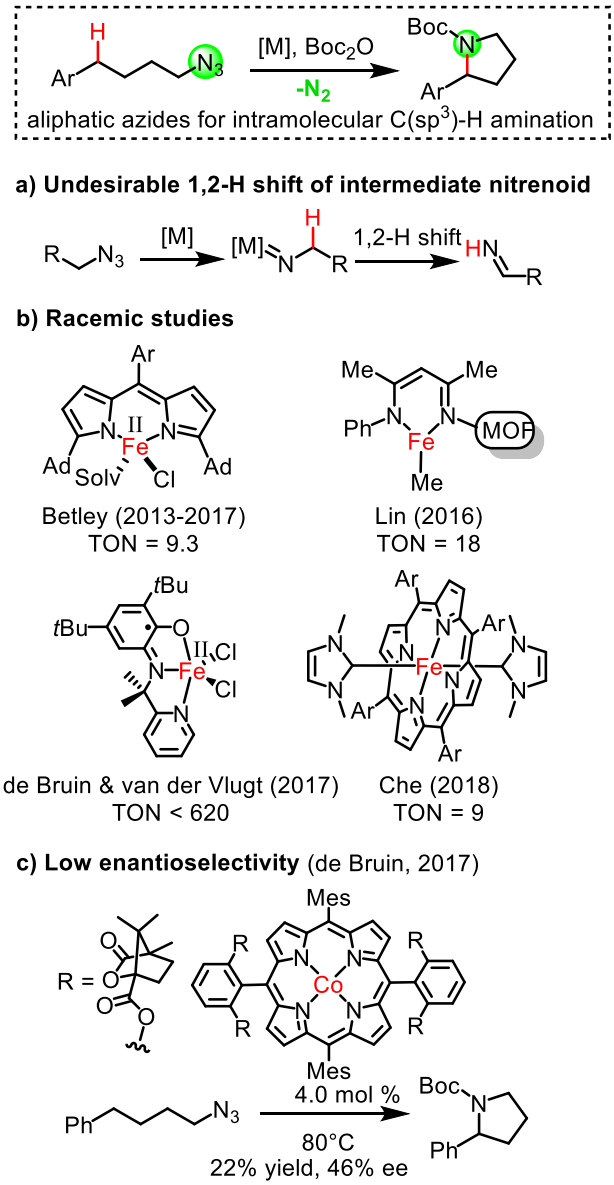

Figure 22. Previous work on ring-closing C(sp^3)-H aminations of primary aliphatic azides.

Ruthenium complexes are well-established for catalyzing C(sp^3)-H aminations of organic azides such as aryl, acyl, and sulfonyl azides,[7] but applying simple primary aliphatic azides has remained elusive and this has been attributed at least in parts to a very efficient 1,2-hydrogen shift of the intermediate Ru-imido complexes.[9] And this reactivity was also reported for other metal complexes when encountering aliphatic azide with α-C-H.[10]

Intrigued by these studies, the author of this thesis wondered if the chiral-at-ruthenium complex with suitable ligand environment is capable of activating primary aliphatic azides like (4-azidobutyl)benzene for intramolecular C-H amination instead of 1,2-hydride shift. Another expectation was that asymmetric induction which is challenging to date may be realized by the

chiral-at-metal ruthenium catalysts if the ring-closing step occurs in the coordination sphere of the metal center.[4c]

3.2.2 Initial Optimization

The study was initiated by investigating the intramolecular C-H amination of 4-azidobutylbenzene (**9a**) to Boc-protected 2-phenylpyrrolidine (**10a**) with *rac*-**Ru1** as the catalyst. The reaction highly depends on the solvent (Table 3, entries 1-6). Toluene gave the best yield of 22% at a conversion of 52% in the presence of one equivalent of Boc_2O at 85 ℃. At the same time, the Boc-protected amine **11** was detected as a side-product in 9% NMR yield. Temperature was optimized next (entries 7-10), and it was found that 95 ℃ was optimal. The substrate **9a** was kept intact at 60 ℃ after 40 hours. Further optimization of the amount of Boc_2O and the concentration of the reaction did not obviously improve the yield of **10a** (entries 11-15).

Table 3. Initial optimization of the intramolecular C-H amination of 4-azidobutylbenzene (**9a**) [a]

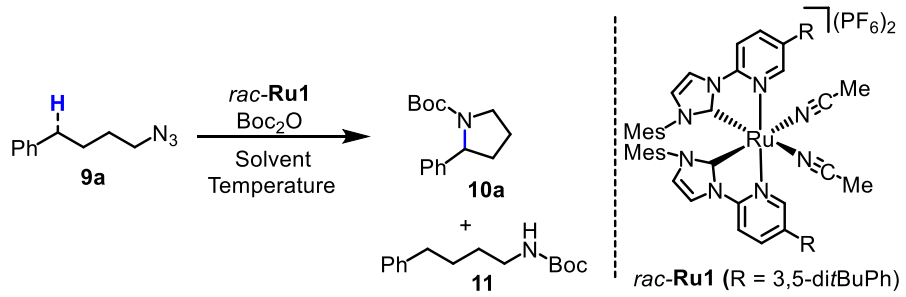

Entry	Solvent	Temperature (℃)	Boc_2O (equiv)	Conversion (%)[b]	Yield of **10a** (%)[b]	Yield of **11** (%)[b]
1	DMF	85	1.0	0	0	0
2	1,4-dioxane	85	1.0	49	18	8
3	Toluene	85	1.0	52	22	9
4	DCE	85	1.0	48	15	12
5	*i*PrOH	85	1.0	43	0	20
6	3-Pentanone	85	1.0	48	9	24
7	Toluene	60	1.0	0	0	0
8	Toluene	75	1.0	17	5	5
9	Toluene	95	1.0	57	26	14
10	Toluene	105	1.0	59	25	15
11	Toluene	95	1.2	58	25	15
12	Toluene	95	2.0	57	20	18
13	Toluene	95	4.0	65	16	21
14[c]	Toluene	95	1.0	22	10	6
15[d]	Toluene	95	1.0	65	27	18

[a]Reaction conditions: **9a** (17.5 mg, 0.1 mmol, 1 equiv), *rac*-**Ru1** catalyst (2.8 mg, 0.002 mmol, 2 mol%) and Boc_2O in indicated solvent (0.25 mL, 0.4 M) were stirred at indicated temperature for 40 h under an atmosphere of nitrogen. [b]Determined by ^1H NMR of the crude products using $Cl_2CHCHCl_2$ as internal standard. [c]0.4 mL toluene (0.25 M) was used instead. [d]0.1 mL toluene (1.0 M) was used instead.

To our surprise, the reaction was fastly improved when performed in the presence of catalytic amounts of PPh_3, providing **10a** in 44% yield with 79% conversion (Table 4, entry 1). Even slightly better yields were obtained with tris(4-fluorophenyl)phosphine, while other phosphines and pyridine provided inferior results (entries 2-9).

Table 4. Survey of additives for the intramolecular C-H amination of 4-azidobutylbenzene (**9a**) [a]

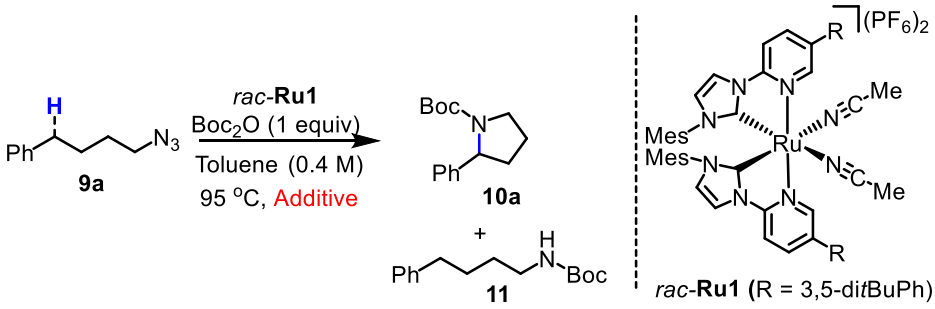

Entry	Additive	Conversion (%)[b]	Yield of **10a** (%)[b]	Yield of **11** (%)[b]
1	$P(Ph)_3$	79	44	17
2	$P(OPh)_3$	65	15	10
3	$P(cy)_3$	58	20	11
4	$P(4\text{-MeO-Ph})_3$	64	18	15
5	$P(4\text{-F-Ph})_3$	81	46	18
6	$P(Pentafluoropheny)_3$	77	31	16
7	$P(4\text{-}CF_3\text{-Ph})_3$	78	35	17
8	$P(2\text{-Me-Ph})_3$	60	20	15
9	Pyridine	39	8	5

[a]Reaction conditions: **9a** (17.5 mg, 0.1 mmol, 1 equiv), *rac*-**Ru1** catalyst (2.8 mg, 0.002 mmol, 2 mol%), indicated additive (0.002 mmol, 2 mol%) and Boc_2O (23 μL, 0.1 mmol, 1 equiv) in toluene (0.25 mL, 0.4 M) were stirred for 40 h at 95 ℃ under an atmosphere of nitrogen. [b]Determined by ^1H NMR of the crude products using $Cl_2CHCHCl_2$ as internal standard.

With this result in hand, the amount of the phosphine was further investigated, and it was found that 1 mol% provided the optimal result (Table 5, entries 1-4). In addition, decrease the catalyst loading from 2 mol% to 1 mol% almost did not affect the yield of **10a** (entry 5 *vs* 2), but increase the catalyst loading to 4 mol% led to worse result (entry 6). It has to be noted that none of the reactions proceed to full conversion. To understand if this is due to the catalyst deactivation, experiments in which the fresh catalyst and optionally also additional phosphine ligand was added after a reaction time of 30 hours were performed but did only slightly improve the yields (entries 7-10).

Table 5. Survey of the amount of $P(4\text{-F-Ph})_3$ and catalyst loading[a]

Entry	*rac*-**Ru1** (mol %)	$P(4\text{-F-Ph})_3$ (mol %)	Conversion (%)[b]	Yield of **10a** (%)[b]	Yield of **11** (%)[b]
1	2	0.5	75	40	16
2	2	1	80	47	17
3	2	2	81	46	18
4	2	5	89	40	17
5	1	1	81	46	18
6	4	1	75	40	19
7[c]	1	1	79	46	15
8[c,d]	2	1	83	48	17
9[c,e]	1	2	84	43	16
10[c,f]	2	2	82	48	17

[a]Reaction conditions: **9a** (17.5 mg, 0.1 mmol, 1 equiv), *rac*-**Ru1** catalyst, $P(4\text{-F-Ph})_3$ and Boc_2O (23 μL, 0.1 mmol, 1 equiv) in toluene (0.25 mL, 0.4 M) were stirred at 95 ℃ for 40 h under an atmosphere of nitrogen. [b]Determined by ^1H NMR of the crude products using $Cl_2CHCHCl_2$ as internal standard. [c]1,2-dichlorobenzene as the solvent. [d]1 mol% Ru catalyst was added initially, and another 1 mol% catalyst was added after 30 h of the reaction. The new mixture was stirred for another 20 h. [e]1 mol% $P(4\text{-F-Ph})_3$ was added initially, and another 1 mol% $P(4\text{-F-Ph})_3$ was added after 30 h of the reaction. The new mixture was stirred for another 20 h. [f]1 mol% Ru catalyst and $P(4\text{-F-Ph})_3$ were added initially, and another 1 mol% Ru catalyst and $P(4\text{-F-Ph})_3$ were added after 30 h of the reaction. The new mixture was stirred for another 20 h.

Although the yield was only modest, an encouraging enantioselectivity of 82% ee was obtained with Λ-**Ru1** as the catalyst (Table 6, entry 1). Next, the optimization of the ruthenium catalyst for this transformation was performed to improve the enantioselectivity (Note: 1,2-dichlorobenzene was finally used as the solvent for this reaction due to the solubility problem of the ruthenium catalyst. Some of the Ru catalysts (e.g. **Ru2**-**4** and **Ru7**) were later found soluble in 1,2-dichlorobenzene but not in toluene, and the reactivity was similar in both solvents). The initial experiments were carried out with the chiral-at-ruthenium catalyst Λ-**Ru1** which bears two very bulky 3,5-di(*tert*-butyl)phenyl substituents at the coordinating pyridine ligands. Interestingly, Λ-**Ru2** with less bulky 3,5-(dimethyl)phenyl substituents at the pyridyl moieties provided an even higher enantioselectivity of 89% ee (entry 2). The phenyl-modified catalyst Λ-**Ru3** afforded a further slightly increased enantioselectivity of 90% ee (entry 3), whereas the plain catalyst devoid of additional substituents (Λ-**Ru4**) yielded the Boc-protected pyrrolidine with reduced 87% ee (entry 4). Furthermore, a

trimethylsilyl (TMS)-functionalized ruthenium complex Λ-**Ru5** did not provide better results here (entry 5). Adding a *t*Bu-moiety at the 4-position of the phenyl groups (Λ-**Ru6**) decreased the enantioselectivity to 80% ee (entry 6). However, the best result was obtained with a 4-(CF_3)Ph modification (Λ-**Ru7**) which afforded (*R*)-**10a** in 54% NMR yield at 77% conversion and with 95% ee (entry 7). Interestingly, even at a catalyst loading of just 0.5 mol%, the Boc-protected pyrrolidine (*R*)-**10a** was still formed with 42% yield (65% conversion) and 94% ee, reflecting a turnover number of 84 (entry 8). Thus, a careful optimization of steric and electronic effects provided a ruthenium catalyst (Λ-**Ru7**) which, in the presence of tris(4-fluorophenyl)phosphine, effectively discriminates between the two benzylic C-H bonds of 4-azidobutylbenzene to provide the corresponding chiral pyrrolidine with outstanding enantioselectivity.

Control experiments revealed that tris(4-fluorophenyl)phosphine is crucial for obtaining a satisfactory yield. In its absence, the yield diminished to merely 12% even after an extended reaction time, while the enantioselectivity was not affected, thus implying that the phosphine is not involved in the stereocontrolling step (entry 9). Finally, Boc_2O is also required for this reaction to proceed (entry 10).

Table 6. Optimization of ruthenium catalyst for enantioselective intramolecular C-H amination of **9a**[a]

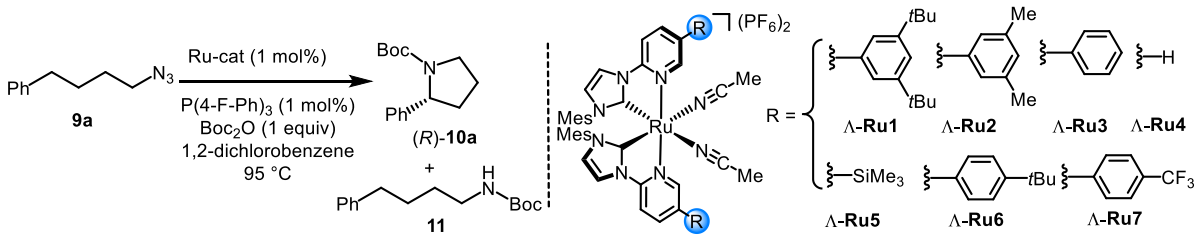

Entry	Catalyst	Additive	Conv. (%)[b]	NMR yield (%)[b]		ee (%)[c]
				10a	**11**	
1[d]	Λ-**Ru1**	$P(4\text{-F-Ph})_3$	81	46	18	82
2	Λ-**Ru2**	$P(4\text{-F-Ph})_3$	77	46	18	89
3	Λ-**Ru3**	$P(4\text{-F-Ph})_3$	79	44	16	90
4	Λ-**Ru4**	$P(4\text{-F-Ph})_3$	75	44	20	87
5	Λ-**Ru5**	$P(4\text{-F-Ph})_3$	70	43	17	89
6	Λ-**Ru6**	$P(4\text{-F-Ph})_3$	65	23	18	80
7	Λ-**Ru7**	$P(4\text{-F-Ph})_3$	77	54 (51)[e]	18	95
8	Λ-**Ru7**[f]	$P(4\text{-F-Ph})_3$	65	42	16	94
9	Λ-**Ru7**	no	45	12	14	95
10[g]	Λ-**Ru7**	$P(4\text{-F-Ph})_3$	<3	0[h]	0[h]	n.a.[i]

[a]Standard conditions: **9a** (35 mg, 0.2 mmol, 1 equiv), Boc_2O (46 μL, 0.2 mmol, 1 equiv), catalyst (0.002 mmol, 1 mol%), and additive (0.002 mmol, 1 mol%) in 1,2-dichlorobenzene (0.5 mL) at 95°C for 60 h under N_2 unless otherwise noted. [b]Determined by ^1H NMR of crude products using $Cl_2CHCHCl_2$ as internal standard. [c]Determined by HPLC of crude main product on a chiral stationary phase. [d]Reaction time was 40 h. [e]Isolated yield in parentheses. [f]0.5 mol% Λ-**Ru7** was used. [g]Without Boc_2O. [h]Refers to cpds without Boc-protection. [i]n.a. = not applicable.

At last, to understand if these chiral-at-metal ruthenium complexes are unique for this transformation, several commercially available ruthenium complexes were tested. However, none of them can catalyze this transformation providing Boc-protected pyrrolidine product no matter in the presence or absence of tris(4-fluorophenyl)phosphine (Table 7). This suggests that the ligand environment of ruthenium complex is very important for the success of the C-H amination.

Table 7. Survey of different ruthenium catalysts for the intramolecular C-H amination of **9a**[a]

Entry	Catalyst (2 mol%)	$P(4\text{-F-Ph})_3$ (2 mol%)	Conversion (%)[b]	Yield of **10a** (%)[b]
1	$RuCl_2(PPh_3)_3$	no	87	0
		yes	80	0
2	[Ru(*p*-cymene)Cl_2]$_2$	no	80	0
		yes	85	0
3	[RuCp*$(CH_3CN)_3$]PF_6	no	0	0
		yes	0	0
4	Cp*RuCl(cod)	no	<5	0
		yes	<5	0
5	CpRuCl[bis(diphenylphosphino)methane]	no	0	0
		yes	0	0

[a]Reaction conditions: **9a** (35.0 mg, 0.2 mmol, 1 equiv), 2 mol% Ru catalyst, $P(4\text{-F-Ph})_3$ (1.3 mg, 0.004 mmol, 2 mol%) and Boc_2O (46 µL, 0.2 mmol, 1 equiv) in 1,2-dichlorobenzene (0.5 mL, 0.4 M) were stirred at 95 °C for 20 h under an atmosphere of nitrogen. [b]Determined by ^1H NMR of the crude products using $Cl_2CHCHCl_2$ as internal standard.

3.2.3 Scope Investigations

With the optimized catalyst Λ-**Ru7** and reaction conditions in hand (1 equiv Boc_2O and 1 mol% $P(4\text{-F-Ph})_3$ in 1,2-dichlorobenzene at 95 °C), the substrate scope of this transformation was investigated. As shown in Figure 23, methyl groups in *para* or *meta* position of the benzene moiety are well tolerated (pyrrolidines **10b**,**c**), but a sterically demanding *ortho*-methyl group leads to vastly diminished yield of 15%. Electron-donating groups appear to be beneficial (pyrrolidines **10e-i**). For example, a *para*-methoxy functionalized benzene provides the Boc-protected pyrrolidine in 53% yield and with excellent 99% ee. Interestingly, potentially coordinating group on the benzene moiety (**10h,i**) do not affect the formation of pyrrolidine product. A bulky phosphite substituent (**10j**) and benzoxy group (**10k**) with active C-H lead to a decreased yield but still with good enantioselectivities of 92% ee. In contrary, electron-withdrawing groups like fluorine substituent leads to a decreased yield of 40% with 94% ee (product **10l**) and a chlorine to a yield of 45% with 95% ee (product **10m**). The phenyl moiety can also be replaced by a naphthyl (pyrrolidine **10n**) and by heteroaromatic moieties (pyrrolidines **10o**-**s**). For example, a carbazole moiety provides the Boc-protected pyrrolidine **10s** in 52% yield and 93% ee. Further substrates including aryl moieties in the bridge could also be

transformed to pyrrolidine products (**10t**,**u**) with 80% and 94% ee respectively.

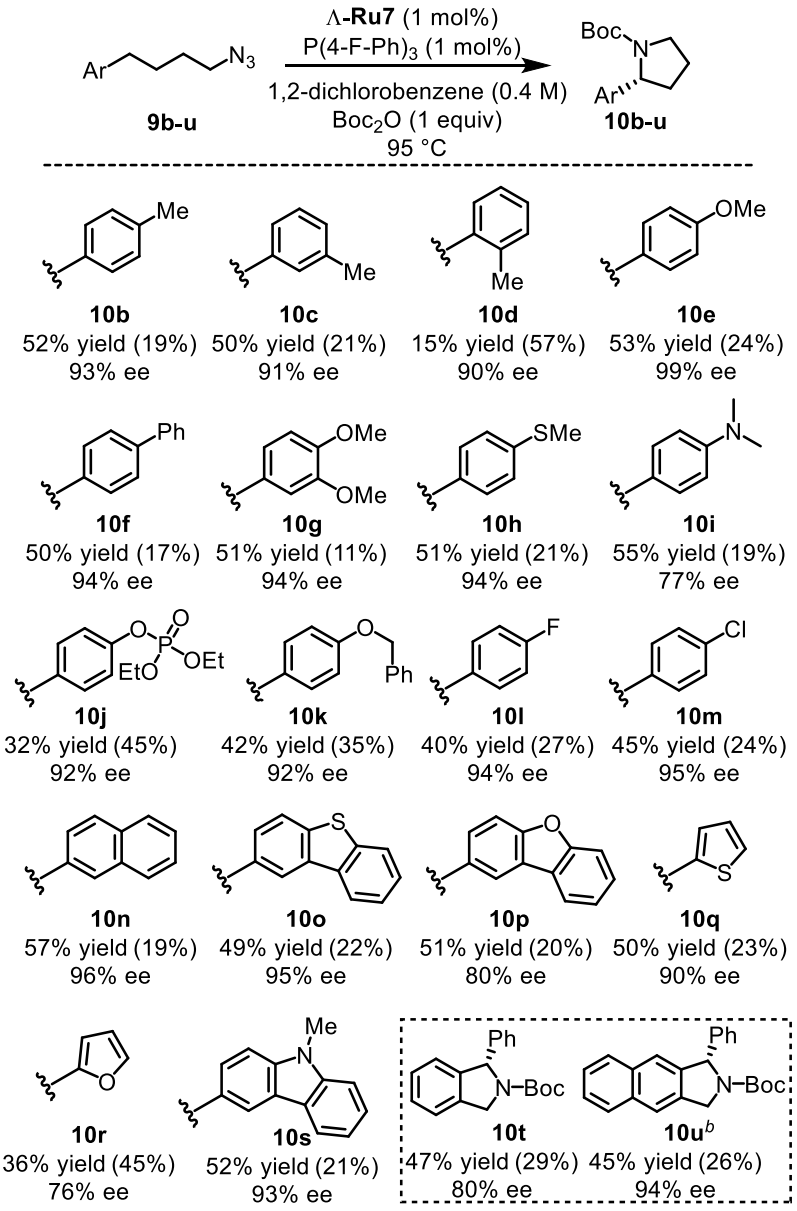

Figure 23. Substrate scope for the enantioselective intramolecular C-H amination of aliphatic azide with isolated yield. [a]Recovered starting materials were showed in parentheses. [b]0.1 M 1,2-dichlorobenzene and 85 ℃ were used instead.

However, replacing the aryl group with alkyl group (**9v**) totally suppresses the C-H amination reaction even after an increased reaction temperature to 105 ℃ (Table 8, entry 1). Further variation of **9w** with an alkynyl group only provided <5% yield of the product under the standard reaction conditions (entry 2). Substrate **9x** with an alkenyl group was also tested, but it totally decomposed even at 85 ℃ (entry 3). Finally, a racemic substrate with a tertiary C-H group only provided a very

modest kinetic resolution (entry 4).

Table 8. Other substrates tested for the intramolecular C-H amination[a]

Entry	Substrate	Product	Yield[b]	ee[c]
1[d]	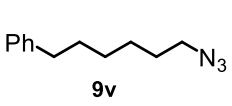 **9v**	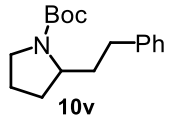 **10v**	0%	n.a.
2	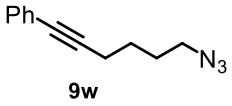 **9w**	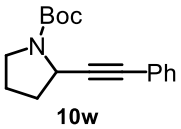 **10w**	< 5%	n.a.
3[e]	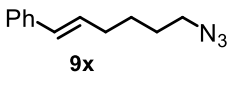 **9x**	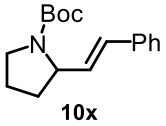 **10x**	0%	n.a.
4[f]	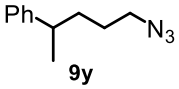 **9y**	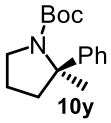 **10y**	22%	46%

[a]Reaction conditions: Organic azide substrate (0.2 mmol), Λ-**Ru7** (0.002 mmol, 1 mol%), P(4-F-Ph)$_3$ (0.002 mmol, 1 mol%) and Boc_2O (0.2 mmol, 1 equiv) in 1,2-dichlorobenzene (0.5 mL, 0.4 M) were stirred at 95 ℃ for 60 h under an atmosphere of nitrogen. [b]NMR yield with $Cl_2CHCHCl_2$ as internal standard. [c]Determined by HPLC of crude main product on a chiral stationary phase. [d]The substrate **9v** was kept infact even at 105 ℃ for 10 h. [e]Organic azide **9x** is not stable at 95 ℃, which is decomposed under the reaction conditions. [f]Reaction time was 35 h. n.a. = not applicable.

Overall, enantioselectivities of 76-99% ee were observed and isolated yields of 15-57%. However it has to be noted that none of the reactions proceed to full conversion and thus allow to reisolated unreacted starting materials (Figure 23). Nevertheless, it is remarkable that within this substrate scope, chiral α-aryl pyrrolidines with enantioselectivities of up to 99% ee can be obtained. Importantly, chiral α-aryl pyrrolidines are prominent structural motifs in bioactive compounds.[20] For example, pyrrolidine **10g** can be converted to the anti-tumor alkaloid (*R*)-(+)-crispine A in 4 steps using a Pummerer cyclization (Figure 24).[20a]

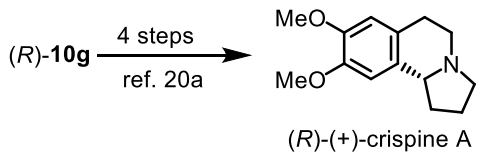

Figure 24. Synthesis of anti-tumor alkaloid (*R*)-(+)-crispine A from pyrrolidine (*R*)-**10g**.

3.2.4 Mechanism Study

Some experiments were performed to gain insight into the mechanism and started with the unusual function of the phosphine. The role of phosphine as co-catalyst to activate the organic azide is advocated by the well-established reactivity of organic azides towards phosphines.[21] Indeed, $P(4\text{-F-Ph})_3$ starts to react with (4-azidobutyl)benzene already at room temperature and full conversion is obtained at 95 ℃ for 2 hours to form the corresponding iminophosphorane **12** (Figure 25a). The iminophosphorane **12** was also confirmed catalytically competent by itself (Figure 25b). Interestingly, although such a role of phosphines in the activation of organic azides towards C-H amination has not been reported to our knowledge, the opposite reaction namely the phosphine-induced extraction of a nitrene from a metal imido complex was disclosed independently by McElwee-White[22a] and Sundermeyer.[22b]

Next, experiments of comparing (4-azidobutyl)benzene and benzyl azide as substrates at a temperature where C-H amination does not yet occur was performed to gain insight into the competing 1,2-hydride shift. As a result, only benzyl azide provided significant amounts of the imine product which can be traced back to the higher activity of the benzylic C-H bond in the ruthenium imido intermediate towards 1,2-H shift (Figure 25c). This is consistent with a recent report by Park who showed that the degree of 1,2-H shift correlates with the nature of the α-C-H bond.[9]

To understand the reactivity of ruthenium nitrene, initial C-H amination rates of electronically distinct substrates **9e** and **9l** were determined. Reaction rate of electron-rich **9e** is 1.7 times faster than electron-deficient **9l** suggesting the electrophilic nature of the ruthenium nitrene (Figure 25d). This is in consistent with the substrate scope that electron-rich substrates provide better yields compared with electron-deficient substrates. The C-H amination with mono-deuterated substrate **9a'** using racemic catalyst provided an intramolecular kinetic isotope effect (KIE) of 1.3 (Figure 25e), which is much lower than the value reported for iron[15,16] and cobalt[17] catalytic systems. This might suggest that the C-H amination appears to occur by a concerted-insertion mechanism or a hydrogen abstraction mechanism with fast radical recombination.[18] However, the interpretation of the intramolecular KIE is complicated by the fact that the ruthenium catalyst is intrinsically chiral, although used as a racemic mixture for this experiment, and the monodeuterated substrate **9a'** as well. Indeed the cyclization of the chiral substrate (*R*)-**9y** to (*R*)-**10y** but not (*S*)-**9y** to (*S*)-**10y** demonstrates the high stereospecificity

of the C-H amination (Figure 25f). Finally, a pronounced (noncompetitive) intermolecular KIE value of 3.1 was determined by measuring initial C-H amination rates of non-deuterated (**9a**) and bis-deuterated (**9a''**) substrates (Figure 25e). Using alternatively a 1:1 mixture of non-deuterated (**9a**) and bis-deuterated substrate (**9a''**) provides a (competitive) intermolecular KIE of 3.9 (see the Experimental Part 5.3.4). An observation of a significant intermolecular KIE reveals that the C-H amination is the rate limiting step in the overall process.

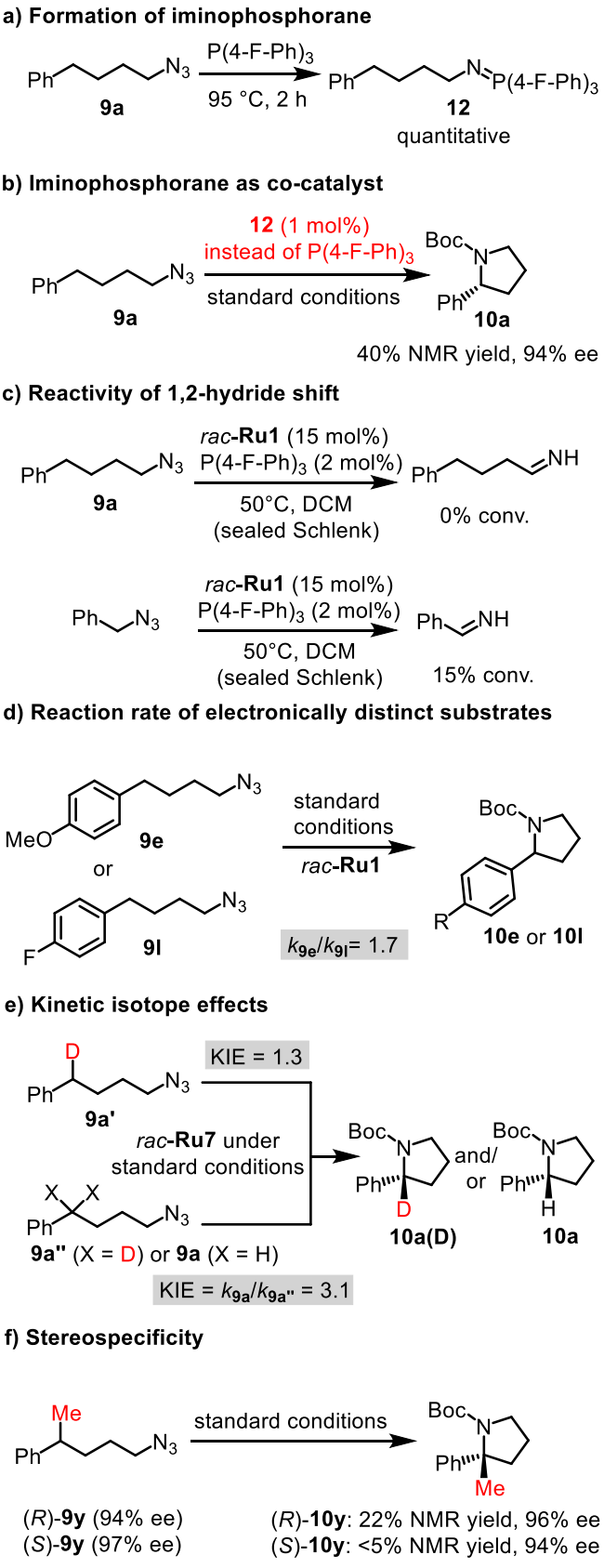

Figure 25. Mechanism studies for the enantioselective intramolecular C-H amination of aliphatic azide.

Based on previous work on the ring-closing C-H amination of (4-azidobutyl)arenes[12,15-17] and all the mechanism studies, the following catalytic cycle is proposed (Figure 26). $P(4\text{-F-Ph})_3$ activates the organic azide to form an intermediate iminophosphorane (**I**) through the well-known Staudinger reaction, which then transfers a nitrene to the ruthenium center to afford a ruthenium imido complex (intermediate **II**), followed by a stereo-controlled insertion of the nitrene moiety into the δ-C-H bond (transition state **III**) to provide a ruthenium-coordinated pyrrolidine (intermediate **IV**). However, a stepwise process through H-atom transfer cannot be totally excluded at this point. Finally, the product is released after Boc-protection.

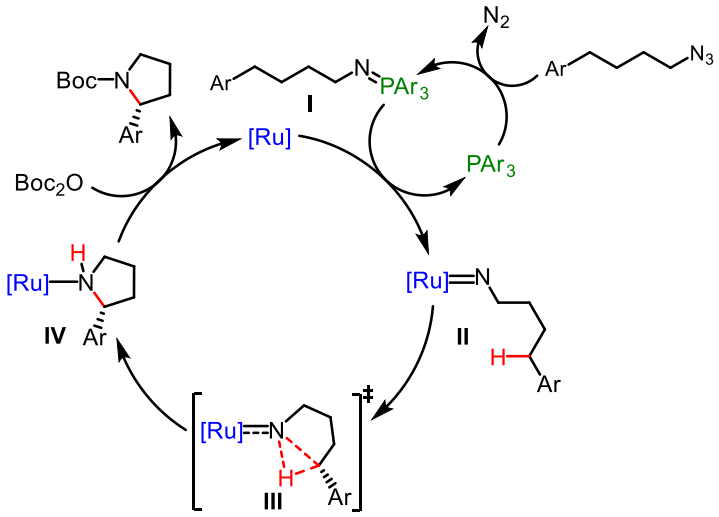

Figure 26. Proposed mechanism for the enantioselective intramolecular C-H amination of aliphatic azide.

3.2.5 Conclusions

In summary, a highly enantioselective catalytic ring-closing benzylic $C(sp^3)$-H amination of primary aliphatic azides to provide chiral 2-aryl pyrrolidines by combining of chiral-at-metal transition metal catalysis with nucleophilic phosphine catalysis is presented here. In this unique dual catalysis system, the phosphine activates the organic azide and transfers a nitrene to the ruthenium complex, which then executes the enantioselective C-H amination. This combination of ruthenium catalysis and Staudinger reaction introduces a novel direction for C-H amination of unactivated aliphatic azides which are very desirable but challenging substrates for this transformation.

References

1 For a recent account, see: L. Zhang, E. Meggers, *Acc. Chem. Res.* **2017**, *50*, 320.

2 For the chiral-at-ruthenium complex, see: Y. Zheng, Y. Tan, K. Harms, M. Marsch, R. Riedel, L. Zhang, E. Meggers, *J. Am. Chem. Soc.* **2017**, *139*, 4322.

3 For ruthenium imido intermediate, see: (*a*) S.-M. Au, J.-S. Huang, W.-Y. Yu, W.-H. Fung, C.-M. Che, *J. Am. Chem. Soc.* **1999**, *121*, 9120; (*b*) D. Intrieri, A. Caselli, F. Ragaini, P. Macchi, N. Casati, E. Gallo, *Eur. J. Inorg. Chem.* **2012**, *2012*, 569.

4 (*a*) G. Dequirez, V. Pons, Dauban, P. *Angew. Chem. Int. Ed.* **2012**, *51*, 7384; (*b*) S. Cenini, E. Gallo, A. Caselli, F. Ragaini, S. Fantauzzi, C. Piangiolino, *Coord. Chem. Rev.* **2006**, *250*, 1234; (*c*) P. F. Kuijpers, J. I. van der Vlugt, S. Schneider, B. de Bruin, *Chem. Eur. J.* **2017**, *23*, 13819.

5 For reviews on catalytic C-H aminations, see: (*a*) C.-M. Che, V. K.-Y. Lo, C.-Y. Zhou, J.-S. Huang, *Chem. Soc. Rev.* **2011**, *40*, 1950; (*b*) F. Collet, C. Lescot, P. Dauban, *Chem. Soc. Rev.* **2011**, *40*, 1926-1936; (*c*) J. L. Jeffrey, R. Sarpong, *Chem. Sci.* **2013**, *4*, 4092; (*d*) D. Hazelard, P.-A. Nocquet, P. Compain, *Org. Chem. Front.* **2017**, *4*, 2500; (*e*) Y. Park, Y. Kim, S. Chang, *Chem. Rev.* **2017**, *117*, 9247.

6 For a review of organic azides, see: S. Bräse, C. Gil, K. Knepper, V. Zimmermann, *Angew. Chem. Int. Ed.* **2005**, *44*, 5188.

7 For C(sp^3)-H aminations with aryl, sulfonyl, and acyl azides, see: (*a*) S. Cenini, E. Gallo, A. Penoni, F. Ragaini, S. Tollari, *Chem. Commun.* **2000**, 2265; (*b*) F. Ragaini, A. Penoni, E. Gallo, S. Tollari, C. L. Gotti, M. Lapadula, E. Mangioni, S. Cenini, *Chem. Eur. J.* **2003**, *9*, 249; (*c*) J. V. Ruppel, R. M. Kamble, X. P. Zhang, *Org. Lett.* **2007**, *9*, 4889; (*d*) A. Caselli, E. Gallo, S. Fantauzzi, S. Morlacchi, F. Ragaini, S. Cenini, *Eur. J. Inorg. Chem.* **2008**, 3009; (*e*) S. Fantauzzi, E. Gallo, A. Caselli, F. Ragaini, N. Casati, P. Macchi, S. Cenini, *Chem. Commun.* **2009**, 3952; (*f*) H. Lu, V. Subbarayan, J. Tao, X. P. Zhang, *Organometallics* **2010**, *29*, 389; (*g*) H. Lu, J. Tao, J. E. Jones, L. Wojtas, X. P. Zhang, *Org. Lett.* **2010**, *12*, 1248; (*h*) Y. Liu, C.-M. Che, *Chem. Eur. J.* **2010**, *16*, 10494; (*i*) M. Ichinose, H. Suematsu, Y. Yasutomi, Y. Nishioka, T. Uchida, T. Katsuki, *Angew. Chem. Int. Ed.* **2011**, *50*, 9884; (*j*) D. Intrieri, A. Caselli, F. Ragaini, P. Macchi, N. Casati, E. Gallo, *Eur. J. Inorg. Chem.* **2012**, 569; (*k*) Q. Nguyen, K. Sun, T. G. Driver, *J. Am. Chem. Soc.* **2012**, *134*, 7262; (*l*) Q. Nguyen, T. Nguyen, T. G. Driver, *J. Am. Chem. Soc.* **2013**, *135*, 620; (*m*) Y. Nishioka, T. Uchida, T. Katsuki, *Angew. Chem. Int. Ed.* **2013**, *52*, 1739; (*n*) G. Tseberlidis, P.

Zardi, A. Caselli, D. Cancogni, M. Fusari, L. Lay, E. Gallo, *Organometallics* **2015**, *34*, 3774; (*o*) O. Villanueva, N. M. Weldy, S. B. Blakey, C. E. MacBeth, *Chem. Sci.* **2015**, *6*, 6672.

8 Y. M. Badiei, A. Dinescu, X. Dai, R. M. Palomino, F. W. Heinemann, T. R. Cundari, T. H. Warren, *Angew. Chem. Int. Ed.* **2008**, *47*, 9961.

9 J. H. Lee, S. Gupta, W. Jeong, Y. H. Rhee, J. Park, *Angew. Chem. Int. Ed.* **2012**, *51*, 10851.

10 (*a*) G. Albertin, S. Antoniutti, D. Baldan, J. Castro, S. Garc á-Font án, *Inorg. Chem.* **2008**, *47*, 742; (*b*) L. Hu, Y. A. Liu, X. Liao, *Sci. Adv.* **2017**, *3*, e1700826.

11 E. R. King, T. A. Betley, *Inorg. Chem.* **2009**, *48*, 2361.

12 (*a*) E. T. Hennessy, T. A. Betley, *Science* **2013**, *340*, 591; (*b*) D. A. Iovan, M. J. T. Wilding, Y. Baek, E. T. Hennessy, T. A. Betley, *Angew. Chem. Int. Ed.* **2017**, *56*, 15599.

13 For a comment, see: T. G. Driver, *Nat. Chem.* **2013**, *5*, 736.

14 For a review of rings in drugs, see: R. D. Taylor, M. MacCoss, A. D. G. Lawson, *J. Med. Chem.* **2014**, *57*, 5845.

15 N. C. Thacker, Z. Lin, T. Zhang, J. C. Gilhula, C. W. Abney, W. Lin, *J. Am. Chem. Soc.* **2016**, *138*, 3501.

16 (*a*) B. Bagh, D. L. J. Broere, V. Sinha, P. F. Kuijpers, N. P. van Leest, B. de Bruin, S. Demeshko, M. A. Siegler, J. I. van der Vlugt, *J. Am. Chem. Soc.* **2017**, *139*, 5117. For a related palladium catalyst, see: (*b*) D. L. J. Broere, B. de Bruin, J. N. H. Reek, M. Lutz, S. Dechert, J. I. van der Vlugt, *J. Am. Chem. Soc.* **2014**, *136*, 11574.

17 P. F. Kuijpers, M. J. Tiekink, W. B. Breukelaar, D. L. J. Broere, N. P. van Leest, J. I. van der Vlugt, J. N. H. Reek, B. de Bruin, *Chem. Eur. J.* **2017**, *23*, 7945.

18 K.-P. Shing, Y. Liu, B. C., X.-Y. Chang, T. You, C.-M. Che, *Angew. Chem. Int. Ed.* **2018**, *57*, 11947.

19 For a review of asymmetric C-H functionalization, see: C. Zheng, S.-L. You, *RSC Adv.* **2014**, *4*, 6173.

20 (*a*) S. C. K. Rotte, A. G. Chittiboyina, I. A. Khan, *Eur. J. Org. Chem.* **2013**, 6355; (*b*) C. H. Mitch, S. J. Quimby, N.; Pedregal, C. Diaz, M. G. de la Torre, A. Jimenez, Q. Shi, E. J. Canada, S. D. Kahl, M. A. Statnick, D. L. McKinzie, D. R. Benesh, K. S. Rash, V. N. Barth, *J. Med. Chem.* **2011**, *54*, 8000; (*c*) A. K. Amegadzie, K. M. Gardinier, E. J. Hembre, P. A. Hipskind, L. N. Jungheim, B. S. Muehl, K. A. Savin, K. J. Thrasher, S. A. Boyd, (Lilly), Patent WO 2005000821A1, **2005**.

21 H. Staudinger, J. Meyer, *Helv. Chim. Acta* **1919**, *2*, 635.

22 (*a*) H. F. Sleiman, S. Mercer, L. McElwee-White, *J. Am. Chem. Soc.* **1989**, *111*, 8007; (*b*) K. Korn, A. Schorm, J. Z. Sundermeyer, *Anorg. Allg. Chem.* **1999**, *625*, 2125.

3.3 Ruthenium Catalyzed Asymmetric Oxidative Homocoupling of 2-Acyl Imidazoles

3.3.1 Project Design and Research Background

Bis-cyclometalated chiral-at-metal iridium and rhodium complexes have been successfully employed as catalysts for a variety of transformations by the Meggers group,[1] especially light-induced enantioselective reactions.[2] The efficiency of this kind of catalysts is attributed at least in parts to the strong σ donating effect of the cyclometalated ligands, which makes the ligand exchange fast in the overall catalytic process. The author of this thesis is quite interested in the asymmetric catalysis of chiral cyclometalated ruthenium complexes.[3] Compared with iridium and rhodium complexes, bis-cyclometalated ruthenium complexes are less reported for catalysis,[4] maybe because they are too electron-rich to be stable. After a literature research, it was found that Nishiyama and co-workers reported a chiral mono-cyclometalated ruthenium complex[3a] which contains one chiral cyclometalated bis-oxazolinyl ligand, one bidentate acetylacetonato ligand in addition to one CO ligand. This complex has been demonstrated to be stable under air. Furthermore, it has been applied for the asymmetric hydrogenation of ketones[3a] and asymmetric alkynylation of aldehydes[3c] providing excellent enantioselectivities (Figure 27).

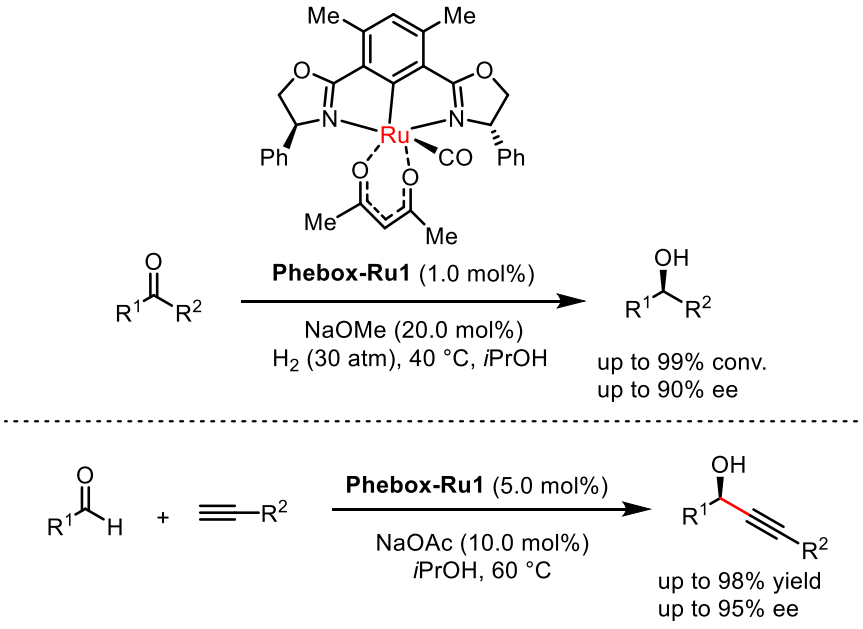

Figure 27. Asymmetric transformations catalyzed by chiral cyclometalated ruthenium complex (**Phebox-Ru1**).

Both the bis-cyclometalated chiral-at-metal iridium and rhodium complexes have been employed as single electron reductants in light-induced photoredox transformations.[2a,b,d,f] For example, a chiral-at-metal iridium (**IrS**) catalyzed enantioselective trichloromethylation of 2-acyl imidazoles and 2-acyl pyridines with enantioselectivities of ≥99% ee was reported in 2015 (Scheme 10).[2b] The author of this thesis wondered if the cyclometalated ruthenium complex could also serve as a single electron reductant. The study was initiated with testing the catalytic performance of mono-cyclometalated ruthenium complex **Phebox-Ru1** for the trichloromethylation of 2-acyl imidazoles.

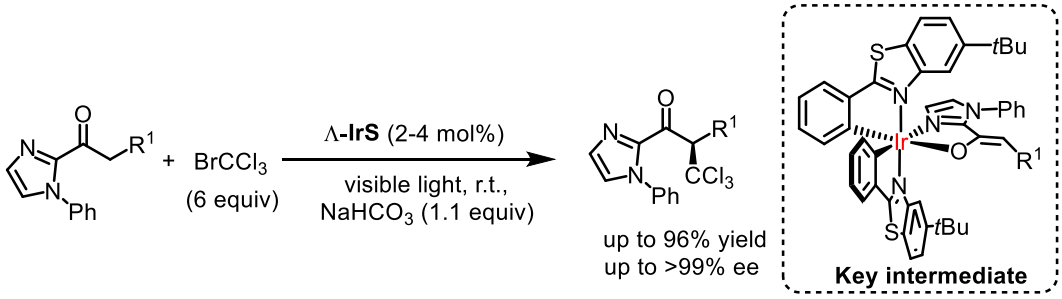

Scheme 10. Visible-light-activated enantioselective trichloromethylation of 2-acyl imidazoles catalyzed by Λ-**IrS**.

3.3.2 Reaction Development and Initial Experiments

Under the established reaction conditions of the above report from the Meggers group,[2b] only 10% of the trichloromethylation product **14** with 74% ee was obtained after 18 hours in the presence of 2 mol% of **Phebox-Ru1** (Table 8, entry 1). Control experiment indicated that light was not necessary for the formation of the product (entry 2). Interestingly, the homocoupling product **15c** was isolated as the major product in 55% yield with 93% ee when the reaction was performed at 40 °C (entry 3). This surprising homocoupling product has never been observed in the transformations catalyzed by the chiral-at-metal iridium (**IrS**) complex. Furthermore, the product containing a 1,4-dicarbonyl motif is an important synthetic building block, and the direct oxidative α-coupling of carbonyl compounds constitutes a direct way to construct 1,4-dicarbonyl moiety which has been reported rarely.

Table 8. Initial study of the catalytic property of **Phebox-Ru1**[a]

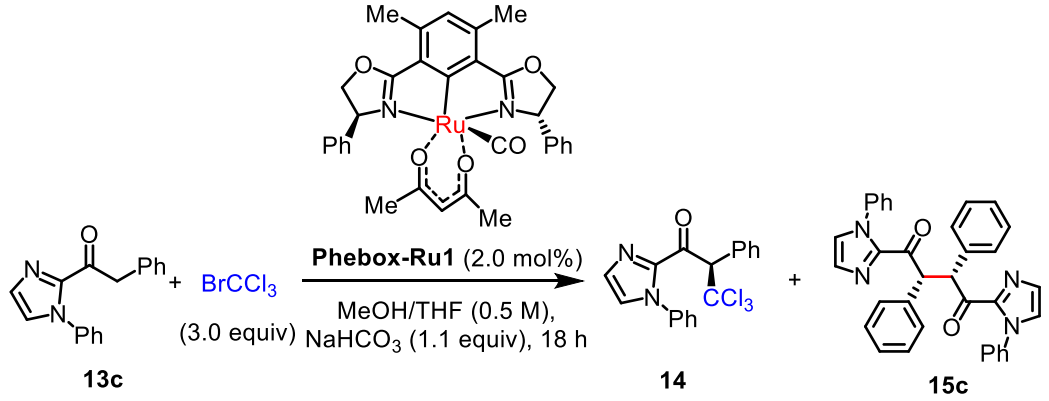

Entry	Light	T (^{o}C)	Yield (%)[b]		ee (%)[c]	
			14	**15c**	**14**	**15c**
1	CFL (20 W)	25	10	0	74	n.a.
2	No	25	10	0	73	n.a.
3	No	40	trace	55	n.a	93

[a]Standard conditions: **13c** (26.2 mg, 0.1 mmol, 1 equiv), $NaHCO_3$ (9.2 mg, 0.11 mmol, 1.1 equiv), **Phebox-Ru1** (1.3 mg, 0.002 mmol, 2 mol%) and $BrCCl_3$ (29.4 μL, 0.3 mmol, 3 equiv) in MeOH/THF (0.2 mL, the volume ratio of MeOH and THF is 3: 1) were stirred at indicated temperature under nitrogen for 19 h. [b]Isolated yield. [c]Determined by HPLC of crude main product on a chiral stationary phase. n.a. = not applicable.

As introduced in Chapter 1.4, although different indirect methods (Figure 28a), like the coupling of pre-formed lithium enolates, have been developed for the oxidative α-coupling of carbonyl compounds,[5] catalytic asymmetric versions are very limited.[6] The ideal way to construct chiral 1,4-dicarbonyl compounds is the direct asymmetric oxidative α-coupling of carbonyl compounds, which is only a recent accomplishment. Jørgensen and coworkers reported the direct enantioselective oxidative homocoupling of α-branched aldehydes with good yields (28-79%) and excellent enantioselectivities (6-96% ee) in the presence of 40 mol% chiral amine catalyst (Figure 28b).[7] All these facts give necessary impetus for the author of this thesis to further investigate this catalytic asymmetric transformation.

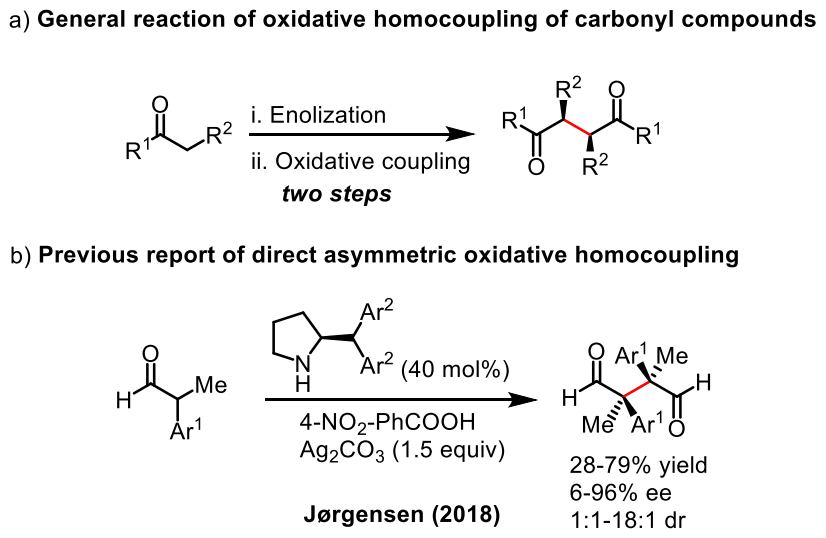

Figure 28. a) General strategy for oxidative homocoupling of carbonyl compounds; b) Previous report on direct asymmetric oxidative homocoupling of carbonyl compounds.

The optimization of the reaction conditions is performed in the presence of 2 mol% ruthenium catalyst and started with testing the substrates with different imidazole moieties. Both the yield and enantioselectivity were improved to 73% and 94% respectively when increasing the size of the substituents from methyl to phenyl (Table 9, entries 1-3). Interestingly, the reaction is very sensitive to the solvent. None of the other investigated solvents (THF, DMF, CH_3CN, and CH_2Cl_2) except methanol could give the homocoupling product (entries 4-8). Next, the base was optimized. Using other bases instead of sodium bicarbonate ($NaHCO_3$) provided decreased yields, even totally supressed the reaction in some cases (entries 9-13). Increase the reaction temperature to 50 or 60 ^oC led to worse results (entries 14,15 *vs* 3). In addition, screening the amount of $BrCCl_3$ indicated that one equivalent provided the best result (entries 16,17 *vs* 3). Finally, using **Phebox-Ru2** with isopropyl groups as the catalyst instead of **Phebox-Ru1** led to a decreased yield and ee (entry 18).

Control experiments confirmed that ruthenium catalyst, base as well as $BrCCl_3$ are all essential for this coupling reaction (entries 19-21). Furthermore, air could obviously suppress the product formation (entry 22). For comparison, the chiral-at-metal complexes Λ-**RhS** and Λ-**IrS** which have been known to activate 2-acyl imidazole could not catalyze this transformation (entries 23,24). It is noteworthy that only *syn*-products can be observed in all cases.

Table 9. Optimization of the ruthenium-catalyzed homocoupling of 2-acyl imidazoles [a]

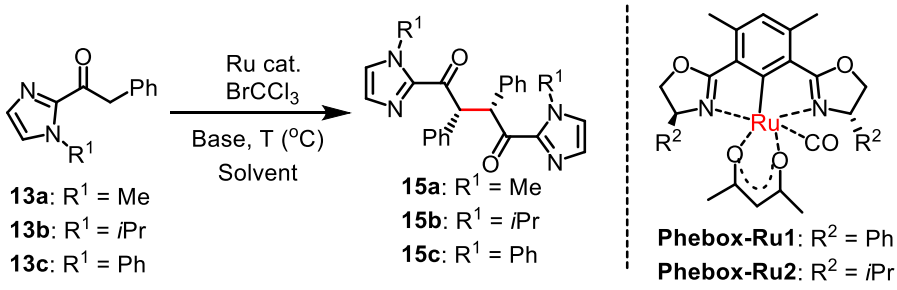

Entry	Base (1.1 equiv)	$BrCCl_3$ (equiv)	T (°C)	Solvent[b]	cpd **13**	Yield (%)[c]	ee (%)[d]
1	$NaHCO_3$	1.0	40	MeOH/THF	**13a**	47	45
2	$NaHCO_3$	1.0	40	MeOH/THF	**13b**	41	67
3	$NaHCO_3$	1.0	40	MeOH/THF	**13c**	73	94
4	$NaHCO_3$	1.0	40	MeOH	**13c**	62	93
5	$NaHCO_3$	1.0	40	THF	**13c**	0	-
6	$NaHCO_3$	1.0	40	DMF	**13c**	0	-
7	$NaHCO_3$	1.0	40	CH_3CN	**13c**	15	n.d.
8	$NaHCO_3$	1.0	40	CH_2Cl_2	**13c**	0	-
9	Na_2HPO_4	1.0	40	MeOH/THF	**13c**	trace	n.a.
10	K_3PO_4	1.0	40	MeOH/THF	**13c**	62	90
11	Et_3N	1.0	40	MeOH/THF	**13c**	trace	n.a.
12	Lutidine	1.0	40	MeOH/THF	**13c**	32	n.d.
13	K_2HPO_4	1.0	40	MeOH/THF	**13c**	trace	n.a.
14	$NaHCO_3$	1.0	50	MeOH/THF	**13c**	63	86
15	$NaHCO_3$	1.0	60	MeOH/THF	**13c**	43	86
16	$NaHCO_3$	0.5	40	MeOH/THF	**13c**	52	90
17	$NaHCO_3$	2.0	40	MeOH/THF	**13c**	47	86
18[e]	$NaHCO_3$	1.0	40	MeOH/THF	**13c**	69	92
19	-	1.0	40	MeOH/THF	**13c**	0	-
20[f]	$NaHCO_3$	1.0	40	MeOH/THF	**13c**	0	-
21[g]	$NaHCO_3$	1.0	40	MeOH/THF	**13c**	0	-
22[h]	$NaHCO_3$	1.0	40	MeOH/THF	**13c**	7	n.d.
23[i]	$NaHCO_3$	1.0	40	MeOH/THF	**13c**	0	-
24[j]	$NaHCO_3$	1.0	40	MeOH/THF	**13c**	7	n.d.

[a]Reaction conditions: **13a-c** (0.1 mmol), base (1.1 equiv), **Phebox-Ru1** (1.3 mg, 0.002 mmol, 2 mol%) and $BrCCl_3$ in indicated solvent (0.2 M) were stirred at indicated temperature under nitrogen for 45 h. [b]When MeOH/THF was used as solvent, the volume ratio of MeOH and THF was 4: 1. [c]Isolated yields. [d]Determined by HPLC on chiral stationary phase. n.d. = not determined. [e]**Phebox-Ru2** was used as the catalyst. [f]Without **Phebox-Ru1**. [g]Without $BrCCl_3$. [h]In the air. [i]Λ-**IrS** was used instead of **Phebox-Ru1**. [j]Λ-**RhS** was used instead of **Phebox-Ru1**.

To obtain the absolute configuration of the homocoupling product, **15c** was transformed to 2,3-diphenylbutane-1,4-diol (**19**) in two steps (Scheme 11). The optical rotation of **19** is determined as $[\alpha]_D^{20}$ = -45.8° (*c* = 1.0, CH_2Cl_2), which indicated that the product is (2*R*,3*R*)-**19** {Lit.[8] **[**$\alpha]_D^{20}$ = +47° (c = 0.25, $CHCl_3$) for (2*S*,3*S*)-**19**}. This suggests that the homocoupling product is (2*R*,3*R*)-**15c**.

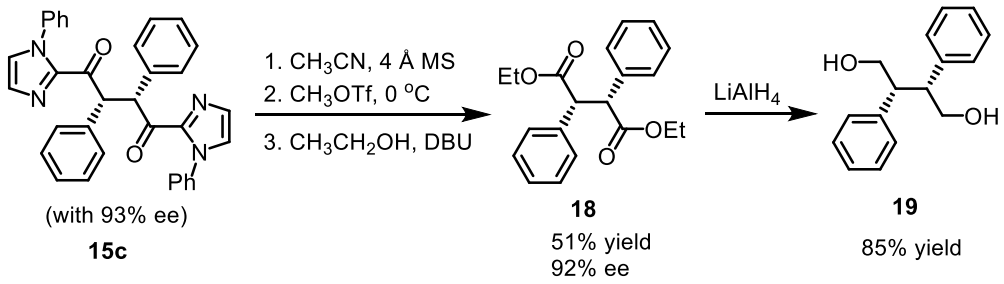

(with 93% ee)
15c

18
51% yield
92% ee

19
85% yield

Scheme 11. Determination of the absolute configuration of the homocoupling product.

3.3.3 Substrate Scope

With the optimized reaction conditions in hand, we investigated the scope of this ruthenium catalyzed homocoupling transformation (Figure 29). Substrates with a methyl group at the *meta*- or *para*-position of the phenyl moiety were successfully transformed to the homocoupling products with good yields and enantioselectivities (**15d**,**e**), but a sterically demanding *ortho*-methyl group totally suppressed the reaction. Electronic property of the phenyl group has great influence on both of the yield and enantioselectivity of this transformation. Typically, substrates with electron-donating groups (**13g**,**i**) gave higher enantioselectivities but lower yields compared with substrates with electron-withdrawing groups (**13j-l**). For example, enantioselectivity of 94% ee with a low yield of 35% was obtained for **13i** with a methoxy group, while a good yield of 72% with a decreased enantioselectivity of 75% ee was provided for **13l** containing a chlorine. Finally, phenyl can also be replaced with other aromatic groups like naphthyl (**13n**) or thiophenyl (**13o**). Importantly, diastereoselectivities were extremely high for all presented substrates, and only *syn*-products were detected in the ^{1}H NMR spectra of the crude reaction mixtures.

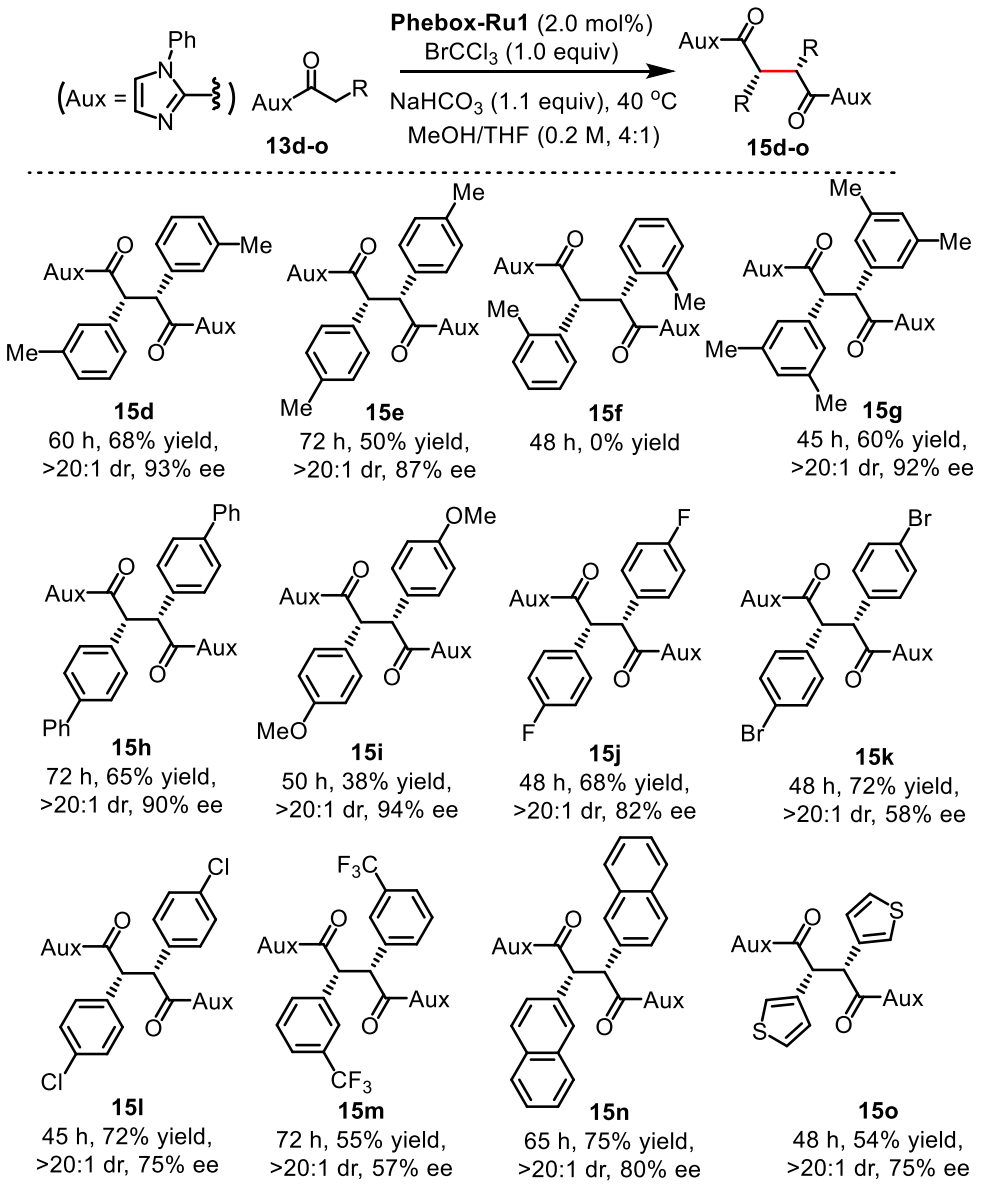

Figure 29. Substrate scope of direct asymmetric oxidative homocoupling of 2-acyl imidazoles with isolated yields.

3.3.4 Mechanism Study

A number of experiments were performed to understand the mechanism. Firstly, ruthenium enolate **16** which was proposed to be the key intermediate was isolated in 70% yield after the stoichiometric reaction of **Phebox-Ru1** and 2-acyl imidazole **13l** (Figure 30a). The accurate structure of **16** was also demonstrated by single crystal X-ray diffraction. Moreover, the chiral ruthenium enolate **16** was confirmed catalytically competent by itself for the homocoupling reaction (Figure 30b). Thus, the chiral ruthenium enolate **16** is a key intermediate which provides the crucial asymmetric

induction in the reaction.

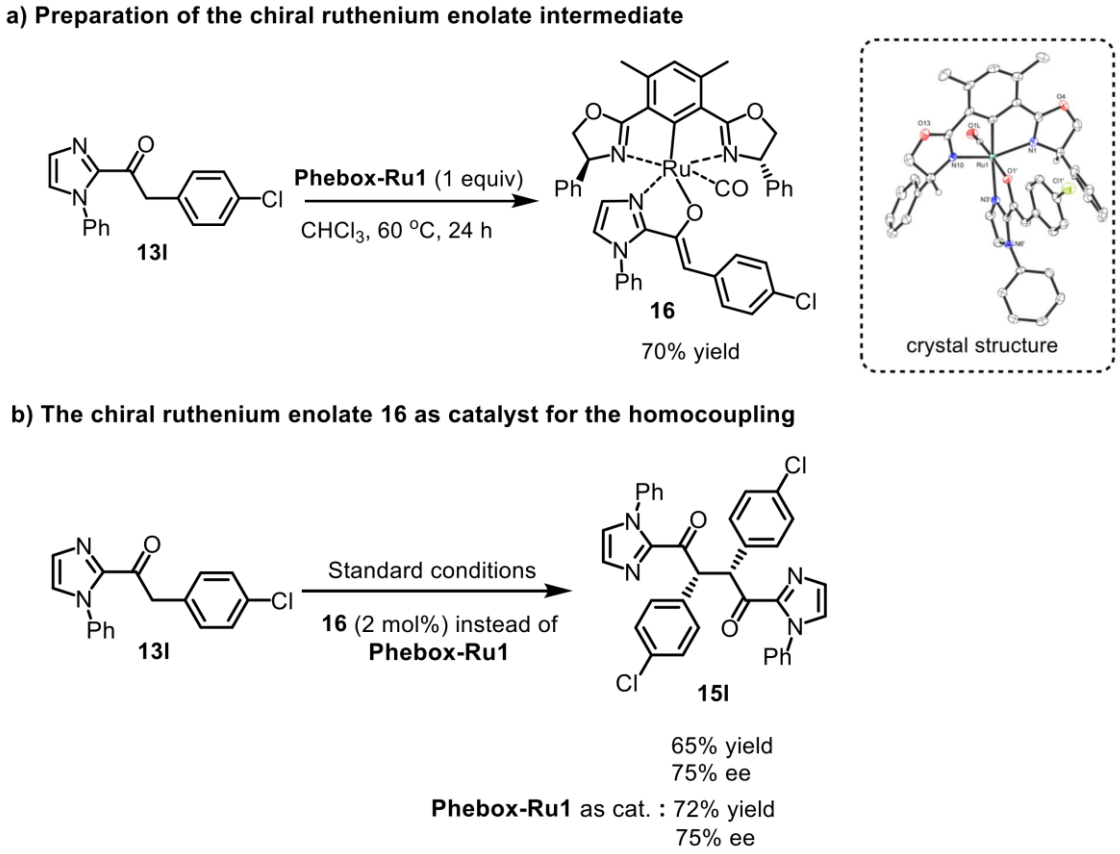

Figure 30. a) Preparation of the chiral ruthenium enolate intermediate; b) The chiral ruthenium enolate intermediate as the catalyst for the homocoupling of **13l**.

Next, monitoring the reaction by ^{1}H NMR indicated that a new species was formed initially and disappeared at the end of the reaction, which was demonstrated to be the brominated compound **17** (Figure 31a). This suggests that the brominated compound **17** is the reaction intermediate. Further verification was offered by the crosscoupling reaction between **17** and 2-acyl imidazole **13c** in the absence of $BrCCl_3$, providing the coupling product **15c** in 54% yield with 94% ee (Figure 31b). Interestingly, three coupling products were obtained in 56% yield when 2-acyl imidazole **13d** was used instead of **13c** under the same reaction conditions (Figure 31b). This could be explained by the bromide-transfer reaction between the bromide-containing compound with the ruthenium enolate intermediate (see the proposed mechanism below).

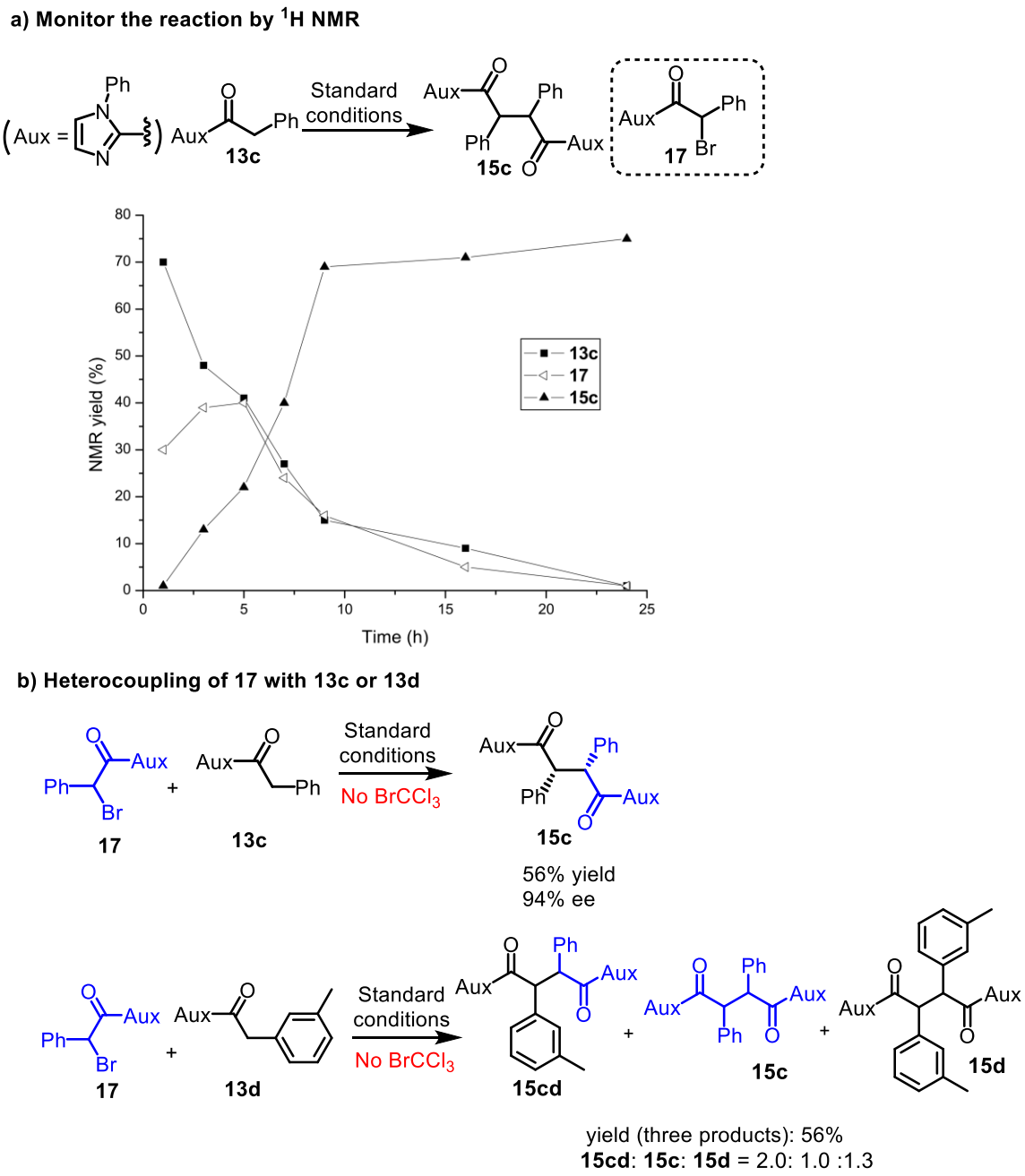

Figure 31. a) Monitor the reation by ^{1}H NMR; b) Heterocoupling of **17** with **13c** or **13d**.

When the standard catalytic reaction was monitored by electron paramagnetic resonance (EPR) using 5,5-dimethyl-1-pyrroline N-oxide (DMPO) as a free radical spin trapping agent, one radical signal was clearly observed (Figure 32a). The exact same signal was also observed for the reaction between **17** and **13c**, which was proposed to be α-carbonyl carbon radical generated from **17**. Furthermore, the catalytic reaction using **17** as the substrate in the absence of $BrCCl_3$ afforded the homocoupling product **15c** in 12% yield (Figure 32b). This also implies that radical species can be formed from **17** in the presence of the ruthenium complex **Phebox-Ru1**.

a) EPR experiment

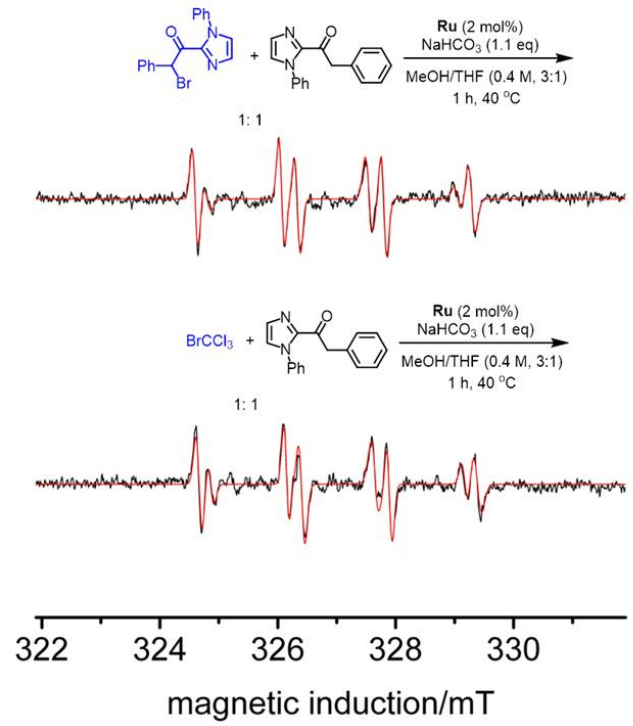

b) Catalytic reaction with 17 as the substrate

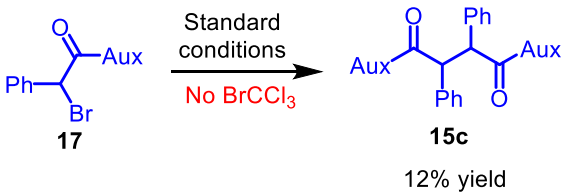

Figure 32. a) EPR experiment; b) Catalytic reaction with **17** as the substrate.

Based on all the observations and previous reports,[5] the following radical-enolate reaction mechanism is proposed (Figure 33). The ruthenium catalyst initially reacts with the substrate affording the electron-rich ruthenium enolate **I**, followed by reaction with $BrCCl_3$ providing brominated intermediate **17**, which is the key to form the free radical **II**. This radical species (**II**) reacts with ruthenium enolate **I** in a stereo-controlled manner providing intermediate **III**, which can be further oxidized by brominated intermediate **17** to afford the product-coordinated ruthenium species **IV**. Finally, the product is released together with regenerating the catalyst. However, the radical-radical coupling mechanism cannot be totally excluded at this stage.

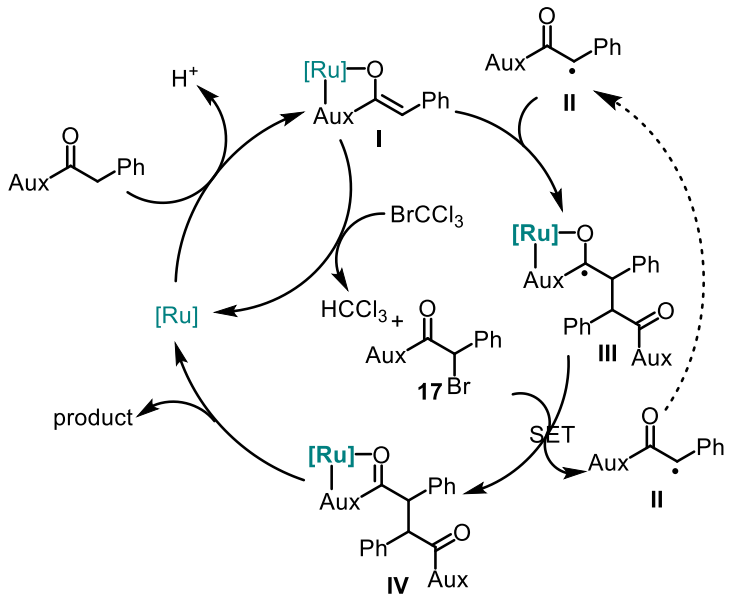

Figure 33. Proposed mechanism for the homocoupling of 2-acyl imidazoles.

3.3.5 Conclusions

In conclusion, the first ruthenium catalyzed asymmetric direct oxidative homocoupling of 2-acyl imidazole providing 1,4-dicarbonyl compounds in good yields with moderate to high enantioselectivities was reported here. To be noted, only one diastereomer is formed for all presented substrates. Moreover, mechanism studies support a two-steps catalytic process, first the bromination of the 2-acyl imidazole, followed by ruthenium catalyzed radical-enolate coupling to afford the final product. This methodology represents a rare example of the catalytically direct synthesis of symmetric chiral 1,4-dicarbonyl compounds.

References

1 L. Zhang, E. Meggers, *Chem. Asian J.* **2017**, *12*, 2335; (*b*) L. Zhang, E. Meggers, *Acc. Chem. Res.* **2017**, *50*, 320.

2 For selected examples, see: (*a*) H. Huo, X. Shen, C. Wang, L. Zhang, P. Röse, L.-A. Chen, K. Harms, M. Marsch, G. Hilt, E. Meggers, *Nature* **2014**, *515*, 100; (*b*) H. Huo, C. Wang, K. Harms, E. Meggers, *J. Am. Chem. Soc.* **2015**, *137*, 9551; (*c*) C. Wang, J. Qin, X. Shen, R. Riedel, K. Harms, E. Meggers, *Angew. Chem. Int. Ed.* **2016**, *55*, 685; (*d*) X. Huang, R. D. Webster, K. Harms, E. Meggers, *J. Am. Chem. Soc.* **2016**, *138*, 12636; (*e*) X. Huang, X. Li, X. Xie, R. Riedel, E. Meggers, *Nat. Commun.* **2017**, *8*, 2245; (*f*) J. Ma, A. R. Rosales, X. Huang, K. Harms, R. Riedel, O. Wiest, E. Meggers, *J. Am. Chem. Soc.* **2017**, *139*, 17245; (*g*) X. Huang, J. Lin, T. Shen, K. Harms, M. Marchini, P. Ceroni, E. Meggers, *Angew. Chem. Int. Ed.* **2018**, *57*, 5454.

3 (*a*) J. Ito, S. Ujiie, H. Nishiyama, *Chem. Commun.* **2008**, 1923; (*b*) J. Ito, S. Ujiie, H. Nishiyama, *Organometallics* **2009**, *28*, 630; (*c*) J. Ito, R. Asai, H. Nishiyama, *Org. Lett.* **2010**, *12*, 3860; (*d*) S. Ubukata, J. Ito, R. Oguri, H. Nishiyama, *J. Org. Chem.* **2016**, *81*, 3347; (*e*) S. Chanthamath, S. Iwasa, *Acc. Chem. Res.* **2016**, *49*, 2080.

4 (*a*) J. Zhang, A. Ugrinov, Y. Zhang, P. Zhao, *Angew. Chem. Int. Ed.* **2014**, *53*, 8437; (*b*) M. Simonetti, D. M. Cannas, X. Just-Baringo, I. J. Vitorica-Yrezabal, I. Larrosa, *Nat. Chem.* **2018**, *10*, 724.

5 For reviews of oxidative coupling of carbonyl compounds, see: (*a*) A. G. Csákÿ, J. Plumet, *Chem. Soc. Rev.* **2001**, *30*, 313; (*b*) F. Guo, M. D. Clift, R. J. Thomson, *Eur. J. Org. Chem.* **2012**, 4881.

6 H.-Y. Jang, J.-B. Hong, D. W. C. MacMillan, *J. Am. Chem. Soc.* **2007**, *129*, 7004.

7 L. Næsborg, L. A. Leth, G. J. Reyes-Rodríguez, T. A. Palazzo, V. Corti, K. A. Jørgensen, *Chem. Eur. J.* **2018**, *24*,14844.

8 V. D. Rao, M. Periasamy, *Synthesis* **2000**, *5*, 703.

Chapter 4: Summary and Outlook

4.1 Summary

1) Kinetic resolution of epoxides with CO_2 catalyzed by a chiral-at-iridium complex

Chiral-at-metal bis-cyclometalated iridium(III) complexes were introduced as a new class of catalysts for the reaction of epoxides with CO_2 to form cyclic carbonates under conditions of kinetic resolution (Figure 34). Reactions were typically performed at room temperature in the presence of 1 mol% iridium catalyst and 1.5 mol% tetraethylammonium bromide as the nucleophilic co-catalyst to provide selectivity factors of up to 16.6. Compared with reported catalytic systems, this system is tolerant of a variety of monosubstituted epoxides including styrene epoxide, epoxides with aliphatic side chains, glycidyl ethers, and a glycidyl ester, and no polymerization side reaction was observed for any of the investigated substrates. Moreover, only sample epoxides were used as substrates in this case. This is different from most of our group's previous reports in which two-point binding substrates are necessary to obtain good asymmetric induction.

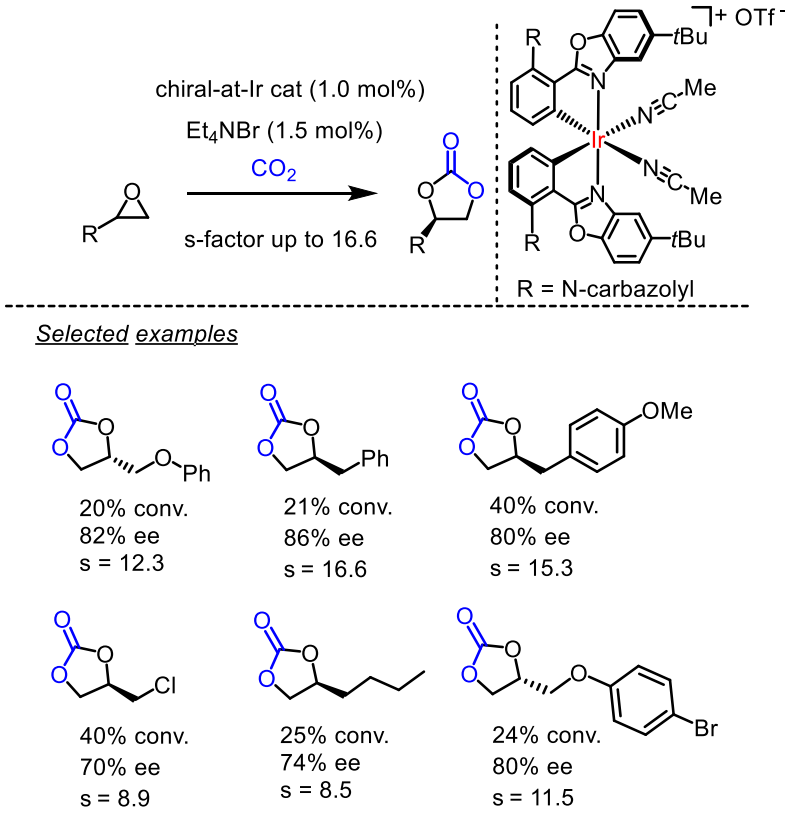

Figure 34. Kinetic resolution of epoxides with CO_2 catalyzed by Λ-**IrO(Carb)**.

2) Enantioselective intramolecular C(sp^3)-H amination of aliphatic azides by dual ruthenium and phosphine catalysis

The previously elusive catalytic enantioselective ring-closing C(sp^3)-H amination of unactivated aliphatic azides affording chiral pyrrolidines has been achieved through dual catalysis with a chiral-at-metal bis(pyridyl-NHC) ruthenium catalyst in combination with tris(*p*-fluorophenyl)phosphine (both 1 mol%) to provide enantioselectivities of up to 99% ee (Figure 35). A number of experiments have been performed, which support a unique catalytic cycle. The phosphine activates the organic azide to form an intermediate iminophosphorane through the well-known Staudinger reaction, which then transfers a nitrene to the ruthenium center to afford a ruthenium imido complex, followed by the stereo-controlled C-H amination.

The application of chiral-at-ruthenium complexes in enantioselective C(sp^3)-H activation demonstrates its interesting reactivity. The high enantioselectivity obtained for this transformation also indicated that the configuration of the chiral-at-ruthenium complex is stable even at a high temperature. This methodology is of significant synthetic value due to the importance of chiral α-aryl pyrrolidines as structural motifs in bioactive compounds.

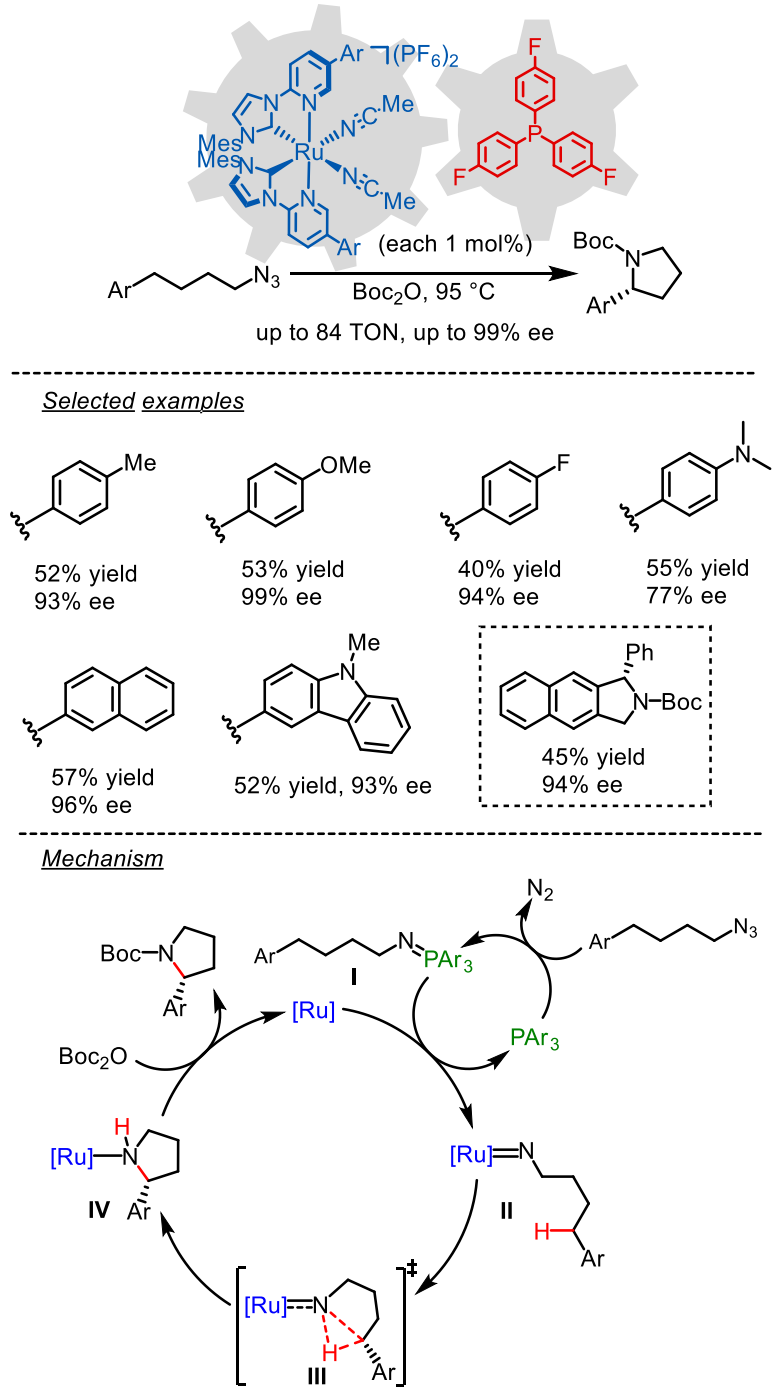

Figure 35. Enantioselective intramolecular C-H amination of aliphatic azides by dual ruthenium and phosphine catalysis.

3) Ruthenium catalyzed asymmetric direct oxidative homocoupling of 2-acyl imidazoles

Enantioselective direct oxidative homocoupling of 2-acyl imidazoles is achieved in the presence of 2 mol% of a mono-cyclometalated ruthenium complex and one equivalent $BrCCl_3$ as the oxidant, providing moderate to excellent enantioselectivities (Figure 36). Furthermore, almost only one diastereomer was obtained for all of the investigated substrates, which is difficult for most of the reported catalytic systems. Interestingly, a unique two-steps mechanism is proposed for this catalytic transformation. First is the ruthenium catalyzed bromination of 2-acyl imidazole affording the key intermediate brominated product, followed by the ruthenium catalyzed stereo-controlled radical-enolate reaction to provide the final product. This methodology represents a rare examples of catalytically synthesizing chiral 1,4-dicarbonyl molecules from carbonyl compounds.

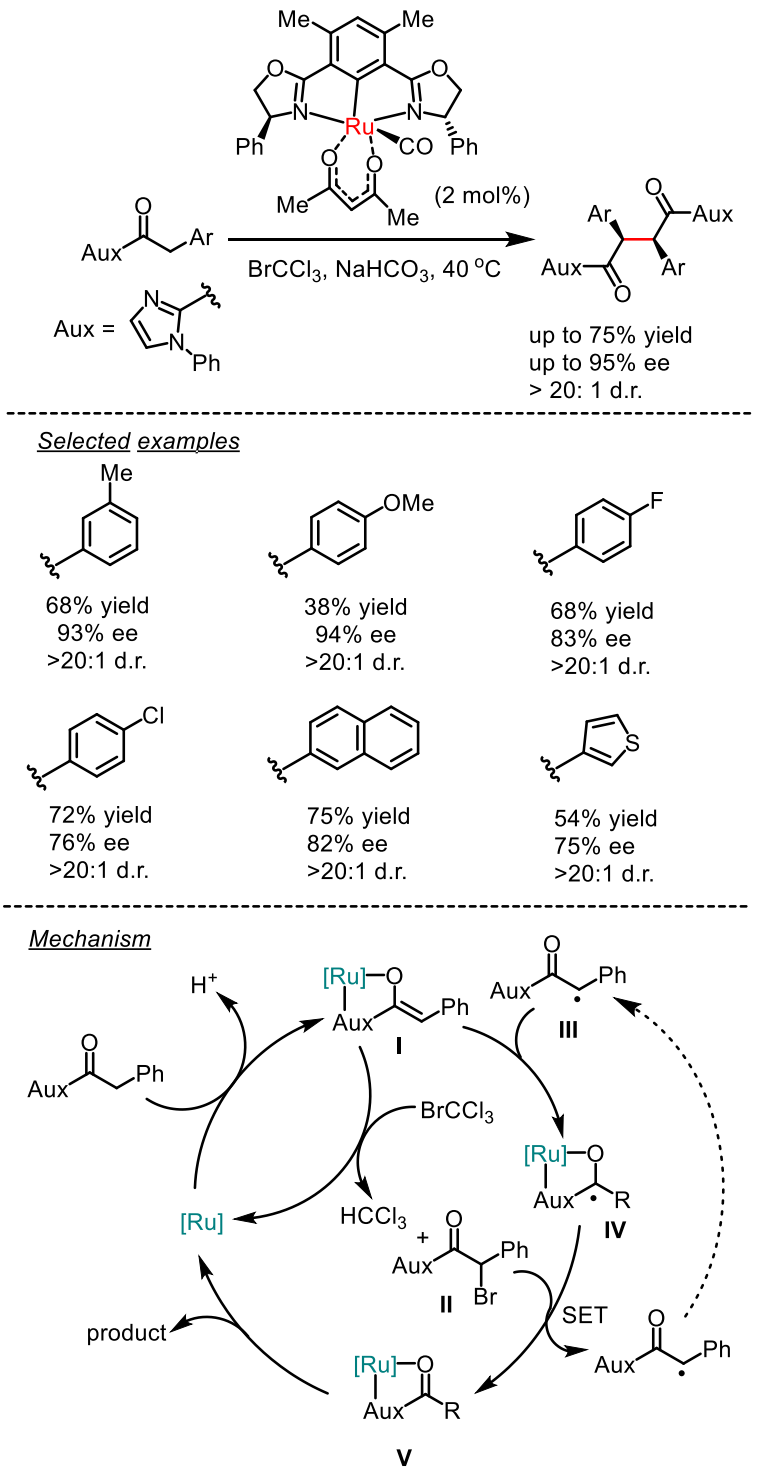

Figure 36. Asymmetric direct oxidative homocoupling of 2-acyl imidazole catalyzed by cyclometalated ruthenium complex.

4.2 Outlook

This thesis displays the versatile catalytic properties of previously established chiral-at-metal

iridium and ruthenium complexes and a cyclometalated ruthenium complex. In particular, the enantioselective intramolecular C-H amination of aliphatic azides demonstrates the attractive catalytic property of our chiral-at-ruthenium complex. Accordingly, further investigations as follows can be considered in the future:

1) Developing new ruthenium complexes with other types of ligands instead of pyridyl-NHC: The chiral-at-metal bis(pyridyl-NHC) ruthenium catalysts displayed high activity and excellent stereocontrol for intramolecular C-H amination of aliphatic azides, but it could not activate electro-deficient organic azides. The study in this thesis also indicated that ligands surrounding the metal center had a great influence on the catalytic activity of the ruthenium complex. Therefore, it is supposed that ruthenium complexes containing other types of ligands (like cyclometalated ligands) which make the metal center more electron-rich is worthy of further development. New ruthenium complexes offer the opportunity to catalyze C-H aminations of other types of organic azides or other precursors, thus making this strategy more general to construct C-N bonds. The precise design of the ligand is necessary when synthesizing electron-rich ruthenium complexes because of the stability problem. Both the steric and electronic effects on the ligand should be considered.

2) Developing new transformations based on nitrene or carbene insertion catalysis: Ruthenium imido complexes are the key intermediate in our catalytic enantioselective C-H animations. The formation of the ruthenium imido intermediate depends on the nature of the ruthenium catalyst and the nitrene precursors employed. The C-H amination of aliphatic azides presented in this thesis was limited to the activation of the benzylic C-H bond. It will be of high significance to achieve the C-H amination of saturated and completely unactivated C-H bonds. Except for the development of new catalysts, testing other aminating reagents is an alternative, for an example using N-tosyloxycarbamates. In addition to the nitrene insertion, C-H functionalization through carbene insertion using our chiral-at-metal ruthenium catalysts is also interesting. Analogously, different kinds of carbene precursors should be carefully screened to achieve the transformation.

Chapter 5: Experimental Part

5.1 Materials and Methods

All reactions were carried out under an atmosphere of nitrogen with magnetic stirring unless indicated ortherwise. The catalytic reactions were performed by using standard Schlenk glassware techniques.

Solvents and Reagents

Solvents were distilled under nitrogen from calcium hydride ($CHCl_3$, CH_2Cl_2 and CH_3CN) or sodium/benzophenone (Et_2O and THF) or sodium (toluene). Extra dry DMF, 1,4-dioxane and 1,2-dichlorobenzene were purchased from Acros. HPLC grade solvents, such as 2-methoxyethanol, methanol and ethanol were used directly without further drying. All reagents were purchased from Acros, Alfa Aesar, Sigma Aldrich, TCI, ChemPur and Fluorochem and used without further purification.

Chromatographic Methods

The course of the reactions and the column chromatographic elution were monitored by thin layer chromatography (TLC) [Macherey-Nagel (ALUGRAM®Xtra Sil G/UV254)]. Flash column chromatography was performed with silica gel from Merck (particle size 0.040-0.063 mm).

Nuclear Magnetic Resonance Spectroscopy (NMR)

^{1}H NMR, proton decoupled ^{13}C NMR, and proton coupled ^{19}F NMR spectra were recorded on Bruker Avance 300 system (^{1}H NMR: 300 MHz, ^{13}C NMR: 75 MHz, ^{19}F NMR: 282 MHz) spectrometers or Bruker AM (^{1}H NMR: 500 MHz) spectrometers at ambient temperature. Chemical shifts are given in ppm on the δ scale, and were determined after calibration to the residual signals of the solvents, which were used as an internal standard. NMR standards were used are as follows: ^{1}H NMR spectroscopy: δ = 7.26 ppm ($CDCl_3$), δ = 5.32 ppm (CD_2Cl_2), δ = 1.96 ppm (CD_3CN), δ = 7.16 ppm (C_6D_6); ^{13}C-NMR spectroscopy: δ = 77.0 ppm ($CDCl_3$), δ = 53.8 ppm (CD_2Cl_2), δ = 118.26, 1.32 ppm (CD_3CN), δ = 206.26, δ = 128.06 ppm (C_6D_6). ^{19}F NMR spectroscopy: δ = 0 ppm ($CFCl_3$). The characteristic signals were specified from the low field to high field with the chemical shifts (δ in ppm). ^{1}H NMR spectra peak multiplicities indicated as singlet (s), doublet (d), doublet of doublet (dd),

doublet of doublet of doublet (ddd), triplet (t), doublet of triplet (dt), quartet (q), multiplet (m). The coupling constant *J* indicated in Hertz (Hz).

High-Performance Liquid Chromatography (HPLC)

Chiral HPLC was performed with an Agilent 1200 Series, Agilent 1260 Series HPLC System or Shimadzu Lc-2030c. All the HPLC conditions were detailed in the individual procedures. The type of the columns, mobile phase and the flow rate were specified in the individual procedures.

Gas Chromatography (GC)

Chiral GC chromatography was performed with an Agilent 7890B GC system. All the GC conditions were detailed in the individual procedures.

Infrared Spectroscopy (IR)

IR measurements were recorded on a Bruker Alpha-P FT-IR spectrometer. The absorption bands were indicated a wave numbers ν (cm^{-1}). All substances were measured as films or solids.

Mass Spectrometry (MS)

High-resolution mass spectra were recorded on a Bruker En Apex Ultra 7.0 TFT-MS instrument using ESI or APCI or FD technique. Ionic masses are given in units of m/z for the isotopes with the highest natural abundance.

Electron Paramagnetic Resonance (EPR)

The EPR spectrometer is from Bruker (model esp300), with a modified Varian rectangular X-band cavity and the modulation frequency was set to 100 kHz, the modulation amplitude was 0.1 mT.

Circular Dichroism Spectroscopy (CD)

CD spectra were recorded on a JASCO J-810 CD spectropolarimeter. The parameters we used as follows: from 600 nm to 200 nm; data pitch (0.5 nm); band with (1 nm); response (1 second); sensitivity (standard); scanning speed (50 nm/min); accumulation (5 times). The concentration of the compounds for the measurements was 0.2 mM. The formula for converting θ to ε is shown as below.

$$\Delta\varepsilon = \frac{\theta[m\,\mathrm{deg}]}{32980 \times c(mol/L) \times L(cm)}$$

C = concentration of the sample; L = thickness of the measurement vessel

Crystal Structure Analysis

Crystal X-ray measurements and the crystal structure analysis were carried out by Dr. Klaus Harms (Chemistry Department, Philipps University of Marburg). X-ray data were collected with a Bruker 3 circuit D8 Quest diffractometer with MoKa radiation (microfocus tube with multilayer optics) and Photon 100 CMOS detector. Scaling and absorption correction was performed by using the SADABS software package of Bruker. Structures were solved using direct methods in SHELXS and refined using the full matrix least squares procedure in SHELXL-2013 or SHELXL-2014. The Flack parameter is a factor used to estimate the absolute configuration of the coumounds. The hydrogen atoms were placed in calculated positions and refined as riding on their respective C atom, and Uiso(H) was set at 1.2 Ueq(Csp^2) and 1.5 Ueq(Csp^3). Disorder of PF_6 ions, solvent molecules or methylene groups was refined using restraints for both the geometry and the anisotropic displacement factors.

Optical Rotation Polarimeter

Optical rotations were measured on a Krüss P8000-T or Perkin-Elmer 241 polarimeter with $[\alpha]_D^{20}$ or $[\alpha]_D^{25}$ values reported in degrees with concentrations reported in g/100 mL.

5.2 Kinetic Resolution of Epoxides with CO_2 Catalyzed by a Chiral-at-Iridium Complex

5.2.1 Synthesis of Iridium Catalysts Λ-IrO(Carb) and Δ-IrO(Carb)

a) Synthesis of ligand

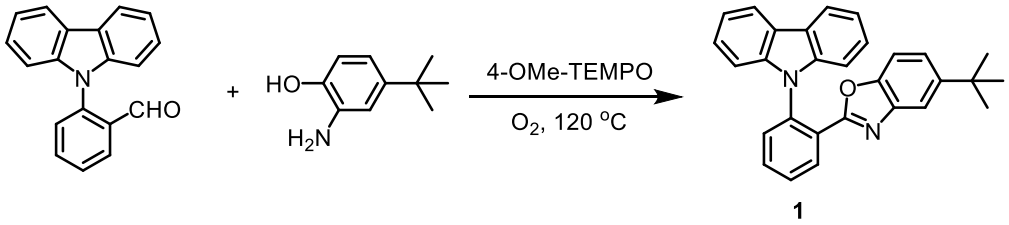

A solution of 2-amino-4-*tert*-butylphenol (0.43 g, 2.58 mmol) and 2-(9H-carbazol-9-yl)benzaldehyde[1] (0.7 g, 2.58 mmol) in *m*-xylene (9 mL) was stirred at 120 ℃ for 1 h. After cooling to r.t., 4-methoxy-TEMPO (24.0 mg, 0.13 mmol) was added to the mixture which was then stirred at 120 ℃ overnight under an oxygen atmosphere (1 atm O_2 gas in a balloon). After cooling to room temperature, all volatiles were removed in vacuo. The residue was purified by flash chromatography on silica gel (*n*-hexane/EtOAc 20:1) to afford the desired product **1** (1.02 g, 2.45 mmol, 95%) as a white solid.

^{1}H NMR (300 MHz, $CDCl_3$) δ 8.56 (dd, J = 7.6, 1.8 Hz, 1H), 8.25-8.15 (m, 2H), 7.82-7.68 (m, 2H), 7.67-7.56 (m, 2H), 7.35-7.21 (m, 4H), 7.20-7.08 (m, 3H), 6.80 (d, J = 8.7 Hz, 1H), 1.30 (s, 9H).

^{13}C NMR (75 MHz, $CDCl_3$) δ 161.2, 148.8, 147. 9, 142.0, 141.2, 136.4, 132. 6, 132.0, 130.9, 129.0, 126.9, 126.1, 123.7, 123.0, 120.3, 119.8, 116.5, 109.64, 109.61, 34.9, 31.8.

IR (film): ν (cm^{-1}) 3056, 2959, 2869, 1591, 1544, 1452, 1315, 1270, 1229, 1197, 1118, 1065, 1029, 908, 842, 812, 720, 640, 425.

HRMS (ESI, *m/z*) calcd. for $C_{29}H_{24}N_2ONa$ $[M+Na]^+$: 439.1786, found: 439.1781.

b) Synthesis of iridium dimer complex

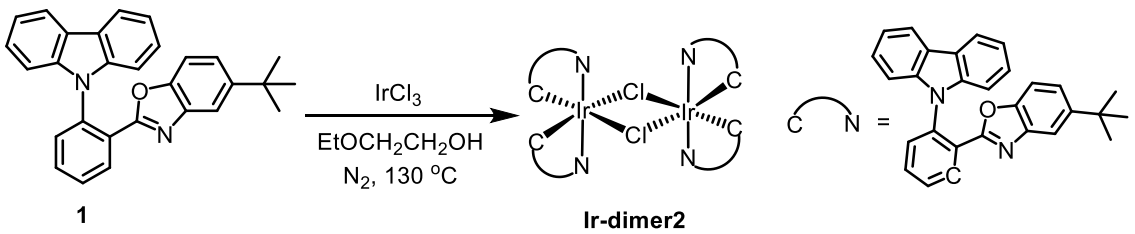

A solution of compound **1** (500 mg, 1.20 mmol) and iridium chloride hydrate (254 mg, 0.72 mmol) in

2-ethoxyethanol (24 mL) was purged with nitrogen gas for 15 min and then stirred at 130 ℃ for 24 h under nitrogen atmosphere. After cooling to room temperature, all volatiles were removed in vacuo and the residue was purified by flash chromatography on silica gel (*n*-hexane/CH_2Cl_2 1:4 to CH_2Cl_2) to afford the desired product **Ir-dimer2** (553 mg, 0.26 mmol, 87%) as a yellow solid.

^{1}H NMR (300 MHz, CD_2Cl_2) δ 8.27-8.13 (m, 12H), 7.52-7.41 (m, 8H), 7.38-7.31 (m, 4H), 7.20-7.14 (m, 4H), 7.12-7.06 (m, 4H), 7.03-6.94 (m, 8H), 6.79-6.72 (m, 4H), 6.62-6.58 (m, 4H), 6.32-6.20 (m, 8H), 0.62 (s, 36H).

^{13}C NMR could not be measured because of the low solubility.

IR (film): ν (cm^{-1}) 3055, 2962, 2869, 2034, 1573, 1481, 1453, 1424, 1364, 1314, 1275, 1231, 1193, 1147, 1109, 965, 929, 888, 808, 749, 719, 646, 425.

HRMS (LIFDI, m/z) calcd. for $C_{116}H_{92}Cl_2Ir_2N_8O_4$: 2116.5887, found: 2116.5921.

c) Synthesis of iridium auxiliary complex

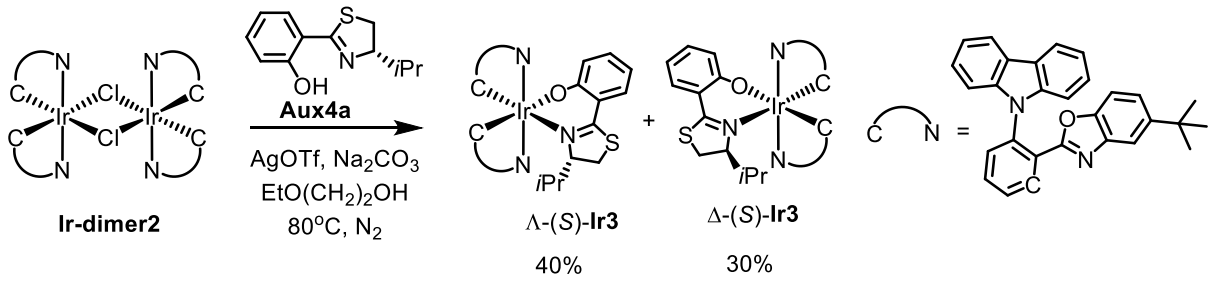

A mixture of dimer complex **Ir-dimer2** (0.5 g, 0.24 mmol), the chiral auxiliary **Aux4a** (125.4 mg, 0.57 mmol), AgOTf (146 mg, 0.57 mmol) and Na_2CO_3 (375 mg, 3.54 mmol) in 2-ethoxyethanol (15 mL) was stirred at 80 ^{o}C for 20 h under nitrogen atmosphere. After cooling to room temperature, all volatiles were removed in vacuo. The residue was dissolved in CH_2Cl_2 and filtered through celite to remove all unsoluble solid. The filtrate was then concentrated under reduced pressure and purified by flash chromatography on silica gel (*n*-hexane/CH_2Cl_2 4:1 to 2:1) to get the two diastereomers. The first eluting diastereomer (236 mg, 0.19 mmol, 40%) was assigned as Λ-(*S*)-**Ir3** and the second eluting diastereomer as Δ-(*S*)-**Ir3** (174 mg, 0.14 mmol, 30%).

Λ-(*S*)-**Ir3**:

^{1}H NMR (300 MHz, CD_2Cl_2) δ 8.35-8.15 (m, 4H), 7.92 (s, 1H), 7.51-7.21 (m, 16H), 7.20-7.05 (m, 5H), 6.99-6.86 (m, 3H), 6.82 (d, J = 8.7 Hz, 1H), 6.71 (d, J = 7.5 Hz, 1H), 6.37-6.27 (m, 1H), 4.97 (d,

J = 8.7 Hz, 1H), 3.46 (t, *J* = 10.8 Hz, 1H), 3.09 (d, *J* = 12.5 Hz, 1H), 1.39 (s, 9H), 1.11 (s, 9H), 0.80-0.65 (m, 1H), 0.48 (d, *J* = 6.7 Hz, 3H), 0.02 (d, *J* = 6.6 Hz, 3H).

^{13}C NMR (75 MHz, CD_2Cl_2) δ 176.8, 176.4, 168.9, 167.7, 154.7, 154.0, 150.8, 150.5, 148.7, 148.3, 143.0, 142.4, 142.3, 142.2, 138.6, 138.3, 136.5, 136.0, 135.8, 134.1, 133.9, 133.1, 132.4, 131.8, 130.4, 129.8, 126.7, 126.5, 126.4, 126.3, 124.9, 124.4, 124.3, 124.03, 123.96, 123.8, 123.6, 122.9, 121.9, 121.0, 120.9, 120.7, 120.6, 120.4, 120.3, 120.3, 119.2, 118.6, 115.2, 114.0, 113.1, 111.1, 110.8, 110.7, 110.6, 110.4, 85.6, 35.9, 35.5, 32.2, 31.8, 31.7, 28.4, 19.8, 14.2.

IR (film): *ν* (cm^{-1}) 2960, 2869, 1562, 1522, 1452, 1362, 1273, 1232, 1194, 1151, 1013, 965, 930, 846, 814, 749, 647.

HRMS (ESI, *m/z*) calcd. for $C_{70}H_{61}IrN_5O_3S$ $[M+H]^+$: 1244.4124, found: 1244.4124.

CD (MeOH): λ, nm (Δε, $M^{-1}cm^{-1}$) 449 (–4), 391 (+19), 357 (+21), 330 (+33), 297 (–22), 275 (+4), 263 (1).

Δ-(*S*)-**Ir3**:

^{1}H NMR (300 MHz, CD_2Cl_2) δ 8.31-8.18 (m, 4H), 7.89 (d, *J* 1.7 Hz, 1H), 7.43-7.01 (m, 22H), 6.92 (d, *J* 8.9 Hz, 1H), 6.80 (dd, *J* 7.7, 5.5 Hz, 2H), 6.62 (d, *J* 7.8 Hz, 1H), 6.29 (t, *J* 6.9 Hz, 1H), 3.64 (d, *J* 10.0 Hz, 1H), 2.93 (dd, *J* 11.3, 2.2 Hz, 1H), 2.57 (t, *J* 10.6 Hz, 1H), 2.38-2.22 (m, 1H), 1.15 (s, 9H), 1.08 (s, 9H), 1.05 (d, *J* 6.9 Hz, 3H), 0.35 (d, *J* 7.0 Hz, 3H).

^{13}C NMR (75 MHz, CD_2Cl_2) δ 177.3, 177.1, 168.3, 167.6, 154.9, 154.0, 151.0, 149.9, 148.9, 148.3, 142.9, 142.8, 142.2, 142.2, 139.0, 137.9, 136.5, 136.1, 133.7, 132.8, 132.8, 132.6, 132.4, 129.8, 129.3, 126.6, 126.6, 126.4, 126.3, 124.5, 124.4, 124.2, 124.1, 123.9, 123.9, 123.7, 122.8, 122.1, 121.0, 120.9, 120.8, 120.7, 120.4, 120.3, 120.2, 119.9, 114.9, 114.1, 113.7, 110.9, 110.5, 110.3, 83.1, 35.6, 35.4, 32.2, 32.0, 31.6, 30.1, 20.8, 17.1.

IR (film): *ν* (cm^{-1}) 2954, 2922, 2856, 1593, 1563, 1450, 1419, 1359, 1339, 1312, 1274, 1231, 1194, 1146, 928, 813, 746, 718, 640.

HRMS (ESI, *m/z*) calcd. for $C_{70}H_{61}IrN_5O_3S$ $[M+H]^+$: 1244.4121, found: 1244.4121.

CD (MeOH): λ, nm (Δε, $M^{-1}cm^{-1}$) 470 (+10), 424 (+1), 412 (+3), 387 (-5), 378 (-3), 331 (-41), 299 (+40), 274 (+9), 238 (-37), 215 (+42).

d) Synthesis of enantiopure iridium complex

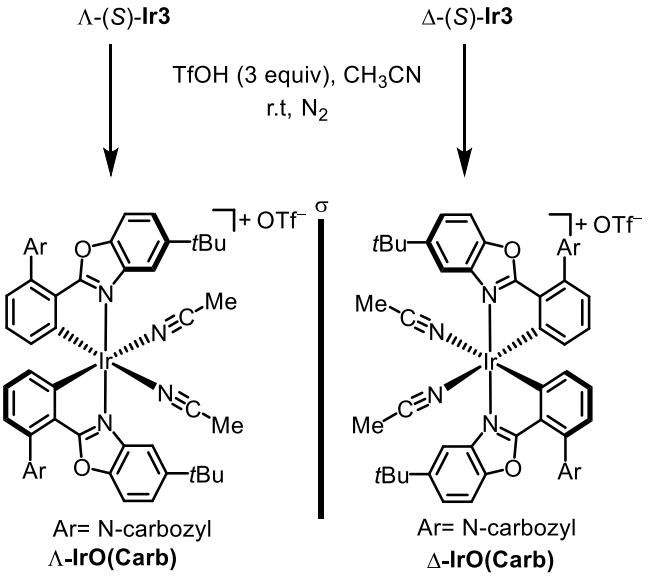

A round flask was charged with Λ-(*S*)-**Ir3** (142 mg, 0.11 mmol), then evacuated and purged with nitrogen gas, and CH_3CN (6 mL) was added. After stirring for 5 min, trifluoromethanesulfonic acid (29 μL, 0.33 mmol) was added. The resulting mixture was stirred for 1 h at room temperature under nitrogen atmosphere. Then all volatiles were removed in vacuo and the residue was purified by flash chromatography on silica gel (CH_2Cl_2/CH_3CN 20:1 to 3:1) to give catalyst Λ-**IrO(Carb)** (125.4 mg, 0.099 mmol, 90%) as a yellow solid. According to the same procedure, catalyst **Δ-IrO(Carb)** (121.6 mg, 0.097 mmol, 88%) was got as a yellow solid.

Λ-**IrO(Carb)**:

^{1}H NMR (300 MHz, CD_3CN) δ 8.30 (d, J = 7.5 Hz, 4H), 7.92 (d, J = 1.7 Hz, 2H), 7.55 (dd, J = 8.9, 1.9 Hz, 2H), 7.46-7.15 (m, 14H), 7.01 (d, J = 8.9 Hz, 2H), 6.90 (d, J = 7.1 Hz, 2H), 6.64 (dd, J = 7.4, 1.1 Hz, 2H), 2.39 (s, 6H), 1.40 (s, 18H).

^{13}C NMR (75 MHz, CD_2Cl_2) δ 175.5, 151.5, 148.6, 145.3, 142.5, 142.1, 137.7, 136.4, 133.8, 132.9, 128.6, 126.6, 126.5, 125.4, 124.8, 124.3, 124.2, 121.7, 121.0, 121.0, 120.7, 120.6, 113.0, 111.9, 110.2, 110.1, 35.8, 31.9, 4.4.

IR (film): $\tilde{\nu}$ (cm^{-1}) 3053, 2961, 2871, 1575, 1453, 1423, 1366, 1313, 1266, 1230, 1195, 1151, 1028, 969, 930, 817, 747, 636, 571, 518, 423.

HRMS (LIFDI, *m*/*z*) calcd. for $C_{62}H_{52}IrN_6O_2$ $[M]^+$: 1105.3776, found: 1105.3780.

CD (MeOH): λ, nm (Δε, M^{-1}cm^{-1}) 448 (-6), 338 (+31), 412 (+3), 293 (-46), 235 (+54), 217 (-11), 207 (+39).

Δ-IrO(Carb):

CD (MeOH): λ, nm (Δε, $M^{-1}cm^{-1}$) 448 (+6), 338 (-31), 412 (-3), 293 (+46), 235 (-54), 217 (+11), 207 (-39).

All other spectroscopic data of **Δ-IrO(Carb)** were in agreement with Λ-**IrO(Carb)**.

5.2.2 Synthesis of Epoxides

Procedure A:

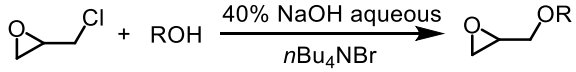

To a solution of ROH (1 equiv), 40% NaOH aqueous (17 equiv) and nBu$_4$NBr (0.05 equiv) in water (0.6 M) was added 2-(chloromethyl)oxirane (4 equiv) in a flask. After being stirred at room temperature for 24 hours, the reaction mixture was extracted three times with diethyl ether. The combined organic phases were dried over Na_2SO_4. After removal of the solvent under reduced pressure, the crude mixture was purified by flash column chromatography on silica gel column resulted in the desired epoxides.

Procedure B:

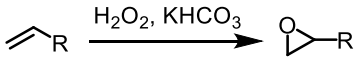

To a solution of alkene (1.0 equiv) in CH_3CN/CH_3CH_2OH (2.1 M, volume ratio = 1: 5), H_2O_2 solution (2.0 equiv) containing $KHCO_3$ (0.3 equiv) was added slowly. The resulting mixture was stirred at room temperature for 24 hours. Another portion of H_2O_2 solution (0.5 equiv) was added and the resulting mixture was stirred at room temperature for another 24 hours. The reaction was quenched by saturated $Na_2S_2O_3$ solution slowly, and the product was extracted three times with diethyl ether. The combined organic phases were dried over Na_2SO_4. After removal of the solvent under reduced pressure, the crude mixture was purified by flash column chromatography on silica gel column resulted in the desired epoxides.

2-((Benzyloxy)methyl)oxirane (**4a**)

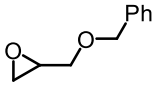

Compound **4a** (985 mg, 6.0 mmol) was synthesized from phenylmethanol (1.08 g, 10 mmol) according to the above Procedure A and obtained as a colorless oil. Yield: 60%. **^{1}H NMR (300 MHz, $CDCl_3$)** δ 7.42-7.27 (m, 5H), 4.69-4.50 (m, 2H), 3.77 (dd, *J* = 11.4, 3.1 Hz, 1H), 3.45 (dd, *J* = 11.4, 5.8 Hz, 1H), 3.19 (ddd, *J* = 7.0, 5.8, 2.9 Hz, 1H), 2.88-2.75 (m, 1H), 2.62 (dd, *J* = 5.0, 2.7 Hz, 1H).

2-((*p*-Tolyloxy)methyl)oxirane (**4c**)

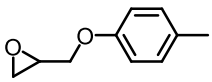

Compound **4c** (969 mg, 5.9 mmol) was synthesized from *p*-cresol (1.08 g, 10 mmol) according to the above Procedure A and obtained as a colorless oil. Yield: 59%. **^{1}H NMR (300 MHz, $CDCl_3$)** δ 7.08 (d, *J* = 8.4 Hz, 2H), 6.82 (d, *J* = 8.4 Hz, 2H), 4.18 (dd, *J* = 11.0, 3.2 Hz, 1H), 3.95 (dd, *J* = 11.0, 5.5 Hz, 1H), 3.35 (s, 1H), 2.90 (t, *J* = 4.5 Hz, 1H), 2.75 (dd, *J* = 4.9, 2.6 Hz, 1H), 2.29 (s, 3H).

2-((*m*-Tolyloxy)methyl)oxirane (**4d**)

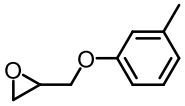

Compound **4d** (903 mg, 5.5 mmol) was synthesized from *m*-cresol (1.08 g, 10 mmol) according to the above Procedure A and obtained as a colorless oil. Yield: 55%. **^{1}H NMR (300 MHz, $CDCl_3$)** δ 7.17 (t, *J* = 7.7 Hz, 1H), 6.76 (dd, *J* = 17.8, 8.0 Hz, 3H), 4.19 (dd, *J* = 11.0, 3.3 Hz, 1H), 3.97 (dd, *J* = 11.0, 5.5 Hz, 1H), 3.35 (ddd, *J* = 8.7, 5.8, 3.3 Hz, 1H), 2.95-2.84 (m, 1H), 2.75 (dd, *J* = 5.0, 2.6 Hz, 1H), 2.33 (s, 3H).

2-((*o*-Tolyloxy)methyl)oxirane (**4e**)

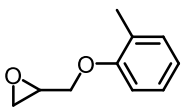

Compound **4e** (969 mg, 5.9 mmol) was synthesized from *o*-cresol (1.08 g, 10 mmol) according to the above Procedure A and obtained as a colorless oil. Yield: 59%. **^{1}H NMR (250 MHz, $CDCl_3$)** δ

7.22-7.08 (m, 2H), 6.93-6.75 (m, 2H), 4.23 (dd, *J* = 11.1, 3.1 Hz, 1H), 3.99 (dd, *J* = 11.1, 5.4 Hz, 1H), 3.38 (ddt, *J* = 5.6, 4.1, 3.0 Hz, 1H), 2.99-2.85 (m, 1H), 2.79 (dd, *J* = 5.0, 2.7 Hz, 1H), 2.26 (s, 3H).

2-((4-Methoxyphenoxy)methyl)oxirane (**4f**)

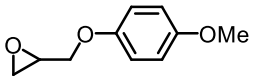

Compound **4f** (1.17 g, 6.5 mmol) was synthesized from 4-methoxyphenol (1.24 g, 10 mmol) according to the above Procedure A and obtained as a colorless oil. Yield: 65%. **^{1}H NMR (250 MHz, CDCl$_3$)** δ 6.97-6.73 (m, 4H), 4.17 (dd, *J* = 11.1, 3.3 Hz, 1H), 3.92 (dd, *J* = 11.1, 5.6 Hz, 1H), 3.77 (s, 3H), 3.42-3.27 (m, 1H), 2.98-2.83 (m, 1H), 2.74 (dd, *J* = 5.0, 2.7 Hz, 1H).

2-((4-Bromophenoxy)methyl)oxirane (**4j**)

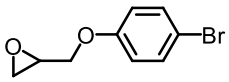

Compound **4j** (1.40 g, 6.1 mmol) was synthesized from 4-bromophenol (1.73 g, 10 mmol) according to the above Procedure A and obtained as a colorless oil. Yield: 61%. **^{1}H NMR (250 MHz, CDCl$_3$)** δ 7.46-7.30 (m, 2H), 6.90-6.73 (m, 2H), 4.21 (dd, *J* = 11.0, 3.0 Hz, 1H), 3.91 (dd, *J* = 11.0, 5.7 Hz, 1H), 3.34 (ddt, *J* = 5.7, 4.1, 2.9 Hz, 1H), 2.97-2.83 (m, 1H), 2.75 (dd, *J* = 4.9, 2.6 Hz, 1H).

2-((4-Chlorophenoxy)methyl)oxirane (**4h**)

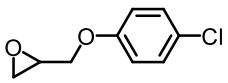

Compound **4h** (1.09 g, 5.9 mmol) was synthesized from 4-chlorophenol (1.29 g, 10 mmol) according to the above Procedure A and obtained as a colorless oil. Yield: 59%. **^{1}H NMR (300 MHz, CDCl$_3$)** δ 7.36-7.16 (m, 2H), 6.97-6.80 (m, 2H), 4.23 (dd, *J* = 11.0, 3.0 Hz, 1H), 3.94 (dd, *J* = 11.0, 5.7 Hz, 1H), 3.36 (ddd, *J* = 6.9, 5.8, 2.9 Hz, 1H), 2.93 (t, *J* = 4.5 Hz, 1H), 2.77 (dd, *J* = 4.9, 2.6 Hz, 1H).

2-((Naphthalen-2-yloxy)methyl)oxirane (**4i**)

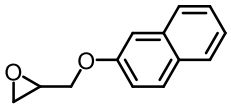

Compound **4i** (981 mg, 4.9 mmol) was synthesized from naphthalen-2-ol (1.44 g, 10 mmol) according to the above Procedure A and obtained as a colorless oil. Yield: 49%. **^{1}H NMR (300 MHz, $CDCl_3$)** δ 7.85-7.66 (m, 3H), 7.44 (dd, *J* = 11.0, 4.1 Hz, 1H), 7.35 (t, *J* = 6.9 Hz, 1H), 7.22-7.12 (m, 2H), 4.35 (dd, *J* = 11.0, 3.2 Hz, 1H), 4.09 (dd, *J* = 11.0, 5.7 Hz, 1H), 3.43 (dt, *J* = 9.8, 3.0 Hz, 1H), 3.01- 2.91 (m, 1H), 2.82 (dd, *J* = 4.9, 2.7 Hz, 1H).

2-(Phenethoxymethyl)oxirane (**4j**)

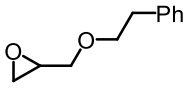

Compound **4j** (1.16 g, 6.5 mmol) was synthesized from 2-phenylethan-1-ol (1.22 g, 10 mmol) according to the above Procedure A and obtained as a colorless oil. Yield: 65%. **^{1}H NMR (250 MHz, $CDCl_3$)** δ 7.38-7.26 (m, 2H), 7.25-7.15 (m, 3H), 3.02-2.91 (m, 1H), 2.91-2.66 (m, 3H), 2.48 (dd, *J* = 5.0, 2.7 Hz, 1H), 2.01-1.73 (m, 2H).

2-((Benzhydryloxy)methyl)oxirane (**4k**)

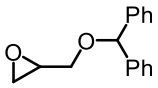

Compound **4k** (1.44 g, 6.0 mmol) was synthesized from diphenylmethanol (1.84 g, 10 mmol) according to the above Procedure A and obtained as a white solid. Yield: 60%. **^{1}H NMR (300 MHz, $CDCl_3$)** δ 7.47-7.20 (m, 10H), 5.48 (s, 1H), 3.76 (dd, *J* = 11.4, 3.1 Hz, 1H), 3.49 (dd, *J* = 11.4, 5.7 Hz, 1H), 3.24 (ddt, *J* = 5.7, 4.0, 3.0 Hz, 1H), 2.81 (dd, *J* = 5.0, 4.2 Hz, 1H), 2.63 (dd, *J* = 5.1, 2.7 Hz, 1H).

2-((Oxiran-2-ylmethoxy)methyl)furan (**4l**)

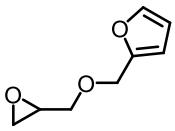

Compound **4l** (693 mg, 4.5 mmol) was synthesized from furan-2-ylmethanol (981 mg, 10 mmol) according to the above Procedure A and obtained as a colorless oil. Yield: 45%. **^{1}H NMR (300 MHz, $CDCl_3$)** δ 7.54-7.31 (m, 1H), 6.34 (s, 2H), 4.67-4.38 (m, 2H), 3.75 (dd, *J* = 11.5, 3.1 Hz, 1H), 3.44 (dd, *J* = 11.5, 5.8 Hz, 1H), 3.16 (ddd, *J* = 7.0, 5.9, 3.0 Hz, 1H), 2.90-2.71 (m, 1H), 2.61 (dd, *J* = 5.0, 2.7 Hz, 1H).

2-((Thiophen-2-ylmethoxy)methyl)oxirane (**4m**)

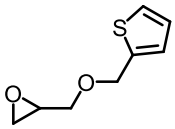

Compound **4m** (953 mg, 5.6 mmol) was synthesized from thiophen-2-ylmethanol (1.14 g, 10 mmol) according to the above Procedure A and obtained as a colorless oil. Yield: 56%. **^{1}H NMR (250 MHz, $CDCl_3$)** δ 7.30 (dd, *J* = 5.0, 1.3 Hz, 1H), 7.00 (ddd, *J* = 8.4, 3.9, 2.0 Hz, 2H), 4.87-4.61 (m, 2H), 3.77 (dd, *J* = 11.4, 3.1 Hz, 1H), 3.45 (dd, *J* = 11.4, 5.8 Hz, 1H), 3.18 (ddt, *J* = 5.8, 4.1, 2.9 Hz, 1H), 2.89-2.76 (m, 1H), 2.62 (dd, *J* = 5.0, 2.7 Hz, 1H).

2-Phenethyloxirane (**4o**)

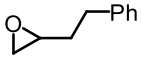

Compound **4o** (934 mg, 6.3 mmol) was synthesized from but-3-en-1-ylbenzene (1.32 g, 10 mmol) according to the above Procedure B and obtained as a colorless oil. Yield: 63%. **^{1}H NMR (250 MHz, $CDCl_3$)** δ 7.38-.26 (m, 2H), 7.25-7.15 (m, 3H), 3.02-2.91 (m, 1H), 2.91-2.66 (m, 3H), 2.48 (dd, *J* = 5.0, 2.7 Hz, 1H), 2.01-1.73 (m, 2H).

2-Benzyloxirane (**4r**)

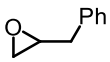

Compound **4r** (671 mg, 5.0 mmol) was synthesized from allylbenzene (1.18 g, 10 mmol) according to the above Procedure B and obtained as a colorless oil. Yield: 50%. **^{1}H NMR (250 MHz, $CDCl_3$)** δ 7.38-7.20 (m, 5H), 3.17 (tdd, *J* = 5.5, 3.9, 2.7 Hz, 1H), 3.00-2.76 (m, 3H), 2.56 (dd, *J* = 5.0, 2.7 Hz, 1H).

2-(4-Methoxybenzyl)oxirane (4s)

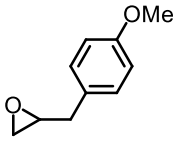

Compound **4s** (969 mg, 5.9 mmol) was synthesized from 1-allyl-4-methoxybenzene (1.48 g, 10 mmol) according to the above Procedure B and obtained as a colorless oil. Yield: 59%. **^{1}H NMR (250 MHz, $CDCl_3$)** δ 7.23-7.11 (m, 2H), 6.93-6.79 (m, 2H), 3.80 (s, 3H), 3.12 (tdd, *J* = 5.5, 3.9, 2.7 Hz, 1H), 2.96-2.70 (m, 3H), 2.53 (dd, *J* = 5.0, 2.7 Hz, 1H).

5.2.3 Ir-Catalyzed Kinetic Resolution of Epoxides with CO_2

A 1.5 mL glass vial with stirrer bar was charged with the Et_4NBr (0.9 mg, 0.0045 mmol, 1.5 mol%), Λ-**IrO(Carb)** (3.8 mg, 0.003 mmol, 1.0 mol%), the corresponding epoxide (0.3 mmol, 1.0 equiv) and 1,4-dioxane (86 μL, 3.5 M). The glass vial was placed into a 300 mL stainless steel autoclave with suitable stainless steel module. The autoclave was closed and then subjected to three cycles of pressurization and depressurization with carbon dioxide, before final stabilization of the pressure to 20 bar. The autoclave was left stirring at room temperature for 30 hours. At the end of the reaction an aliquot of the resulting mixture was taken and the conversion was determined by means of ^{1}H NMR spectroscopy using $CDCl_3$ as the solvent. The analytically pure cyclic carbonate product was isolated by column chromatography, and then analysed by chiral HPLC or chiral GC to determine the enantiomeric excess.

(*R*)-4-((Benzyloxy)methyl)-1,3-dioxolan-2-one (5a)[2a]

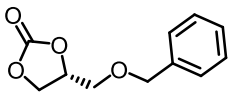

Starting from **4a** (49.2 mg, 0.3 mmol) according to the general procedure to give **5a** in 14% conversion. Enantiomeric excess was determined by HPLC analysis on a chiral stationary phase, ee = 81%. HPLC conditions: Chiralpak OD-H column (4.6 × 250 mm), UV detection at 216 nm, mobile phase *n*-hexane/isopropanol = 80:20, flow rate 1.0 mL/min, column temperature = 25 ℃, t_r (minor) = 17.3 min, t_r (major) = 22.3 min.

^{1}H NMR (300 MHz, $CDCl_3$) δ 7.42-7.27 (m, 5H), 4.86-4.76 (m, 1H), 4.62 (d, *J* = 12.0 Hz, 1H), 4.56 (d, *J* = 12.0 Hz, 1H), 4.48 (t, *J* = 8.3 Hz, 1H), 4.38 (dd, *J* = 8.3, 6.1 Hz, 1H), 3.71 (dd, *J* = 10.9, 4.0 Hz, 1H), 3.71 (dd, *J* = 10.9, 3.8 Hz, 1H) ppm.

^{13}C NMR (75 MHz, $CDCl_3$) δ 155.0, 137.2, 128.7, 128.2, 127.9, 75.1, 73.9, 69.0, 66.4 ppm.

(*R*)-4-(Phenoxymethyl)-1,3-dioxolan-2-one (5b)[2a]

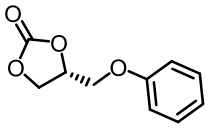

Starting from **4b** (45.0 mg, 0.3 mmol) according to the general procedure to give **5b** in 20% conversion. Enantiomeric excess was determined by HPLC analysis on a chiral stationary phase, ee = 82%. HPLC conditions: Chiralpak OD-H column (4.6 × 250 mm), UV detection at 216 nm, mobile phase *n*-hexane/isopropanol = 80:20, flow rate 1.0 mL/min, column temperature = 25 ℃, t_r (minor) = 24.0 min, t_r (major) = 31.8 min.

^{1}H NMR (300 MHz, $CDCl_3$) δ 7.35-7.26 (m, 2H), 7.02 (t, *J* = 7.4 Hz, 1H), 6.91 (d, *J* = 7.8 Hz, 2H), 5.07-4.97 (m, 1H), 4.65-4.57 (m, 1H), 4.56-4.49 (m, 1H), 4.24 (dd, *J* = 10.6, 4.2 Hz, 1H), 4.14 (dd, *J* = 10.6, 3.6 Hz, 1H) ppm.

^{13}C NMR (75 MHz, $CDCl_3$) δ 157.9, 154.8, 129.8, 122.1, 114.8, 74.3, 67.1, 66.4 ppm.

(*R*)-4-((*p*-Tolyloxy)methyl)-1,3-dioxolan-2-one (5c)[2b]

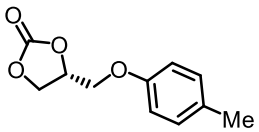

Starting from **4c** (49.2 mg, 0.3 mmol) according to the general procedure to give **5c** in 20% conversion. Enantiomeric excess was determined by HPLC analysis on a chiral stationary phase, ee = 82%. HPLC conditions: Chiralpak OD-H column (4.6 × 250 mm), UV detection at 216 nm, mobile phase *n*-hexane/isopropanol = 80:20, flow rate 1.0 mL/min, column temperature = 25 ℃, t_r (minor) = 16.1 min, t_r (major) = 29.6 min.

^{1}H NMR (300 MHz, $CDCl_3$) δ 7.15-7.05 (m, 2H), 6.85-6.77 (m, 2H), 5.06-4.95 (m, 1H), 4.65-4.48 (m, 2H), 4.22 (dd, *J* = 10.6, 4.3 Hz, 1H), 4.12 (dd, *J* = 10.6, 3.7 Hz, 1H), 2.29 (s, 3H).

^{13}C NMR (75 MHz, $CDCl_3$) δ 155.9, 154.8, 131.5, 130.3, 114.7, 74.3, 67.3, 66.4, 20.6.

(*R*)-4-((*m*-Tolyloxy)methyl)-1,3-dioxolan-2-one (5d)[2b]

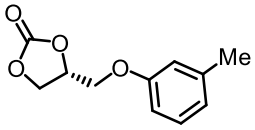

Starting from **4d** (49.2 mg, 0.3 mmol) according to the general procedure to give **5d** in 20% conversion. Enantiomeric excess was determined by HPLC analysis on a chiral stationary phase, ee = 82%. HPLC conditions: Chiralpak OD-H column (4.6 × 250 mm), UV detection at 216 nm, mobile phase *n*-hexane/isopropanol = 80:20, flow rate 1.0 mL/min, column temperature = 25 ℃, t_r (minor) = 18.2 min, t_r (major) = 28.1 min.

^{1}H NMR (300 MHz, $CDCl_3$) δ 7.18 (t, *J* = 7.8 Hz, 1H), 6.83 (d, *J* = 7.5 Hz, 1H), 6.76-6.67 (m, 2H), 5.06-4.95 (m, 1H), 4.64-4.48 (m, 2H), 4.21 (dd, *J* = 10.7, 4.2 Hz, 1H), 4.12 (dd, *J* = 10.7, 3.7 Hz, 1H), 2.33 (s, 3H) ppm.

^{13}C NMR (75 MHz, $CDCl_3$) δ 157.9, 154.8, 140.0, 129.5, 122.9, 115.7, 111.5, 74.3, 67.0, 66.4, 21.6 ppm.

(*R*)-4-((*o*-Tolyloxy)methyl)-1,3-dioxolan-2-one (5e)[2b]

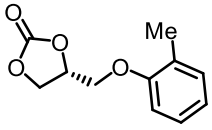

Starting from **4e** (49.2 mg, 0.3 mmol) according to the general procedure to give **5e** in 12% conversion. Enantiomeric excess was determined by HPLC analysis on a chiral stationary phase, ee = 80%. HPLC

conditions: Chiralpak OD-H column (4.6 × 250 mm), UV detection at 216 nm, mobile phase *n*-hexane/isopropanol = 80:20, flow rate 1.0 mL/min, column temperature = 25 ℃, t_r (minor) = 22.5 min, t_r (major) = 24.2 min.

^{1}H NMR (300 MHz, $CDCl_3$) δ 7.21-7.12 (m, 2H), 6.92 (t, *J* = 7.5 Hz, 1H), 6.82-6.75 (m, 1H), 5.09-5.00 (m, 1H), 4.67-4.52 (m, 2H), 4.26 (dd, *J* = 10.7, 3.6 Hz, 1H), 4.13 (dd, *J* = 10.7, 3.1 Hz, 1H), 2.22 (s, 3H) ppm.

^{13}C NMR (75 MHz, $CDCl_3$) δ 155.9, 154.9, 131.2, 127.3, 127.0, 121.8, 111.1, 74.3, 67.2, 66.4, 16.1.

(*R*)-4-((4-Methoxyphenoxy)methyl)-1,3-dioxolan-2-one (5f)[2b]

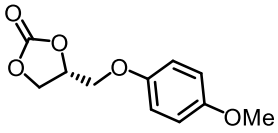

Starting from **4f** (54.0 mg, 0.3 mmol) according to the general procedure to give **5f** in 17% conversion. Enantiomeric excess was determined by HPLC analysis on a chiral stationary phase, ee = 80%. HPLC conditions: Chiralpak OD-H column (4.6 × 250 mm), UV detection at 216 nm, mobile phase *n*-hexane/isopropanol = 70:30, flow rate 1.0 mL/min, column temperature = 25 ℃, t_r (minor) = 15.1 min, t_r (major) = 27.0 min.

^{1}H NMR (300 MHz, $CDCl_3$) δ 6.90-6.78 (m, 4H), 5.04-4.93 (m, 1H), 4.63-4.47 (m, 2H), 4.18 (dd, *J* = 10.7, 4.1 Hz, 1H), 4.09 (dd, *J* = 10.7, 3.6 Hz, 1H), 3.76 (s, 3H) ppm.

^{13}C NMR (75 MHz, $CDCl_3$) δ 154.9, 154.8, 152.1, 116.0, 114.9, 74.4, 68.0, 66.3, 55.8 ppm.

(*R*)-4-((4-Bromophenoxy)methyl)-1,3-dioxolan-2-one (5g)[2c]

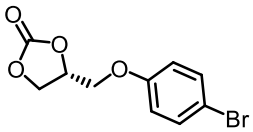

Starting from **4g** (68.7 mg, 0.3 mmol) according to the general procedure to give **5g** in 24% conversion. Enantiomeric excess was determined by HPLC analysis on a chiral stationary phase, ee = 80%. HPLC conditions: Chiralpak OD-H column (4.6 × 250 mm), UV detection at 216 nm, mobile phase *n*-hexane/isopropanol = 80:20, flow rate 1.0 mL/min, column temperature = 25 ℃, t_r (minor) = 19.4 min, t_r (major) = 24.0 min.

^{1}H NMR (300 MHz, $CDCl_3$) δ 7.47-7.34 (m, 2H), 6.85-6.75 (m, 2H), 5.07-4.96 (m, 1H), 4.62 (t, *J* = 8.5 Hz, 1H), 4.51 (dd, *J* = 8.6, 5.9 Hz, 1H), 4.21 (dd, *J* = 10.6, 4.1 Hz, 1H), 4.11 (dd, *J* = 10.6, 3.6 Hz, 1H) ppm.

^{13}C NMR (75 MHz, $CDCl_3$) δ = 157.0, 154.6, 132.7, 116.6, 114.5, 74.1, 67.4, 66.2 ppm.

(*R*)-4-((4-Chlorophenoxy)methyl)-1,3-dioxolan-2-one (5h)[2c]

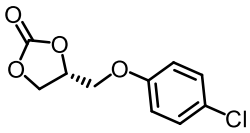

Starting from **4h** (55.4 mg, 0.3 mmol) according to the general procedure to give **5h** in 23% conversion. Enantiomeric excess was determined by HPLC analysis on a chiral stationary phase, ee = 78%. HPLC conditions: Chiralpak OD-H column (4.6 × 250 mm), UV detection at 216 nm, mobile phase *n*-hexane/isopropanol = 80:20, flow rate 1.0 mL/min, column temperature = 25 ℃, t_r (minor) = 18.6 min, t_r (major) = 22.5 min.

^{1}H NMR (300 MHz, $CDCl_3$) δ 7.30-7.22 (m, 2H), 6.88-6.80 (m, 2H), 5.06-4.97 (m, 1H), 4.61 (t, *J* = 8.5 Hz, 1H), 4.51 (dd, *J* = 8.6, 5.9 Hz, 1H), 4.21 (dd, *J* = 10.6, 4.0 Hz, 1H), 4.11 (dd, *J* = 10.6, 3.6 Hz, 1H) ppm.

^{13}C NMR (75 MHz, $CDCl_3$) δ 156.5, 154.6, 129.8, 127.2, 116.1, 74.1, 67.5, 66.2.

(*R*)-4-((Naphthalen-2-yloxy)methyl)-1,3-dioxolan-2-one (5i)[2b]

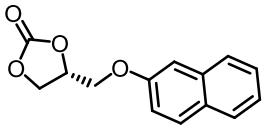

Starting from **4i** (60.0 mg, 0.3 mmol) according to the general procedure to give **5i** in 22% conversion. Enantiomeric excess was determined by HPLC analysis on a chiral stationary phase, ee = 80%. HPLC conditions: Chiralpak IG column (4.6 × 250 mm), UV detection at 254 nm, mobile phase *n*-hexane/isopropanol = 80:20, flow rate 1.0 mL/min, column temperature = 25 ℃, t_r (minor) = 20.1 min, t_r (major) = 21.3 min.

^{1}H NMR (300 MHz, $CDCl_3$) δ 7.85-7.68 (m, 3H), 7.51-7.43 (m, 1H), 7.42-7.34 (m, 1H), 7.20-7.10 (m, 2H), 5.15-5.04 (m, 1H), 4.71-4.54 (m, 2H), 4.36 (dd, *J* = 10.6, 4.3 Hz, 1H), 4.27 (dd, *J* = 10.6, 3.7

Hz, 1H) ppm.

^{13}C NMR (75 MHz, $CDCl_3$) δ 155.9, 154.7, 134.4, 130.0, 129.7, 127.9, 127.0, 126.9, 124.5, 118.5, 107.3, 74.2, 67.1, 66.4 ppm.

(*R*)-4-(Phenethoxymethyl)-1,3-dioxolan-2-one (5j)

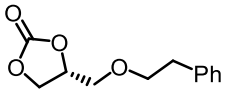

Starting from **4j** (53.4 mg, 0.3 mmol) according to the general procedure (70 h was used instead) to give **5j** in 16% conversion. Enantiomeric excess was determined by HPLC analysis on a chiral stationary phase, ee = 82%. HPLC conditions: Chiralpak OD-H column (4.6 × 250 mm), UV detection at 216 nm, mobile phase *n*-hexane/isopropanol = 80:20, flow rate 1.0 mL/min, column temperature = 25 ℃, t_r (minor) = 15.4 min, t_r (major) = 19.7 min.

^{1}H NMR (300 MHz, $CDCl_3$) δ 7.34-7.26 (m, 2H), 7.25-7.17 (m, 3H), 4.81-4.70 (m, 1H), 4.42 (t, *J* = 8.3 Hz, 1H), 4.29 (dd, *J* = 8.3, 6.1 Hz, 1H), 3.81-3.64 (m, 3H), 3.58 (dd, *J* = 11.0, 3.6 Hz, 1H), 2.89 (t, *J* = 6.8 Hz, 2H) ppm.

^{13}C NMR (75 MHz, $CDCl_3$) δ 155.0, 138.6, 129.0, 128.5, 126.5, 75.1, 72.9, 69.9, 66.3, 36.3 ppm.

IR (film): *v* (cm^{-1}) 2922, 2863, 1787, 1486, 1455, 1393, 1362, 1167, 1128, 1105, 1045, 749, 701, 576, 499.

HRMS (ESI, *m/z*) calcd. for $C_{12}H_{14}O_4Na$ $[M+Na]^+$: 245.0784, found: 245.0780.

(*R*)-4-((Benzhydryloxy)methyl)-1,3-dioxolan-2-one (5k)

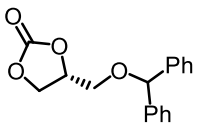

Starting from **4k** (72.2 mg, 0.3 mmol) according to the general procedure (70 h was used instead) to give **5k** in 12% conversion. Enantiomeric excess was determined by HPLC analysis on a chiral stationary phase, ee = 82%. HPLC conditions: Chiralpak OD-H column (4.6 × 250 mm), UV detection at 216 nm, mobile phase *n*-hexane/isopropanol = 80:20, flow rate 1.0 mL/min, column temperature = 25 ℃, t_r (minor) = 24.2 min, t_r (major) = 35.9 min.

^{1}H NMR (300 MHz, $CDCl_3$) δ 7.38-7.25 (m, 10H), 5.42 (s, 1H), 4.90-4.78 (m, 1H), 4.57-4.39 (m, 2H), 3.74 (dd, *J* = 10.9, 3.9 Hz, 1H), 3.61 (dd, *J* = 10.8, 3.6 Hz, 1H) ppm.

^{13}C NMR (75 MHz, $CDCl_3$) δ 155.0, 141.3, 141.2, 128.8, 128.7, 128.1, 128.0, 127.1, 127.0, 84.6, 75.1, 68.0, 66.5 ppm.

IR (film): *v* (cm^{-1}) 2925, 2873, 1779, 1486, 1452, 1393, 1331, 1168, 1124, 1097, 1033, 973, 919, 845, 793, 747, 696, 656, 625, 593, 524, 469.

HRMS (ESI, *m/z*) calcd. for $C_{17}H_{16}O_4Na[M+ Na]^+$: 307.0941, found: 307.0934.

(*R*)-4-((Furan-2-ylmethoxy)methyl)-1,3-dioxolan-2-one (5l)[2d]

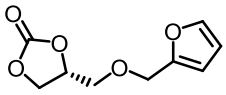

Starting from **4l** (46.2 mg, 0.3 mmol) according to the general procedure to give **5l** in 13% conversion. Enantiomeric excess was determined by HPLC analysis on a chiral stationary phase, ee = 74%. HPLC conditions: Chiralpak OD-H column (4.6 × 250 mm), UV detection at 216 nm, mobile phase *n*-hexane/isopropanol = 80:20, flow rate 1.0 mL/min, column temperature = 25 ℃, t_r (minor) = 14.7 min, t_r (major) = 15.8 min.

^{1}H NMR (300 MHz, $CDCl_3$) δ 7.47-7.38 (m, 1H), 6.42-6.30 (m, 2H), 4.84-4.73 (m, 1H), 4.61-4.42 (m, 3H), 4.34 (dd, *J* = 8.4, 6.2 Hz, 1H), 3.70 (dd, *J* = 10.9, 4.4 Hz, 1H), 3.64 (dd, *J* = 10.9, 3.9 Hz, 1H) ppm.

^{13}C NMR (75 MHz, $CDCl_3$) δ 154.9, 150.8, 143.3, 110.5, 110.2, 75.0, 68.6, 66.4, 65.4 ppm.

(*R*)-4-((Thiophen-2-ylmethoxy)methyl)-1,3-dioxolan-2-one (5m)

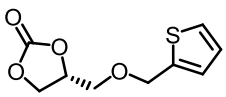

Starting from **4m** (51.0 mg, 0.3 mmol) according to the general procedure to give **5m** in 11% conversion. Enantiomeric excess was determined by HPLC analysis on a chiral stationary phase, ee = 76%. HPLC conditions: Chiralpak OD-H column (4.6 × 250 mm), UV detection at 216 nm, mobile phase *n*-hexane/isopropanol = 80:20, flow rate 1.0 mL/min, column temperature = 25 ℃, t_r (minor) = 19.4 min, t_r (major) = 22.3 min.

^{1}H NMR (300 MHz, $CDCl_3$) δ 7.32 (dd, J = 4.9, 1.4 Hz, 1H), 7.06-6.95 (m, 2H), 4.85-4.68 (m, 3H), 4.47 (t, J = 8.3 Hz, 1H), 4.36 (dd, J = 8.4, 6.1 Hz, 1H), 3.70 (dd, J = 10.8, 4.2 Hz, 1H), 3.63 (dd, J = 10.8, 3.8 Hz, 1H) ppm.

^{13}C NMR (75 MHz, $CDCl_3$) δ 154.9, 139.7, 127.3, 127.0, 126.6, 75.0, 68.4, 68.1, 66.4 ppm.

IR (film): ν (cm^{-1}) 2918, 2857, 1786, 1392, 1360, 1166, 1098, 1040, 845, 771, 710.

HRMS (ESI, *m/z*) calcd. for $C_9H_{10}O_4SNa$ $[M+Na]^+$: 237.0192, found: 237.0149.

(*R*)-(2-Oxo-1,3-dioxolan-4-yl)methyl benzoate (5n)[2c]

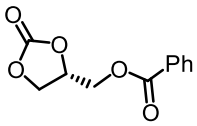

Starting from **4n** (53.4 mg, 0.3 mmol) according to the general procedure to give **5n** in 15% conversion. Enantiomeric excess was determined by HPLC analysis on a chiral stationary phase, ee = 74%. HPLC conditions: Chiralpak OD-H column (4.6 × 250 mm), UV detection at 216 nm, mobile phase *n*-hexane/isopropanol = 80:20, flow rate 1.0 mL/min, column temperature = 25 ℃, t_r (minor) = 17.2 min, t_r (major) = 19.1 min.

^{1}H NMR (300 MHz, $CDCl_3$) δ 8.06-7.98 (m, 2H), 7.64-7.56 (m, 1H), 7.51-7.42 (m, 2H), 5.11-5.00 (m, 1H), 4.67-4.55 (m, 2H), 4.51 (dd, J = 12.6, 3.9 Hz, 1H), 4.42 (dd, J = 8.8, 5.7 Hz, 1H) ppm.

^{13}C NMR (75 MHz, $CDCl_3$) δ 166.1, 154.6, 133.9, 129.9, 128.9, 128.8, 74.0, 66.2, 63.8 ppm.

(*R*)-4-Phenethyl-1,3-dioxolan-2-one (5o)[2e]

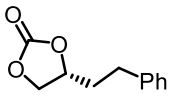

Starting from **4o** (29.6 mg, 0.2 mmol) according to the general procedure (reaction time is 70 h) to give **5o** in 12% conversion. Enantiomeric excess was determined by HPLC analysis on a chiral stationary phase, ee = 78%. HPLC conditions: Chiralpak OD-H column (4.6 × 250 mm), UV detection at 216 nm, mobile phase *n*-hexane/isopropanol = 80:20, flow rate 1.0 mL/min, column temperature = 25 ℃, t_r (minor) = 21.5 min, t_r (major) = 24.2 min.

^{1}H NMR (300 MHz, $CDCl_3$) δ 7.36-7.16 (m, 5H), 4.73-4.62 (m, 1H), 4.47 (t, J = 8.1 Hz, 1H), 4.04

(dd, *J* = 8.4, 7.2 Hz, 1H), 2.93-2.81 (m, 1H), 2.80-2.68 (m, 1H), 2.23-2.09 (m, 1H), 2.05-1.91 (m, 1H) ppm.

^{13}C NMR (75 MHz, $CDCl_3$) δ 155.0, 139.8, 128.9, 128.6, 126.7, 76.1, 69.4, 35.8, 31.0 ppm.

(*S*)-4-Butyl-1,3-dioxolan-2-one (5p)[2a]

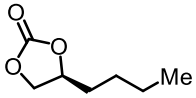

Starting from **4p** (21.5 µL, 0.2 mmol) according to the general procedure (1 mol% **Δ-IrO(Carb)**, 2 mol% *n*Bu_4NBr and 45 h were used instead) to give **5p** in 25% conversion. Enantiomeric excess was determined by GC analysis on a chiral stationary phase, ee = 74%. GC conditions: BGB column (30 m × 0.25 mm), column temperature 115 °C, isothermal, t_r (minor) = 12.1 min, t_r (major) = 12.4 min.

^{1}H NMR (300 MHz, $CDCl_3$) δ 4.70 (ddd, *J* = 14.8, 7.4, 5.5 Hz, 1H), 4.52 (t, *J* = 8.1 Hz, 1H), 4.07 (dd, *J* = 8.3, 7.2 Hz, 1H), 1.90-1.60 (m, 2H), 1.50-1.29 (m, 4H), 0.93 (dd, *J* = 8.8, 5.3 Hz, 3H) ppm.

^{13}C NMR (75 MHz, $CDCl_3$) δ 155.2, 69.5, 33.8, 26.6, 22.4, 13.9 ppm.

(*S*)-4-Ethyl-1,3-dioxolan-2-one (5q)[2a]

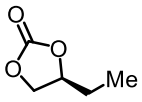

Starting from **4q** (26.1 µL, 0.3 mmol) according to the general procedure (1 mol% **Δ-IrO(Carb)**, 2 mol% *n*Bu_4NBr and 45 h were used instead) to give **5q** in 23% conversion. Enantiomeric excess was determined by GC analysis on a chiral stationary phase, ee = 68%. GC conditions: BGB column (30 m × 0.25 mm), column temperature 110 °C, isothermal, t_r (minor) = 5.6 min, t_r (major) = 5.7 min.

^{1}H NMR (300 MHz, $CDCl_3$) δ 4.65 (dt, *J* = 13.5, 7.0 Hz, 1H), 4.51 (t, *J* = 8.1 Hz, 1H), 4.07 (dd, *J* = 8.3, 7.0 Hz, 1H), 1.88-1.67 (m, 2H), 1.02 (t, *J* = 7.4 Hz, 3H) ppm.

^{13}C NMR (75 MHz, $CDCl_3$) δ 155.2, 78.1, 69.1, 27.1, 8.6 ppm.

(*S*)-4-Benzyl-1,3-dioxolan-2-one (5r)[2f]

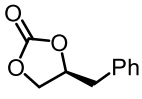

Starting from **4q** (26.8 mg, 0.2 mmol) according to the general procedure (1 mol% **Δ-IrO(Carb)**, 2 mol% *n*Bu_4NBr and 45 h were used instead) to give **5q** in 21% conversion. Enantiomeric excess was determined by HPLC analysis on a chiral stationary phase, ee = 86%. HPLC conditions: Chiralpak OD-H column (4.6 × 250 mm), UV detection at 216 nm, mobile phase *n*-hexane/isopropanol = 80:20, flow rate 1.0 mL/min, column temperature = 25 ℃, t_r (minor) = 18.7 min, t_r (major) = 20.1 min.

^{1}H NMR (300 MHz, $CDCl_3$) δ 7.41-7.27 (m, 3H), 7.25-7.19 (dd, *J* = 7.6, 1.7 Hz, 2H), 4.93 (td, *J* = 13.5, 6.7 Hz, 1H), 4.50-4.39 (m, 1H), 4.17 (dd, *J* = 8.6, 6.9 Hz, 1H), 3.17 (dd, *J* = 14.2, 6.2 Hz, 1H), 2.99 (dd, *J* = 14.2, 6.7 Hz, 1H) ppm.

^{13}C NMR (75 MHz, $CDCl_3$) δ 154.9, 134.0, 129.5, 129.2, 127.8, 77.0, 68.6, 39.8 ppm.

(*S*)-4-(4-Methoxybenzyl)-1,3-dioxolan-2-one (5s)

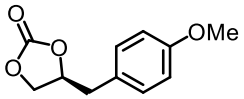

Starting from **4s** (32.8 mg, 0.2 mmol) according to the general procedure (1 mol% **Δ-IrO(Carb)**, 2 mol% *n*Bu_4NBr and 45 h were used instead) to give **5s** in 40% conversion. Enantiomeric excess was determined by HPLC analysis on a chiral stationary phase, ee = 80%. HPLC conditions: Chiralpak OD-H column (4.6 × 250 mm), UV detection at 216 nm, mobile phase *n*-hexane/isopropanol = 80:20, flow rate 1.0 mL/min, column temperature = 25 ℃, t_r (minor) = 15.7 min, t_r (major) = 18.0 min.

^{1}H NMR (300 MHz, $CDCl_3$) δ 7.13 (d, *J* = 8.5 Hz, 2H), 6.87 (d, *J* = 8.6 Hz, 2H), 4.98-4.81 (m, 1H), 4.42 (t, *J* = 8.2 Hz, 1H), 4.15 (dd, *J* = 8.5, 7.0 Hz, 1H), 3.79 (s, 3H), 3.08 (dd, *J* = 14.3, 6.0 Hz, 1H), 2.93 (dd, *J* = 14.3, 6.6 Hz, 1H) ppm.

^{13}C NMR (75 MHz, $CDCl_3$) δ 159.2, 154.9, 130.6, 125.8, 114. 6, 77.1, 68.5, 55.4, 38.8 ppm.

HRMS (ESI, *m/z*) calcd. for $C_{11}H_{12}O_4Na$ $[M+Na]^+$: 231.0628, found: 231.0625.

(*R*)-4-(Chloromethyl)-1,3-dioxolan-2-one (5t)[2a]

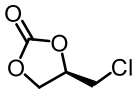

Starting from **4r** (23.6 μL, 0.3 mmol) according to the general procedure (1 mol% **Δ-IrO(Carb)**, 2 mol% *n*Bu_4NBr and 45 h were used instead) to give **5r** in 40% conversion. Enantiomeric excess was

determined by GC analysis on a chiral stationary phase, ee = 70%. GC conditions: BGB column (30 m × 0.25 mm), column temperature 110 °C, isothermal, t_r (minor) = 12.8 min, t_r (major) = 13.0 min.

^{1}H NMR (300 MHz, $CDCl_3$) δ 4.96 (dtd, J = 8.2, 5.6, 4.3 Hz, 1H), 4.59 (t, J = 8.5 Hz, 1H), 4.41 (dd, J = 8.9, 5.8 Hz, 1H), 3.85-3.67 (m, 2H) ppm.

^{13}C NMR (75 MHz, $CDCl_3$) δ 154.2, 74.3, 67.1, 43.7 ppm.

(*R*)-4-Phenyl-1,3-dioxolan-2-one (5v)[2a]

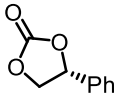

Starting from **4v** (24.0 mg, 0.20 mmol) according to the general procedure (reaction time was 70 h) to give **5v** as a white solid in 10% conversion. Enantiomeric excess was determined by HPLC analysis on a chiral stationary phase, ee = 74%. HPLC conditions: Chiralpak OD-H column (4.6 × 250 mm), UV detection at 216 nm, mobile phase *n*-hexane/isopropanol = 80:20, flow rate 1.0 mL/min, column temperature = 25 ℃, t_r (minor) = 13.0 min, t_r (major) = 15.7 min.

^{1}H NMR (300 MHz, $CDCl_3$) δ 7.48-7.41 (m, 3H), 7.40-7.33 (m, 2H), 5.67 (t, J = 8.0 Hz, 1H), 4.80 (t, J = 8.4 Hz, 1H), 4.38-4.30 (m, 1H) ppm.

^{13}C NMR (75 MHz, $CDCl_3$) δ 154.9, 136.0, 129.9, 129.4, 126.0, 78.1, 71.3 ppm.

5.2.4 Reaction of *n*Bu_4NBr with Iridium Catalyst Λ-IrO(Carb)

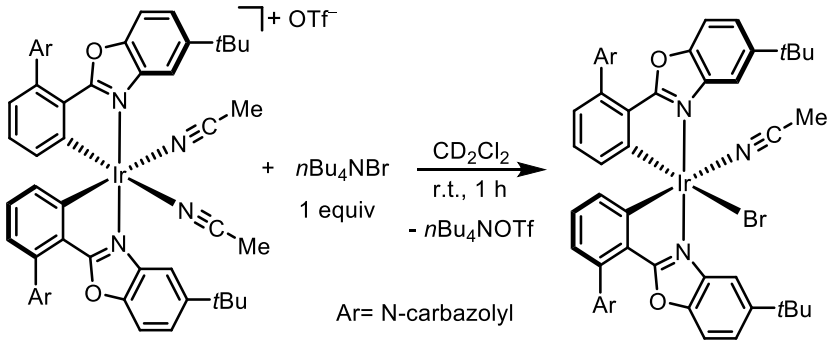

A NMR tube was charged with iridium catalyst Λ-**IrO(Carb)** (20 mg, 0.016 mmol), *n*Bu_4NBr (5.2 mg, 0.016 mmol, 1 equiv) and CD_2Cl_2 (0.5 mL). The mixture was left at room temperature for 1 h, and then analyzed by ^{1}H NMR. See the change of the corresponding spectrum below. Free acetonitrile signal could be clearly observed after mixing iridium catalyst Λ-**IrO(Carb)** and *n*Bu_4NBr**,** which

might result from the coordination of bromide to the iridium metal center.

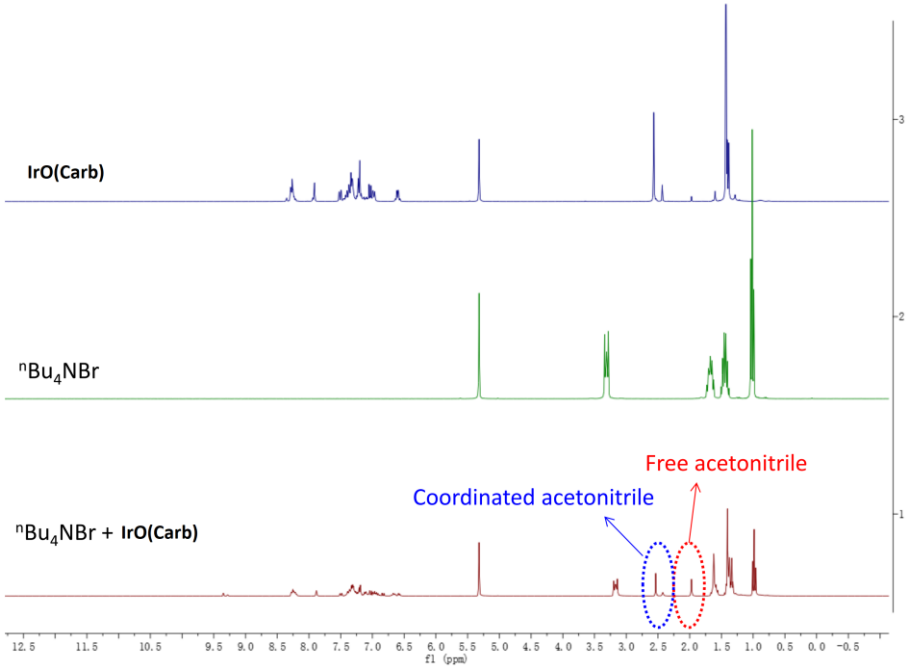

5.2.5 Single Crystal X-Ray Diffraction Study of Δ-IrO(Carb)

Crystals of **Δ-IrO(Carb)** was obtained by slow diffusion from a solution of the compound in CH_2Cl_2 layered with *n*-hexane at room temperature for several days.

Crystal data and details of the structure determination are presented in Table 10. Data was collected with an STOE STADIVARI diffractometer equipped with with CuK_a radiation, a graded multilayer mirror monochromator (l = 1.54178 Å) and a DECTRIS PILATUS 300K detector using an oil-coated shock-cooled crystal at 100(2) K. Absorption effects were corrected semi-empirical using multiscanned reflexions (STOE LANA, absorption correction by scaling of reflection intensities.). Cell constants were refined using 522626 of observed reflections of the data collection. The structure was solved by direct methods by using the program XT V2014/1 (Bruker AXS Inc., 2014) and refined by full matrix least squares procedures on F^2 using SHELXL-2018/3 (Sheldrick, 2018). The non-hydrogen atoms have been refined anisotropically, carbon bonded hydrogen atoms were included at calculated positions and refined using the 'riding model' with isotropic temperature factors at 1.2 times (for CH_3 groups 1.5 times) that of the preceding carbon atom. CH_3 groups were allowed to rotate

about the bond to their next atom to fit the electron density. Nitrogen or oxygen bonded hydrogen atoms were located and allowed to refine isotropically.

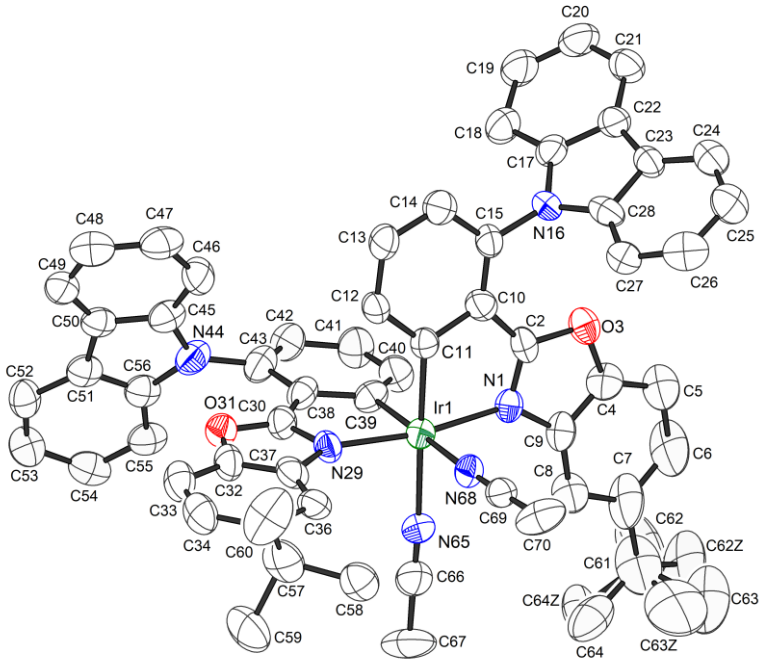

Figure 37. Crystal structure of **Δ-IrO(Carb)**. ORTEP drawing with 50% probability thermal ellipsoids.

Table 10 Crystal data and details of the structure determination of **Δ-IrO(Carb)**.

Empiric formula	$C_{67}H_{60}Cl_8F_3IrN_6O_5S$
Formula weight	1594.07
Crystal system, space group	Tetragonal, $P4_1$
a, *b*, *c* (Å)	27.8771(1), 27.8771(1), 38.0822(2)
α, β, γ (°)	90, 90, 90
V (Å^3)	29594.9(3)
Z	16
Crystal size (mm)	0.30 x 0.20 x 0.10
Data collection software	X-Area Pilatus3_SV 1.31.127.0 (STOE, 2016)[3]
Cell refinement software	X-Area Recipe 1.33.0.0 (STOE, 2015)[4]
Data reduction software	X-Area Integrate 1.71.0.0 (STOE, 2016)[5] X-Area LANA 1.68.2.0 (STOE, 2016)[6]
T_{max}, T_{min}	0.2441, 0.0522
No. of measured, independent and observed [$I > 2\ (I)$] reflections	503295, 60310, 57821
R_{int}	0.0436
$R[F^2 > 2\ (F^2)]$, $wR(F^2)$, S	0.0579, 0.1582, 1.054
No. of used reflections	60310
No. of parameters	3459
No. of restraints	2130
ρ_{max}, ρ_{min} (e Å^{-3})	4.366, -1.393
Absolute structure parameter	0.012(4)[7]
Programs used	XT V2014/1 (Bruker AXS Inc., 2014)[8] SHELXL-2018/3 (Sheldrick, 2018)[9] DIAMOND (Crystal Impact)[10] ShelXle (Hübschle, Sheldrick, Dittrich, 2011)[11]
CCDC	1864089

References

1 L.-A. Chen, X. Tang, J. Xi, W. Xu, L. Gong, E. Meggers, *Angew. Chem. Int. Ed.* **2013**, *52*, 14021.

2 (*a*) H. Zhou, G.-X. Wang, W.-Z. Zhang, X.-B. Lu, *ACS Catal.* **2015**, *5*, 6773; (*b*) G. D. Yadav, P. S. Surve, *Catal. Sci. Technol.* **2013**, *3*, 2668; (*c*) S. Wu, Y. Zhang, B. Wang, E. H. M. Elageed, L. Ji, H. Wu, G. Gao, *Eur. J. Org. Chem.* **2017**, 753; (*d*) E. Dolci, G. Michaud, F. Simon, B. Boutevin, S. Fouquay, S. Caillol, *Polym. Chem.* **2015**, *6*, 7851; (*e*) R. D. Aher, B. S. Kumar, A. Sudalai, *Synlett* **2014**, *25*, 97; (*f*) F. Zhou, S.-L. Xie, X.-T. Gao, R. Zhang, C.-H. Wang, G.-Q. Yina, J. Zhou, *Green Chem.* **2017**, 19, 3908.

3 *X-Area Pilatus3_SV*, STOE & Cie GmbH, Darmstadt, Germany, **2016**.

4 *X-Area Recipe*, STOE & Cie GmbH, Darmstadt, Germany, **2015**.

5 *X-Area Integrate*, STOE & Cie GmbH, Darmstadt, Germany, **2016**.

6 *X-Area LANA*, STOE & Cie GmbH, Darmstadt, Germany, **2016**.

7 S. Parsons, H. D. Flack, T. Wagner, *Acta Cryst. B* **2013**, *69*, 249.

8 G. M. Sheldrick, *Acta Cryst. A* **2015**, *71*, 3.

9 G. M. Sheldrick, *Acta Cryst. C* **2015**, *71*, 3.

10 K. Brandenburg, *Diamond - Crystal and Molecular Structure Visualization*, Crystal Impact - Dr. H. Putz & Dr. K. Brandenburg GbR, Bonn, Germany, **2014**.

11 C. B. Hübschle, G. M. Sheldrick, B. Dittrich, *J. Appl. Cryst.* **2011**, *44*, 1281.

5.3 Enantioselective Intramolecular C-H Amination of Aliphatic Azides by Dual Ruthenium and Phosphine Catalysis

5.3.1 Synthesis of Ruthenium Catalysts

1) Synthesis of imidazolium ligands

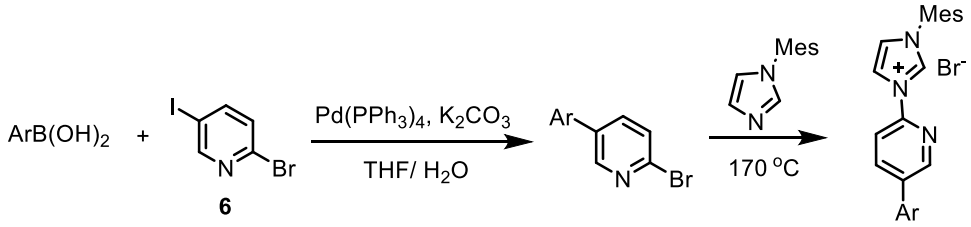

7a (Ar = 3,5-di*t*Bu-Ph)
7b (Ar = Ph)
7c (Ar = 4-*t*Bu-Ph)
7d (Ar = 4-CF_3-Ph)

8a (Ar = 3,5-di*t*Bu-Ph)
8b (Ar = Ph)
8c (Ar = 4-*t*Bu-Ph)
8d (Ar = 4-CF_3-Ph)

Compound **7b** was synthesized by following a published procedure.[1]

Compound **7a** was synthesized according to the published procedure with slight modifications.[1] A mixture of 2-bromo-5-iodopyridine (1.42 g, 5 mmol), (3,5-di(*tert*-butyl)phenyl)boronic acid (1.17 g, 5 mmol), $Pd(PPh_3)_4$ (289 mg, 0.25 mmol) and K_2CO_3 (2.07 g, 15 mmol) in THF (8.6 mL) and water (4.3 mL) in a round bottomed flask was allowed to heat at 70 ℃ for 1 day. After cooling to room temperature, the layers were separated and aqueous layer was extracted with CH_2Cl_2 (3×15 mL). The combined organic layers were washed with water, dried with Na_2SO_4 and concentrated under reduced pressure. The crude mixture was purified by flash column chromatography on a silica gel column resulted in the compound **7a** (693 mg, 2.0 mmol, 40% yield) as a white solid.

^{1}H NMR (300 MHz, $CDCl_3$) δ 8.57 (d, J = 2.2 Hz, 1H), 7.73 (dd, J = 8.2, 2.6 Hz, 1H), 7.54 (d, J = 8.2 Hz, 1H), 7.51 (t, J = 1.8 Hz, 1H), 7.34 (d, J = 1.8 Hz, 2H), 1.38 (s, 18H).

^{13}C NMR (75 MHz, $CDCl_3$) δ 152.0, 148.9, 140.7, 137.4, 137.4, 136.1, 128.0, 122.8, 121.6, 35.2, 31.6.

IR (film): ν (cm^{-1}) 3050, 2956, 2866, 1593, 1553, 1456, 1426, 1391, 1358, 1249, 1203, 1126, 1093, 1068, 1017, 929, 900, 869, 828, 799, 738, 705, 639, 615, 568, 541, 493, 403.

HRMS (ESI, *m/z*) calcd. for $C_{19}H_{25}NBr$ $[M+H]^+$: 346.1165, 348.1146, found: 346.1174, 348.1154.

Following the above procedure, compound **7c** (606 mg, 2.1 mmol, 41% yield) was obtained as a white

solid from (4-(*tert*-butyl)phenyl)boronic acid (890 mg, 5 mmol).

^{1}H NMR (300 MHz, $CDCl_3$) δ 8.58 (dd, J = 2.6, 0.5 Hz, 1H), 7.73 (dd, J = 8.3, 2.6 Hz, 1H), 7.55-7.47 (m, 5H), 1.36 (s, 9H).

^{13}C NMR (75 MHz, $CDCl_3$) δ 152.0, 148.6, 140.7, 136.9, 136.0, 133.7, 128.1, 126.8, 126.4, 34.8, 31.4.

IR (film): ν (cm^{-1}) 2957, 2864, 1572, 1543, 1444, 1401, 1359, 1268, 1112, 1083, 1031, 995, 931, 851, 822, 776, 738, 707, 631, 572, 528, 441, 414.

HRMS (ESI, *m/z*) calcd. for $C_{15}H_{17}NBr$ $[M+H]^+$: 290.0539, 292.0520, found: 290.0547, 292.0527.

Following the above procedure, compound **7d** (1.28 g, 4.2 mmol, 84% yield) was obtained as a white solid from (4-(trifluoromethyl)phenyl)boronic acid (950 mg, 5 mmol).

^{1}H NMR (300 MHz, $CDCl_3$) δ 8.60 (d, J = 2.3 Hz, 1H), 7.79-7.57 (m, 6H).

^{13}C NMR (75 MHz, $CDCl_3$) δ 148.7, 142.1, 140.2, 137.1, 134.8, 131.5, 131.1, 130.6, 130.2, 128.4, 127.5, 126.4, 126.4, 126.3, 126.3, 122.3.

^{19}F NMR (282 MHz, $CDCl_3$) δ -63.51.

IR (film): ν (cm^{-1}) 3028, 2955, 2867, 1592, 1534, 1477, 1418, 1376, 1329, 1244, 1093, 1052, 1007, 825, 754, 730, 663, 627, 576, 541, 502, 438, 405.

HRMS (ESI, *m/z*) calcd. for $C_{12}H_8BrF_3N$ $[M+H]^+$: 301.9787, 303.9767, found: 301.9795, 303.9774.

Compound **8a** was synthesized following the reported procedure.[2] Mesitylimidazole (391 mg, 2.1 mmol) and 2-bromo-5-(3,5-di-*tert*-butylphenyl)pyridine (**7a**) (693 mg, 2.0 mmol) were stirred in a sealed tube at 170 ℃ for 30 h. After cooling to room temperature, the resulting brown solid was washed with diethyl ether for several times until no starting materials were visible by TLC, and then the solvent was removed to give **8a** as a light brown solid (905 mg, 1.7 mmol, 85% yield).

^{1}H NMR (300 MHz, $CDCl_3$) δ 11.47 (t, J = 1.5 Hz, 1H), 9.40 (d, J = 8.5 Hz, 1H), 8.94 (t, J = 1.8 Hz, 1H), 8.73 (d, J = 2.0 Hz, 1H), 8.34 (dd, J = 8.6, 2.4 Hz, 1H), 7.55 (t, J = 1.7 Hz, 1H), 7.44 (d, J = 1.7 Hz, 2H), 7.36 – 7.30 (m, 1H), 7.07 (s, 2H), 2.37 (s, 3H), 2.22 (s, 6H), 1.39 (s, 18H).

^{13}C NMR (75 MHz, $CDCl_3$) δ 151.4, 146.5, 144.1, 140.6, 138.9, 138.2, 134.9, 134.7, 133.4, 130.1, 129.3, 124. 5, 122.5, 120.9, 119.9, 115.3, 34.4, 30.9, 20.5, 17.3.

IR (film): ν (cm^{-1}) 3037, 2957, 2867, 1595, 1535, 1483, 1443, 1367, 1327, 1248, 1088, 1049, 1027,

963, 929, 849, 743, 711, 662, 626, 574, 555, 517, 480, 412.

HRMS (ESI, *m*/*z*) calcd. for $C_{31}H_{38}N_3$ $[M\text{-}Br]^+$: 452.3060, found: 452.3064.

Following the above procedure, compound **8b** (673 mg, 1.6 mmol, 80% yield) was obtained as a light brown solid from **7b** (468 mg, 2.0 mmol).

^{1}H NMR (300 MHz, $CDCl_3$) δ 11.78 (s, 1H), 9.38 (d, J = 8.5 Hz, 1H), 8.95 (s, 1H), 8.72 (d, J = 2.0 Hz, 1H), 8.27 (dd, J = 8.5, 2.2 Hz, 1H), 7.60 (d, J = 6.9 Hz, 2H), 7.55-7.43 (m, 4H), 7.04 (s, 2H), 2.34 (s, 3H), 2.21 (s, 6H).

^{13}C NMR (75 MHz, $CDCl_3$) δ 146.8, 145.1, 141.5, 139.0, 138.6, 136.9, 136.0, 134.1, 130.8, 130.1, 129.4, 129.0, 127.2, 124.0, 120.0, 116.3, 21.2, 17.8.

IR (film): ν (cm^{-1}) 1592, 1535, 1473, 1451, 1383, 1242, 1148, 1088, 1031, 997, 968, 914, 857, 767, 724, 699, 666, 635, 575, 515, 489, 409.

HRMS (ESI, *m*/*z*) calcd. for $C_{23}H_{22}N_3$ $[M\text{-}Br]^+$: 340.1808, found: 340.1816.

Following the above procedure, compound **8c** (754 mg, 1.6 mmol, 79% yield) was obtained as a light brown solid from **7c** (580 mg, 2.0 mmol).

^{1}H NMR (300 MHz, $CDCl_3$) δ 11.29 (s, 1H), 9.23 (d, J = 8.5 Hz, 1H), 8.99 (s, 1H), 8.75 (d, J = 1.6 Hz, 1H), 8.28 (dd, J = 8.5, 1.9 Hz, 1H), 7.56 (d, J = 7.8 Hz, 5H), 7.05 (s, 2H), 2.36 (s, 3H), 2.22 (s, 6H), 1.40 (s, 9H).

^{13}C NMR (75 MHz, $CDCl_3$) δ 152.3, 146.7, 144.6, 141.5, 138.5, 138.4, 135.7, 134.0, 132.9, 130.6, 130.0, 126.7, 126.3, 124.3, 120.3, 116.1, 34.7, 31.2, 21.1, 17.8.

IR (film): ν (cm^{-1}) 3028, 2955, 2867, 1592, 1534, 1477, 1418, 1376, 1329, 1244, 1093, 1052, 1007, 825, 754, 730, 663, 627, 576, 541, 502, 438, 405.

HRMS (ESI, *m*/*z*) calcd. for $C_{27}H_{30}N_3$ $[M\text{-}Br]^+$: 396.2434, found: 396.2444.

Following the above procedure, compound **8d** (930 mg, 1.9 mmol, 95% yield) was obtained as a light brown solid from **7d** (604 mg, 2.0 mmol).

^{1}H NMR (300 MHz, $CDCl_3$) δ 11.39 (t, J = 1.4 Hz, 1H), 9.39 (d, J = 8.6 Hz, 1H), 8.93 (t, J = 1.8 Hz, 1H), 8.74 (d, J = 2.2 Hz, 1H), 8.32 (dd, J = 8.6, 2.4 Hz, 1H), 7.75 (q, J = 8.4 Hz, 4H), 7.38 (t, J = 1.7 Hz, 1H), 7.05 (s, 2H), 2.35 (s, 3H), 2.20 (s, 6H).

^{13}C NMR (75 MHz, $CDCl_3$) δ 147.0, 145.6, 141.9, 139.5, 139.5, 137.4, 136.4, 134.1, 131.5, 131.0,

130.7, 130.2, 127.7, 126.6, 126.5, 126.5, 126.4, 125.8, 124.1, 122.2, 120.3, 116.9, 21.3, 18.0.

^{19}F NMR (282 MHz, $CDCl_3$) δ -62.65.

IR (film): ν (cm^{-1}) 3018, 1595, 1533, 1479, 1381, 1323, 1245, 1164, 1115, 1066, 1009, 964, 830, 728, 671, 603, 510, 435.

HRMS (ESI, *m/z*) calcd. for $C_{24}H_{21}F_3N_3$ $[M\text{-}Br]^+$: 408.1682, found: 408.1691.

2) Synthesis of racemic ruthenium catalysts

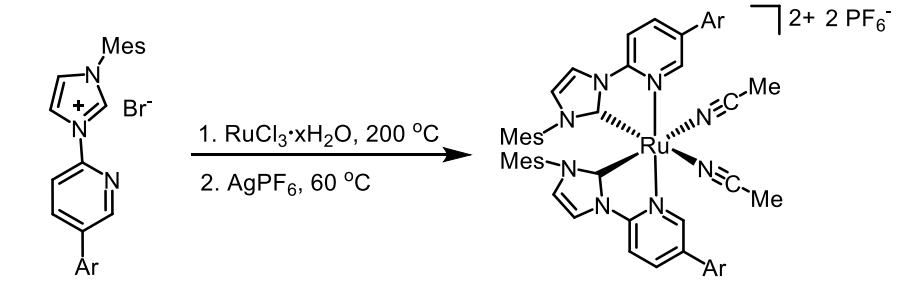

8a (Ar = 3,5-di*t*Bu-Ph)
8b (Ar = Ph)
8c (Ar = 4-*t*Bu-Ph)
8d (Ar = 4-CF_3-Ph)

rac-**Ru1** (Ar = 3,5-di*t*Bu-Ph)
rac-**Ru3** (Ar = Ph)
rac-**Ru6** (Ar = 4-*t*Bu-Ph)
rac-**Ru7** (Ar = 4-CF_3-Ph)

Racemic ruthenium catalyst *rac*-**Ru1** was synthesized following the published procedure with slight modifications.[2] A solution of $RuCl_3$•xH_2O (25.0 mg, 0.12 mmol) and compound **8a** (128 mg, 0.24 mmol) in ethylene glycol (2.4 mL) was heated at 200 ℃ for 6 h. The reaction mixture was treated with saturated aqueous NH_4PF_6 after cooling down to room temperature. A yellow precipitate was formed, which was extracted by CH_2Cl_2 for three times. The combined organic layers were washed with water and concentrated under reduced pressure to obtain an orange solid, which was dissolved in CH_3CN (3 mL) followed by adding $AgPF_6$ (38 mg, 0.15 mmol). The mixture was stirred at 60 ℃ overnight. After cooling to room temperature, the mixture was filtered, and the filtrate was collected, evaporated to dryness and purified by column chromatograph on silica gel (CH_2Cl_2/CH_3CN = 100:1 to 20:1) to give *rac*-**Ru1** (139 mg, 0.10 mmol, 84% yield for two steps) as a pale yellow solid.

^{1}H NMR (300 MHz, CD_2Cl_2) δ 8.51 (d, J = 1.9 Hz, 2H), 8.15 (dd, J = 8.7, 2.1 Hz, 2H), 8.08 (d, J = 2.3 Hz, 2H), 7.66 (d, J = 8.7 Hz, 2H), 7.62 (t, J = 1.6 Hz, 2H), 7.43 (d, J = 1.7 Hz, 4H), 6.97 (d, J = 2.3 Hz, 2H), 6.65 (s, 2H), 6.60 (s, 2H), 2.25 (s, 6H), 2.10 (s, 6H), 1.89 (s, 6H), 1.54 (s, 6H), 1.45 (s, 36H).

^{13}C NMR (75 MHz, CD_2Cl_2) δ 189.2, 152.9, 152.3, 149.0, 140.7, 136.8, 136.1, 135.1, 134.4, 134.3,

134.2, 130.4, 129.4, 125.8, 124.5, 124.2, 121.0, 118.3, 112.0, 35.7, 31.9, 21.0, 17.9, 17.5, 4.0.

^{19}F NMR (235 MHz, CD_2Cl_2) δ -71.22, -74.25.

IR (film): v (cm^{-1}) 2957, 1604, 1499, 1436, 1367, 1307, 1250, 1154, 1106, 1034, 931, 833, 702, 628, 589, 555, 423.

Following the above procedure, *rac*-**Ru3** (102 mg, 0.09 mmol, 74% yield for two steps) was obtained as a yellow solid from compound **8b** (252 mg, 0.6 mmol).

^{1}H NMR (300 MHz, CD_2Cl_2) δ 8.53 (d, J = 2.0 Hz, 2H), 8.08 (dd, J = 8.6, 2.1 Hz, 2H), 8.02 (d, J = 2.3 Hz, 2H), 7.65-7.52 (m, 12H), 6.93 (d, J = 2.3 Hz, 2H), 6.60 (d, J = 6.3 Hz, 4H), 2.31 (s, 6H), 2.01 (s, 6H), 1.97 (s, 6H), 1.52 (s, 6H).

^{13}C NMR (75 MHz, CD_2Cl_2) δ 189.6, 152.4, 149.2, 140.6, 137.1, 135.6, 135.3, 135.1, 134.3, 134.2, 130.2, 130.2, 129.8, 129.6, 127.0, 126.0, 125.0, 118.0, 111.8, 21.1, 17.7, 17.5, 4.0.

^{19}F NMR (282 MHz, CD_2Cl_2) δ -71.32, -73.84.

IR (film): v (cm^{-1}) 2922, 2852, 1511, 1483, 1453, 1422, 1290, 1247, 1142, 1081, 1036, 952, 930, 835, 764, 745, 696, 678, 620, 591, 556, 542, 488, 457, 434, 388.

Following the above procedure, *rac*-**Ru6** (212 mg, 0.17 mmol, 56% yield for two steps) was obtained as a yellow solid from compound **8c** (286 mg, 0.6 mmol).

^{1}H NMR (300 MHz, CD_2Cl_2) δ 8.51 (d, J = 1.9 Hz, 2H), 8.07 (dd, J = 8.6, 2.1 Hz, 2H), 8.02 (d, J = 2.3 Hz, 2H), 7.68 - 7.52 (m, 10H), 6.93 (d, J = 2.3 Hz, 2H), 6.60 (s, 4H), 2.31 (s, 6H), 2.03 (s, 6H), 1.95 (s, 6H), 1.51 (s, 6H), 1.41 (s, 18H).

^{13}C NMR (75 MHz, CD_2Cl_2) δ 189.3, 153.0, 151.9, 148.7, 140.3, 136.5, 135.2, 135.0, 134.0, 134.0, 131.9, 130.0, 129.4, 127.0, 126.4, 125.6, 124.7, 117.8, 111.7, 35.1, 31.4, 20.8, 17.5, 17.2, 3.7.

^{19}F NMR (282 MHz, CD_2Cl_2) δ -72.21, -74.73.

IR (film): v (cm^{-1}) 3138, 2959, 1611, 1490, 1425, 1373, 1309, 1258, 1103, 1033, 932, 834, 738, 629, 588, 554, 434.

Following the above procedure, *rac*-**Ru7** (348 mg, 0.27 mmol, 89% yield for two steps) was obtained as a yellow solid from compound **8d** (293 mg, 0.6 mmol).

^{1}H NMR (300 MHz, CD_2Cl_2) δ 8.57 (d, J = 1.9 Hz, 2H), 8.10 (dd, J = 8.7, 2.1 Hz, 2H), 8.03 (d, J = 2.3 Hz, 2H), 7.89 (d, J = 8.3 Hz, 4H), 7.78 (d, J = 8.2 Hz, 4H), 7.67 (d, J = 8.6 Hz, 2H), 6.93 (d, J =

2.3 Hz, 2H), 6.64 (s, 2H), 6.57 (s, 2H), 2.31 (s, 6H), 2.00 (s, 12H), 1.52 (s, 6H).

^{13}C NMR (75 MHz, CD_2Cl_2) δ 189.7, 152.9, 149.4, 140.4, 138.6, 137.3, 135.2, 134.2, 134.1, 134.0, 131.6, 131.1, 130.2, 129.3, 127.5, 127.1, 127.0, 127.0, 126.9, 126.3, 126.0, 125.2, 122.7, 117.9, 111.9, 21.0, 17.5, 17.3, 3.7.

^{19}F NMR (282 MHz, CD_2Cl_2) δ -62.90, -71.13, -73.65.

IR (film): ν (cm^{-1}) 1612, 1492, 1426, 1322, 1255, 1166, 1117, 1069, 823, 689, 552.

3) Synthesis of enantiomerically pure ruthenium catalysts

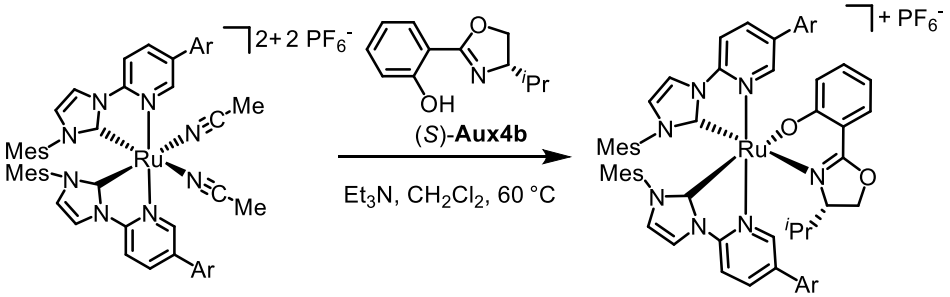

rac-**Ru3** (Ar = Ph)
rac-**Ru6** (Ar = 4-*t*Bu-Ph)
rac-**Ru7** (Ar = 4-CF_3-Ph)

Λ-(*S*)-**Ru3** (Ar = Ph)
Λ-(*S*)-**Ru6** (Ar = 4-*t*Bu-Ph)
Λ-(*S*)-**Ru7**(Ar = 4-CF_3-Ph)

Chiral ruthenium complex Λ-(*S*)-**Ru3** was synthesized following our published procedure with slight modifications.[2] A mixture of *rac*-**Ru3** (124.7 mg, 0.11 mmol), chiral auxiliary (*S*)-**Aux4b** (45.6 mg, 0.22 mmol) and triethylamine (153 μL, 1.09 mmol) in CH_2Cl_2 (1.8 mL) was heated at 60 ℃ for 18 h. The reaction mixture was cooled to room temperature and concentrated to dryness. The residue was subjected to a flash silica gel chromatography (CH_3CN/CH_2Cl_2 = 1:600 to 1:50) to isolate one diastereomer (orange solid, 33.8 mg, 0.03 mmol, yield: 28%) which was assigned as Λ-(*S*)-**Ru3**.

^{1}H NMR (500 MHz, CD_2Cl_2) δ 8.74 (d, J = 2.0 Hz, 1H), 8.19 (d, J = 2.0 Hz, 1H), 7.95 (d, J = 2.3 Hz, 1H), 7.92 (dd, J = 8.6, 2.2 Hz, 1H), 7.87 (d, J = 2.3 Hz, 1H), 7.74 (dd, J = 8.6, 2.2 Hz, 1H), 7.54-7.43 (m, 7H), 7.42-7.38 (m, 3H), 7.37-7.31 (m, 3H), 7.00 (ddd, J = 8.7, 6.9, 1.9 Hz, 1H), 6.89 (d, J = 2.3 Hz, 1H), 6.84 (d, J = 2.2 Hz, 1H), 6.56 (s, 1H), 6.51 (s, 1H), 6.50-6.45 (m, 3H), 6.24-6.18 (m, 1H), 4.29 (dd, J = 9.3, 3.2 Hz, 1H), 4.12 (t, J = 9.1 Hz, 1H), 3.91 (dt, J = 8.9, 3.1 Hz, 1H), 2.28 (s, 3H), 2.05 (s, 3H), 2.00 (s, 3H), 1.95 (s, 3H), 1.61 (s, 3H), 1.42 (s, 3H), 0.55 (d, J = 7.0 Hz, 3H), 0.30-0.19 (m, 1H), -0.03 (d, J = 6.8 Hz, 3H).

^{13}C NMR (126 MHz, CD_2Cl_2) δ 197.5, 196.2, 172.0, 165.2, 153.0, 152.9, 148.5, 148.0, 139.5, 137.3,

135.8, 135.4, 135.1, 135.0, 134.7, 134.4, 134.2, 133.9, 133.9, 133.6, 133.4, 130.2, 129.8, 129.6, 129.4, 129.4, 129.1, 129.0, 126.4, 125.6, 125.1, 123.8, 116.6, 115.9, 112.7, 110.8, 110.5, 110.0, 74.9, 66.6, 30.1, 30.0, 20.9, 20.9, 18.8, 18.5, 17.9, 17.9, 17.4, 13.5.

^{19}F NMR (282 MHz, CD_2Cl_2) δ -71.73, -74.25.

HRMS (ESI, *m/z*) calcd. for $C_{58}H_{56}RuN_7O_2$ $[M\text{-}PF_6]^+$: 984.3549, found: 984.3565.

IR (film): ν (cm^{-1}) 1605, 1537, 1507, 1471, 1413, 1355, 1322, 1250, 1222, 1067, 969, 921, 836, 756, 685, 580, 553.

CD (MeOH): λ, nm (Δε, $M^{-1}cm^{-1}$) 478 (–7), 408 (+33), 365 (0), 334 (+20), 315 (+10), 291 (-2), 269 (+13).

Following the above procedure, Λ-(*S*)-**Ru6** (45.9 mg, 0.037 mmol, yield: 34%) was obtained as an orange solid from *rac*-**Ru6** (139 mg, 0.11 mmol).

^{1}H NMR (300 MHz, CD_2Cl_2) δ 8.73 (d, *J* = 2.0 Hz, 1H), 8.20 (d, *J* = 1.9 Hz, 1H), 7.95-7.82 (m, 3H), 7.75 (dd, *J* = 8.6, 2.1 Hz, 1H), 7.49 (dt, *J* = 20.9, 9.3 Hz, 6H), 7.40-7.22 (m, 5H), 6.99 (ddd, *J* = 8.7, 6.9, 1.9 Hz, 1H), 6.87 (dd, *J* = 13.1, 2.3 Hz, 2H), 6.61-6.37 (m, 5H), 6.22 (t, *J* = 7.1 Hz, 1H), 4.29 (dd, *J* = 9.2, 3.2 Hz, 1H), 4.15 (t, *J* = 9.0 Hz, 1H), 3.96-3.87 (m, 1H), 2.28 (s, 3H), 2.06 (s, 3H), 1.99 (s, 3H), 1.93 (s, 3H), 1.60 (s, 3H), 1.42 (s, 3H), 1.39 (s, 9H), 1.35 (s, 9H), 0.55 (d, *J* = 6.9 Hz, 3H), 0.33-0.16 (m, 1H), -0.03 (d, *J* = 6.8 Hz, 3H).

^{13}C NMR (75 MHz, CD_2Cl_2) δ 197.1, 195.9, 171.7, 165.0, 152.7, 152.7, 152.4, 152.3, 148.1, 147.7, 139.5, 139.5, 137.2, 135.0, 134.9, 134.7, 134.3, 134.1, 133.9, 133.8, 133.4, 133.3, 132.6, 132.4, 130.1, 129.7, 129.4, 129.4, 129.0, 126.8, 126.5, 126.0, 126.0, 125.5, 125.0, 123.8, 116.6, 115.8, 112.6, 110.8, 110.5, 109.9, 74.9, 66.5, 35.0, 34.9, 31.4, 31.3, 30.0, 20.9, 20.8, 18.8, 18.5, 17.9, 17.9, 17.4, 13.5.

^{19}F NMR (282 MHz, CD_2Cl_2) δ -71.68, -74.19.

IR (film): ν (cm^{-1}) 2958, 1607, 1486, 1420, 1372, 1320, 1251, 1151, 1068, 1032, 926, 836, 747, 688, 553.

HRMS (ESI, *m/z*) calcd. for $C_{66}H_{72}RuN_7O_2$ $[M\text{-}PF_6]^+$: 1096.4804, found: 1096.4824.

CD (MeOH): λ, nm (Δε, $M^{-1}cm^{-1}$) 469 (–8), 405 (+43), 366 (-5), 332 (+22), 293 (-60), 270 (+58), 250 (-17), 225 (+21).

Following the above procedure, Λ-(*S*)-**Ru7** (56.7 mg, 0.045 mmol, yield: 41%) was obtained as an orange solid from *rac*-**Ru7** (142 mg, 0.11 mmol).

^{1}H NMR (300 MHz, CD_2Cl_2) δ 8.78 (d, J = 2.2 Hz, 1H), 8.22-8.17 (m, 1H), 8.02-7.99 (m, 1H), 7.97 (dd, J = 8.6, 1.9 Hz, 1H), 7.93-7.89 (m, 1H), 7.82-7.76 (m, 3H), 7.73 (s, 1H), 7.71 (s, 1H), 7.58 (d, J = 8.7 Hz, 1H), 7.53-7.41 (m, 6H), 7.05-6.97 (m, 1H), 6.91 (d, J = 2.3 Hz, 1H), 6.86 (d, J = 2.3 Hz, 1H), 6.58 (s, 1H), 6.54 (s, 1H), 6.51-6.44 (m, 3H), 6.28-6.22 (m, 1H), 4.33-4.27 (m, 1H), 4.10 (t, J = 9.1 Hz, 1H), 3.92-3.85 (m, 1H), 2.27 (s, 3H), 2.04 (s, 3H), 2.02 (s, 3H), 1.96 (s, 3H), 1.61 (s, 3H), 1.43 (s, 3H), 0.55 (d, J = 7.0 Hz, 3H), 0.27–0.15 (m, 1H), –0.04 (d, J = 6.9 Hz, 3H).

^{13}C NMR (75 MHz, CD_2Cl_2) δ 197.5, 196.12 172.0, 165.3, 153.8, 153.6, 148.7, 148.2, 139.6, 139.5, 139.0, 137.2, 135.2, 134.9, 134.7, 134.7, 134.5, 134.4, 134.1, 134.0, 132.1, 131.8, 130.9, 130.8, 130.7, 130.5, 130.1, 129.9, 129.6, 129.2, 128.8, 126.9, 126.8, 126.8, 126.6, 126.6, 126.6, 126.5, 125.75, 125.56, 125.54, 125.34, 123.79, 123.40, 123.38, 116.84, 116.13, 112.87, 110.82, 110.32, 74.8, 66.6, 30.1, 20.9, 20.9, 18.8, 18.5, 17.9, 17.8, 17.4, 13.5.

^{19}F NMR (282 MHz, CD_2Cl_2) δ -63.02, -63.04, -71.64, -74.16.

IR (film): ν (cm^{-1}) 2925, 1608, 1531, 1489, 1422, 1379, 1322, 1285, 1251, 1166, 1117, 1068, 1018, 925, 836, 757, 686, 596, 553, 507, 458, 429.

HRMS (ESI, *m/z*) calcd. for $C_{60}H_{54}RuF_6N_7O_2$ $[M\text{-}PF_6]^+$: 1120.3298, found: 1120.3317.

CD (MeOH): λ, nm (Δε, $M^{-1}cm^{-1}$) 484 (–6), 411 (+25), 369 (+1), 338 (+12), 316 (0), 304 (+6), 288 (-5), 262 (+11).

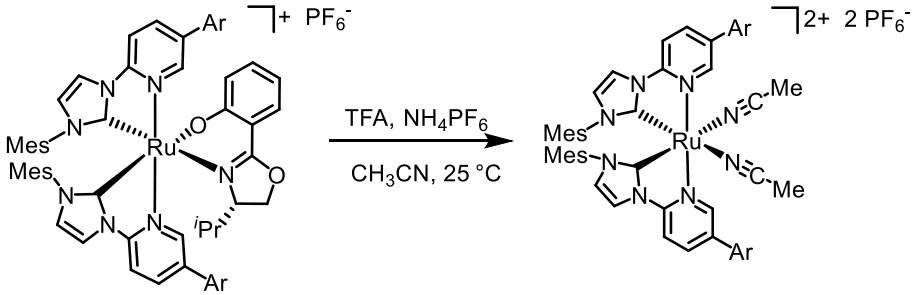

Λ-(*S*)-**Ru3** (Ar = Ph)
Λ-(*S*)-**Ru6** (Ar = 4-*t*Bu-Ph)
Λ-(*S*)-**Ru7** (Ar = 4-CF_3-Ph)

Λ-**Ru3** (Ar = Ph)
Λ-**Ru6** (Ar = 4-*t*Bu-Ph)
Λ-**Ru7** (Ar = 4-CF_3-Ph)

To a suspension of Λ-(*S*)-**Ru3** (50 mg, 0.044 mmol) in CH_3CN (4.4 mL) was added trifluoroacetic acid (32.6 μL, 0.44 mmol, 10 equiv) dropwise and stirred at room temperature for 0.5 h, followed by the addition of an excess of NH_4PF_6 (215 mg, 1.32 mmol, 30 equiv), and then stirred at room temperature for another 0.5 h. The mixture was filtered by a thin pad of silica gel, the pale yellow filtrate was concentrated, and then subjected to the column chromatography on silica gel (CH_3CN/CH_2Cl_2 = 50:1

to 5:1) to give the enantiopure catalyst Λ-**Ru3** (44.8 mg, 0.039 mmol, 88% yield) as a yellow solid. **CD (MeOH)**: λ, nm (Δε, $M^{-1}cm^{-1}$) 345 (+8), 326 (0), 305 (+39), 289 (-14), 266 (+69), 235 (-63), 216 (-28). All the other spectroscopic data of enantiopure ruthenium catalyst Λ-**Ru3** were in agreement with the racemic catalyst *rac*-**Ru3**.

Following the above procedure, Λ-**Ru6** (46.0 mg, 0.036 mmol, yield: 82%) was obtained as a yellow solid from Λ-(*S*)-**Ru6** (54.7 mg, 0.044 mmol).

CD (MeOH): λ, nm (Δε, $M^{-1}cm^{-1}$) 344 (+13), 328 (+7), 309 (+34), 292 (-11), 270 (+87), 238 (-82), 220 (-25). All the other spectroscopic data of enantiopure ruthenium catalyst Λ-**Ru6** were in agreement with the racemic catalyst *rac*-**Ru6**.

Following the above procedure, Λ-**Ru7** (54.0 mg, 0.042 mmol, yield: 95%) was obtained as a yellow solid from Λ-(*S*)-**Ru7** (55.8 mg, 0.044 mmol).

CD (MeOH): λ, nm (Δε, $M^{-1}cm^{-1}$) 353 (+7), 324 (-5), 302 (+40), 287 (-1), 266 (+60), 240 (-52), 212 (-19). All the other spectroscopic data of enantiopure ruthenium catalyst Λ-**Ru7** were in agreement with the one of racemic catalyst *rac*-**Ru7**.

5.3.2 Synthesis of Organic Azide Substrates

CAUTION: Organic azides are known to be potentially explosive compounds. All azidation reactions and subsequent workups should be performed carefully. Once isolated, organic azides were stored in a -20 ℃ freezer.

Organic azides **9a**, **9e**, **9r** and **9y** were synthesized according to published procedures.[3,4,5]

Procedure A:

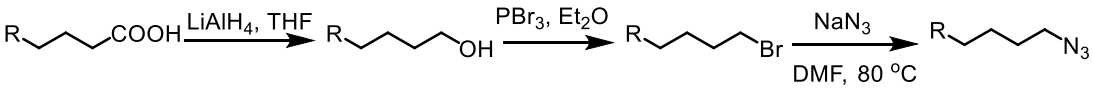

To a solution of the desired alkyl carboxylic acid (10 mmol, 1 equiv) in THF (0.5 M) was added $LiAlH_4$ (1.5 g, 40 mmol, 4 equiv) portionwise at 0 ℃ under N_2 atmosphere. Then the solution was stirred at 25 ℃ for 24 h. After that, to the reaction was added H_2O (0.2 mL), aqueous 1 M NaOH (0.2 mL), H_2O (0.5 mL) consecutively at 0 ℃ to quench the reaction, and then filtered. The aqueous phase

was extracted three times with diethyl ether, the combined organic phases were dried over Na_2SO_4, and concentrated in vacuo to get the alcohol compound which was directly used for the next step without further purification.

To the above alcohol compound (1 equiv) in diethyl ether (0.9 M) was added PBr_3 (0.5 equiv) dropwise at 0 ℃ under N_2 atmosphere. The solution was stirred at 25 ℃ for 20 h. After the alcohol compound was totally consumed, the reaction was quenched by slowly by adding H_2O at 0 ℃. The aqueous phase was extracted three times with diethyl ether, the combined organic phases were washed with saturated aqueous solution of $NaHCO_3$ and brine, dried over Na_2SO_4 and concentrated in *vacuo* to get the alkyl bromide compound which was directly used for next step without further purification.

To a solution of the above alkyl bromide (1 equiv) in DMF (0.5 M) was added sodium azide (1.2 equiv), and the solution was stirred for 24 h at 80 ℃. A 1:1 mixture of H_2O/diethyl ether was added to the reaction mixture, and the aqueous phase was extracted three times with diethyl ether. The combined organic phases were washed several times with H_2O to remove DMF, then brine, and dried over Na_2SO_4. After removal of the solvent under reduced pressure, the crude mixture was purified by flash column chromatography on a silica gel column resulted in the analytically pure azides.

Procedure B:

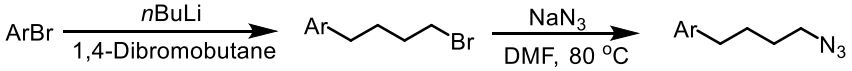

To a solution of the desired aryl bromide (10 mmol, 1 equiv) in diethyl ether (0.5 M) was added *n*BuLi (12 mmol, 1.2 equiv) dropwise at 0 ℃, followed by 1,4-dibromobutane. The mixture was then refluxed for 4 h. After cooling to room temperature, the reaction was quenched by slowly adding H_2O at 0 ℃. The aqueous phase was extracted three times with diethyl ether. The combined organic phases were dried over Na_2SO_4. After removal of the solvent under reduced pressure, the crude mixture was purified by flash column chromatography on silica gel column resulted in the desired alkyl bromide.

To a solution of the above alkyl bromide (1 equiv) in DMF (0.5 M) was added sodium azide (1.2 equiv), and the solution was stirred for 24 h at 80 ℃. A 1:1 mixture of H_2O/diethyl ether was added to

the reaction mixture, and the aqueous phase was extracted three times with diethyl ether. The combined organic phases were washed several times with H_2O to remove DMF, then brine, and dried over Na_2SO_4. After removal of the solvent under reduced pressure, the crude mixture was purified by flash column chromatography on a silica gel column which resulted in the analytically pure azides.

1-(4-Azidobutyl)-4-methylbenzene (**9b**)

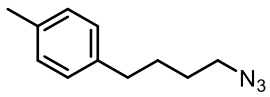

Compound **9b** (927 mg, 4.9 mmol) was synthesized from 4-(*p*-tolyl)butanoic acid (1.78 g, 10 mmol) according to the above Procedure A and obtained as a colorless oil. Yield: 49%.

^{1}H NMR (300 MHz, $CDCl_3$) δ 7.17-6.99 (m, 4H), 3.28 (t, J = 6.5 Hz, 2H), 2.62 (t, J = 7.2 Hz, 2H), 2.33 (s, 3H), 1.80-1.55 (m, 4H).

^{13}C NMR (75 MHz, $CDCl_3$) δ 138.9, 135.5, 129.2, 128.4, 51.5, 35.1, 28.7, 28.6, 21.1.

IR (film): ν (cm^{-1}) 3014, 2932, 2861, 2089, 1514, 1452, 1349, 1256, 1112, 1033, 886, 805, 639, 548, 488.

1-(4-Azidobutyl)-3-methylbenzene (**9c**)

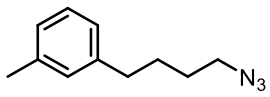

Compound **9c** (965 mg, 5.1 mmol) was synthesized from 4-(*m*-tolyl)butanoic acid (1.78 g, 10 mmol) according to the above Procedure A and obtained as a colorless oil. Yield: 51%.

^{1}H NMR (300 MHz, $CDCl_3$) δ 7.22-7.14 (m, 1H), 7.05-6.94 (m, 3H), 3.29 (t, J = 6.5 Hz, 2H), 2.62 (t, J = 7.2 Hz, 2H), 2.34 (s, 3H), 1.78-1.57 (m, 4H).

^{13}C NMR (75 MHz, $CDCl_3$) δ 141.9, 138.1, 129.3, 128.4, 126.8, 125.5, 51.5, 35.4, 28.6, 28.6, 21.5.

IR (film): ν (cm^{-1}) 3019, 2933, 2861, 2089, 1607, 1487, 1454, 1349, 1257, 1165, 1095, 1039, 884, 778, 696, 556, 437.

1-(4-Azidobutyl)-2-methylbenzene (**9d**)

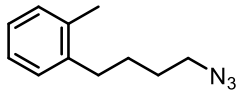

Compound **9d** (852 mg, 4.5 mmol) was synthesized from 4-(*o*-tolyl)butanoic acid (1.78 g, 10 mmol) according to the above Procedure A and obtained as a colorless oil. Yield: 45%.

^{1}H NMR (300 MHz, $CDCl_3$) δ 7.22-7.07 (m, 4H), 3.32 (t, J = 6.3 Hz, 2H), 2.65 (dd, J = 8.7, 5.8 Hz, 2H), 2.33 (s, 3H), 1.79-1.59 (m, 4H).

^{13}C NMR (75 MHz, $CDCl_3$) δ 140.1, 135.9, 130.4, 128.9, 126.2, 126.1, 51.5, 32.9, 28.9, 27.4, 19.4.

IR (film): ν (cm^{-1}) 3018, 2937, 2865, 2089, 1490, 1457, 1349, 1255, 1117, 1057, 887, 742, 666, 554, 447.

4-(4-Azidobutyl)-1,1'-biphenyl (**9f**)

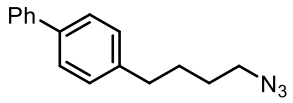

Compound **9f** (1.53 g, 6.1 mmol) was synthesized from 4-bromo-1,1'-biphenyl (1.86 g, 8 mmol) according to the above Procedure B and obtained as a colorless oil. Yield: 76%.

^{1}H NMR (300 MHz, $CDCl_3$) δ 7.64-7.48 (m, 4H), 7.44 (dd, J = 10.2, 4.8 Hz, 2H), 7.37-7.29 (m, 1H), 7.27 (s, 1H), 7.24 (s, 1H), 3.31 (t, J = 6.6 Hz, 2H), 2.70 (t, J = 7.3 Hz, 2H), 1.83-1.60 (m, 4H).

^{13}C NMR (75 MHz, $CDCl_3$) δ 141.2, 141.1, 139.1, 128.9, 128.9, 127.3, 127.2, 127.1, 51.5, 35.1, 28.6, 28.6.

IR (film): ν (cm^{-1}) 3027, 2934, 2860, 2089, 1602, 1486, 1453, 1407, 1349, 1257, 1115, 1073, 1004, 832, 757, 695, 590, 552, 503.

1-(4-Azidobutyl)-4-methoxybenzene (**9g**)

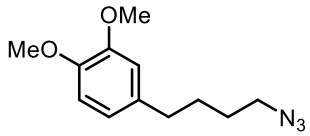

Compound **9g** (1.29 g, 5.5 mmol) was synthesized from 4-(3,4-dimethoxyphenyl)butanoic acid (2.24 g,

10 mmol) according to the above Procedure A and obtained as a pale yellow oil. Yield: 55%.

^{1}H NMR (300 MHz, $CDCl_3$) δ 6.80 (d, J = 8.7 Hz, 1H), 6.74-6.68 (m, 2H), 3.88 (s, 3H), 3.86 (s, 3H), 3.29 (t, J = 6.5 Hz, 2H), 2.60 (t, J = 7.2 Hz, 2H), 1.77-1.57 (m, 4H).

^{13}C NMR (75 MHz, $CDCl_3$) δ 149.1, 147.5, 134.6, 120.3, 111.9, 111.5, 56.1, 56.0, 51.5, 35.1, 28.8, 28.6.

HRMS (ESI, *m/z*) calcd. for $C_{12}H_{17}N_3O_2Na$ $[M+Na]^+$: 258.1213, found: 258.1222.

IR (film): ν (cm^{-1}) 2999, 2935, 2861, 2090, 1590, 1512, 1457, 1417, 1257, 1234, 1145, 1026, 931, 853, 804, 760, 632, 597, 556.

(4-(4-Azidobutyl)phenyl)(methyl)sulfane (**9h**)

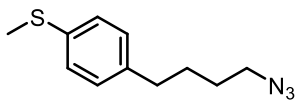

Compound **9h** (288 mg, 1.3 mmol) was synthesized from (4-bromophenyl)(methyl)sulfane (2.03 g, 10 mmol) according to the above Procedure B and obtained as a colorless oil. Yield: 13%.

^{1}H NMR (300 MHz, $CDCl_3$) δ 7.24–7.17 (m, 2H), 7.14–7.06 (m, 2H), 3.28 (t, J = 6.5 Hz, 2H), 2.61 (t, J = 7.2 Hz, 2H), 2.47 (s, 3H), 1.75–1.56 (m, 4H).

^{13}C NMR (75 MHz, $CDCl_3$) δ 139.1, 135.6, 129.0, 127.4, 51.5, 34.9, 28.5, 16.5.

IR (film): ν (cm^{-1}) 2924, 2857, 2091, 1492, 1442, 1349, 1259, 1094, 1016, 962, 885, 806, 738, 658, 627, 527, 489.

4-(4-Azidobutyl)-N,N-dimethylaniline (**9i**)

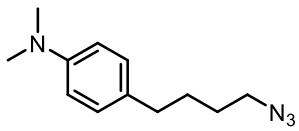

Compound **9i** (327 mg, 1.5 mmol) was synthesized from 4-bromo-*N*,*N*-dimethylaniline (2.0 g, 10 mmol) according to the above Procedure B and obtained as a colorless oil. Yield: 15%.

^{1}H NMR (300 MHz, $CDCl_3$) δ 7.06 (d, J = 8.5 Hz, 2H), 6.72 (d, J = 8.5 Hz, 2H), 3.28 (t, J = 6.4 Hz, 2H), 2.92 (s, 6H), 2.56 (t, J = 7.0 Hz, 2H), 1.75–1.55 (m, 4H).

^{13}C NMR (75 MHz, $CDCl_3$) δ 149.2, 129.1, 113.3, 51.6, 41.1, 34.5, 28.8, 28.6.

IR (film): ν (cm^{-1}) 2930, 2857, 2798, 2089, 1614, 1519, 1449, 1342, 1259, 1161, 1130, 1062, 946, 887, 808, 743, 673, 554, 516.

4-(4-Azidobutyl)phenyl diethyl phosphate (**9j**)

Compound **9j** was synthesized according to the method below.

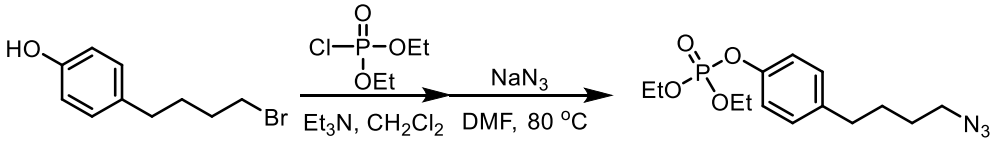

To the above 4-(4-bromobutyl)phenol (2.29 g, 10 mmol, 1 equiv) in dry CH_2Cl_2 (20 mL, 0.5 M) was added triethylamine (2.8 mL, 20 mmol, 2 equiv), followed by diethyl phosphorochloridate (1.6 mL, 11 mmol, 1.1 equiv) dropwise at 0 ℃ under N_2 atmosphere. The solution was stirred at 25 ℃ overnight. The reaction was quenched by slowly adding HCl aqueous (1 M). The aqueous phase was extracted with CH_2Cl_2, the combined organic phases were washed with saturated aqueous solution of $NaHCO_3$ and brine, dried over Na_2SO_4. The crude mixture was purified by flash column chromatography on a silica gel column resulting in the analytically pure alkyl bromide.

To a solution of the above alkyl bromide (475 mg, 1.3 mmol, 1 equiv) in DMF (2.6 mL,0.5 M) was added sodium azide (104 mg, 1.6 mmol, 1.2 equiv), and the solution was stirred for 24 h at 80 ℃. A 1:1 mixture of H_2O/ethyl acetate was added to the reaction mixture, and the aqueous phase was extracted five times with ethyl acetate. The combined organic phases were washed several times with H_2O to remove DMF, then brine, and dried over Na_2SO_4. After removal of the solvent under reduced pressure, the crude mixture was purified by flash column chromatography on a silica gel column resulted in the analytically pure alkyl azides **9j** as a colorless oil (393 mg, 1.2 mmol). Yield: 12% for two steps.

^{1}H NMR (300 MHz, $CDCl_3$) δ 7.12 (s, 4H), 4.20 (p, J = 7.3 Hz, 4H), 3.27 (t, J = 6.4 Hz, 2H), 2.61 (t, J = 7.2 Hz, 2H), 1.71–1.54 (m, 4H), 1.34 (t, J = 7.1 Hz, 6H).

^{13}C NMR (75 MHz, $CDCl_3$) δ 149.2, 149.1, 138.6, 129.6, 120.0, 120.0, 64. 7, 64.6, 51.4, 34.7, 28.6, 28.5, 16.3, 16.2.

IR (film): ν (cm^{-1}) 2985, 2935, 2864, 2093, 1606, 1506, 1451, 1365, 1274, 1215, 1165, 1101, 1024, 955, 933, 812, 765, 689, 637, 545, 511.

1-(4-Azidobutyl)-4-(benzyloxy)benzene (**9k**)

Compound **9k** was synthesized according to the method below.

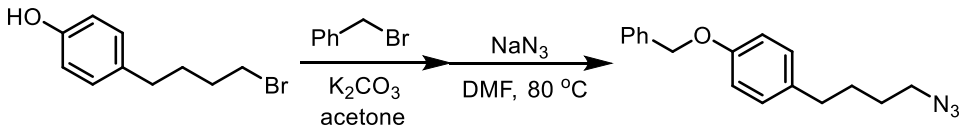

A mixture of 4-(4-bromobutyl)phenol (2.29 g, 10 mmol, 1 equiv), K_2CO_3 (2.76 g, 20 mmol, 2 equiv) and benzyl bromide (1.71 g, 10 mmol, 1 equiv) in acetone (100 mL, 0.1 M) was stirred at 50 ℃ overnight. After the reaction was finished, acetone was removed under reduced pressure. A 1:1 mixture of H_2O/CH_2Cl_2 was added to the residue, and the organic phase washed with water for several times, then brine, dried over Na_2SO_4. The crude mixture was purified by flash column chromatography on a silica gel column resulting in the analytically pure alkyl bromide.

To a solution of the above alkyl bromide (2.23 g, 7.0 mmol, 1 equiv) in DMF (14 mL, 0.5 M) was added sodium azide (546 mg, 8.4 mmol, 1.2 equiv), and the solution was stirred for 24 h at 80 ℃. A 1:1 mixture of H_2O/ethyl acetate was added to the reaction mixture, and the aqueous phase was extracted five times with ethyl acetate. The combined organic phases were washed several times with H_2O to remove DMF, then brine, and dried over Na_2SO_4. After removal of the solvent under reduced pressure, the crude mixture was purified by flash column chromatography on a silica gel column resulting in the analytically pure alkyl azides **9k** as a colorless oil (1.74 g, 6.5 mmol). Yield: 62% for two steps.

^{1}H NMR (300 MHz, $CDCl_3$) δ 7.12 (s, 4H), 4.20 (p, J = 7.3 Hz, 4H), 3.27 (t, J = 6.4 Hz, 2H), 2.61 (t, J = 7.2 Hz, 2H), 1.71–1.54 (m, 4H), 1.34 (t, J = 7.1 Hz, 6H).

^{13}C NMR (75 MHz, $CDCl_3$) δ 149.2, 149.1, 138.6, 129.6, 120.0, 120.0, 64. 7, 64.6, 51.4, 34.7, 28.6, 28.5, 16.3, 16.2.

IR (film): ν (cm^{-1}) 3032, 2933, 2861, 2090, 1610, 1583, 1508, 1456, 1378, 1350, 1293, 1233, 1175, 1112, 1077, 1018, 912, 859, 824, 735, 695, 642, 611, 552, 510, 455.

1-(4-Azidobutyl)-4-fluorobenzene (**9l**)

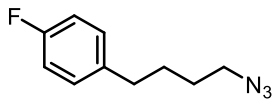

Compound **9l** (928 mg, 4.8 mmol) was synthesized from 4-(4-fluorophenyl)butanoic acid (1.46 g, 8 mmol) according to the above Procedure A and obtained as a colorless oil. Yield: 60%.

^{1}H NMR (300 MHz, $CDCl_3$) δ 7.18-7.06 (m, 2H), 7.04-6.91 (m, 2H), 3.29 (t, *J* = 6.5 Hz, 2H), 2.62 (t, *J* = 7.2 Hz, 2H), 1.75-1.55 (m, 4H).

^{13}C NMR (75 MHz, $CDCl_3$) δ 163.1, 159.9, 137.6, 137.5, 129.9, 129.8, 115.4, 115.1, 51.5, 34.7, 28.7, 28.5.

^{19}F NMR (282 MHz, $CDCl_3$) δ -117.64.

IR (film): *v* (cm^{-1}) 2937, 2863, 2090, 1602, 1507, 1456, 1350, 1221, 1156, 1100, 1013, 826, 759, 703, 637, 547, 500, 422.

1-(4-Azidobutyl)-4-chlorobenzene (**9m**)

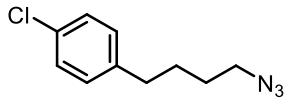

Compound **9m** (1.17 g, 5.6 mmol) was synthesized from 4-(4-chlorophenyl)butanoic acid (1.99 g, 10 mmol) according to the above Procedure A and obtained as a colorless oil. Yield: 56%.

^{1}H NMR (300 MHz, $CDCl_3$) δ 7.25 (dd, *J* = 6.5, 1.9 Hz, 2H), 7.10 (d, *J* = 8.3 Hz, 2H), 3.28 (t, *J* = 6.5 Hz, 2H), 2.62 (t, *J* = 7.3 Hz, 2H), 1.79-1.55 (m, 4H).

^{13}C NMR (75 MHz, $CDCl_3$) δ 140.4, 131.8, 129.8, 128.6, 51.4, 34.9, 28.51, 28.49.

IR (film): *v* (cm^{-1}) 2936, 2862, 2090, 1490, 1457, 1407, 1349, 1255, 1091, 1014, 887, 811, 711, 661, 630, 525, 485.

2-(4-Azidobutyl)naphthalene (**9n**)

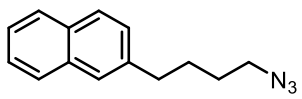

Compound **9n** (1.35 g, 6.0 mmol) was synthesized from 2-bromonaphthalene (2.07 g, 10 mmol) according to the above Procedure B and obtained as a colorless oil. Yield: 60%.

^{1}H NMR (300 MHz, $CDCl_3$) δ 7.87 (dd, J = 10.1, 7.9 Hz, 3H), 7.68 (s, 1H), 7.58-7.47 (m, 2H), 7.39 (dd, J = 8.4, 1.5 Hz, 1H), 3.33 (t, J = 6.7 Hz, 2H), 2.86 (t, J = 7.4 Hz, 2H), 1.92-1.79 (m, 2H), 1.78-1.64 (m, 2H).

^{13}C NMR (75 MHz, $CDCl_3$) δ 139.4, 133.7, 132.1, 128.0, 127.7, 127.5, 127.2, 126.5, 126.0, 125.3, 51.4, 35.5, 28.5, 28.3.

IR (film): ν (cm^{-1}) 3052, 2935, 2860, 2088, 1632, 1599, 1507, 1455, 1353, 1261, 1151, 1075, 1015, 954, 891, 853, 814, 744, 643, 555, 473, 403.

2-(4-Azidobutyl)dibenzo[b,d]thiophene (**9o**)

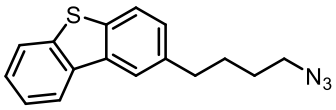

Compound **9o** (985 mg, 3.5 mmol) was synthesized from 2-bromodibenzo[*b*,*d*]thiophene (2.63 g, 10 mmol) according to the above Procedure B and obtained as a colorless oil. Yield: 35%.

^{1}H NMR (300 MHz, $CDCl_3$) δ 8.20-8.11 (m, 1H), 7.96 (d, J = 0.9 Hz, 1H), 7.89-7.82 (m, 1H), 7.77 (d, J = 8.2 Hz, 1H), 7.51-7.41 (m, 2H), 7.29 (dd, J = 8.2, 1.6 Hz, 1H), 3.32 (t, J = 6.7 Hz, 2H), 2.83 (t, J = 7.5 Hz, 2H), 1.82 (tt, J = 8.1, 7.0 Hz, 2H), 1.75-1.63 (m, 2H).

^{13}C NMR (75 MHz, $CDCl_3$) δ 140.0, 138.4, 137.2, 135.9, 135.6, 127.6, 126.8, 124.4, 123.0, 122.8, 121.7, 121.3, 51.5, 35.6, 29.0, 28.6.

IR (film): ν (cm^{-1}) 2932, 2859, 2088, 1464, 1428, 1349, 1262, 1156, 1069, 1022, 933, 884, 810, 762, 729, 674, 610, 556, 505, 417.

2-(4-Azidobutyl)dibenzo[b,d]furan (**9p**)

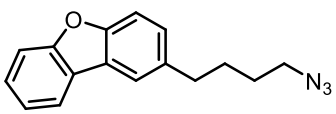

Compound **9p** (557 mg, 2.1 mmol) was synthesized from 2-bromodibenzo[*b*,*d*]furan (2.47 g, 10 mmol) according to the above Procedure B and obtained as a colorless oil. Yield: 21%.

^{1}H NMR (300 MHz, $CDCl_3$) δ 7.94 (dd, J = 7.6, 0.7 Hz, 1H), 7.75 (d, J = 1.3 Hz, 1H), 7.56 (d, J = 8.2 Hz, 1H), 7.45 (dt, J = 8.3, 5.0 Hz, 2H), 7.37-7.25 (m, 2H), 3.32 (t, J = 6.7 Hz, 2H), 2.81 (t, J = 7.4 Hz, 2H), 1.89-1.60 (m, 4H).

^{13}C NMR (75 MHz, $CDCl_3$) δ 156.7, 155.0, 136.5, 127.7, 127.2, 124.5, 124.4, 122.7, 120.7, 120.2, 111.8, 111.5, 51.5, 35.5, 29.2, 28.6.

IR (film): ν (cm^{-1}) 3050, 2934, 2861, 2089, 1594, 1478, 1445, 1347, 1270, 1248, 1191, 1114, 1074, 1018, 930, 884, 841, 810, 746, 649, 617, 559, 421.

2-(4-Azidobutyl)thiophene (**9q**)

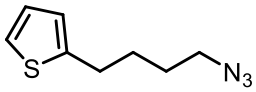

Compound **9q** (870 mg, 4.8 mmol) was synthesized from 4-(thiophen-2-yl)butanoic acid (1.70 g, 10 mmol) according to the above Procedure A and obtained as a colorless oil. Yield: 48%.

^{1}H NMR (300 MHz, $CDCl_3$) δ 7.13 (dd, J = 5.1, 1.2 Hz, 1H), 6.92 (dd, J = 5.1, 3.4 Hz, 1H), 6.82-6.76 (m, 1H), 3.30 (t, J = 6.6 Hz, 2H), 2.87 (t, J = 7.1 Hz, 2H), 1.84-1.60 (m, 4H).

^{13}C NMR (75 MHz, $CDCl_3$) δ 144.7, 126.9, 124.4, 123.3, 51.4, 29.5, 29.0, 28.4.

IR (film): ν (cm^{-1}) 2936, 2861, 2089, 1446, 1350, 1249, 1135, 1076, 1035, 890, 848, 824, 692, 557, 475.

3-(4-Azidobutyl)-9-methyl-9H-carbazole (**9s**)

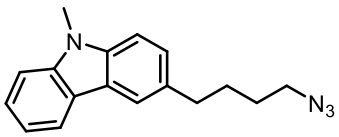

Compound **9s** (1.73 g, 6.2 mmol) was synthesized from 3-bromo-9-methyl-9*H*-carbazole (2.60 g, 10 mmol) according to the above Procedure B and obtained as a pale yellow oil. Yield: 62%.

^{1}H NMR (300 MHz, $CDCl_3$) δ 8.09 (d, J = 7.7 Hz, 1H), 7.90 (s, 1H), 7.48 (t, J = 7.6 Hz, 1H), 7.42-7.27 (m, 3H), 7.23 (t, J = 7.4 Hz, 1H), 3.84 (s, 3H), 3.31 (t, J = 6.8 Hz, 2H), 2.85 (t, J = 7.4 Hz, 2H), 1.89-1.62 (m, 4H).

^{13}C NMR (75 MHz, $CDCl_3$) δ 141.5, 139.8, 132.5, 126.5, 125.7, 123.1, 122.8, 120.4, 119.9, 118.8, 108.5, 108.4, 51.6, 35.6, 29.4, 29.2, 28.6.

IR (film): ν (cm^{-1}) 3051, 3021, 2930, 2858, 2089, 1602, 1483, 1355, 1326, 1244, 1148, 1122, 1058, 1015, 924, 883, 847, 800, 773, 741, 681, 623, 589, 559, 423.

5.3.3 Catalytic Enantioselective Intramolecular C-H Amination of Aliphatic Azides

1) General procedure for the initial optimization of the intramolecular C-H amination reaction (for Tables 3-6 in Chapter 3.2)

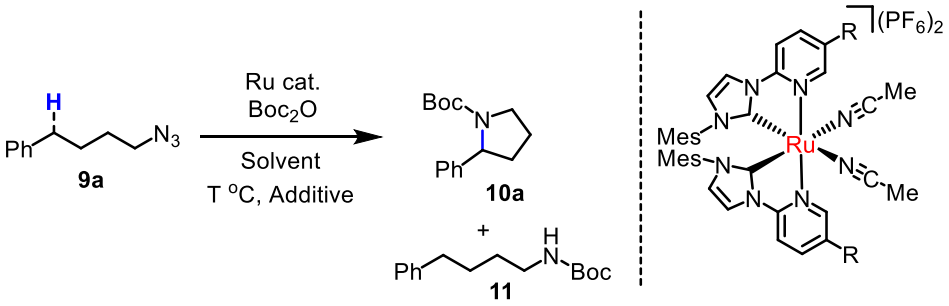

A dried 10 mL Schlenk tube was charged with azides **9a** (17.5 mg, 0.1 mmol, 1 equiv) and *rac*-**Ru1** (or Λ-**Ru1-7)** under an atmosphere of nitrogen. The indicated solvent and corresponding additive were added then, followed by Boc_2O. The reaction mixture was stirred at indicated temperature for indicated time under an atmosphere of nitrogen. The crude mixture was cooled down to room temperature and transferred to a 25 mL flask. All volatiles were removed from the solution via rotary evaporation. The residue was then analyzed by ^{1}H NMR spectroscopy using $Cl_2CHCHCl_2$ as internal standard to determine the conversion, yield of **10a** and **11**. The analytically pure product **10a** for the determination of the enantiomeric excess was obtained by preparative TLC. Enantiomeric excess was determined by HPLC analysis on chiral stationary phase.

2) Standard procedure for the substrate scope of the C-H amination reaction

A dried 10 mL Schlenk tube was charged with azides **9a-u** (0.2 mmol) and Λ-**Ru7** (2.6 mg, 0.002 mmol, 1 mol%) under an atmosphere of nitrogen. A solution of P(4-F-Ph)$_3$ (0.5 mL, 0.002 mmol, 4 mM in 1,2-dichlorobenzene) was added via syringe, followed by Boc_2O (45.8 μL, 0.2 mmol, 1 equiv). The reaction mixture was stirred at 95 ℃ for 60 h under an atmosphere of nitrogen. Afterwards, the

mixture was concentrated under reduced pressure, and the residue was purified by flash chromatography on silica gel (*n*-hexane/EtOAc = 60:1 to 15:1) to afford the analytically pure products **10a-u**. Enantiomeric excess was determined by HPLC analysis on chiral stationary phase. The absolute configuration of the product was determined by comparing the optical rotation with the reported literature.[6]

***tert*-Butyl (*R*)-2-phenylpyrrolidine-1-carboxylate (10a)**[6]

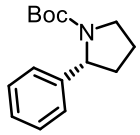

Starting from **9a** (35.0 mg, 0.20 mmol) according to the general procedure to provide **10a** as a white solid (25.0 mg, 0.102 mmol, 51% yield). Enantiomeric excess was determined by HPLC analysis on a chiral stationary phase, ee = 95%. HPLC conditions: Chiralpak IG column (4.6 × 250 mm), UV detection at 220 nm, mobile phase *n*-hexane/isopropanol = 97:3, flow rate 1.0 mL/min, column temperature = 25 ℃, t_r (major) = 9.6 min, t_r (minor) = 10.4 min. $[\alpha]_D^{22}$ = +82.9° (*c* = 1.0, CH_2Cl_2).

^{1}H NMR (300 MHz, $CDCl_3$) δ 7.34-7.26 (m, 2H), 7.24-7.14 (m, 3H), 5.05-4.65 (br, m, 1H), 3.74-3.45 (br, m, 2H), 2.41-2.19 (br, m, 1H), 1.99-1.78 (m, 3H), 1.55-1.11 (br, m, 9H).

^{13}C NMR (75 MHz, $CDCl_3$) δ 154.7, 145.3, 128.3, 126.6, 125.6, 79.3, 61.5, 60.9, 47.3, 36.1, 34.9, 28.3, 23.4.

HRMS (ESI, *m/z*) calcd. for $C_{15}H_{21}NO_2Na$ $[M+Na]^+$: 270.1465, found: 270.1463.

***tert*-Butyl (*R*)-2-(p-tolyl)pyrrolidine-1-carboxylate (10b)**[6]

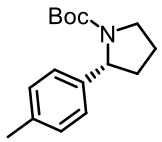

Starting from **9b** (37.9 mg, 0.20 mmol) according to the general procedure to give **10b** as a white solid (27.1 mg, 0.104 mmol, 52% yield). Enantiomeric excess was determined by HPLC analysis on a chiral stationary phase, ee = 93%. HPLC conditions: Chiralpak IG column (4.6 × 250 mm), UV detection at 220 nm, mobile phase *n*-hexane/isopropanol = 99:1, flow rate 1.0 mL/min, column temperature = 25 ℃, t_r (major) = 13.0 min, t_r (minor) = 15.9 min. $[\alpha]_D^{22}$ = +91.6° (*c* = 1.0, CH_2Cl_2).

^{1}H NMR (300 MHz, $CDCl_3$) δ 7.13-7.01 (m, 4H), 5.04-4.64 (br, m, 1H), 3.70-3.42 (br, m, 2H), 2.38-2.20 (m, 4H), 1.97-1.75 (m, 3H), 1.53-1.12 (br, m, 9H).

^{13}C NMR (75 MHz, $CDCl_3$) δ 154.7, 142.2, 136.1, 128.9, 125.5, 79.2, 61.2, 47.2, 36.1, 28.4, 23.3, 21.1.

HRMS (ESI, *m/z*) calcd. for $C_{16}H_{23}NO_2Na$ $[M+Na]^+$: 284.1621, found: 284.1621.

***tert*-Butyl (*R*)-2-(m-tolyl)pyrrolidine-1-carboxylate (10c)**[6]

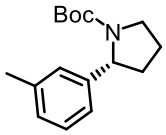

Starting from **9c** (37.9 mg, 0.2 mmol) according to the general procedure to give **10c** as a white solid (26.1 mg, 0.10 mmol, 50% yield). Enantiomeric excess was determined by HPLC analysis on a chiral stationary phase, ee = 91%. HPLC conditions: Chiralpak IG column (4.6 × 250 mm), UV detection at 220 nm, mobile phase *n*-hexane/isopropanol = 99:1, flow rate 1.0 mL/min, column temperature = 25 ℃, t_r (major) = 14.6 min, t_r (minor) = 16.6 min. $[\alpha]_D^{22}$ = +83.5° (*c* = 1.0, CH_2Cl_2).

^{1}H NMR (300 MHz, $CDCl_3$) δ 7.22-7.12 (m, 1H), 7.05-6.92 (m, 3H), 5.04-4.59 (br, m, 1H), 3.75-3.37 (br, m, 2H), 2.38-2.22 (m, 4H), 1.98-1.74 (m, 3H), 1.53-1.09 (br, m, 9H).

^{13}C NMR (75 MHz, $CDCl_3$) δ 154.8, 145.2, 137.8, 128.2, 127.3, 126.4, 122.8, 79.3, 61.5, 47.3, 36.1, 28.3, 23.4, 21.6.

HRMS (ESI, *m/z*) calcd. for $C_{16}H_{23}NO_2Na$ $[M+Na]^+$: 284.1621, found: 284.1622.

***tert*-Butyl (*R*)-2-(o-tolyl)pyrrolidine-1-carboxylate (10d)**[7]

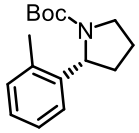

Starting from **9d** (37.9 mg, 0.2 mmol) according to the general procedure to give **10d** as a white solid (7.8 mg, 0.03 mmol, 15% yield). Enantiomeric excess was determined by HPLC analysis on a chiral stationary phase, ee = 90%. HPLC conditions: Chiralpak IG column (4.6 × 250 mm), UV detection at 220 nm, mobile phase *n*-hexane/isopropanol = 99:1, flow rate 1.0 mL/min, column temperature = 25 ℃, t_r (major) = 13.9 min, t_r (minor) = 15.4 min. $[\alpha]_D^{22}$ = +89.1° (*c* = 1.0, CH_2Cl_2).

^{1}H NMR (300 MHz, $CDCl_3$) δ 7.18-7.02 (m, 4H), 5.20-4.89 (br, m, 1H), 3.75-3.39 (br, m, 2H), 2.40-2.21(m, 4H), 2.00-1.65 (m, 3H), 1.50-1.10 (br, m, 9H).

^{13}C NMR (75 MHz, $CDCl_3$) δ 154.6, 143.5, 134.0, 130.1, 126.4, 126.0, 124.6, 79.2, 58.2, 47.3, 34.3, 33.0, 28.6, 28.2, 23.3, 19.4.

HRMS (ESI, *m/z*) calcd. for $C_{16}H_{23}NO_2Na$ $[M+Na]^+$: 284.1621, found: 284.1620.

***tert*-Butyl (*R*)-2-(4-methoxyphenyl)pyrrolidine-1-carboxylate (10e)**[6]

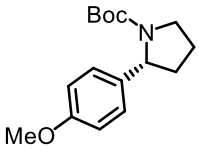

Starting from **9e** (41.1 mg, 0.2 mmol) according to the general procedure to give **10e** as a white solid (29.3 mg, 0.106 mmol, 53% yield). Enantiomeric excess was determined by HPLC analysis on a chiral stationary phase, ee = 99%. HPLC conditions: Chiralpak IG column (4.6 × 250 mm), UV detection at 220 nm, mobile phase *n*-hexane/isopropanol = 99:1, flow rate 1.0 mL/min, column temperature = 25 ℃, t_r (minor) = 26.3 min, t_r (major) = 28.2 min. $[\alpha]_D^{22}$ = +108.6° (*c* = 1.0, CH_2Cl_2).

^{1}H NMR (300 MHz, $CDCl_3$) δ 7.15-7.03 (m, 2H), 6.90-6.76 (m, 2H), 5.05-4.57 (br, m, 1H), 3.79 (s, 3H), 3.69-3.40 (br, m, 2H), 2.37-2.16 (m, 1H), 1.99-1.73 (m, 3H), 1.48-1.13 (br, m, 9H).

^{13}C NMR (75 MHz, $CDCl_3$) δ 158.4, 154.8, 129.4, 126.7, 113.7, 79.2, 60.8, 55.4, 47.2, 36.2, 28.4, 23.4.

HRMS (ESI, *m/z*) calcd. for $C_{16}H_{23}NO_3Na$ $[M+Na]^+$: 300.1570, found: 300.1571.

***tert*-Butyl (*R*)-2-([1,1'-biphenyl]-4-yl)pyrrolidine-1-carboxylate (10f)**[8]

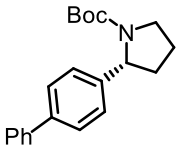

Starting from **9f** (50.3 mg, 0.2 mmol) according to the general procedure to give **10f** as a white solid (32.2 mg, 0.10 mmol, 50% yield). Enantiomeric excess was determined by HPLC analysis on a chiral stationary phase, ee = 94%. HPLC conditions: Chiralpak IG column (4.6 × 250 mm), UV detection at 254 nm, mobile phase *n*-hexane/isopropanol = 99:1, flow rate 1.0 mL/min, column temperature = 25 ℃, t_r (major) = 21.2 min, t_r (minor) = 27.2 min. $[\alpha]_D^{22}$ = +69.7° (*c* = 1.0, CH_2Cl_2).

^{1}H NMR (300 MHz, $CDCl_3$) δ 7.64-7.51 (m, 4H), 7.48-7.40 (m, 2H), 7.37-7.30 (m, 1H), 7.28-7.22 (m, 2H), 5.11-4.71 (br, m, 1H), 3.77-3.45 (br, m, 2H), 2.46-2.21 (m, 1H), 2.05-1.79 (m, 3H), 1.48 (br, s, 3H), 1.22 (br, s, 6H).

^{13}C NMR (75 MHz, $CDCl_3$) δ 154.7, 144.4, 141.1, 139.6, 128.8, 127.2, 127.1, 127.0, 126.1, 79.4, 61.2, 47.3, 36.1, 28.4, 23.4.

HRMS (ESI, *m/z*) calcd. for $C_{21}H_{25}NO_2Na$ $[M+Na]^+$: 346.1778, found: 346.1776.

***tert*-Butyl (*R*)-2-(3,4-dimethoxyphenyl)pyrrolidine-1-carboxylate (10g)**[6]

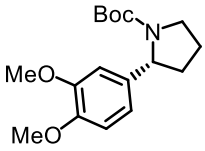

Starting from **9g** (47 mg, 0.2 mmol) according to the general procedure to give **10g** as a white solid (31.3 mg, 0.102 mmol, 51% yield). Enantiomeric excess was determined by HPLC analysis on a chiral stationary phase, ee = 94%. HPLC conditions: Chiralpak IC column (4.6 × 250 mm), UV detection at 220 nm, mobile phase *n*-hexane/isopropanol = 80:20, flow rate 1.0 mL/min, column temperature = 25 ℃, t_r (major) = 17.1 min, t_r (minor) = 20.6 min. **$[\alpha]_D^{22}$** = +75.6° (c = 1.0, CH_2Cl_2).

^{1}H NMR (300 MHz, $CDCl_3$) δ 6.85-6.76 (m, 1H), 6.75-6.62 (m, 2H), 5.05-4.60 (br, m, 1H), 3.85 (s, 6H), 3.68-3.43 (br, m, 2H), 2.40-2.15 (m, 1H), 1.98-1.75 (m, 3H), 1.50-1.13 (br, m, 9H).

^{13}C NMR (75 MHz, $CDCl_3$) δ 154.8, 149.0, 147.8, 138.0, 117.7, 111.2, 109.1, 79.3, 61.1, 56.1, 56.0, 47.3, 36.1, 28.4, 23.4.

HRMS (ESI, *m/z*) calcd. for $C_{17}H_{25}NO_4Na$ $[M+Na]^+$: 330.1676, found: 330.1673.

***tert*-Butyl (*R*)-2-(4-(methylthio)phenyl)pyrrolidine-1-carboxylate (10h)**

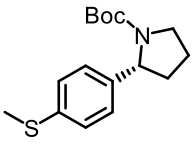

Starting from **9h** (44.3 mg, 0.2 mmol) according to the general procedure to give **10h** as a colourless oil (29.9 mg, 0.102 mmol, 51% yield). (**Note**: The side product *tert*-butyl (4-(4-(methylthio)phenyl)butyl)carbamate could not be removed from the target product.) Enantiomeric excess was determined by HPLC analysis on a chiral stationary phase, ee = 94%. HPLC

conditions: Chiralpak IG column (4.6 × 250 mm), UV detection at 220 nm, mobile phase *n*-hexane/isopropanol = 99:1, flow rate 1.0 mL/min, column temperature = 25 ℃, t_r (major) = 24.7 min, t_r (minor) = 30.1 min. $[\alpha]_D^{22}$ = +28.2° (*c* = 1.0, CH_2Cl_2).

^{1}H NMR (300 MHz, $CDCl_3$) δ 7.23-7.17 (m, 2H), 7.12-7.06 (m, 2H), 5.04-4.65 (br, m, 1H), 3.72-3.39 (br, m, 2H), 2.47 (s, 3H), 2.33-2.21 (m, 1H), 1.94-1.73 (m, 3H), 1.44 (br, s, 3H), 1.21 (br, s, 6H).

^{13}C NMR (75 MHz, $CDCl_3$) δ 154.7, 136.3, 129.1, 127.4, 126.2, 79.4, 60.9, 47.3, 35.6, 28.5, 23.4, 16.4.

IR (film): *v* (cm^{-1}) 2972, 2926, 2874, 1689, 1490, 1445, 1390, 1251, 1161, 1112, 1016, 967, 901, 871, 818, 774, 569, 521.

HRMS (ESI, *m/z*) calcd. for $C_{16}H_{23}NSO_2Na[M+Na]^+$: 316.1342, found: 316.1342.

***tert*-Butyl (*R*)-2-(4-(dimethylamino)phenyl)pyrrolidine-1-carboxylate (10i)**

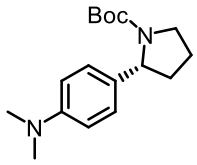

Starting from **9i** (43.6 mg, 0.2 mmol) according to the general procedure to give **10i** as a white solid (32.0 mg, 0.11 mmol, 55% yield). Enantiomeric excess was determined by HPLC analysis on a chiral stationary phase, ee = 77%. HPLC conditions: Chiralpak IG column (4.6 × 250 mm), UV detection at 254 nm, mobile phase *n*-hexane/isopropanol = 95:5, flow rate 1.0 mL/min, column temperature = 25 ℃, t_r (major) = 12.1 min, t_r (minor) = 15.2 min. $[\alpha]_D^{22}$ = +86.2° (*c* = 1.0, CH_2Cl_2).

^{1}H NMR (300 MHz, $CDCl_3$) δ 7.03 (d, *J* = 8.5 Hz, 2H), 6.68 (d, *J* = 8.7 Hz, 2H), 5.05-4.51 (br, m, 1H), 3.70-3.40 (br, m, 2H), 2.92 (s, 6H), 2.35-2.11 (m, 1H), 1.98-1.74 (m, 3H), 1.44 (br, s, 3H), 1.23 (br, s, 6H).

^{13}C NMR (75 MHz, $CDCl_3$) δ 154.8, 149.7, 133.3, 126.5, 112.7, 79.1, 60.8, 47.1, 41.0, 36.0, 28.5, 23.3.

IR (film): *v* (cm^{-1}) 2964, 2924, 2862, 2803, 2095, 1678, 1614, 1565, 1520, 1480, 1450, 1394, 1353, 1226, 1159, 1106, 1026, 946, 895, 865, 816, 769, 696, 611, 571, 529, 469, 432.

HRMS (ESI, *m/z*) calcd. for $C_{17}H_{27}N_2O_2$ $[M+H]^+$: 291.2067, found: 291.2065.

***tert*-Butyl (*R*)-2-(4-((diethoxyphosphoryl)oxy)phenyl)pyrrolidine-1-carboxylate (10j)**

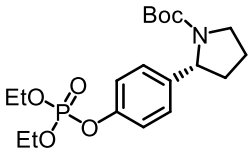

Starting from **9j** (65.3 mg, 0.2 mmol) according to the general procedure to give **10j** as a colourless oil (25.6 mg, 0.064 mmol, 32% yield). Enantiomeric excess was determined by HPLC analysis on a chiral stationary phase, ee = 92%. HPLC conditions: Chiralpak IG column (4.6 × 250 mm), UV detection at 220 nm, mobile phase *n*-hexane/isopropanol = 80:20, flow rate 1.0 mL/min, column temperature = 25 ℃, t_r (minor) = 19.0 min, t_r (major) = 20.8 min. $\mathbf{[\alpha]_D^{22}}$ = +54.7° (*c* = 1.0, CH_2Cl_2).

^{1}H NMR (300 MHz, $CDCl_3$) δ 7.17-7.09 (m, 4H), 5.05-4.60 (br, m, 1H), 4.27-4.13 (m, 4H), 3.72-3.40 (br, m, 2H), 2.39-2.18 (m, 1H), 1.95-1.72 (m, 3H), 1.45-1.10 (m, 15H).

^{13}C NMR (75 MHz, $CDCl_3$) δ 154.7, 149.5, 149.5, 129.7, 126.9, 119.9, 119.8, 79.5, 64.7, 64.6, 60.6, 47.3, 36.1, 28.4, 23.4, 16.3, 16.2.

IR (film): *v* (cm^{-1}) 2977, 2932, 1691, 1506, 1451, 1391, 1274, 1216, 1162, 1109, 1025, 958, 872, 833, 803, 767, 697, 632, 538.

HRMS (ESI, *m/z*) calcd. for $C_{19}H_{30}NPO_6Na$ $[M+Na]^+$: 422.1703, found: 422.1698.

***tert*-Butyl (*R*)-2-(4-(benzyloxy)phenyl)pyrrolidine-1-carboxylate (10k)**

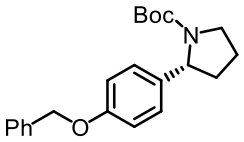

Starting from **9k** (56.3 mg, 0.2 mmol) according to the general procedure to give **10k** as a white solid (29.5 mg, 0.084 mmol, 42% yield). Enantiomeric excess was determined by HPLC analysis on a chiral stationary phase, ee = 92%. HPLC conditions: Chiralpak IG column (4.6 × 250 mm), UV detection at 220 nm, mobile phase *n*-hexane/isopropanol = 98:2, flow rate 1.0 mL/min, column temperature = 25 ℃, t_r (major) = 16.5 min, t_r (minor) = 17.6 min. $\mathbf{[\alpha]_D^{22}}$ = +66.7° (*c* = 1.0, CH_2Cl_2).

^{1}H NMR (300 MHz, $CDCl_3$) δ 7.47-7.28 (m, 5H), 7.08 (d, *J* = 8.5 Hz, 2H), 6.95-6.86 (m, 2H), 5.05 (s, 2H), 4.98-4.65 (br, m, 1H), 3.70-3.40 (br, m, 2H), 2.37-2.17 (m, 1H), 1.99–1.74 (m, 3H), 1.44 (br, s, 3H), 1.20 (br, s, 6H).

^{13}C NMR (75 MHz, $CDCl_3$) δ 157.6, 154.8, 137.3, 128.7, 128.0, 127.6, 126.7, 114.8, 79.3, 70.2, 60.9,

47.2, 36.2, 28.4, 23.4.

IR (film): ν (cm^{-1}) 2968, 2925, 2880, 1689, 1609, 1508, 1453, 1390, 1246, 1159, 1098, 1039, 969, 877, 821, 768, 734, 695, 636, 552, 506, 462, 436.

HRMS (ESI, *m/z*) calcd. for $C_{22}H_{27}NO_3Na$ $[M+Na]^+$: 376.1883, found: 376.1878.

***tert*-Butyl (*R*)-2-(4-fluorophenyl)pyrrolidine-1-carboxylate (10l)**[6]

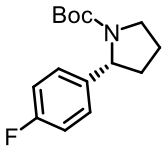

Starting from **9l** (38.6 mg, 0.2 mmol) according to the general procedure to give **10l** as a white solid (21.1 mg, 0.08 mmol, 40% yield). Enantiomeric excess was determined by HPLC analysis on a chiral stationary phase, ee = 94%. HPLC conditions: Chiralpak IG column (4.6 × 250 mm), UV detection at 220 nm, mobile phase *n*-hexane/isopropanol = 99:1, flow rate 1.0 mL/min, column temperature = 25 ℃, t_r (major) = 14.5 min, t_r (minor) = 16.1 min. $[\alpha]_D^{22}$ = +76.3° (*c* = 1.0, CH_2Cl_2).

^{1}H NMR (300 MHz, $CDCl_3$) δ 7.17-7.05 (m, 2H), 7.02-6.92 (m, 2H), 5.03-4.63 (br, m, 1H), 3.69-3.42 (br, m, 2H), 2.39-2.18 (m, 1H), 1.96-1.71 (m, 3H), 1.45-1.08 (br, m, 9H).

^{13}C NMR (126 MHz, $CDCl_3$) δ 162.7, 160.7, 154.6, 141.0, 127.1, 127.1, 115.1, 114.9, 79.5, 60.9, 60.3, 47. 5, 47.2, 36.2, 35.0, 28.7, 28.3, 23.6, 23.3.

HRMS (ESI, *m/z*) calcd. for $C_{15}H_{20}FNO_2Na$ $[M+Na]^+$: 288.1370, found: 288.1369.

***tert*-Butyl (*R*)-2-(4-chlorophenyl)pyrrolidine-1-carboxylate (10m)**[6]

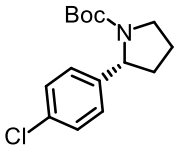

Starting from **9m** (41.9 mg, 0.2 mmol) according to the general procedure to give **10m** as a white solid (25.3 mg, 0.09 mmol, 45% yield). Enantiomeric excess was determined by HPLC analysis on a chiral stationary phase, ee = 95%. HPLC conditions: Chiralpak IG column (4.6 × 250 mm), UV detection at 220 nm, mobile phase *n*-hexane/isopropanol = 99:1, flow rate 1.0 mL/min, column temperature = 25 ℃, t_r (major) = 13.8 min, t_r (minor) = 17.1 min. $[\alpha]_D^{22}$ = +72.0° (*c* = 1.0, CH_2Cl_2).

^{1}H NMR (300 MHz, $CDCl_3$) δ 7.29-7.24 (m, 2H), 7.13-7.07 (m, 2H), 4.98-4.63 (br, m, 1H), 3.70-3.42

(br, m, 2H), 2.39-2.18 (m, 1H), 1.96-1.71 (m, 3H), 1.43 (br, m, 3H), 1.20 (br, m, 6H).

^{13}C NMR (75 MHz, $CDCl_3$) δ 154.6, 143.9, 132.3, 128. 5, 127.0, 79.6, 60.9, 47.3, 36.1, 28.4, 23.3.

HRMS (ESI, *m/z*) calcd. for $C_{15}H_{20}NO_2ClNa$ $[M+Na]^+$: 304.1075, found: 304.1087.

***tert*-butyl (*R*)-2-(naphthalen-2-yl)pyrrolidine-1-carboxylate (10n)**[6]

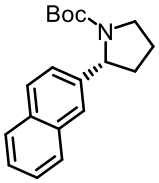

Starting from **9m** (45.0 mg, 0.2 mmol) according to the general procedure to give **10m** as a white solid (34.0 mg, 0.114 mmol, 57% yield). Enantiomeric excess was determined by HPLC analysis on a chiral stationary phase, ee = 96%. HPLC conditions: Chiralpak IG column (4.6 × 250 mm), UV detection at 220 nm, mobile phase *n*-hexane/isopropanol = 99:1, flow rate 1.0 mL/min, column temperature = 25 ℃, t_r (major) = 19.4 min, t_r (minor) = 25.3 min. **$[\alpha]_D^{22}$** = +103.2° (*c* = 1.0, CH_2Cl_2).

^{1}H NMR (300 MHz, $CDCl_3$) δ 7.88-7.74 (m, 3H), 7.59 (s, 1H), 7.51-7.39 (m, 2H), 7.36-7.28 (m, 1H), 5.23-4.83 (br, m, 1H), 3.84-3.52 (br, m, 2H), 2.47-2.26 (m, 1H), 2.04-1.82 (m, 3H), 1.48 (br, s, 3H), 1.16 (br, s, 6H).

^{13}C NMR (75 MHz, $CDCl_3$) δ 154.8, 142.6, 133.5, 132.6, 128.2, 127.8, 127.7, 126.1, 125.5, 124.3, 124.0, 79.4, 61.5, 47.3, 36.0, 28.3, 23.3.

HRMS (ESI, *m/z*) calcd. for $C_{19}H_{23}NO_2Na$ $[M+Na]^+$: 320.1621, found: 320.1622.

***tert*-Butyl (*R*)-2-(dibenzo[b,d]thiophen-2-yl)pyrrolidine-1-carboxylate (10o)**

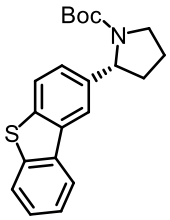

Starting from **9o** (56.3 mg, 0.2 mmol) according to the general procedure to give **10o** as a pale yellow oil (34.5 mg, 0.098 mmol, 49% yield). Enantiomeric excess was determined by HPLC analysis on a chiral stationary phase, ee = 95%. HPLC conditions: Chiralpak IG column (4.6 × 250 mm), UV detection at 220 nm, mobile phase *n*-hexane/isopropanol = 99:1, flow rate 1.0 mL/min, column

temperature = 25 ℃, t_r (major) = 11.7 min, t_r (minor) = 19.3 min. **$[\alpha]_D^{22}$** = +62.0° (*c* = 1.0, CH_2Cl_2).

^{1}H NMR (300 MHz, $CDCl_3$) δ 8.22-8.07 (m, 1H), 7.94 (s, 1H), 7.87-7.73 (m, 2H), 7.44 (dd, *J* = 5.7, 2.9 Hz, 2H), 7.29 (d, *J* = 7.8 Hz, 1H), 5.25-4.85 (br, m, 1H), 3.83-3.53 (br, m, 2H), 2.50-2.30 (m, 1H), 2.07-1.85 (m, 3H), 1.49 (br, s, 3H), 1.17 (br, s, 6H).

^{13}C NMR (75 MHz, $CDCl_3$) δ 154.7, 141.8, 139.8, 137.5, 135.6, 126.6, 124.6, 124.4, 122.9, 122.6, 121.5, 118.4, 79.4, 61.3, 47.3, 36.4, 28.3, 23.4.

IR (film): *v* (cm^{-1}) 2971, 2928, 2874, 1686, 1469, 1390, 1256, 1160, 1111, 1078, 1022, 911, 876, 810, 764, 731, 624, 523, 421.

HRMS (ESI, *m/z*) calcd. for $C_{21}H_{23}NO_2SNa$ $[M+Na]^+$: 376.1342, found: 376.1341.

***tert*-Butyl (*R*)-2-(dibenzo[b,d]furan-2-yl)pyrrolidine-1-carboxylate (10p)**

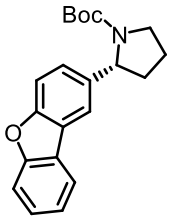

Starting from **9p** (53.1 mg, 0.2 mmol) according to the general procedure to give **10p** as a pale yellow oil (34.3 mg, 0.102 mmol, 51% yield). Enantiomeric excess was determined by HPLC analysis on a chiral stationary phase, ee = 80%. HPLC conditions: Chiralpak IG column (4.6 × 250 mm), UV detection at 220 nm, mobile phase *n*-hexane/isopropanol = 95:5, flow rate 1.0 mL/min, column temperature = 25 ℃, t_r (major) = 10.7 min, t_r (minor) = 16.5 min. **$[\alpha]_D^{22}$** = +22.4° (*c* = 1.0, CH_2Cl_2).

^{1}H NMR (300 MHz, $CDCl_3$) δ 7.93 (d, *J* = 7.3 Hz, 1H), 7.74 (d, *J* = 1.0 Hz, 1H), 7.60-7.40 (m, 3H), 7.38-7.26 (m, 2H), 5.24-4.83 (br, m, 1H), 3.87-3.43 (br, m, 1H), 2.53-2.22 (m, 1H), 2.05-1.84 (m, 3H), 1.47 (br, s, 3H), 1.17 (br, s, 6H).

^{13}C NMR (75 MHz, $CDCl_3$) δ 156.7, 155.3, 154.8, 139.9, 127.2, 125.0, 124.4, 124.2, 122.7, 120.7, 117.5, 111.8, 111.4, 79.4, 61.4, 47.4, 36.4, 28.4, 23.4.

IR (film): *v* (cm^{-1}) 2971, 2928, 2874, 1687, 1478, 1447, 1390, 1250, 1192, 1161, 1110, 1021, 972, 912, 871, 844, 811, 748, 659, 626, 545, 424.

HRMS (ESI, *m/z*) calcd. for $C_{21}H_{23}NO_3Na$ $[M+Na]^+$: 360.1570, found: 360.1570.

***tert*-Butyl (*R*)-2-(thiophen-2-yl)pyrrolidine-1-carboxylate (10q)**[6]

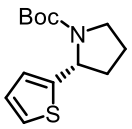

Starting from **9q** (36.3 mg, 0.2 mmol) according to the general procedure to give **10q** as a yellow oil (25.3 mg, 0.10 mmol, 50% yield). Enantiomeric excess was determined by HPLC analysis on a chiral stationary phase, ee = 90%. HPLC conditions: Chiralpak IG column (4.6 × 250 mm), UV detection at 220 nm, mobile phase *n*-hexane/isopropanol = 95:5, flow rate 1.0 mL/min, column temperature = 25 ℃, t_r (major) = 16.7 min, t_r (minor) = 19.3 min. $[\alpha]_D^{22}$ = +69.6° (*c* = 1.0, CH_2Cl_2).

^{1}H NMR (300 MHz, $CDCl_3$) δ 7.20-7.06 (m, 1H), 6.97-6.75 (m, 2H), 5.29-4.96 (br, m, 1H), 3.64-3.35 (br, m, 2H), 2.35-2.16 (m, 1H), 2.10-1.85 (m, 3H), 1.52-1.25 (br, m, 9H).

^{13}C NMR (75 MHz, $CDCl_3$) δ 154. 6, 149.0, 126.5, 123.4, 123.2, 79.7, 56.9, 46.4, 35.7, 28.5, 23.3.

HRMS (ESI, *m/z*) calcd. for $C_{13}H_{19}SNO_2Na$ $[M+Na]^+$: 276.1029, found: 276.1028.

***tert*-Butyl (*R*)-2-(furan-2-yl)pyrrolidine-1-carboxylate (10r)**[9]

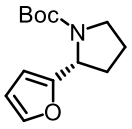

Starting from **9r** (33.0 mg, 0.2 mmol) according to the general procedure to give **10r** as a pale yellow oil (17.0 mg, 0.072 mmol, 36% yield). Enantiomeric excess was determined by HPLC analysis on a chiral stationary phase, ee = 76%. HPLC conditions: Chiralpak IG column (4.6 × 250 mm), UV detection at 220 nm, mobile phase *n*-hexane/isopropanol = 99:1, flow rate 1.0 mL/min, column temperature = 25 ℃, t_r (major) = 12.4 min, t_r (minor) = 13.4 min. $[\alpha]_D^{22}$ = +31.0° (*c* = 1.0, CH_2Cl_2).

^{1}H NMR (300 MHz, $CDCl_3$) δ 7.29 (dd, *J* = 1.8, 0.8 Hz, 1H), 6.27 (dd, *J* = 3.1, 1.8 Hz, 1H), 6.07 (s, 1H), 5.10-4.70 (br, m, 1H), 3.62-3.28 (m, 2H), 2.21-1.79 (m, 4H), 1.51-1.26 (br, m, 9H).

^{13}C NMR (75 MHz, $CDCl_3$) δ 154.5, 141.2, 110.2, 105.5, 79.5, 54.8, 46.3, 32.3, 28.5, 23.6.

HRMS (ESI, *m/z*) calcd. for $C_{13}H_{19}O_3NNa$ $[M+Na]^+$: 260.1257, found: 260.1258.

***tert*-Butyl (*R*)-2-(9-methyl-9H-carbazol-3-yl)pyrrolidine-1-carboxylate (10s)**

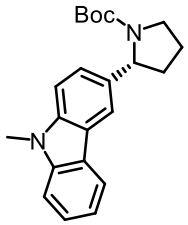

Starting from **9s** (55.7 mg, 0.2 mmol) according to the general procedure to give **10s** as a pale yellow solid (35.0 mg, 0.10 mmol, 50% yield). Enantiomeric excess was determined by HPLC analysis on a chiral stationary phase, ee = 93%. HPLC conditions: Chiralpak IG column (4.6 × 250 mm), UV detection at 254 nm, mobile phase *n*-hexane/isopropanol = 90:10, flow rate 1.0 mL/min, column temperature = 25 ℃, t_r (major) = 12.1 min, t_r (minor) = 24.7 min. $[\alpha]_D^{22}$ = +76.5° (*c* = 1.0, CH_2Cl_2).

^{1}H NMR (300 MHz, $CDCl_3$) δ 8.09 (d, *J* = 7.7 Hz, 1H), 7.89 (s, 1H), 7.48 (t, *J* = 7.5 Hz, 1H), 7.42-7.28 (m, 3H), 7.22 (d, *J* = 7.3 Hz, 1H), 5.26-4.85 (br, m, 1H), 3.90-3.60 (m, 5H), 2.50-2.28 (m, 1H), 2.08-1.82 (m, 3H), 1.59-1.08 (br, m, 9H).

^{13}C NMR (75 MHz, $CDCl_3$) δ 155.0, 141.5, 140.2, 135.9, 125.7, 123.7, 122.9, 122.7, 120.3, 118.8, 117.2, 108.5, 108.2, 79.2, 61.7, 47.4, 36.6, 29.2, 28.4, 23.4.

IR (film): *v* (cm^{-1}) 3045, 2965, 2925, 2857, 1679, 1600, 1478, 1397, 1357, 1330, 1248, 1153, 1115, 1022, 971, 915, 875, 826, 770, 743, 706, 631, 598, 563, 545, 456, 427.

HRMS (ESI, *m/z*) calcd. for $C_{22}H_{26}O_2N_2Na$ $[M+Na]^+$: 373.1886, found: 373.1899.

***tert*-Butyl (*S*)-1-phenylisoindoline-2-carboxylate (10t)**

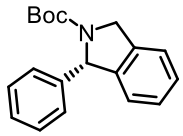

Starting from **9t** (44.7 mg, 0.2 mmol) according to the general procedure to give **10t** as a pale yellow solid (27.7 mg, 47% yield). Enantiomeric excess was determined by HPLC analysis on a chiral stationary phase, ee = 80%. HPLC conditions: Chiralpak IG column (4.6 × 250 mm), UV detection at 254 nm, mobile phase *n*-hexane/isopropanol = 95:5, flow rate 1.0 mL/min, column temperature = 25 ℃, t_r (minor) = 9.4 min, t_r (major) = 13.0 min. $[\alpha]_D^{22}$ = +142.3° (*c* = 1.0, CH_2Cl_2).

^{1}H NMR (300 MHz, $CDCl_3$) δ 7.36-7.18 (m, 8H), 7.02 (dd, *J* = 17.1, 7.3 Hz, 1H), 6.06-5.81 (br, m, 1H), 4.99-4.84 (m, 2H), 1.48 (s, 3H), 1.25 (s, 6H).

^{13}C NMR (75 MHz, $CDCl_3$) δ 154.6, 144.3, 142.0, 135.8, 128.7, 128.4, 127.8, 127.3, 126.8, 123.7, 122.9, 80.0, 67.7, 67.4, 53.1, 52.7, 28.7, 28.3.

IR (film): ν (cm^{-1}) 2977, 2925, 2883, 1680, 1598, 1468, 1394, 1310, 1261, 1176, 1121, 1028, 894, 870, 829, 786, 740, 704, 628, 597, 559, 459, 418.

HRMS (ESI, *m/z*) calcd. for $C_{19}H_{21}O_2N_1Na$ $[M+Na]^+$: 318.1465, found: 318.1472.

***tert*-Butyl (*S*)-1-phenyl-1,3-dihydro-2H-benzo[f]isoindole-2-carboxylate (10u)**

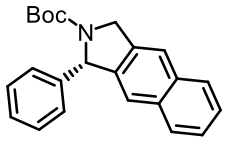

Starting from **9u** (54.7 mg, 0.2 mmol) according to the general procedure with slight modifications (85 ℃ and 0.2 mL 1,2-dichlorobenzene were used) to give **10u** as a white solid (31.0 mg, 45% yield). Enantiomeric excess was determined by HPLC analysis on a chiral stationary phase, ee = 94%. HPLC conditions: Chiralpak IG column (4.6 × 250 mm), UV detection at 254 nm, mobile phase *n*-hexane/isopropanol = 95:5, flow rate 1.0 mL/min, column temperature = 25 ℃, t_r (minor) = 13.4 min, t_r (major) = 20.3 min. $[\alpha]_D^{22}$ = +35.4° (*c* = 1.0, CH_2Cl_2).

^{1}H NMR (300 MHz, $CDCl_3$) δ 7.77 (dd, *J* = 35.3, 7.8 Hz, 3H), 7.53-7.37 (m, 3H), 7.35-7.21 (m, 5H), 6.26-5.92 (br, m, 1H), 5.19-4.95 (m, 2H), 1.51 (s, 3H), 1.28 (s, 6H).

^{13}C NMR (75 MHz, $CDCl_3$) δ 154.6, 144.7, 141.1, 134.7, 133.4, 128.5, 128.1, 127.9, 127.4, 126.8, 126.0, 125.8, 122.5, 121.4, 80.1, 67.1, 52.2, 28.4.

IR (film): ν (cm^{-1}) 2975, 2924, 1681, 1606, 1476, 1379, 1312, 1255, 1175, 1121, 1079, 1025, 959, 889, 862, 818, 772, 741, 700, 633, 601, 554, 519, 478, 431, 399.

HRMS (ESI, *m/z*) calcd. for $C_{23}H_{23}O_2N_1Na$ $[M+Na]^+$: 368.1621, found: 368.1630.

5.3.4 Mechanism Study

1) Preparation of iminophosphorane

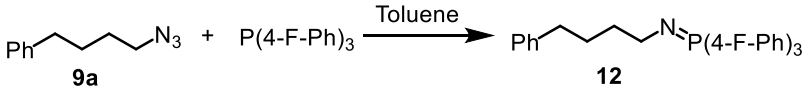

9a **12**

A mixture of azide **9a** (35 mg, 0.2 mmol) and $P(4\text{-F-Ph})_3$ (63 mg, 0.2 mmol) in toluene (0.2 mL, 1 M) were stirred at 95 ℃ for 6 h under an atmosphere of nitrogen. Afterwards, the mixture was

concentrated under reduced pressure to remove the solvent. The analytically pure iminophosphorane **12** was obtained as a colorless oil (29.4 mg, 0.2 mmol, 100% yield).

^{1}H NMR (300 MHz, C_6D_6) δ 7.61-7.48 (m, 6H), 7.24 (dd, J = 9.6, 6.4 Hz, 5H), 6.88-6.79 (m, 6H), 3.41 (dt, J = 16.2, 6.2 Hz, 2H), 2.74 (t, J = 7.3 Hz, 2H), 2.09-1.90 (m, 4H).

^{13}C NMR (75 MHz, C_6D_6) δ 166.6, 166.5, 163.3, 163.2, 143.4, 135.1, 135.0, 134.9, 134.8, 129.7, 129.6, 128.8, 128.6, 125.9, 116.0, 115.8, 115.8, 115.7, 115.5, 45.2, 45.2, 36.4, 35.9, 35.6, 29.8.

^{19}F NMR (282 MHz, C_6D_6) δ -109.14.

IR (film): ν (cm^{-1}) 3062, 3029, 2927, 2852, 2809, 2127, 1674, 1588, 1495, 1457, 1395, 1358, 1296, 1225, 1157, 1103, 1014, 826, 745, 701, 659, 573, 528, 473.

HRMS (ESI, *m/z*) calcd. for $C_{28}H_{26}F_3NP$ $[M+H]^+$: 464.1749, found: 464.1763.

2) Catalytic asymmetric C-H amination using iminophosphorane 12 as the co-catalyst

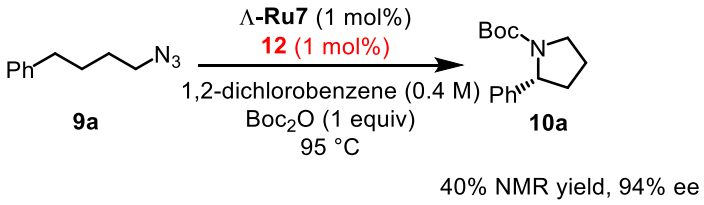

A dried 10 mL Schlenk tube was charged with azide **9a** (35 mg, 0.2 mmol) and Λ-**Ru7** (2.6 mg, 0.002 mmol, 1 mol%) under an atmosphere of nitrogen. A solution of iminophosphorane **12** (0.5 mL, 0.002 mmol, 4 mM in 1,2-dichlorobenzene) was added via syringe, followed by Boc_2O (45.8 μL, 0.2 mmol). The reaction mixture was stirred at 95 ℃ for 30 h under an atmosphere of nitrogen. Afterwards, the mixture was concentrated under reduced pressure, and the residue was analized by ^{1}H NMR to determine the yield using $Cl_2CHCHCl_2$ as internal standard. Analytically pure product was obtained by preparative TLC for chiral HPLC analysis to determine the enantiomeric excess.

3) Comparison of 1,2-hydride shift of benzyl azide and standard substrate 9a

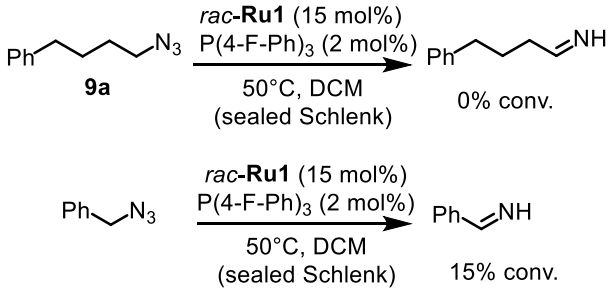

A dried 10 mL Schlenk tube was charged with benzyl azide or **9a** (8.8 mg, 0.05 mmol) and *rac*-**Ru1** (10.3 mg, 0.0075 mmol, 15 mol%) under an atmosphere of nitrogen. A solution of $P(4\text{-F-Ph})_3$ (0.15 mL, 0.001 mmol, 6.7 mM in CH_2Cl_2) was added via syringe. The reaction mixture was stirred at 50 ℃ for 20 h under an atmosphere of nitrogen. Afterwards, the mixture was concentrated under reduced pressure, and the residue was analized by ^{1}H NMR to determine the conversion of the imine.[8] See the ^{1}H NMR spectrum below.

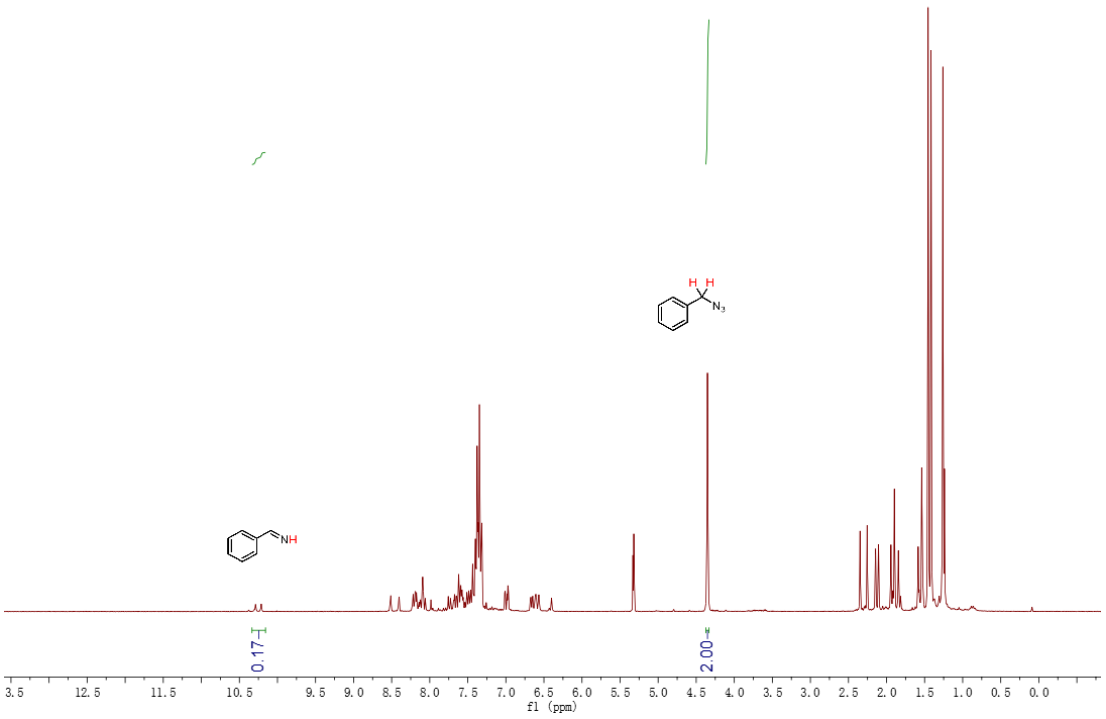

4) Reaction rates of electronically distinct substrates

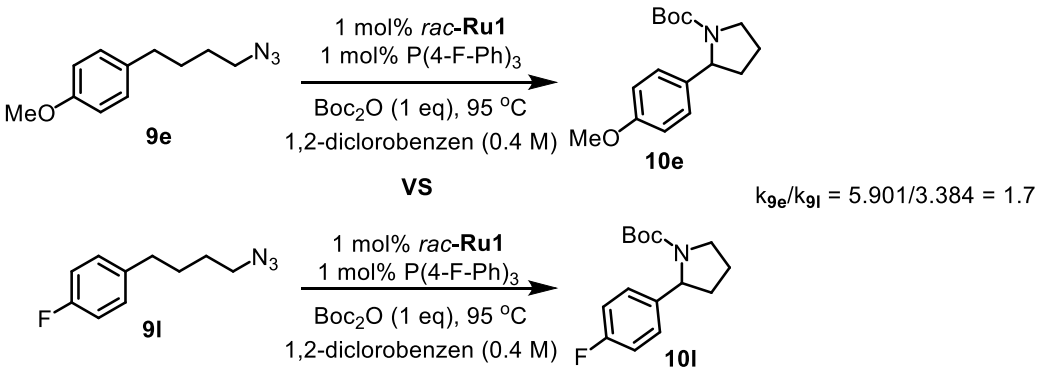

A dried 10 mL Schlenk tube was charged with azide **9e** or **9l** (0.2 mmol) and *rac*-**Ru1** (2.8 mg, 0.002 mmol, 1 mol%) under an atmosphere of nitrogen. A solution of $P(4\text{-F-Ph})_3$ (0.5 mL, 0.002 mmol, 4 mM in 1,2-dichlorobenzene) was added via syringe, followed by Boc_2O (46 μL, 0.2 mmol). Then 10 μL $Cl_2CHCHCl_2$ was added as the internal standard. The reaction mixture was stirred at 95 ℃ under an atmosphere of nitrogen. Aliquots were taken at time intervals as indicated in the figure below. The aliquot was analyzed by ^1H NMR spectroscopy for the formation of product (square for **9e**, triangle for **9l**).

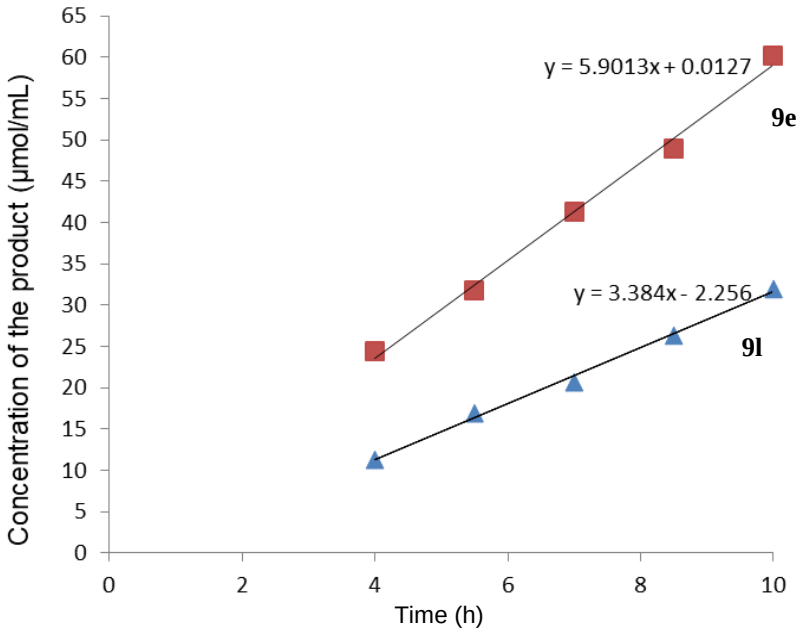

5) KIE experiments

The synthesis of both monodeuterated substrate **9a'** and bis-deuterated substrate **9a''** are reported in the literature.[9]

Intramolecular KIE

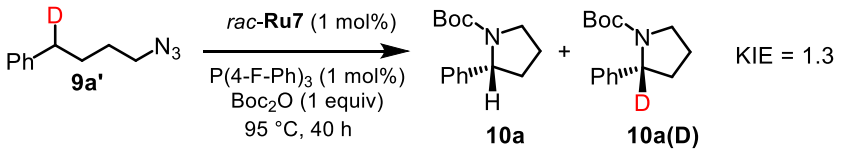

A dried 10 mL Schlenk tube was charged with azide **9a'** (35.2 mg, 0.2 mmol) and *rac*-**Ru7** (2.6 mg, 0.002 mmol, 1 mol%) under an atmosphere of nitrogen. A solution of P(4-F-Ph)$_3$ (0.5 mL, 0.002 mmol, 4 mM in 1,2-dichlorobenzene) was added via syringe, followed by Boc_2O (46 μL, 0.2 mmol). The reaction mixture was stirred at 95 ℃ for 40 h under an atmosphere of nitrogen. Afterwards, the mixture was concentrated under reduced pressure, and the residue was purified by a short silica gel column. The ratio of k_D/k_H was determined by ^{1}H NMR by integration of the methine proton against the methylene protons at the 2- and 4-positions, respectively. A intramolecular KIE value of 1.3 was obtained. See the ^{1}H NMR spectrum below.

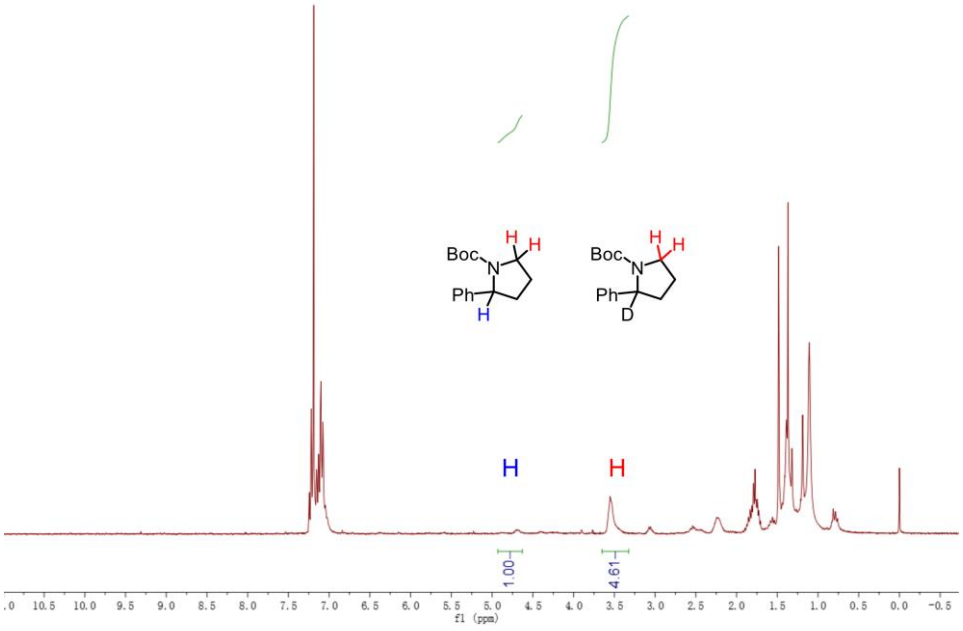

Intermolecular KIE

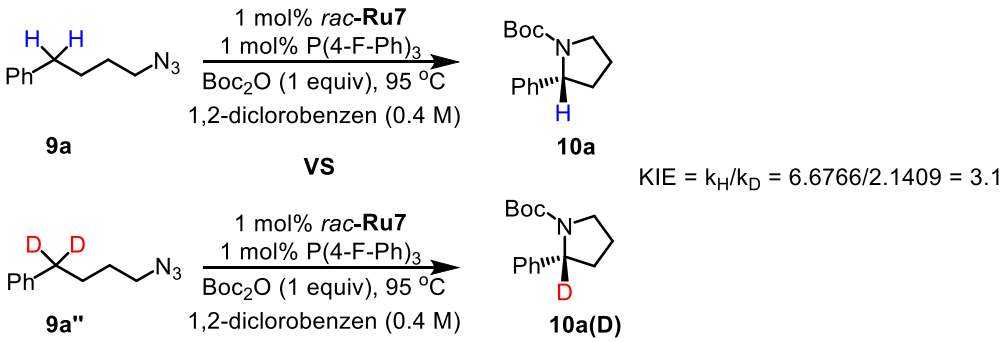

The intermolecular KIE (noncompetitive) was obtained by measuring the initial reaction rates with **9a** and **9a''** following the procedure below.

A dried 10 mL Schlenk tube was charged with azide **9a** (35.0 mg, 0.2 mmol) or **9a''** (35.4 mg, 0.2 mmol), and *rac*-**Ru7** (2.6 mg, 0.002 mmol, 1 mol%) under an atmosphere of nitrogen. A solution of $P(4\text{-F-Ph})_3$ (0.5 mL, 0.002 mmol, 4 mM in 1,2-dichlorobenzene) was added via syringe, followed by Boc_2O (46 μL, 0.2 mmol). Then 10 μL $Cl_2CHCHCl_2$ was added as the internal standard. The reaction mixture was stirred at 95 ℃ under an atmosphere of nitrogen. Aliquots were taken at time intervals as indicated in the figure below. The aliquot was analyzed by ^1H NMR spectroscopy for the formation of product (square for **9a**, triangle for **9a''**).

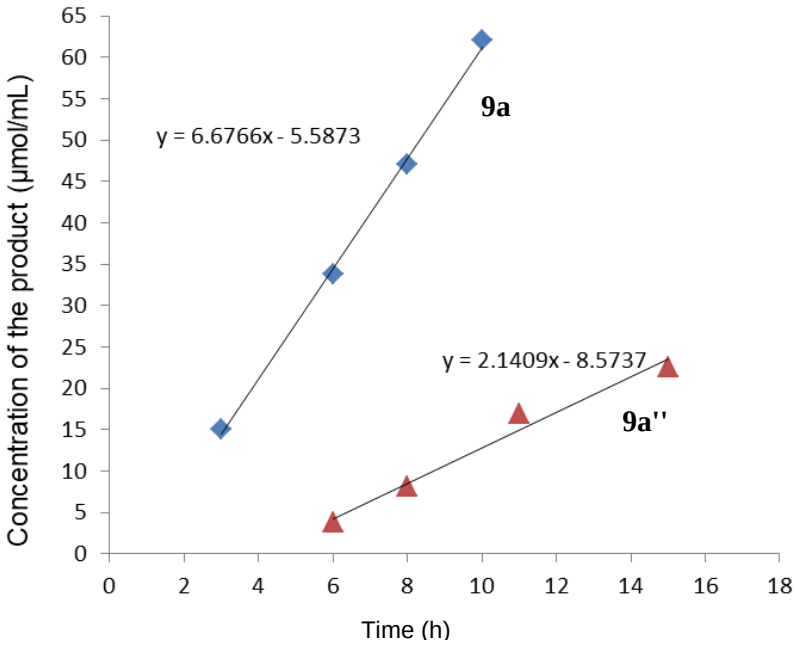

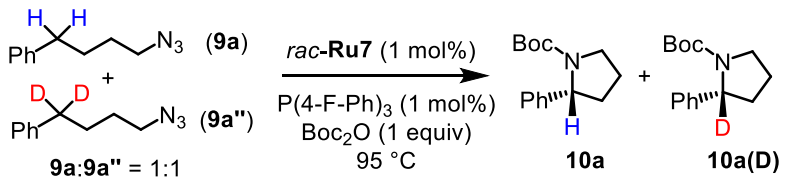

The intermolecular KIE (competitive) was obtained by taking a 1:1 mixture of the non- and bis-deuterated substrate and looking at the ratio of products.

A dried 10 mL Schlenk tube was charged with azides **9a** (17.5 mg, 0.1 mmol), **9a''** (17.7 mg, 0.1 mmol), and *rac*-**Ru7** (2.6 mg, 0.002 mmol, 1 mol%) under an atmosphere of nitrogen. A solution of $P(4\text{-F-Ph})_3$ (0.5 mL, 0.002 mmol, 4 mM in 1,2-dichlorobenzene) was added via syringe, followed by Boc_2O (46 μL, 0.2 mmol). The reaction mixture was stirred at 95 ℃ for 30 h under an atmosphere of nitrogen. Afterwards, the mixture was concentrated under reduced pressure, and the residue was purified by a short silica gel column. The ratio of k_H/k_D was determined by ^{1}H NMR by integration of the methine proton against the methylene protons at the 2- and 4-positions, respectively. A KIE value of 3.9 was obtained. See the ^{1}H NMR below.

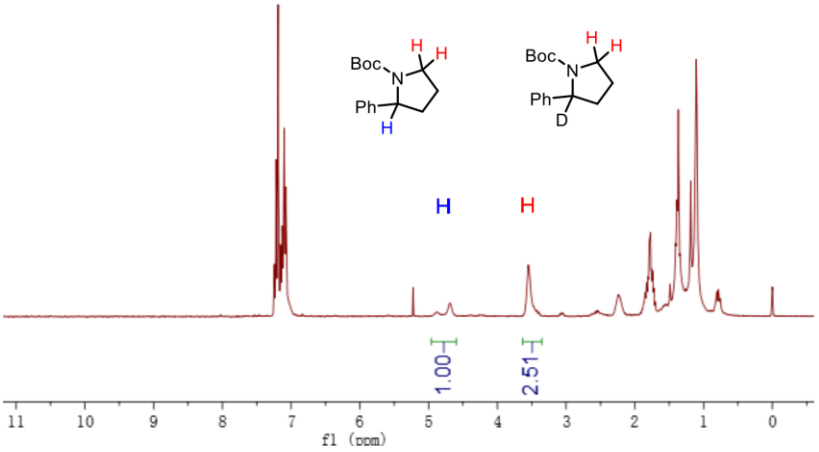

c) Stereospecificity of the intramolecular C-H amination

The synthesis of chiral compound (*R*)-**9y** (with 94% ee) and (*S*)-**9y** (with 97% ee) were reported in the literature.[2]

A dried 10 mL Schlenk tube was charged with azide (*R*)-**9y** or (*S*)-**9y** (37.9 mg, 0.2 mmol) and *rac*-**Ru7** or Λ-**Ru7** (2.6 mg, 0.002 mmol, 1 mol%) under an atmosphere of nitrogen. A solution of $P(4\text{-F-Ph})_3$ (0.5 mL, 0.002 mmol, 4 mM in 1,2-dichlorobenzene) was added via syringe, followed by Boc_2O (46 μL, 0.2 mmol). The reaction mixture was stirred at 95 ℃ for 35 h under an atmosphere of nitrogen. Afterwards, the mixture was concentrated under reduced pressure, and the residue was analized by ^1H NMR to determine the yield using $Cl_2CHCHCl_2$ as internal standard. Analytically pure product was obtained by preparative TLC. Enantiomeric excess was determined by HPLC analysis on a chiral stationary phase. HPLC conditions: Chiralpak OD-H column (4.6 × 250 mm), UV detection at 220 nm, mobile phase *n*-hexane/isopropanol = 99:1, flow rate 0.7 mL/min, column temperature = 25 ℃. See the chromatographys of (*R*)-**10y** or (*S*)-**10y**[10] on chiral stationary phase below.

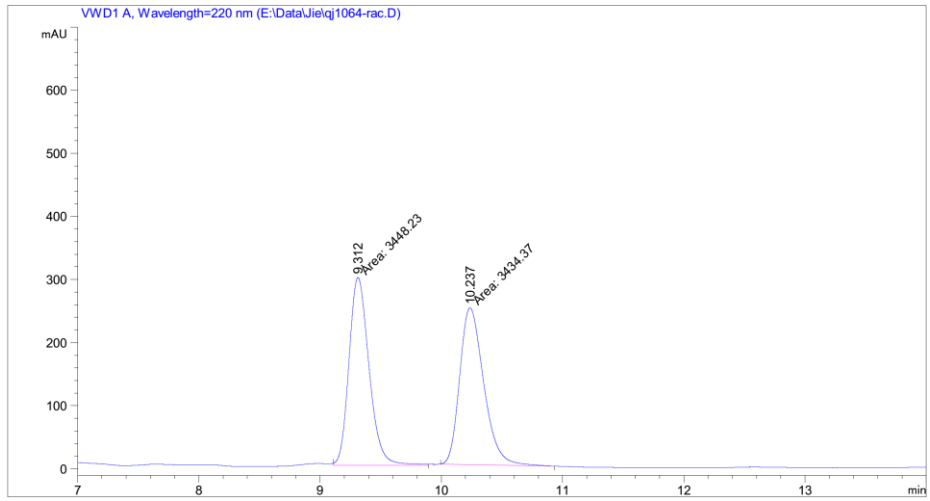

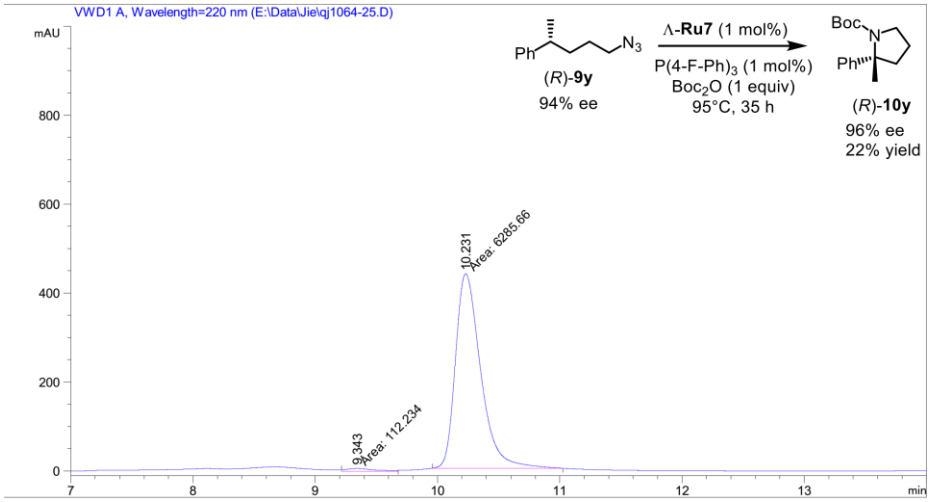

Peak #	RetTime [min]	Type	Width [min]	Area [mAU*s]	Height [mAU]	Area %
1	9.343	MM	0.2734	112.23387	6.84132	1.7542
2	10.231	MM	0.2394	6285.66357	437.60370	98.2458

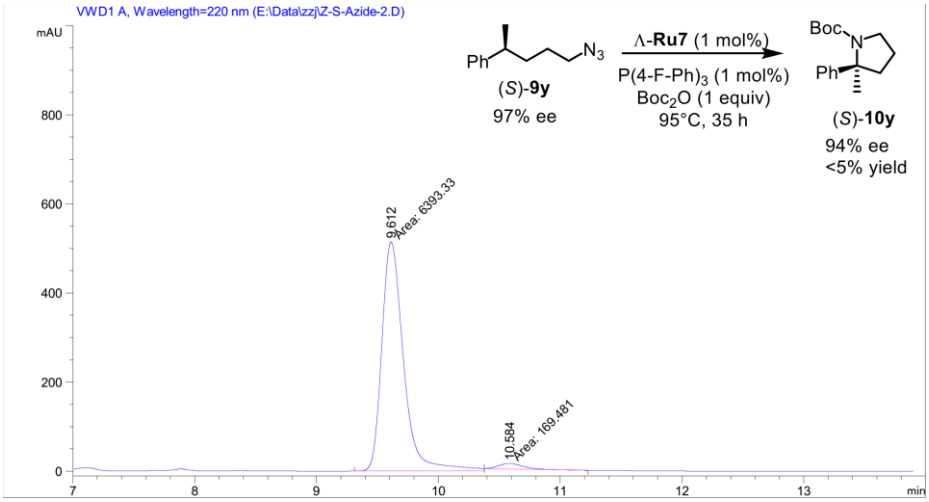

Peak #	RetTime [min]	Type	Width [min]	Area [mAU*s]	Height [mAU]	Area %
1	9.612	MM	0.2075	6393.33447	513.56226	97.4176
2	10.584	MM	0.2292	169.48105	12.32413	2.5824

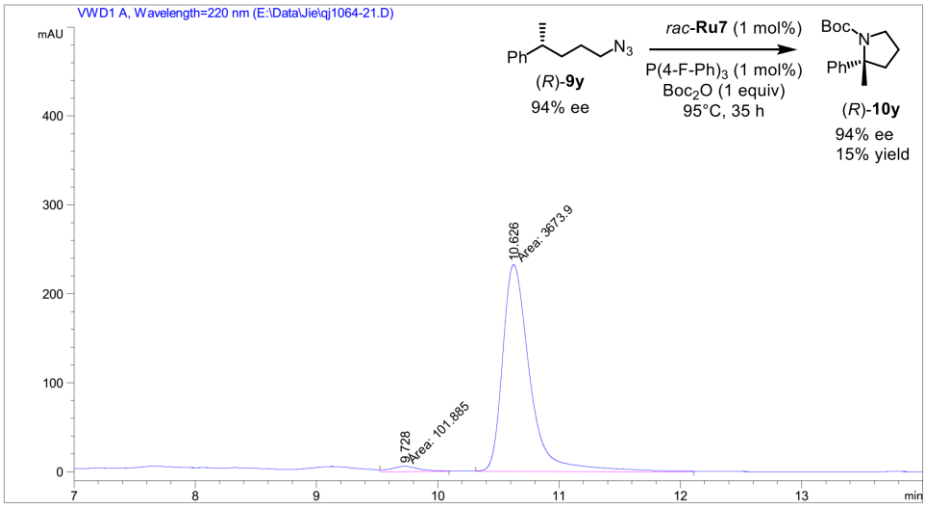

Peak #	RetTime [min]	Type	Width [min]	Area [mAU*s]	Height [mAU]	Area %
1	9.728	MM	0.2774	101.88550	6.12222	2.6984
2	10.626	MM	0.2629	3673.89673	232.93057	97.3016

References

1 B. Sahoo, M. N. Hopkinson, F. Glorius, *Angew. Chem. Int. Ed.* **2015**, *54*, 15545.

2 Y. Zheng, Y. Tan, K. Harms, M. Marsch, R. Riedel, L. Zhang, E. Meggers, *J. Am. Chem. Soc.* **2017**, *139*, 4322.

3 E. T. Hennessy, T. A. Betley, *Science* **2013**, *340*, 591.

4 A. J. Hirsh, B. F. Molino, J. Zhang, N. Astakhova, W. B. Geiss, B. J. Sargent, B. D. Swenson, A. Usyatinsky, M. J. Wyle, R. C. Boucher, R. T. Smith, A. Zamurs, M. R. Johnson, *J. Med. Chem.* **2006**, *49*, 4098.

5 D. Kalaitzakis, M. Triantafyllakis, M. Sofiadis, D. Noutsias, G. Vassilikogiannakis, *Angew. Chem. Int. Ed.* **2016**, *55*, 4605.

6 F. Chen, Z. Ding, J. Qin, T. Wang, Y. He, Q.-H. Fan, *Org. Lett.* **2008**, *13*, 4348.

7 S. C. K. Rotte, A. G. Chittiboyina, I. A. Khan, *Eur. J. Org. Chem.* **2013**, 6355.

8 J. H. Lee, S. Gupta, W. Jeong, Y. H. Rhee, J. Park, *Angew. Chem. Int. Ed.* **2012**, *51*, 10851.

9 P. F. Kuijpers, M. J. Tiekink, W. B. Breukelaar, D. L. J. Broere, N. P. van Leest, J. I., Reek, J. N. H. van der Vlugt, B. de Bruin, *Chem. Eur. J.* **2017**, *23*, 7945.

10 Y. Wang, X. Wen, X. Cui, X. P. Zhang, *J. Am. Chem. Soc.* **2018**, *140*, 4792.

5.4 Ruthenium Catalyzed Asymmetric Oxidative Homocoupling of 2-Acyl Imidazoles

5.4.1 Synthesis of Substrates

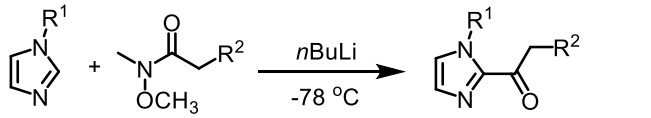

Weinreb amide 2-acyl imidazoles **13a-o**

To a solution of *N*-phenylimidazole (1.1 equiv) in THF at −78 °C was added *n*BuLi (1.1 equiv) dropwise. The mixture was stirred at −78 °C for 30 min, then stirred at room temperature for another 30 min. The corresponding Weinreb amide (1.0 equiv, 0.4 M in THF) was added dropwise to the flask after the reaction was cooled back down to −78 °C. The reaction was allowed to warm to room temperature slowly (over a period of 3-4 h) and stirred overnight. The reaction was quenched with AcOH (6.0 equiv) at room temperature and extracted with EtOAc. The organic layer was washed with aqueous saturated $NaHCO_3$ and brine. The combined organic layers were dried over anhydrous Na_2SO_4, filtered, and concentrated under reduced pressure. The residue was purified by flash chromatography on silica gel (EtOAc/hexane = 1:5) to produce **13a-o**.

The experimental data of unknown compound **13g** and **13m** are shown below. The other 2-acyl imidazoles have been reported previously.[1,2,3]

2-(3,5-Dimethylphenyl)-1-(1-phenyl-1H-imidazol-2-yl)ethan-1-one (13g)

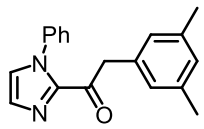

Following the general procedure, 2-acyl imidazole **13g** (870 mg, 3.0 mmol, yield: 75%) was obtained as a yellow oil from the corresponding Weinreb amide (829 mg, 4.0 mmol).

^{1}H NMR (300 MHz, $CDCl_3$) δ 7.45-7.39 (m, 3H), 7.34- 7.30 (m, 1H), 7.28-7.21 (m, 2H), 7.19 (d, J = 1.0 Hz, 1H), 6.94 (s, 2H), 6.87 (s, 1H), 4.38 (s, 2H), 2.28 (s, 6H).

^{13}C NMR (75 MHz, $CDCl_3$) δ 188.9, 143.1, 138.5, 138.0, 134.3, 129.9, 129.1, 128.8, 128.7, 127.9, 127.5, 126.0, 45.6, 21.4.

IR (film): ν (cm^{-1}) 3110, 3016, 2916, 1683, 1600, 1496, 1446, 1397, 1336, 1304, 1216, 1147, 1100, 1044, 962, 910, 854, 792, 761, 691, 636, 551, 521, 492, 419.

HRMS (ESI, *m/z*) calcd for $C_{19}H_{19}N_2O^+$ $[M+H]^+$: 291.1492, found: 291.1494.

1-(1-Phenyl-1H-imidazol-2-yl)-2-(3-(trifluoromethyl)phenyl)ethan-1-one (13m)

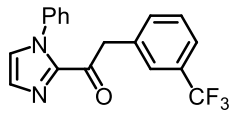

Following the general procedure, 2-acyl imidazole **13m** (793 mg, 2.4 mmol, yield: 60%) was obtained as a white solid from the corresponding Weinreb amide (989 mg, 4.0 mmol).

^{1}H NMR (300 MHz, $CDCl_3$) δ 7.60 (s, 1H), 7.55-7.48 (m, 2H), 7.47-7.41 (m, 4H), 7.35 (d, J = 0.7 Hz, 1H), 7.28-7.22 (m, 3H), 4.54 (s, 2H).

^{13}C NMR (75 MHz, $CDCl_3$) δ 187.7, 142.7, 138.3, 135.5, 133.6, 130.9 (q, J = 31.9 Hz), 130.1, 129.1, 129.0, 128.9, 127.9, 126.8 (q, J = 3.8 Hz), 126.0, 123.8 (q, J = 3.8 Hz), 122.5, 45.3.

^{19}F NMR (282 MHz, $CDCl_3$) δ -62.53 (s, 3F).

IR (film): ν (cm^{-1}) 3120, 1678, 1595, 1496, 1451, 1397, 1330, 1302, 1204, 1163, 1125, 1072, 1027, 961, 910, 877, 821, 787, 771, 696, 657, 621, 591, 536, 420.

HRMS (ESI, *m/z*) calcd for $C_{18}H_{13}F_3N_2ONa^+$ $[M+Na]^+$: 353.0872, found: 353.0874.

5.4.2 Ruthenium Catalyzed Asymmetric Homocoupling of 2-Acyl Imidazoles

1) General procedure for the optimization of the reaction conditions (for Table 9 in Chapter 3.3)

A dried 10 mL Schlenk tube was charged with the corresponding 2-acyl imidazoles substrate (0.20 mmol, 1.0 equiv), the corresponding ruthenium catalyst (2 mol%) and the corresponding base (0.22 mmol, 1.1 equiv). The corresponding solvent was added, then was $BrCCl_3$. The reaction mixture was degassed *via* freeze-pump-thaw for three cycles. After the mixture was thoroughly degassed, the vial was sealed and put in pre-heated silicone oil bath. The reaction was stirred at indicated temperature for the indicated time (monitored by TLC) under nitrogen atmosphere. Afterwards, the mixture was concentrated under reduced pressure, and the residue was purified by flash chromatography on silica gel (EtOAc/hexane = 1:5 to 1:3) to afford the analytically pure product. Enantiomeric excess was determined by HPLC analysis on chiral stationary phase.

2) Standard procedure for the substrate scope of the ruthenium-catalyzed homocoupling

A dried 10 mL Schlenk tube was charged with **Phebox-Ru1** (2.5 mg, 0.004 mmol, 2 mol%), $NaHCO_3$ (18.5 mg, 0.22 mmol, 1.1 equiv) and the corresponding 2-acyl imidazoles (0.20 mmol, 1.0 equiv). MeOH/THF (1 mL, the volume ratio of MeOH/THF is 4:1) was added, then was $BrCCl_3$ (19.6 μL, 0.20 mmol, 1.0 equiv). The reaction mixture was degassed via freeze-pump-thaw for three cycles. After the mixture was thoroughly degassed, the vial was sealed and put in pre-heated silicone oil bath. The reaction was stirred at 40 °C for the indicated time (monitored by TLC) under nitrogen atmosphere. Afterwards, the mixture was concentrated under reduced pressure, and the residue was purified by flash chromatography on silica gel (EtOAc/hexane = 1:5 to 1:3) to afford the analytically pure product **15a-o**. Enantiomeric excess was determined by HPLC analysis on chiral stationary phase.

(2*R*,3*R*)-1,4-Bis(1-methyl-1H-imidazol-2-yl)-2,3-diphenylbutane-1,4-dione (15a)

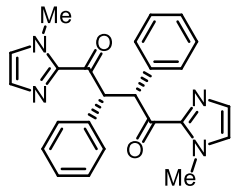

Starting from **13a** (40 mg, 0.20 mmol) according to the general procedure to give **15a** as a white solid (18.7 mg, 0.047 mmol, 47% yield). Enantiomeric excess was determined by HPLC analysis on a chiral stationary phase, ee = 45%. HPLC conditions: Chiralpak OJ-H column (4.6 × 250 mm), UV detection at 254 nm, mobile phase *n*-hexane/isopropanol = 80: 20, flow rate 1.0 mL/min, column temperature = 25 ℃, t_r (minor) = 9.4 min, t_r (major) = 10.8 min. $[\alpha]_D^{20}$ = -16.2° (*c* 0.05, CH_2Cl_2).

^{1}H NMR (300 MHz, $CDCl_3$) δ 7.31-7.27 (m, 2H), 7.26-7.24 (m, 2H), 7.16-7.04 (m, 8H), 6.92 (s, 2H), 5.91 (s, 2H), 3.90 (s, 6H).

^{13}C NMR (75 MHz, $CDCl_3$) δ 191.6, 142.8, 136.7, 129.7, 129.5, 128.4, 127.0, 126.9, 57.2, 36.1.

IR (film): ν (cm^{-1}) 2922, 2854, 2175, 2022, 1965, 1663, 1594, 1456, 1397, 1328, 1285, 1251, 1153, 1076, 1009, 967, 908, 888, 778, 740, 695, 665, 623, 585, 561, 520.

HRMS (ESI, *m*/*z*) calcd for $C_{24}H_{23}N_4O_2^+$ $[M+H]^+$: 399.1816, found: 399.1819.

(2*R*,3*R*)-1,4-Bis(1-isopropyl-1H-imidazol-2-yl)-2,3-diphenylbutane-1,4-dione (15b)

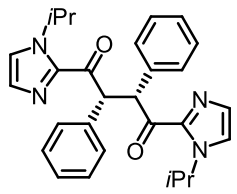

Starting from **13b** (45.7 mg, 0.2 mmol) according to the general procedure to give **15b** as a white solid (18.7 mg, 0.041 mmol, 41% yield). Enantiomeric excess was determined by HPLC analysis on a chiral stationary phase, ee = 58%. HPLC conditions: Chiralpak IA column (4.6 × 250 mm), UV detection at 254 nm, mobile phase *n*-hexane/isopropanol = 85: 15, flow rate 1.0 mL/min, column temperature = 25 ℃, t_r (major) = 6.3 min, t_r (minor) = 8.7 min. **$[\alpha]_D^{20}$** = -118.1° (*c* 1.0, CH_2Cl_2).

^{1}H NMR (300 MHz, $CDCl_3$) δ 7.26-7.21 (m, 4H), 7.17-7.03 (m, 10H), 5.89 (s, 2H), 5.53-5.40 (m, 2H), 1.36 (d, *J* = 6.6 Hz, 6H), 1.26 (d, *J* = 6.7 Hz, 6H).

^{13}C NMR (75 MHz, $CDCl_3$) δ 191.9, 142.3, 137.0, 130.1, 129.4, 128.3, 126.9, 120.9, 58.1, 49.1, 23.7, 23.6.

IR (film): *v* (cm^{-1}) 2971, 2929, 2181, 1664, 1595, 1493, 1458, 1391, 1333, 1253, 1195, 1154, 1081, 1004, 964, 918, 888, 816, 776, 748, 697, 671, 645, 600, 572, 522, 447, 406.

HRMS (ESI, *m/z*) calcd for $C_{28}H_{30}N_4O_2Na^+$ $[M+Na]^+$: 477.2261, found: 477.2264.

(2*R*,3*R*)-2,3-Diphenyl-1,4-bis(1-phenyl-1H-imidazol-2-yl)butane-1,4-dione (15c)

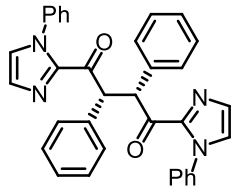

Starting from **13c** (52.4 mg, 0.20 mmol) according to the general procedure to give **15c** as a white solid (38.1 mg, 0.073 mmol, 73% yield). Enantiomeric excess was determined by HPLC analysis on a chiral stationary phase, ee = 94%. HPLC conditions: Chiralpak IA column (4.6 × 250 mm), UV detection at 254 nm, mobile phase *n*-hexane/isopropanol = 85: 15, flow rate 1.0 mL/min, column temperature = 25 ℃, t_r (major) = 9.7 min, t_r (minor) = 17.7 min. **$[\alpha]_D^{20}$** = -310.6° (*c* 1.0, CH_2Cl_2).

^{1}H NMR (300 MHz, $CDCl_3$) δ 7.45-7.36 (m, 6H), 7.27-7.23 (m, 4H), 7.22-7.07 (m, 12H), 7.00 (s, 2H), 5.81 (s, 2H).

^{13}C NMR (75 MHz, $CDCl_3$) δ 189.7, 142.7, 138.5, 136.5, 129.9, 129.5, 128.9, 128.5, 128.4, 127.1,

126.6, 125.6, 57.6.

IR (film): *v* (cm^{-1}) 2175, 2012, 1974, 1676, 1594, 1494, 1447, 1396, 1305, 1147, 1071, 1030, 980, 955, 906., 887, 818, 756, 692, 663, 603, 545, 517, 450, 411.

HRMS (ESI, *m/z*) calcd for $C_{34}H_{27}N_4O_2^+$ $[M+H]^+$: 523.2129, found: 523.2133.

(2*R*,3*R*)-1,4-Bis(1-phenyl-1H-imidazol-2-yl)-2,3-di-m-tolylbutane-1,4-dione (15d)

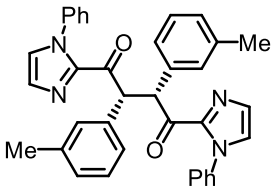

Starting from **13d** (55.2 mg, 0.20 mmol) according to the general procedure to give **15d** as a white solid (37.4 mg, 0.068 mmol, 68% yield). Enantiomeric excess was determined by HPLC analysis on a chiral stationary phase, ee = 93%. HPLC conditions: Chiralpak OD-H column (4.6 × 250 mm), UV detection at 254 nm, mobile phase *n*-hexane/isopropanol = 90: 10, flow rate 1.0 mL/min, column temperature = 25 ℃, t_r (major) = 8.8 min, t_r (minor) = 10.9 min. $[\alpha]_D^{20}$ = -270.5° (*c* 1.0, CH_2Cl_2).

^{1}H NMR (300 MHz, $CDCl_3$) δ 7.43-7.36 (m, 6H), 7.20-7.15 (m, 2H), 7.13-7.09 (m, 4H), 7.08-7.04 (m, 3H), 7.03-6.90 (s, 7H), 5.69 (s, 2H), 2.23 (s, 6H).

^{13}C NMR (75 MHz, $CDCl_3$) δ 190.0, 142.9, 138.6, 137.9, 136.4, 129.9, 129.9, 129.0, 128.6, 128.3, 127.9, 126.9, 126.5, 125.7, 57.6, 21.4.

IR (film): *v* (cm^{-1}) 2922, 2854, 2175, 2022, 1965, 1663, 1594, 1456, 1397, 1328, 1285, 1251, 1153, 1076, 1009, 967, 908, 888, 778, 740, 695, 665, 623, 585, 561, 520.

HRMS (ESI, *m/z*) calcd for $C_{36}H_{30}N_4O_2Na^+$ $[M+Na]^+$: 573.2261, found: 573.2267.

(2*R*,3*R*)-1,4-Bis(1-phenyl-1H-imidazol-2-yl)-2,3-di-p-tolylbutane-1,4-dione (15f)

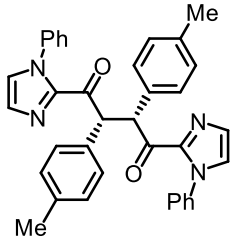

Starting from **13f** (55.2 mg, 0.20 mmol) according to the general procedure to give **15f** as a white solid (25.3 mg, 0.046 mmol, 46% yield). Enantiomeric excess was determined by HPLC analysis on a chiral

stationary phase, ee = 87%. HPLC conditions: Chiralpak OD-H column (4.6 × 250 mm), UV detection at 254 nm, mobile phase *n*-hexane/isopropanol = 90: 10, flow rate 1.0 mL/min, column temperature = 25 ℃, t_r (major) = 9.9 min, t_r (minor) = 12.2 min. **$[\alpha]_D^{20}$** = -359.5° (*c* 1.0, CH_2Cl_2).

^{1}H NMR (300 MHz, $CDCl_3$) δ 7.41-7.36 (m, 6H), 7.17-7.16 (m, 2H), 7.13-7.06 (m, 8H), 6.99-6.94 (m, 6H), 5.72 (s, 2H), 2.22 (s, 6H).

^{13}C NMR (75 MHz, $CDCl_3$) δ 190.0, 142.8, 138.6, 136.6, 133.4, 129.9, 129.4, 129.2, 129.0, 128.5, 126.5, 125.7, 57.1, 21.2.

IR (film): *v* (cm^{-1}) 3131, 2230, 2200, 2146, 1672, 1595, 1497, 1446, 1399, 1342, 1307, 1237, 1144, 1081, 1029, 955, 910, 890, 761, 693, 644, 597, 532, 486, 409.

HRMS (ESI, *m/z*) calcd for $C_{36}H_{30}N_4O_2Na^+$ $[M+Na]^+$: 573.2261, found: 573.2263.

(2*R*,3*R*)-2,3-Bis(3,5-dimethylphenyl)-1,4-bis(1-phenyl-1H-imidazol-2-yl)butane-1,4-dione (15g)

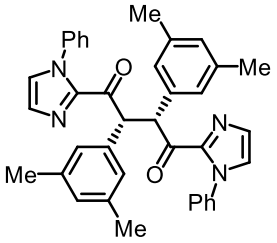

Starting from **13g** (58.2 mg, 0.20 mmol) according to the general procedure to give **15g** as a white solid (34.8 mg, 0.060 mmol, 60% yield). Enantiomeric excess was determined by HPLC analysis on a chiral stationary phase, ee = 92%. HPLC conditions: Chiralpak OD-H column (4.6 × 250 mm), UV detection at 254 nm, mobile phase *n*-hexane/isopropanol = 90: 10, flow rate 1.0 mL/min, column temperature = 25 ℃, t_r (major) = 6.9 min, t_r (minor) = 8.1 min. **$[\alpha]_D^{20}$** = -306.3° (*c* 1.0, CH_2Cl_2).

^{1}H NMR (300 MHz, $CDCl_3$) δ 7.43-7.36 (m, 6H), 7.17 (d, *J* = 0.9 Hz, 2H), 7.13-7.06 (m, 4H), 6.99 (d, *J* = 0.9 Hz, 2H), 6.79 (s, 4H), 6.73 (s, 2H), 5.59 (s, 2H), 2.17 (s, 12H).

^{13}C NMR (75 MHz, $CDCl_3$) δ 190.2, 143.1, 138.6, 137.6, 136.2, 129.9, 129.0, 128.8, 128.6, 127.3, 126.4, 125.7, 57.6, 21.3.

IR (film): *v* (cm^{-1}) 2960, 2916, 2050, 1678, 1599, 1495, 1446, 1399, 1340, 1304, 1263, 1205, 1148, 1096, 1029, 968, 911, 812, 760, 694, 602, 556, 517, 479, 398.

HRMS (ESI, *m/z*) calcd for $C_{38}H_{34}N_4O_2Na^+$ $[M+Na]^+$: 601.2574, found: 601.2581.

(2*R*,3*R*)-2,3-Di([1,1'-biphenyl]-4-yl)-1,4-bis(1-phenyl-1H-imidazol-2-yl)butane-1,4-dione (15h)

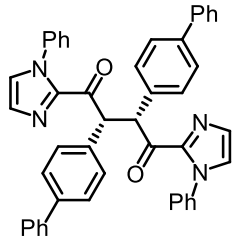

Starting from **13h** (67.7 mg, 0.20 mmol) according to the general procedure to give **15h** as a yellow solid (43.9 mg, 0.065 mmol, 65% yield). Enantiomeric excess was determined by HPLC analysis on a chiral stationary phase, ee = 90%. HPLC conditions: Chiralpak AD-H column (4.6 × 250 mm), UV detection at 254 nm, mobile phase *n*-hexane/isopropanol = 80: 20, flow rate 1.0 mL/min, column temperature = 25 ℃, t_r (minor) = 17.1 min, t_r (major) = 22.6 min. $\mathbf{[\alpha]_D^{20}}$ = -433.4° (*c* 1.0, CH_2Cl_2).

^{1}H NMR (300 MHz, $CDCl_3$) δ 7.55-7.50 (m, 4H), 7.44-7.27 (m, 20H), 7.23-7.19 (m, 2H), 7.17-7.09 (m, 4H), 7.04-7.01 (m, 2H), 5.86 (s, 2H).

^{13}C NMR (75 MHz, $CDCl_3$) δ 190.0, 142.8, 140.7, 139.8, 138.6, 135.6, 130.0, 129.9, 129.0, 128.8, 128.6, 127.3, 127.1, 127.0, 126.7, 125.8, 57.2.

IR (film): ν (cm^{-1}) 3098, 1684, 1591, 1487, 1449, 1400, 1337, 1307, 1209, 1144, 1105, 1076, 1034, 1008, 954, 913, 863, 792, 756, 691, 597, 542, 515, 491, 413.

HRMS (ESI, *m/z*) calcd for $C_{46}H_{34}N_4O_2Na^+$ $[M+Na]^+$: 697.2574, found: 697.2575.

(2*R*,3*S*)-2,3-Bis(4-methoxyphenyl)-1,4-bis(1-phenyl-1H-imidazol-2-yl)butane-1,4-dione (15i)

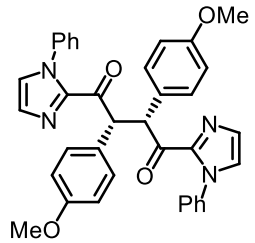

Starting from **13i** (58.5 mg, 0.20 mmol) according to the general procedure to give **15i** as a white solid (20.4 mg, 0.035 mmol, 35% yield). Enantiomeric excess was determined by HPLC analysis on a chiral stationary phase, ee = 94%. HPLC conditions: Chiralpak IA column (4.6 × 250 mm), UV detection at 254 nm, mobile phase *n*-hexane/isopropanol = 80: 20, flow rate 1.0 mL/min, column temperature = 25 ℃, t_r (minor) = 15.8 min, t_r (major) = 20.3 min. $\mathbf{[\alpha]_D^{20}}$ = -304.2° (*c* 1.0, CH_2Cl_2).

^{1}H NMR (300 MHz, $CDCl_3$) δ 7.40-7.35 (m, 6H), 7.18-7.05 (m, 10H), 7.00-6.98 (m, 2H), 6.72-6.67 (m, 4H), 5.66 (s, 2H), 3.71 (s, 6H).

^{13}C NMR (75 MHz, $CDCl_3$) δ 190.1, 158.7, 142.9, 138.6, 130.6, 129.9, 129.0, 128.6, 128.6, 126.5, 125.7, 114.0, 56.7, 55.2.

IR (film): ν (cm^{-1}) 2932, 2835, 1723, 1676, 1603, 1503, 1446, 1398, 1341, 1302, 1248, 1176, 1148, 1102, 1029, 957, 911, 889, 833, 799, 760, 692, 646, 599, 537, 444.

HRMS (ESI, *m/z*) calcd for $C_{36}H_{30}N_4O_4Na^+$ $[M+Na]^+$: 605.2159, found: 605.2164.

(2*R*,3*R*)-2,3-Bis(4-fluorophenyl)-1,4-bis(1-phenyl-1H-imidazol-2-yl)butane-1,4-dione (15j)

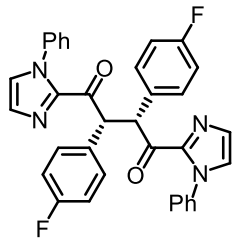

Starting from **13j** (56.1 mg, 0.20 mmol) according to the general procedure to give **15j** as a white solid (38.1 mg, 0.068 mmol, 68% yield). Enantiomeric excess was determined by HPLC analysis on a chiral stationary phase, ee = 82%. HPLC conditions: Chiralpak OD-H column (4.6 × 250 mm), UV detection at 254 nm, mobile phase *n*-hexane/isopropanol = 90: 10, flow rate 1.0 mL/min, column temperature = 25 ℃, t_r (major) = 9.6 min, t_r (minor) = 12.2 min. **$[\alpha]_D^{20}$** = -260.1° (*c* 1.0, CH_2Cl_2).

^{1}H NMR (300 MHz, $CDCl_3$) δ 7.45-7.36 (m, 6H), 7.22-7.14 (m, 6H), 7.13-7.06 (m, 4H), 7.02 (d, *J* = 1.0 Hz, 2H), 6.90-6.80 (m, 4H), 5.71 (s, 2H).

^{13}C NMR (75 MHz, $CDCl_3$) δ 189.4, 163.7, 160.5, 142.5, 138.5, 132.3, 132.3, 131.0, 130.9, 130.1, 129.1, 128.7, 126.9, 125.7, 115.7, 115.4, 56.8.

^{19}F NMR (282 MHz, $CDCl_3$) δ -115.28 (s, 2F).

IR (film): ν (cm^{-1}) 3051, 2150, 2063, 2027, 1996, 1677, 1597, 1500, 1446, 1397, 1342, 1306, 1224, 1154, 1087, 1029, 957, 911, 891, 815, 790, 761, 692, 646, 598, 535, 494, 472, 415.

HRMS (ESI, *m/z*) calcd for $C_{34}H_{24}F_2N_4O_2Na^+$ $[M+Na]^+$: 581.1760, found: 581.1764.

(2*R*,3*R*)-2,3-Bis(4-bromophenyl)-1,4-bis(1-phenyl-1H-imidazol-2-yl)butane-1,4-dione (15k)

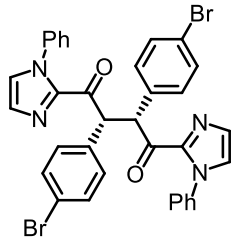

Starting from **13k** (68.2 mg, 0.20 mmol) according to the general procedure to give **15k** as a white solid (48.9 mg, 0.072 mmol, 72% yield). Enantiomeric excess was determined by HPLC analysis on a chiral stationary phase, ee = 58%. HPLC conditions: Chiralpak OD-H column (4.6 × 250 mm), UV detection at 254 nm, mobile phase *n*-hexane/isopropanol = 90: 10, flow rate 1.0 mL/min, column temperature = 25 ℃, t_r (major) = 10.4 min, t_r (minor) = 12.4 min. $[\alpha]_D^{20}$ = -250.2° (*c* 1.0, CH_2Cl_2).

^{1}H NMR (300 MHz, $CDCl_3$) δ 7.44-7.37 (m, 6H), 7.33-7.26 (m, 4H), 7.18-7.16 (m, 2H), 7.14-7.06 (m, 8H), 7.03 (d, *J* = 0.9 Hz, 2H), 5.70 (s, 2H).

^{13}C NMR (75 MHz, $CDCl_3$) δ 188.9, 142.4, 138.4, 135.5, 131.8, 131.1, 130.1, 129.1, 128.8, 127.0, 125.7, 121.5, 56.7.

IR (film): *v* (cm^{-1}) 3064, 2192, 2083, 1996, 1940, 1680, 1593, 1488, 1445, 1397, 1340, 1307, 1235, 1208, 1149, 1074, 1032, 1009, 952, 915, 887, 823, 763, 692, 598, 531, 404.

HRMS (ESI, *m/z*) calcd for $C_{34}H_{24}Br_2N_4O_2Na^+$ $[M+Na]^+$:703.0141, found: 703.0140.

(2*R*,3*R*)-2,3-Bis(4-chlorophenyl)-1,4-bis(1-phenyl-1H-imidazol-2-yl)butane-1,4-dione (15l)

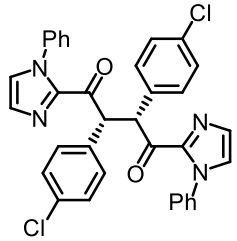

Starting from **13l** (59.4 mg, 0.20 mmol) according to the general procedure to give **15l** as a white solid (42.6 mg, 0.072 mmol, 72% yield). Enantiomeric excess was determined by HPLC analysis on a chiral stationary phase, ee = 75%. HPLC conditions: Chiralpak IA column (4.6 × 250 mm), UV detection at 254 nm, mobile phase *n*-hexane/isopropanol = 85: 15, flow rate 1.0 mL/min, column temperature = 25 ℃, t_r (major) = 12.2 min, t_r (minor) = 20.5 min. $[\alpha]_D^{20}$ = -244.3° (*c* 1.0, CH_2Cl_2).

^{1}H NMR (300 MHz, $CDCl_3$) δ 7.44-7.36 (m, 6H), 7.20-7.06 (m, 14H), 7.02 (s, 2H), 5.71 (s, 2H).

^{13}C NMR (75 MHz, $CDCl_3$) δ 189.0, 142.4, 138.4, 135.0, 133.3, 130.8, 130.1, 129.1, 128.9, 128.8,

127.0, 125.7, 56.7.

IR (film): *v* (cm^{-1}) 3108, 2038, 1905, 1677, 1595, 1492, 1447, 1398, 1308, 1234, 1150, 1090, 1018, 955, 913, 889, 826, 785, 760, 692, 591, 533, 484, 409.

HRMS (ESI, *m/z*) calcd for $C_{34}H_{24}Cl_2N_4O_2Na^+$ $[M+Na]^+$: 613.1169, found: 613.1171.

(2*R*,3*R*)-1,4-Bis(1-phenyl-1H-imidazol-2-yl)-2,3-bis(3-(trifluoromethyl)phenyl)butane-1,4-dione (15m)

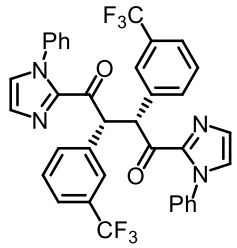

Starting from **13m** (66.1 mg, 0.20 mmol) according to the general procedure to give **15m** as a white solid (36.2 mg, 0.055 mmol, 55% yield). Enantiomeric excess was determined by HPLC analysis on a chiral stationary phase, ee = 57%. HPLC conditions: Chiralpak OD-H column (4.6 × 250 mm), UV detection at 254 nm, mobile phase *n*-hexane/isopropanol = 90: 10, flow rate 1.0 mL/min, column temperature = 25 ℃, t_r (major) = 7.5 min, t_r (minor) = 9.6 min. $[\alpha]_D^{20}$ = -147.9° (*c* 1.0, CH_2Cl_2).

^{1}H NMR (300 MHz, $CDCl_3$) δ 7.47-7.30 (m, 12H), 7.28-7.23 (m, 2H), 7.20-7.16 (m, 2H), 7.15-7.07 (m, 4H), 7.03-7.04 (m, 2H), 5.81 (s, 2H).

^{13}C NMR (75 MHz, $CDCl_3$) δ 188.5, 142.4, 138.3, 137.5, 133.1, 131.0 (q, *J* = 32.2 Hz), 130.3, 129.2, 128.1, 128.9, 127.1, 125.8, 125.7, 124.2 (q, *J* = 3.9 Hz), 122.2, 57.2.

^{19}F NMR (282 MHz, $CDCl_3$) δ -62.69 (s, 6F).

IR (film): *v* (cm^{-1}) 3049, 3130, 2285, 2215, 2158, 1982, 1904, 1679, 1595, 1495, 1446, 1398, 1324, 1164, 1121, 1072, 1031, 958, 910, 831, 786, 761, 695, 653, 572, 521, 484, 409.

HRMS (ESI, *m/z*) calcd for $C_{36}H_{24}F_6N_4O_2Na^+$ $[M+Na]^+$: 681.1696, found: 681.1708.

(2*R*,3*R*)-2,3-Di(naphthalen-2-yl)-1,4-bis(1-phenyl-1H-imidazol-2-yl)butane-1,4-dione (15n)

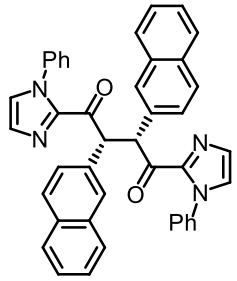

Starting from **13n** (62.5 mg, 0.20 mmol) according to the general procedure to give **15n** as a white solid (46.7 mg, 0.075 mmol, 75% yield). Enantiomeric excess was determined by HPLC analysis on a chiral stationary phase, ee = 80%. HPLC conditions: Chiralpak IA column (4.6 × 250 mm), UV detection at 254 nm, mobile phase *n*-hexane/isopropanol = 80: 20, flow rate 1.0 mL/min, column temperature = 25 ℃, t_r (major) = 10.1 min, t_r (minor) = 15.0 min. $[\alpha]_D^{20}$ = -429.9° (*c* 1.0, CH_2Cl_2).

^{1}H NMR (300 MHz, $CDCl_3$) δ 7.80 (s, 2H), 7.72-7.62 (m, 4H), 7.59 (s, 1H), 7.56 (s, 1H), 7.42-7.34 (m, 12H), 7.19-7.15 (m, 2H), 7.12-7.05 (m, 4H), 6.99-6.96 (m, 2H), 6.10 (s, 2H).

^{13}C NMR (75 MHz, $CDCl_3$) δ 189.6, 142.8, 138.5, 134.0, 133.5, 132.6, 130.0, 129.0, 128.6, 128.5, 128.2, 128.0, 127.8, 127.6, 126.7, 125.9, 125.8, 125.7, 57.6.

IR (film): *v* (cm^{-1}) 3054, 1677, 1595, 1496, 1445, 1398, 1304, 1148, 1030, 959, 912, 844., 793, 756, 691, 656, 535, 474.

HRMS (ESI, *m/z*) calcd for $C_{42}H_{30}N_4O_2Na^+$ $[M+Na]^+$: 645.2261, found: 645.2270.

(2*R*,3*R*)-1,4-Bis(1-phenyl-1H-imidazol-2-yl)-2,3-di(thiophen-3-yl)butane-1,4-dione (15o)

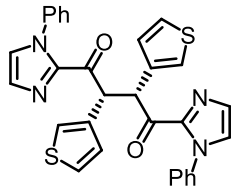

Starting from **13o** (53.7 mg, 0.20 mmol) according to the general procedure to give **15o** as a white solid (28.9 mg, 0.054 mmol, 54% yield). Enantiomeric excess was determined by HPLC analysis on a chiral stationary phase, ee = 75%. HPLC conditions: Chiralpak AD-H column (4.6 × 250 mm), UV detection at 254 nm, mobile phase *n*-hexane/isopropanol = 85: 15, flow rate 1.0 mL/min, column temperature = 25 ℃, t_r (major) = 15.5 min, t_r (minor) = 18.0 min. $[\alpha]_D^{20}$ = -167.2° (*c* 1.0, CH_2Cl_2).

^{1}H NMR (300 MHz, $CDCl_3$) δ 7.42-7.34 (m, 6H), 7.21-7.18 (m, 2H), 7.15-7.04 (m, 8H), 7.04-7.01 (m, 2H), 6.96-6.90 (m, 2H), 5.90 (s, 2H).

^{13}C NMR (75 MHz, $CDCl_3$) δ 189.2, 142.6, 138.5, 136.9, 130.0, 129.0, 128.6, 128.1, 126.8, 125.7, 125.4, 123.7, 52.5.

IR (film): ν (cm^{-1}) 3102, 1676, 1594, 1495, 1446, 1397, 1338, 1304, 1260, 1203, 1146, 1078, 1029, 958, 913, 866, 822, 760, 689, 649, 572, 544, 515, 484, 455, 417.

HRMS (ESI, *m/z*) calcd for $C_{30}H_{22}S_2N_4O_2Na^+$ $[M+Na]^+$: 557.1076, found: 557.1080.

5.4.3 Determination of the Absolute Configuration of the Homocoupling Product

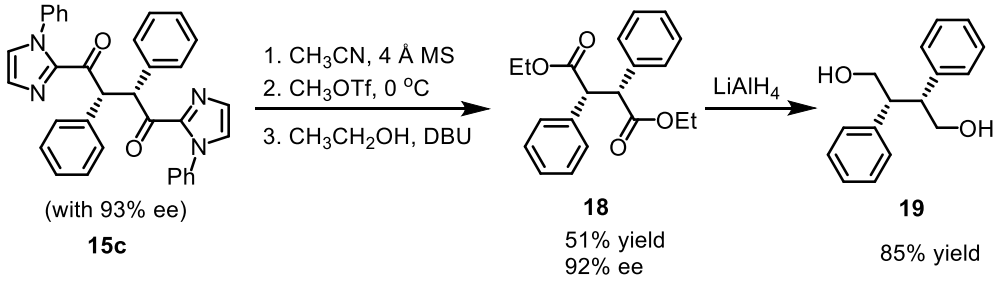

(with 93% ee)
15c

18
51% yield
92% ee

19
85% yield

4 Å MS (167 mg, 100 mg/0.1 mmol of **15c**) was added to a solution of **15c** (87.8 mg, 0.167 mmol) in CH_3CN (1.7 mL, 0.1 M) under nitrogen atmosphere. The suspension was stirred vigorously under a positive pressure of nitrogen for 3 h at 0 °C. Then methyl trifluoromethansulfonate (30.3 mg, 0.184 mmol, 1.1 equiv) was added dropwise at 0 °C. After being stirred at 0 °C for 6 h, EtOH (1.0 mL) and DBU (28.0 mg, 0.184 mmol, 1.1 equiv) were subsequently added to the reaction mixture at 0 °C. After being stirred at 0 °C for 60 min, 10 mL of saturated $NaHCO_3$ aqueous solution was added. And the mixture was extracted with CH_2Cl_2, washed with $NaHCO_3$ aqueous solution, water. The organic layer was dried and the solvent was evaporated and the residue was purified by flash chromatography on silica gel to give **18** (27.8 mg, 0.085 mmol, 51% yield) as a white solid.[4] Compound **18** was further reduced to **19** (17.4 mg, 0.072 mmol, 85% yield) according to a reported procedure[5] using $LiAlH_4$ as the reductant. The optical rotation of **19** is determined as $\mathbf{[\alpha]_D^{20}}$ = -45.8° (*c* 1.0, CH_2Cl_2), which indicated that our product is (2*R*,3*R*)-**19** {Lit.[5] $\mathbf{[\alpha]_D^{20}}$ +47° (c = 0.25, $CHCl_3$) for (2*S*,3*S*)-**19**}. Thus the homocoupling product is (2*R*,3*R*)-**15c**.

5.4.4 Mechanism Study

1) Preparation of ruthenium enolate intermediate

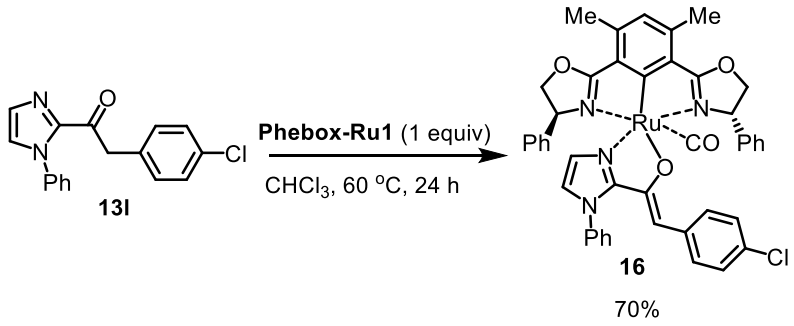

The ruthenium enolate complex was obtained by reacting substrate **13l** (14.6 mg, 0.049 mmol) with **Phebox-Ru1** (30.0 mg, 0.048 mmol) at 60 °C for 24 h in $CHCl_3$ (0.8 mL) under N_2 atmosphere. After removing the solvent, the residue was recrystallized in the mixture solvent of CH_2Cl_2 and n-hexane. The analytically pure ruthenium enolate complex **16** (27.5 mg, 0.034 mmol, 70% yield) was obtained as crystals after several days.

^{1}H NMR (300 MHz, CD_2Cl_2) δ 7.57-7.48 (m, 3H), 7.31-7.22 (m, 5H), 7.20-7.14 (m, 2H), 7.06-6.85 (m, 9H), 6.81 (s, 1H), 6.55-6.47 (m, 2H), 5.10-5.00 (m, 1H), 4.53-4.95 (m, 2H), 4.60-4.50 (m, 1H), 4.48-4.39 (m, 1H), 4.38-4.29 (m, 2H), 2.68 (s, 3H), 2.67 (s, 3H).

^{13}C NMR (75 MHz, CD_2Cl_2) δ 205.0, 195.6, 176.9, 176.1, 157.0, 149.8, 140.4, 140.3, 140.2, 140.1, 134.0, 139.0, 130.7, 130.5, 129.8, 129.5, 128.9, 128.8, 128.6, 128.3, 128.3, 128.0, 127.9, 127.9, 127.5, 127.5, 127.4, 126.8, 122.8, 100.1, 78.6, 78.2, 69.8, 67.1, 54.7, 54.6, 54.4, 54.2, 54.0, 53.8, 53.6, 53.3, 19.7, 19.6.

IR (film): ν (cm^{-1}) 3030, 2952, 1890, 1654, 1585, 1542, 1477, 1448, 1374, 1317, 1255, 1211, 1161, 1088, 1054, 1015, 941, 872, 831, 759, 692, 624, 597, 548, 517, 476, 438.

HRMS (APCI, *m*/*z*) calcd for $C_{44}H_{36}N_4O_4ClRu^+$ $[M+H]^+$: 821.1472, found: 821.1480.

2) Ruthenium enolate intermediate 16 as catalyst for the catalytic homocoupling of 13l

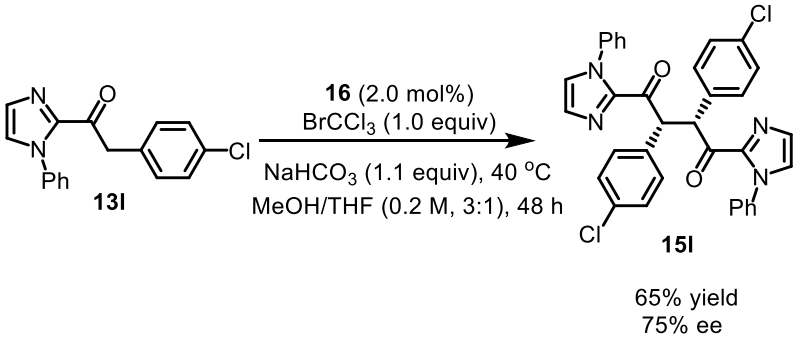

A dried 10 mL Schlenk tube was charged with the catalyst **16** (3.3 mg, 0.004 mmol, 2 mol%),

$NaHCO_3$ (18.5 mg, 0.22 mmol, 1.1 equiv) and **13l** (59.4 mg, 0.20 mmol, 1.0 equiv). MeOH/THF (1 mL, the volume ratio of MeOH/THF is 4:1) was added, then was $BrCCl_3$ (19.6 μL, 0.20 mmol, 1.0 equiv). The reaction mixture was degassed via freeze-pump-thaw for three cycles. After the mixture was thoroughly degassed, the vial was sealed and put in pre-heated silicone oil bath. The reaction was stirred at 40 °C for 48 h under nitrogen atmosphere. Afterwards, the mixture was concentrated under reduced pressure, and the residue was purified by flash chromatography on silica gel (EtOAc/hexane = 1:5 to 1:3) to afford the analytically pure product **15l** as a white solid (38.4 mg, 0.065 mmol, 65% yield). Enantiomeric excess was determined by HPLC analysis on a chiral stationary phase, ee = 75%. HPLC conditions: Chiralpak IA column (4.6 × 250 mm), UV detection at 254 nm, mobile phase *n*-hexane/isopropanol = 85: 15, flow rate 1.0 mL/min, column temperature = 25 ℃, t_r (major) = 12.2 min, t_r (minor) = 20.5 min.

3) Moniter the reaction by ^{1}H NMR

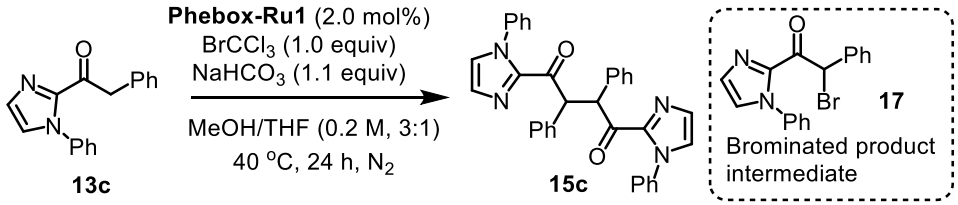

A dried 10 mL Schlenk tube was charged with **Phebox-Ru1** (3.7 mg, 0.006 mmol, 2 mol%), $NaHCO_3$ (27.8 mg, 0.33 mmol, 1.1 equiv) and **13c** (78.7 mg, 0.30 mmol, 1.0 equiv). 1.1 mL MeOH and 0.4 mL THF were added, then was $BrCCl_3$ (29.4 μL, 0.30 mmol, 1.0 equiv). The reaction mixture was degassed via freeze-pump-thaw for three cycles. After the mixture was thoroughly degassed, the vial was sealed and put in pre-heated silicone oil bath. The reaction was stirred at 40 °C under nitrogen atmosphere. The reaction was monitored by ^{1}H NMR analysis of aliquots taken out from the reaction mixture via syringe at indicated time with $Cl_2CHCHCl_2$ as internal standard (see the below profile).

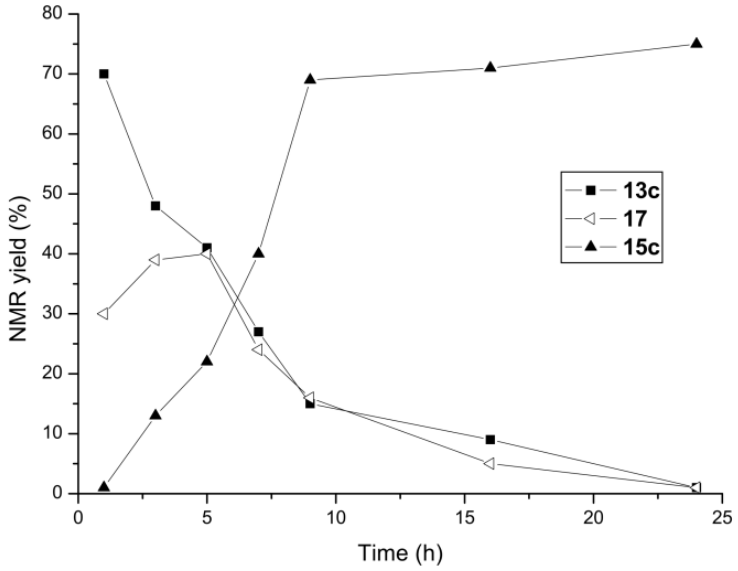

4) Heterocoupling of brominated compound 17 with 2-acyl imidazole 13c or 13d

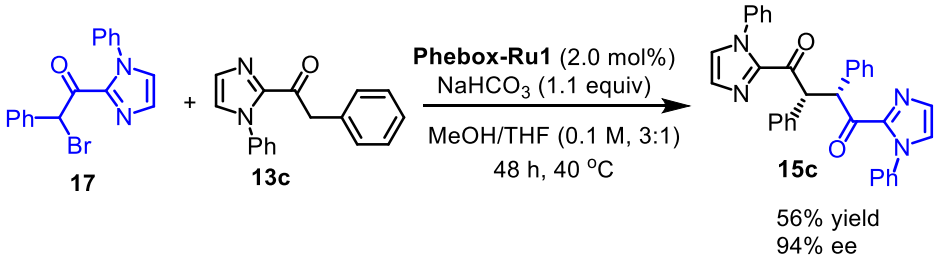

A dried 10 mL Schlenk tube was charged with **Phebox-Ru1** (3.7 mg, 0.006 mmol, 2 mol%), $NaHCO_3$ (27.8 mg, 0.33 mmol, 1.1 equiv), **17** (122.8 mg, 0.36 mmol, 1.2 equiv) and **13c** (78.7 mg, 0.30 mmol, 1.0 equiv), then 1.1 mL MeOH and 0.4 mL THF were added. The reaction mixture was degassed via freeze-pump-thaw for three cycles. After the mixture was thoroughly degassed, the vial was sealed and put in pre-heated silicone oil bath. The reaction was stirred at 40 °C under nitrogen atmosphere. Afterwards, the mixture was concentrated under reduced pressure, and the residue was purified by flash chromatography on silica gel (EtOAc/hexane = 1:5 to 1:3) to afford the analytically pure heterocoupling product **15c** (87.8 mg, 0.168 mmol, 56% yield). Enantiomeric excess was determined by HPLC analysis on chiral stationary phase.

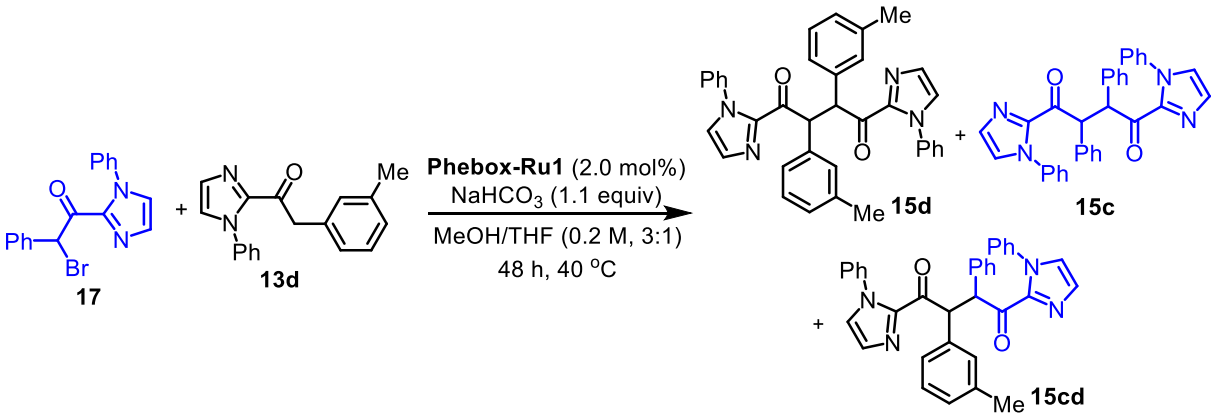

Following the above procedure, three coupling products (30.2 mg, 0.056 mmol, 56% yield, **15d**: **15c**: **15cd** = 1.3: 1.0: 2.0) were obtained between the reaction of **17** (40.9 mg, 0.12 mmol, 1.2 equiv) and **13d** (27.6 mg, 0.10 mmol, 1.0 equiv). These three products could only be isolated as a mixture but could be analyzed by ^{1}H NMR and MS.

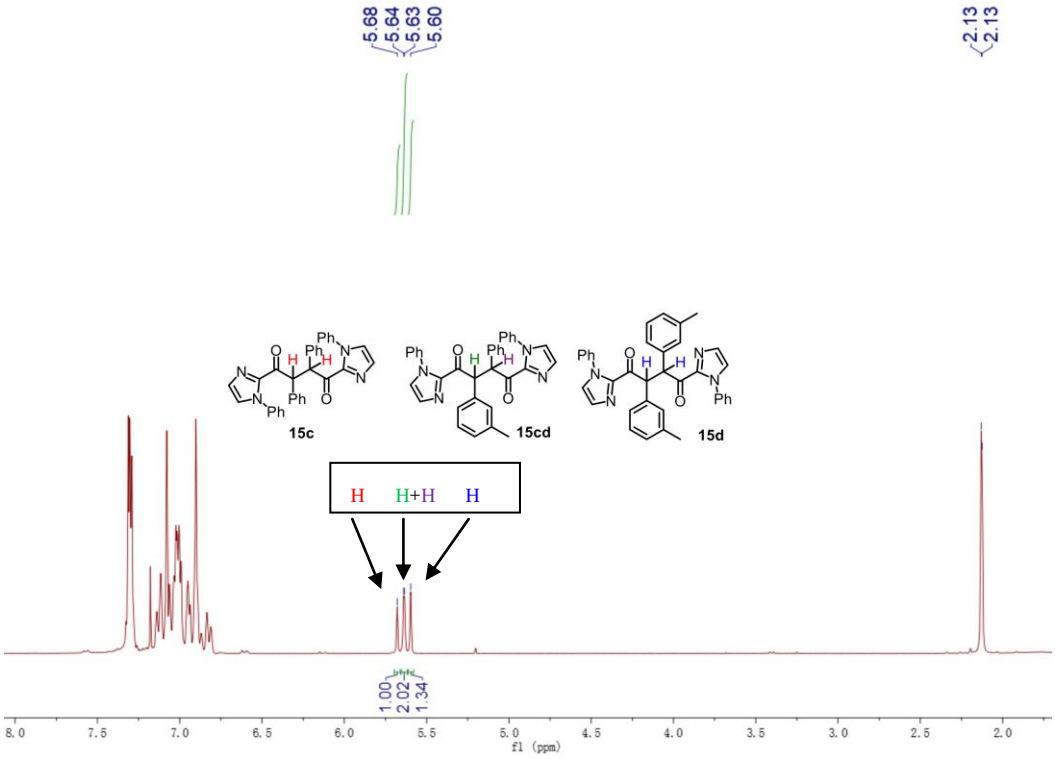

5) EPR experiments

EPR spectra were recorded at room temperature using DMPO (5,5-dimethyl-1-pyrroline *N*-oxide) as free radical spin trapping agent.

A dried 10 mL Schlenk tube was charged with **Phebox-Ru1** (1.3 mg, 0.002 mmol, 2 mol%), $NaHCO_3$

(9.3 mg, 0.11 mmol, 1.1 equiv), **17** (40.9 mg, 0.12 mmol, 1.2 equiv) and **13c** (26.2 mg, 0.10 mmol, 1.0 equiv), then 0.37 mL MeOH and 0.13 mL THF were added. The reaction mixture was degassed via freeze-pump-thaw for three cycles. After the mixture was thoroughly degassed, the vial was sealed and put in pre-heated silicone oil bath. The reaction was stirred at 40 °C under nitrogen atmosphere for 1 hour. 10 μL the reaction solution was taken out to a vial, followed by the addition of 10 μL DMPO (5,5-dimethylM-1-pyrroline *N*-oxide) solution (1 M in H_2O). The resulting mixture was stirred for 5 min. Then, a portion of the reaction mixture was taken out to an EPR tube and measured by EPR (9.17965 GHz; Mod. Frequency = 100 kHz; Mod. Ampl. = 0.12 mT).

The EPR experiment was also performed for the standard catalytic reaction according to the above same procedure.

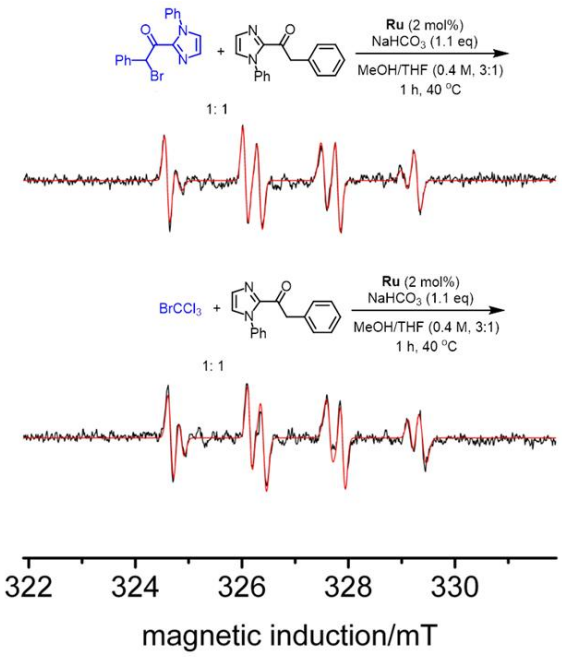

6) Catalytic homocoupling reaction with 17 as the substrate

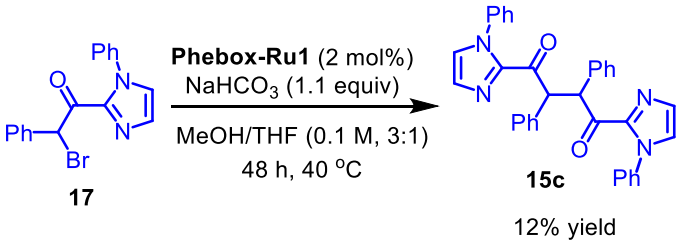

A dried 10 mL Schlenk tube was charged with **Phebox-Ru1** (3.7 mg, 0.006 mmol, 2 mol%), $NaHCO_3$

(27.8 mg, 0.33 mmol, 1.1 equiv) and **17** (102.3 mg, 0.30 mmol, 1.0 equiv), then 1.1 mL MeOH and 0.4 mL THF were added. The reaction mixture was degassed via freeze-pump-thaw for three cycles. After the mixture was thoroughly degassed, the vial was sealed and put in pre-heated silicone oil bath. The reaction was stirred at 40 °C for 48 hours under nitrogen atmosphere. Afterwards, the mixture was concentrated under reduced pressure, and the residue was purified by flash chromatography on silica gel (EtOAc/hexane = 1:5 to 1:3) to afford the analytically pure homocoupling product **15c** (11.8 mg, 0.023 mmol, 12% yield).

5.4.5 Single Crystal X-Ray Diffraction Study of Ruthenium Enolate 16

Crystals of ruthenium enolate **16** was obtained by slow diffusion from a solution of the compounds in CH_2Cl_2 layered with *n*-hexane at room temperature for several days.

Crystal data and details of the structure determination are presented in Table 11. X-ray data were collected with a Bruker 3 circuit D8 Quest diffractometer with MoKa radiation (microfocus tube with multilayer optics) and Photon 100 CMOS detector at 115 K. Scaling and absorption correction was performed by using the SADABS[6] software package of Bruker. Structures were solved using direct methods in SHELXS or SHELXT[7] and refined using the full matrix least squares procedure in SHELXL-2014[8]. The hydrogen atoms were placed in calculated positions and refined as riding on their respective C atom, and Uiso(H) was set at 1.2 Ueq(Csp^2) and 1.5 Ueq(Csp^3). Disorder of PF_6 ions, solvent molecules or phenyl and *tert*-butyl groups was refined using restraints for both the geometry and the anisotropic displacement factors.

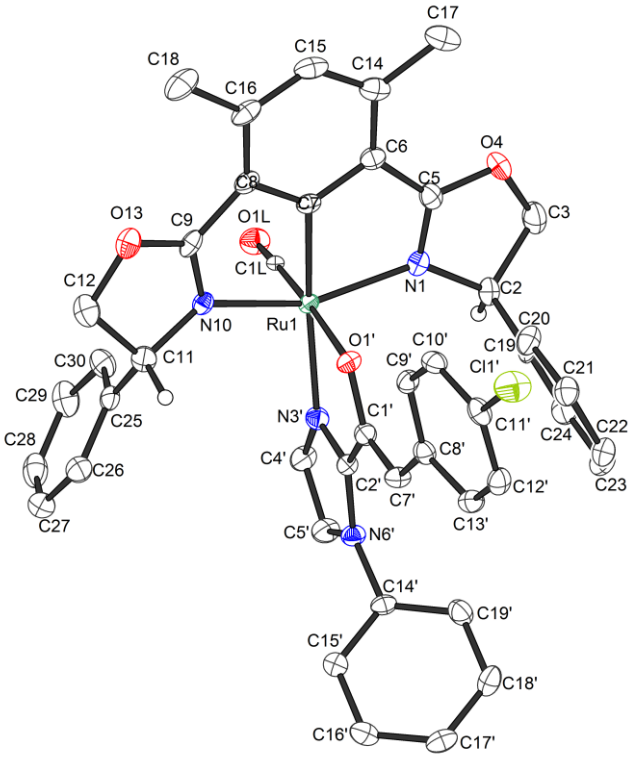

Figure 38. Crystal structure of ruthenium enolate **16**. ORTEP drawing with 50% probability thermal ellipsoids.

Table 11. Crystal data and details of the structure determination of ruthenium enolate **16**.

Empiric formula	$C_{44}H_{35}ClN_4O_4Ru$
Formula weight	820.28
Crystal system, space group	Orthorhombic, $P2_12_12_1$
a, *b*, *c* (Å)	13.4250(9), 13.8917(10), 19.6840(13)
α, β, γ (°)	90, 90, 90
V (Å^3)	3671.0(4)
Z	4
(mm^{-1})	0.551
Crystal size (mm)	0.333 x 0.187 x 0.143
T_{max}, T_{min}	0.93, 0.86
No. of measured, independent and observed [$I > 2\ (I)$] reflections	63761, 8119, 8158
R_{int}	0.0615
$R[F^2 > 2\ (F^2)]$, $wR(F^2)$, S	0.0308, 0.0697, 1.051
No. of used reflections	8519
No. of parameters	489
No. of restraints	0
ρ_{max}, ρ_{min} (e Å^{-3})	0.725, -0.561
Absolute structure parameter	-0.039(19)

References

1 H. Huo, X. Shen, C. Wang, L. Zhang, P. Röse, L.-A. Chen, K. Harms, M. Marsch, G. Hilt, E. Meggers, *Nature* **2014**, *515*, 100.

2 H. Huo, C. Wang, K. Harms, E. Meggers, *J. Am. Chem. Soc.* **2015**, *137*, 9551.

3 Y. Tan, W. Yuan, L. Gong, E. Meggers, *Angew. Chem. Int. Ed.* **2015**, *54*, 13045.

4 B. J. Fallon, V. Corcé, M. Amatore, C. Aubert, F. Chemla, F. Ferreira, A. Perez-Lunaa, M. Petit, *New J. Chem.* **2016**, *40*, 9912.

5 V. D. Rao, M. Periasamy, *Synthesis* **2000**, *5*, 703.

6 *SADABS. Bruker AXS area detector scaling and absorption correction*, Bruker AXS Inc., Madison, Wisconsin, USA, **2014**.

7 G. M. Sheldrick, *Acta Cryst. A* **2008**, *64*, 112.

8 G. M. Sheldrick, *SHELXT*, Universität Göttingen, Göttingen, Germany, **2014**.

Chapter 6: Appendices

6.1 List of Abbreviations

^{1}H NMR	proton nuclear magnetic resonance spectroscopy
^{13}C NMR	carbon nuclear magnetic resonance spectroscopy
^{9}F NMR	fluorine nuclear magnetic resonance spectroscopy
δ	chemical shift
J	coupling constant
br	broad
s	singlet
d	doublet
t	triplet
q	quartet
m	multiplet
ppm	parts per million
AcOH	acetic acid
Al	aluminum
APCI	atmospheric pressure chemical ionization
aq	aqueous
Aux	auxiliary
CD	circular dichroism
C_6D_6	deuterated benzene
$CDCl_3$	deuterochloroform
CD_2Cl_2	dideuteromethylenechloride
$CHCl_3$	chloroform
CH_3CN/ MeCN	acetonitrile
Co	cobalt
Cr	chromium
DBU	1,8-diazabicyclo[5.4.0]undec-7-ene

DMF	dimethylformamide
DMSO	dimethyl sulfoxide
dr	diastereomeric ratio
ee	enantiomeric excesses
e.g.	exempli gratia (lat.: for example)
equiv	equivalent
et al.	et alii (lat.: and others)
ESI	electrospray ionization
EtOH	ethanol
Et_2O	diethyl ether
Et_3N	triethyl amine
EtOAc	ethyl acetate
GC	gas chromatography
HAT	hydrogen atom transfer
h	hour(s)
HPLC	high performance liquid chromatography
HRMS	high resolution mass spectrometry
Hz	Hertz
IR spectra	infrared spectra
Ir	iridium
L	liter(s)
LDA	lithium diisopropylamide
LIFDI	liquid injection field desorption ionization
M	mol/liter
m	meta-
MeOH	methanol
min	minute(s)
mL	milliliter(s)
mmol	millimole

Mn	manganese
MS	mass spectroscopy
N_2	nitrogen
Nu	nucleophile
Ph	phenyl
PPh_3	triphenylphosphine
ppm	parts per million
rac	racemate
Rh	rhodium
r.t.	room temperature
Ru	ruthenium
SET	single-electron transfer
TEMPO	2,2,6,6-tetramethyl-1-piperidinyloxy
TFA	trifluoroacetic acid
THF	tetrahydrofuran
TLC	thin layer chromatography
Tol	toluene

6.2 List of Figures

Figure 19. Additional experiments. a) Investigation of match and mismatch of chiral catalyst and epoxide substrate. b) Dependence of enantioselectivity and s-factor on the conversion. Reaction conditions: glycidyl ether **4b** (0.2 mmol) with Λ-**IrO(Carb)** (2.0 mol%), Et_4NBr (3.0 mol%) in 1,4-dioxane (57 μL) at room temperature under 20 bar CO_2. c) Stoichiometric reaction of **IrO(Carb)** with $n$$Bu_4NBr$.

Figure 20. Proposed mechanism for the kinetic resolution of epoxides with CO_2.

Figure 21. Transformations via the ruthenium imido intermediate.

Figure 22. Previous work on ring-closing C(sp^3)-H aminations of primary aliphatic azides.

Figure 23. Substrate scope for the enantioselective intramolecular C-H amination of aliphatic azide with isolated yield. [a]Recovered starting materials were showed in parentheses. [b]0.1 M 1,2-dichlorobenzene and 85 ℃ were used instead.

Figure 24. Synthesis of anti-tumor alkaloid (*R*)-(+)-crispine A from pyrrolidine (*R*)-**10g**.

Figure 25. Mechanism studies for the enantioselective intramolecular C-H amination of aliphatic azide.

Figure 26. Proposed mechanism for the enantioselective intramolecular C-H amination of aliphatic azide.

Figure 27. Asymmetric transformations catalyzed by chiral cyclometalated ruthenium complex (**Phebox-Ru1**).

Figure 28. a) General strategy for oxidative homocoupling of carbonyl compounds; b) Previous report on direct asymmetric oxidative homocoupling of carbonyl compounds.

Figure 29. Substrate scope of direct asymmetric oxidative homocoupling of 2-acyl imidazoles with isolated yields.

Figure 30. a) Preparation of the chiral ruthenium enolate intermediate; b) The chiral ruthenium enolate intermediate as the catalyst for the homocoupling of **13l**.

Figure 31. a) Monitor the reation by ^{1}H NMR; b) Heterocoupling of **17** with **13c** or **13d**.

Figure 32. a) EPR experiment; b) Catalytic reaction with **17** as the substrate.

Figure 33. Proposed mechanism for the homocoupling of 2-acyl imidazoles.

Figure 34. Kinetic resolution of epoxides with CO_2 catalyzed by Λ-**IrO(Carb)**.

Figure 35. Enantioselective intramolecular C-H amination of aliphatic azides by dual ruthenium and phosphine catalysis.

Figure 63. GC traces of *rac*-**5t** and (*R*)-**5t** (70% ee).

Figure 64. HPLC traces of *rac*-**5v** and (*R*)-**5v** (74% ee).

Figure 65. HPLC traces of (*R*)-**10a** (95% ee) and *rac*-**10a**.

Figure 66. HPLC traces of (*R*)-**10b** (93% ee) and *rac*-**10b**.

Figure 67. HPLC traces of (*R*)-**10c** (91% ee) and *rac*-**10c**.

Figure 68. HPLC traces of (*R*)-**10d** (90% ee) and *rac*-**10d**.

Figure 69. HPLC traces of (*R*)-**10e** (99% ee) and *rac*-**10e**.

Figure 70. HPLC traces of (*R*)-**10f** (94% ee) and *rac*-**10f**.

Figure 71. HPLC traces of (*R*)-**10g** (94% ee) and *rac*-**10g**.

Figure 72. HPLC traces of (*R*)-**10h** (94% ee) and *rac*-**10h**.

Figure 73. HPLC traces of (*R*)-**10i** (77% ee) and *rac*-**10i**.

Figure 74. HPLC traces of (*R*)-**10j** (92% ee) and *rac*-**10j**.

Figure 75. HPLC traces of (*R*)-**10k** (92% ee) and *rac*-**10k**.

Figure 76. HPLC traces of (*R*)-**10l** (94% ee) and *rac*-**10l**.

Figure 77. HPLC traces of (*R*)-**10m** (95% ee) and *rac*-**10m**.

Figure 78. HPLC traces of (*R*)-**10n** (96% ee) and *rac*-**10n**.

Figure 79. HPLC traces of (*R*)-**10o** (95% ee) and *rac*-**10o**.

Figure 80. HPLC traces of (*R*)-**10p** (80% ee) and *rac*-**10p**.

Figure 81. HPLC traces of (*R*)-**10q** (90% ee) and *rac*-**10q**.

Figure 82. HPLC traces of (*R*)-**10r** (76% ee) and *rac*-**10r**.

Figure 83. HPLC traces of (*R*)-**10s** (93% ee) and *rac*-**10s**.

Figure 84. HPLC traces of (*S*)-**10t** (80% ee) and *rac*-**10t**.

Figure 85. HPLC traces of (*S*)-**10u** (94% ee) and *rac*-**10u**.

Figure 86. HPLC traces of (*R*)-**10y** (46% ee) and *rac*-**10y**.

Figure 87. HPLC traces of *rac*-**15a** and (2*R*, 3*R*)-**15a** (45% ee).

Figure 88. HPLC traces of *rac*-**15b** and (2*R*, 3*R*)-**15b** (67% ee).

Figure 89. HPLC traces of *rac*-**15c** and (2*R*, 3*R*)-**15c** (94% ee).

Figure 90. HPLC traces of *rac*-**15d** and (2*R*, 3*R*)-**15d** (93% ee).

Figure 91. HPLC traces of *rac*-**15e** and (2*R*, 3*R*)-**15e** (87% ee).

Figure 92. HPLC traces of *rac*-**15g** and (2*R*, 3*R*)-**15g** (92% ee).

Figure 93. HPLC traces of *rac*-**15h** and (2*R*, 3*R*)-**15h** (91% ee).

Figure 94. HPLC traces of *rac*-**15i** and (2*R*, 3*R*)-**15i** (94% ee).

Figure 95. HPLC traces of *rac*-**15j** and (2*R*, 3*R*)-**15j** (82% ee).

Figure 96. HPLC traces of *rac*-**15k** and (2*R*, 3*R*)-**15k** (58% ee).

Figure 97. HPLC traces of *rac*-**15l** and (2*R*, 3*R*)-**15l** (75% ee).

Figure 98. HPLC traces of *rac*-**15m** and (2*R*, 3*R*)-**15m** (57% ee).

Figure 99. HPLC traces of *rac*-**15n** and (2*R*, 3*R*)-**15n** (80% ee).

Figure 100. HPLC traces of *rac*-**15o** and (2*R*, 3*R*)-**15o** (75% ee).

6.3 List of Tables

6.4 List of Schemes

6.5 List of Synthesized Compounds

1) Chapter 3.1 and its Experimental Part

Metal complexes

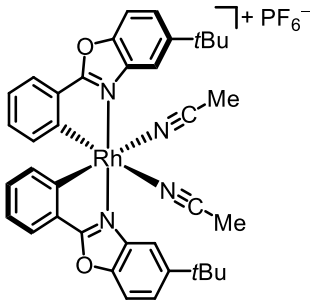

Λ-**RhO**

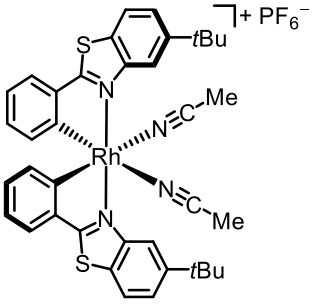

Λ-**RhS**

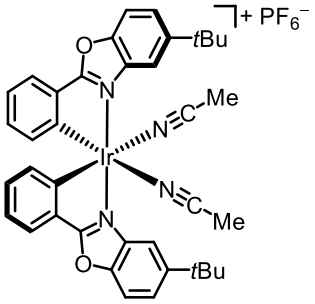

Λ-**IrO**

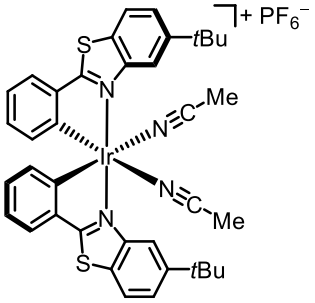

Λ-**IrS**

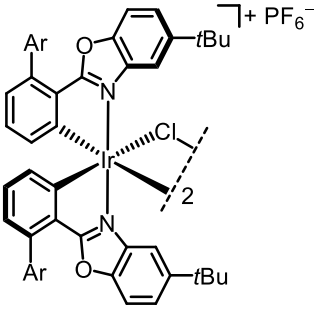

Ar = N-carbazoyl
Ir-dimer2

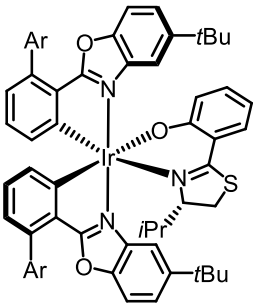

Ar = N-carbazoyl
Λ-(*S*)-**Ir3**

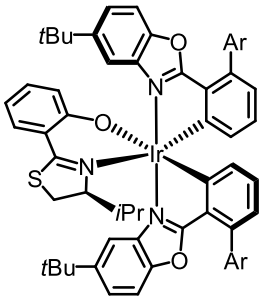

Ar = N-carbazoyl
Δ-(*S*)-**Ir3**

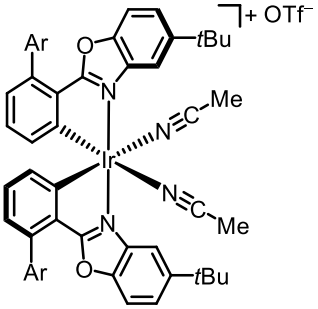

Ar = N-carbazoyl
Λ-**IrO(Carb)**

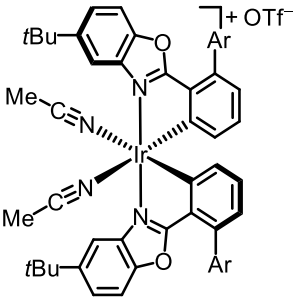

Ar= N-carbozyl
Δ-**IrO(Carb)**

Organic compounds

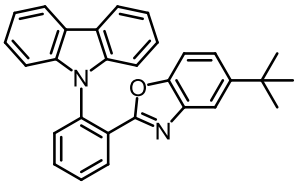

1

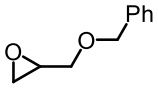

4a

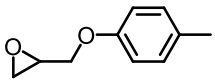

4c

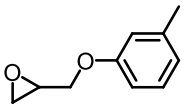

4d

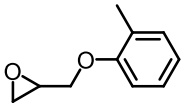

4e

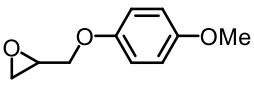

4f

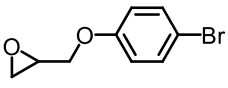

4g

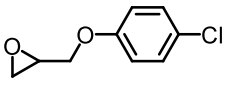

4h

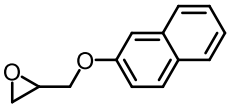

4i

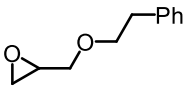

4j

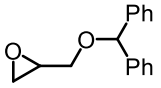

4k

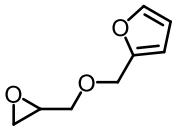

4l

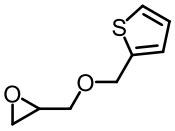

4m

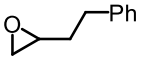

4o

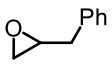

4r

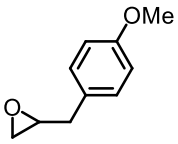

4s

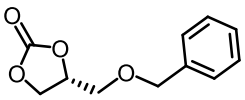

5a

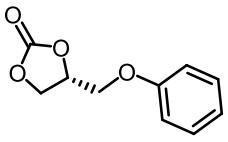

5b

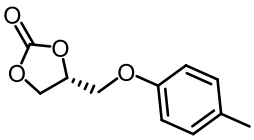

5c

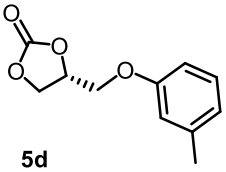

5d

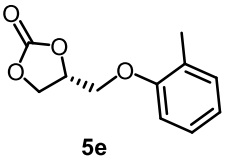

5e

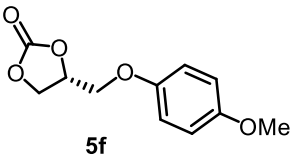

5f

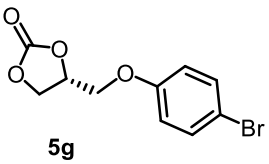

5g

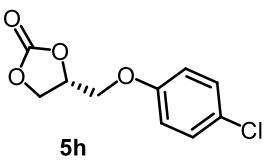

5h

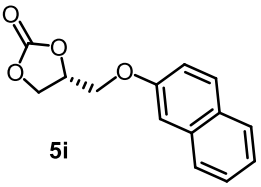

5i

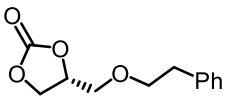

5j

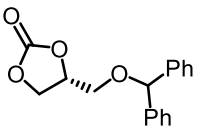

5k

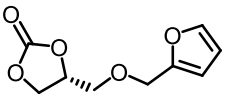

5l

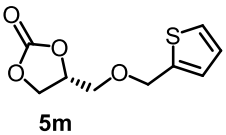

5m

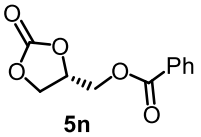

5n

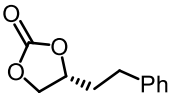

5o

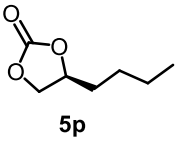

5p

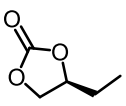

5q

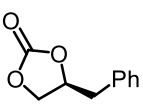

5r

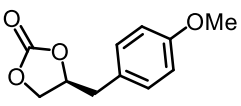

5s

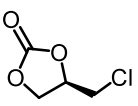

5t

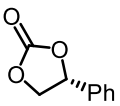

5v

2) Chapter 3.2 and its Experimental Part

Metal complexes

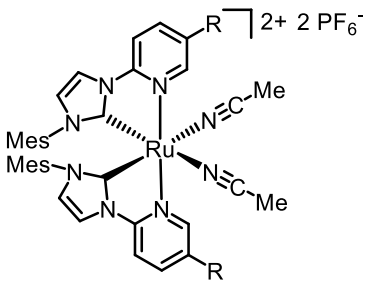

rac- and Λ-**Ru1** (R = 3,5-di*t*Bu-Ph)

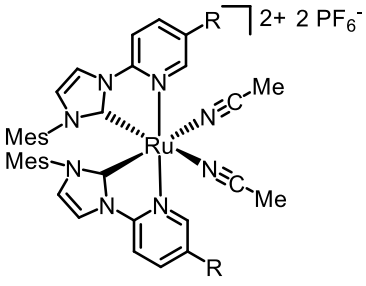

rac- and Λ-**Ru2** (R = 3,5-diMe-Ph)

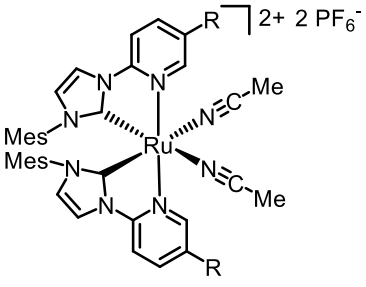

rac- and Λ-**Ru3** (R = Ph)

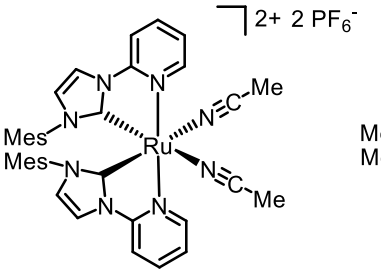

rac- and Λ-**Ru4**

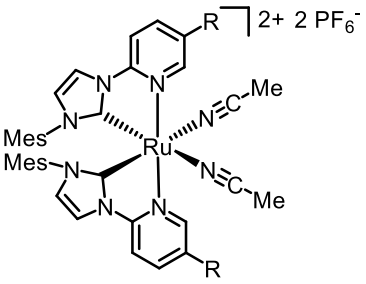

rac- and Λ-**Ru6** (R = 4-*t*Bu-Ph)

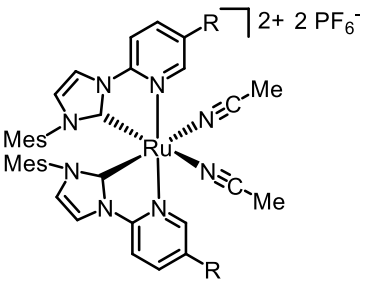

rac- and Λ-**Ru7** (R = 4-CF_3-Ph)

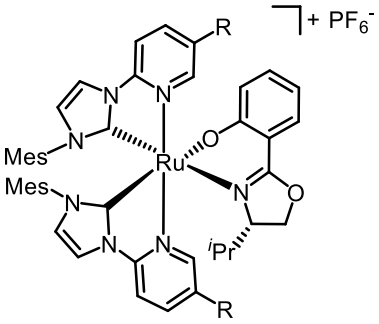

Λ-(*S*)-**Ru3** (R = Ph)

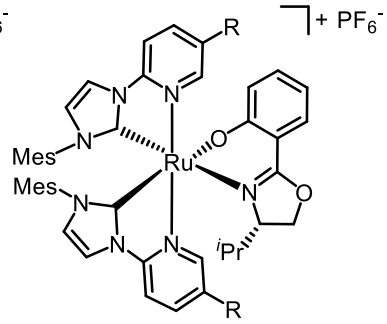

Λ-(*S*)-**Ru6** (R = 4-*t*Bu-Ph)

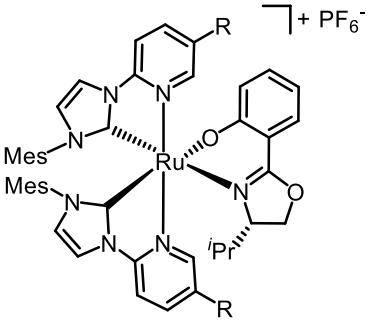

Λ-(*S*)-**Ru7** (R = 4-CF_3-Ph)

Organic compounds

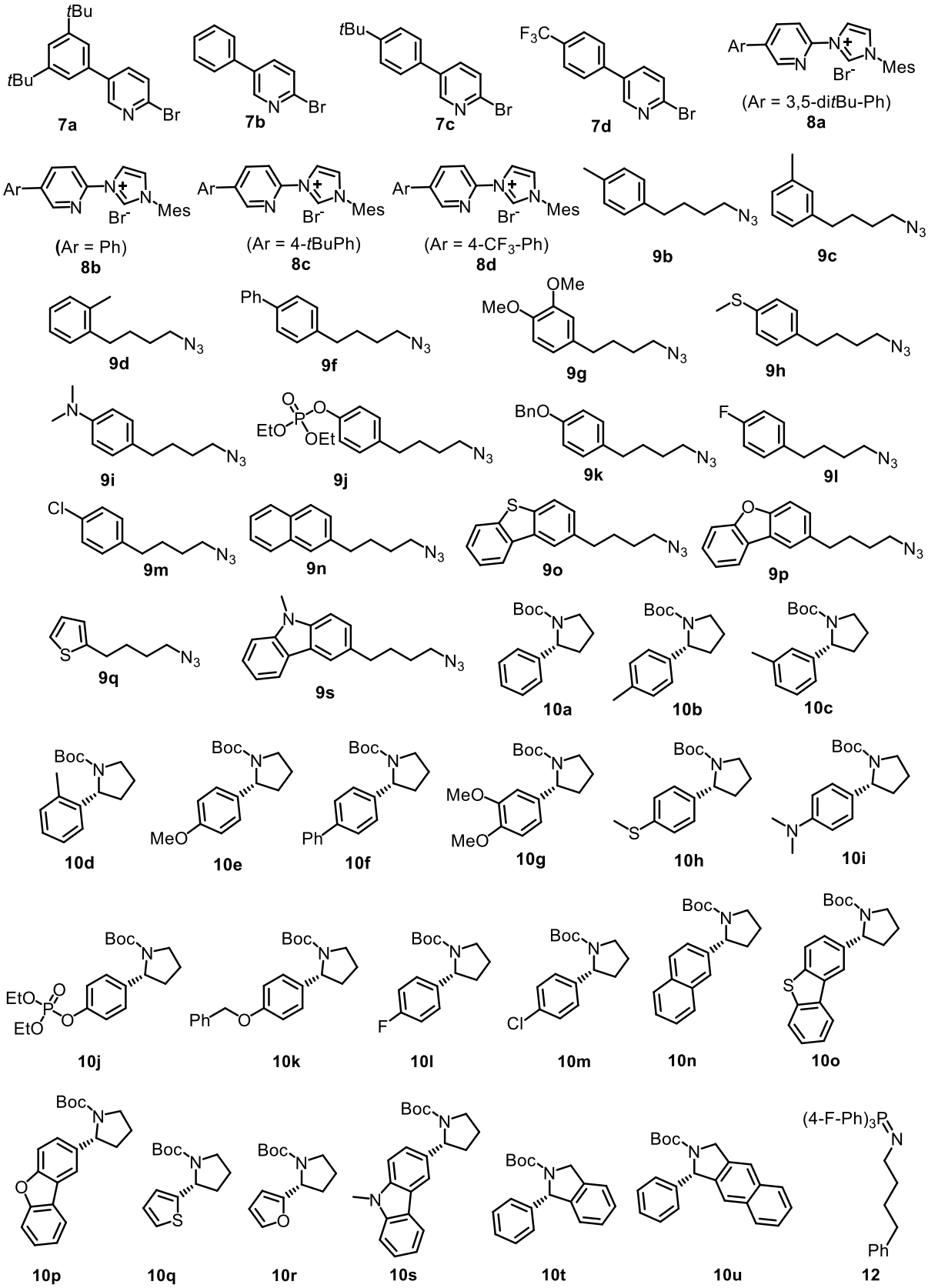

3) Chapter 3.3 and its Experimental Part

Metal complexes

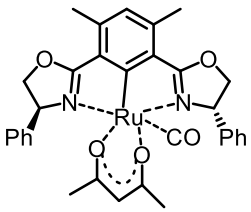

Phebox-Ru1

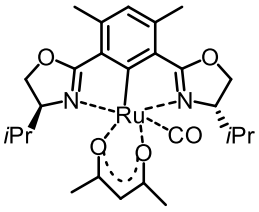

Phebox-Ru2

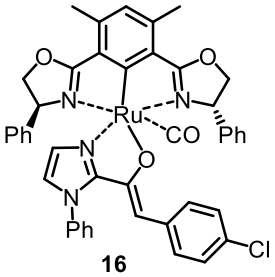

16

Organic compounds

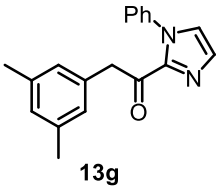

13g

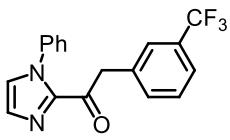

13m

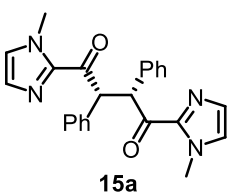

15a

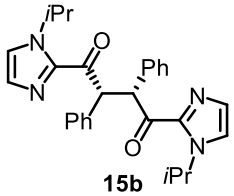

15b

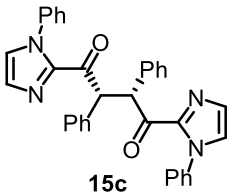

15c

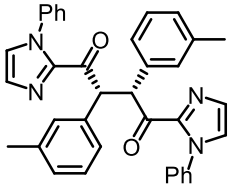

15e

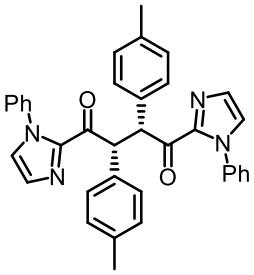

15f

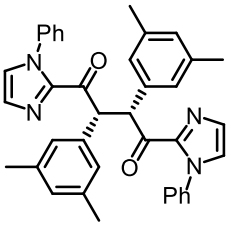

15g

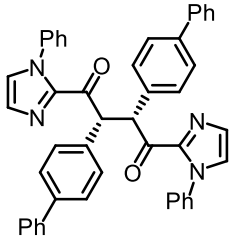

15h

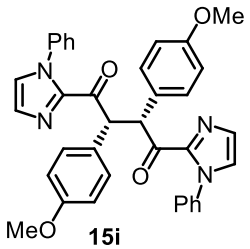

15i

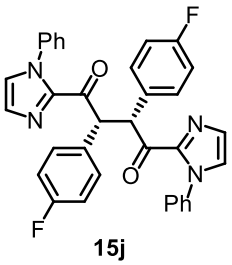

15j

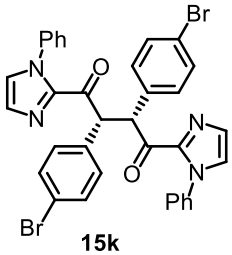

15k

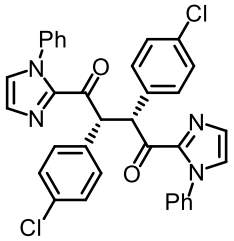

15l

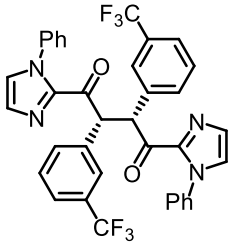

15m

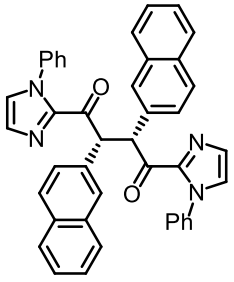

15n

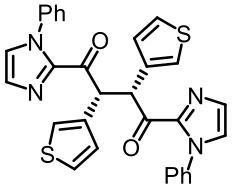

15o

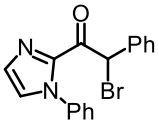

17

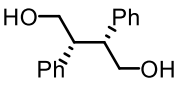

19

6.6 List of Spectra of Complexes

1) NMR spectrum of metal catalysts

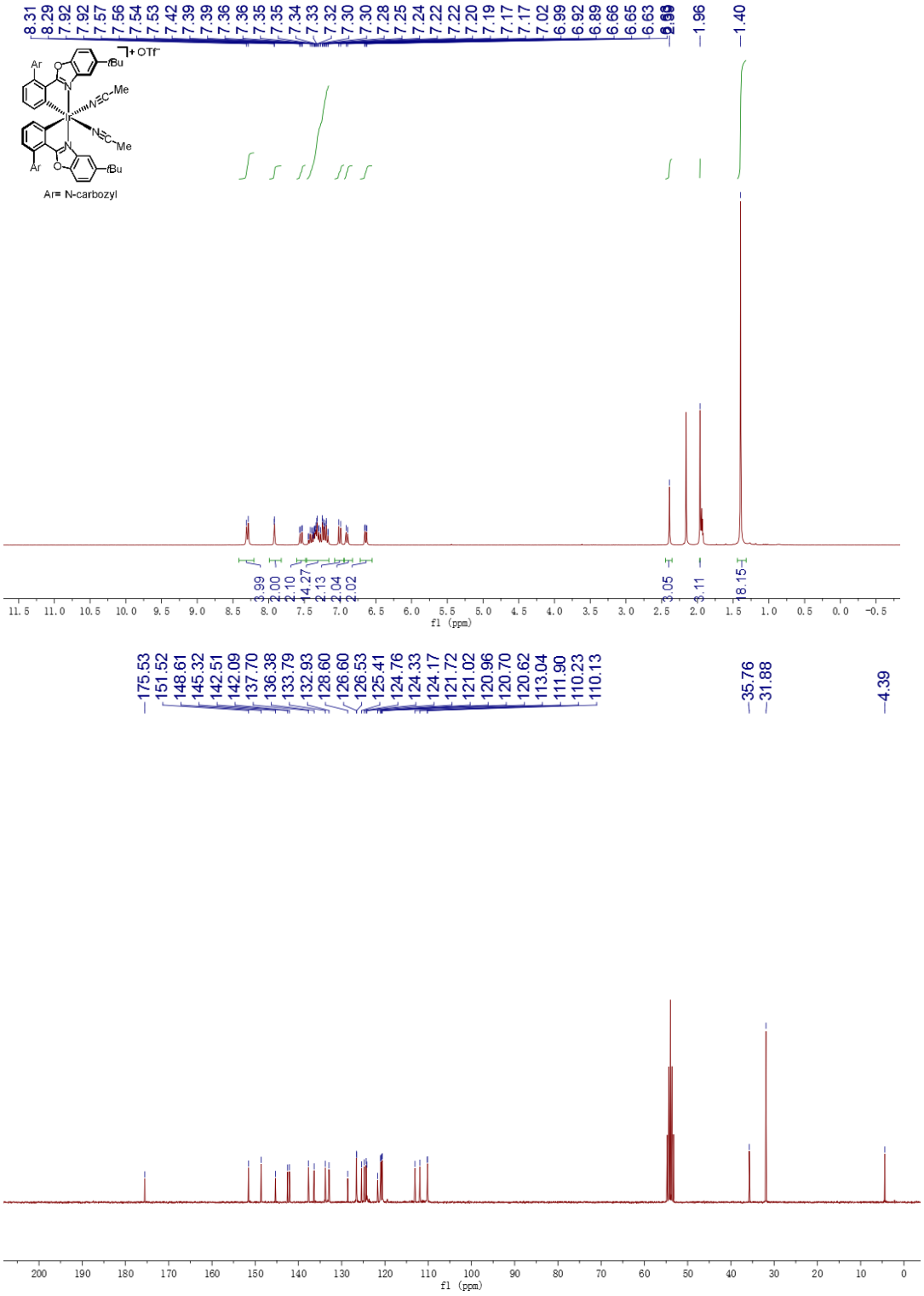

Figure 39. ^{1}H NMR (in CD_3CN) and ^{13}C NMR (in CD_2Cl_2) spectrum of Λ-**IrO(Carb)**.

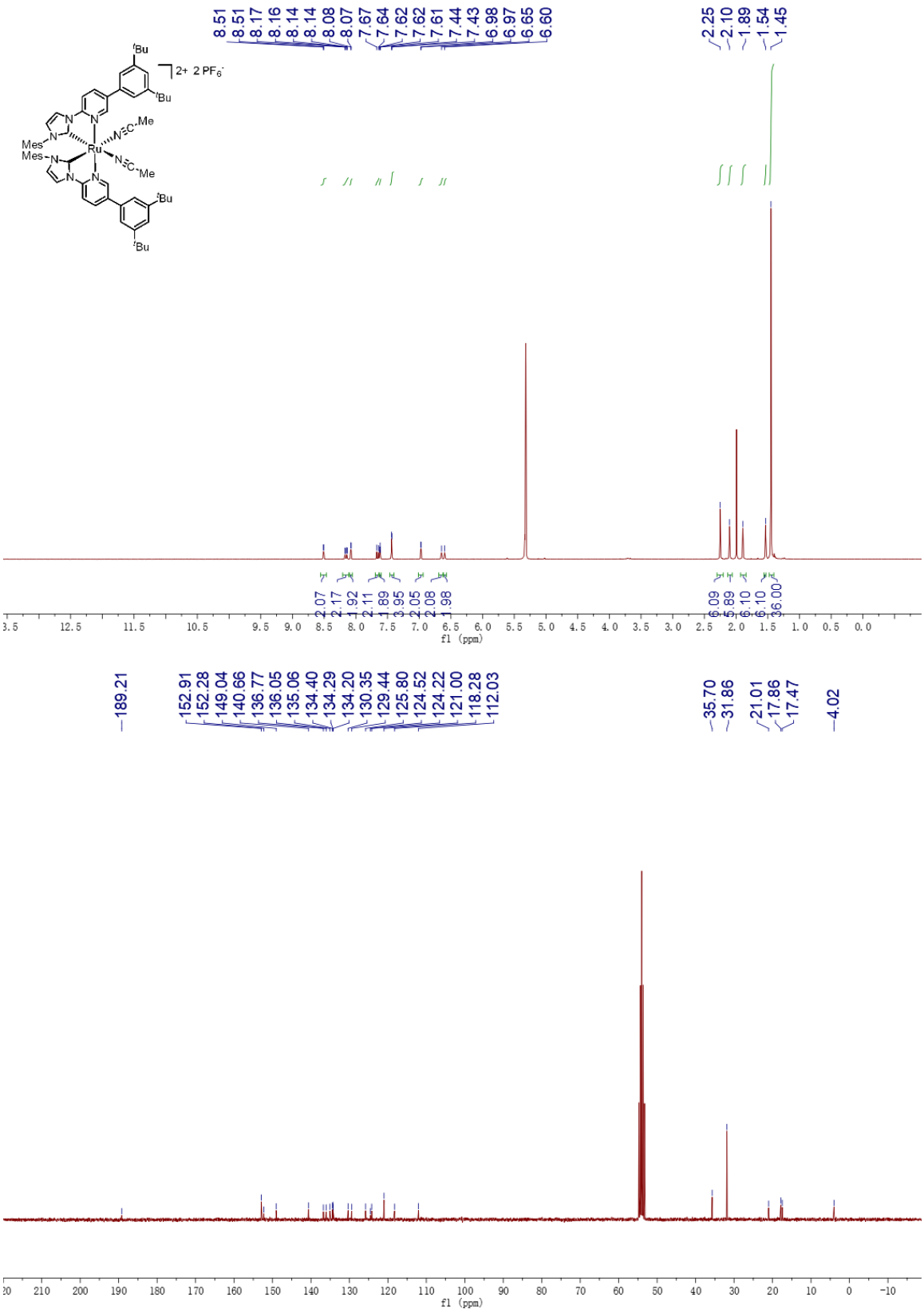

Figure 40. ^{1}H NMR and ^{13}C NMR spectrum of *rac*-**Ru1** in CD_2Cl_2.

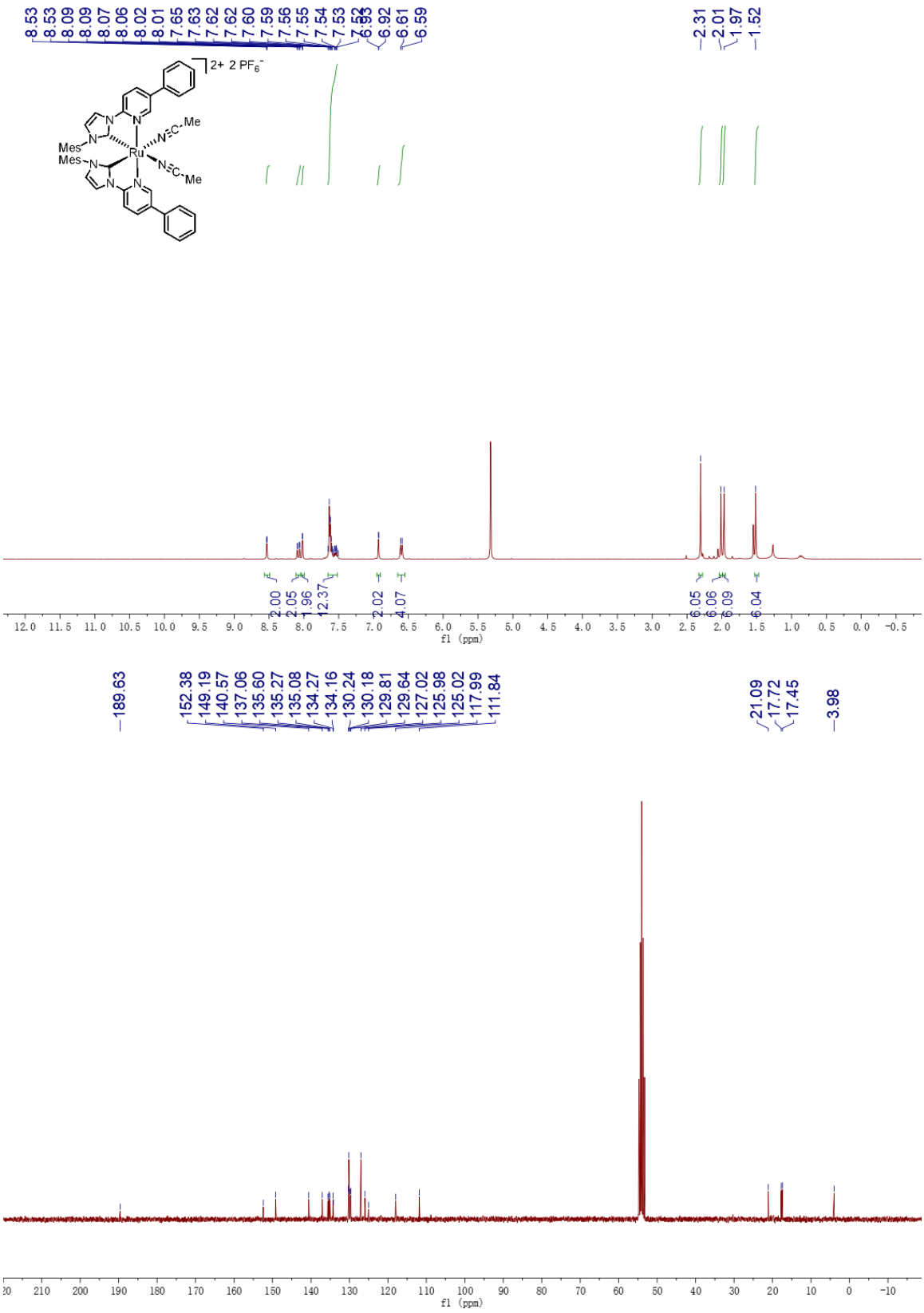

Figure 41. ^{1}H NMR and ^{13}C NMR spectrum of *rac*-**Ru4** in CD_2Cl_2.

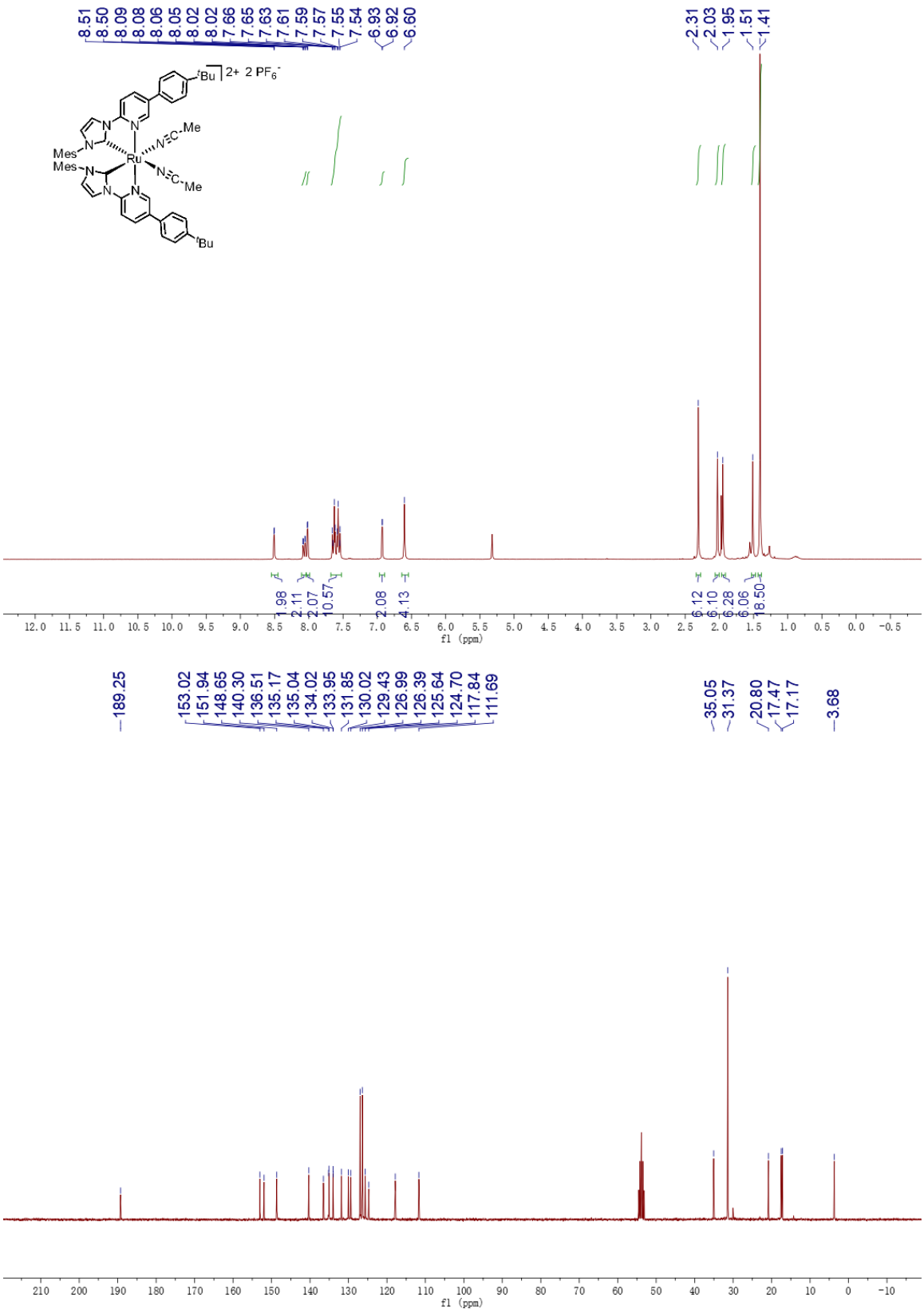

Figure 42. ^{1}H NMR and ^{13}C NMR spectrum of *rac*-**Ru6** in CD_2Cl_2.

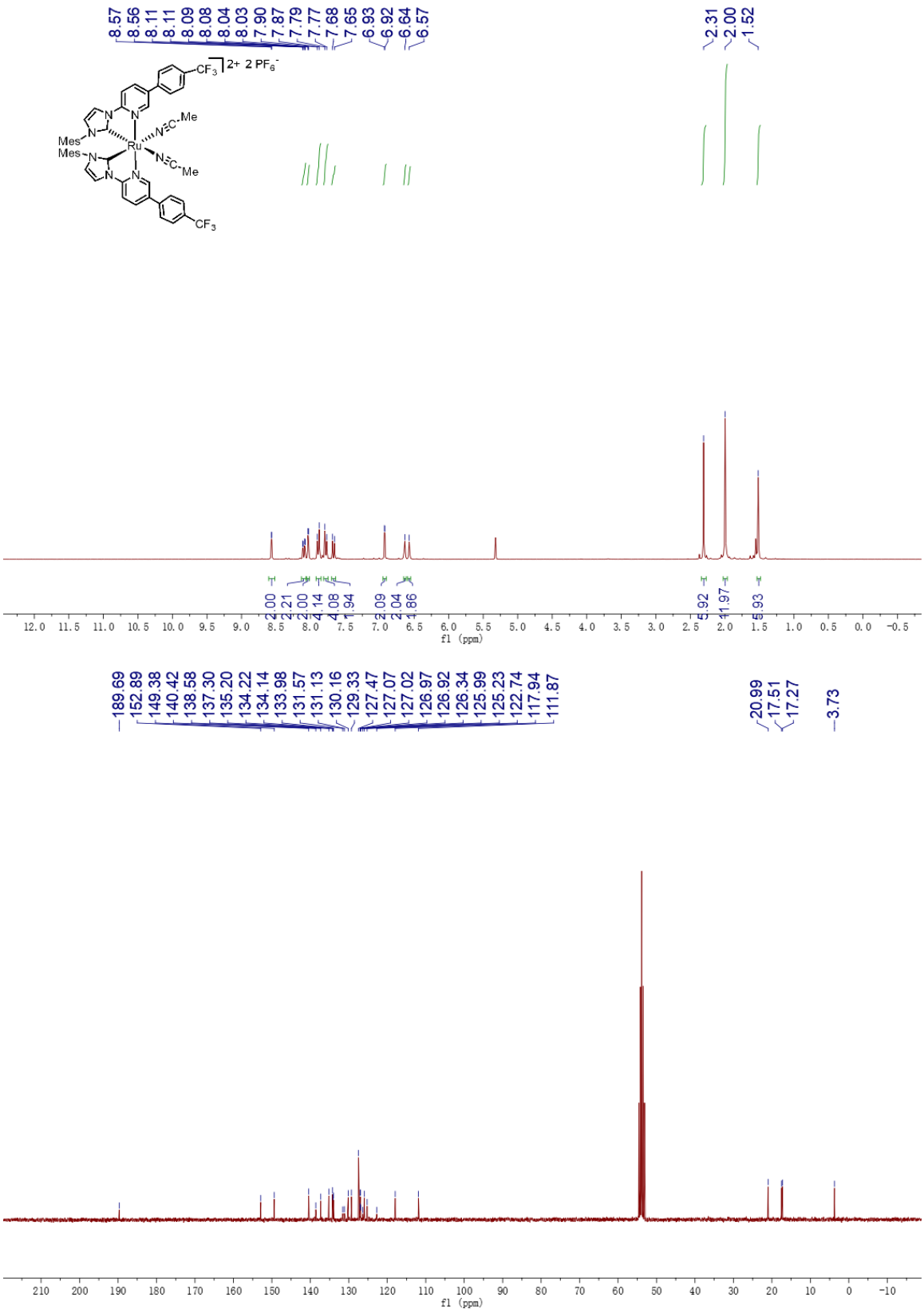

Figure 43. ^{1}H NMR and ^{13}C NMR spectrum of *rac*-**Ru7** in CD_2Cl_2.

2) Chromatography on chiral stationary phase

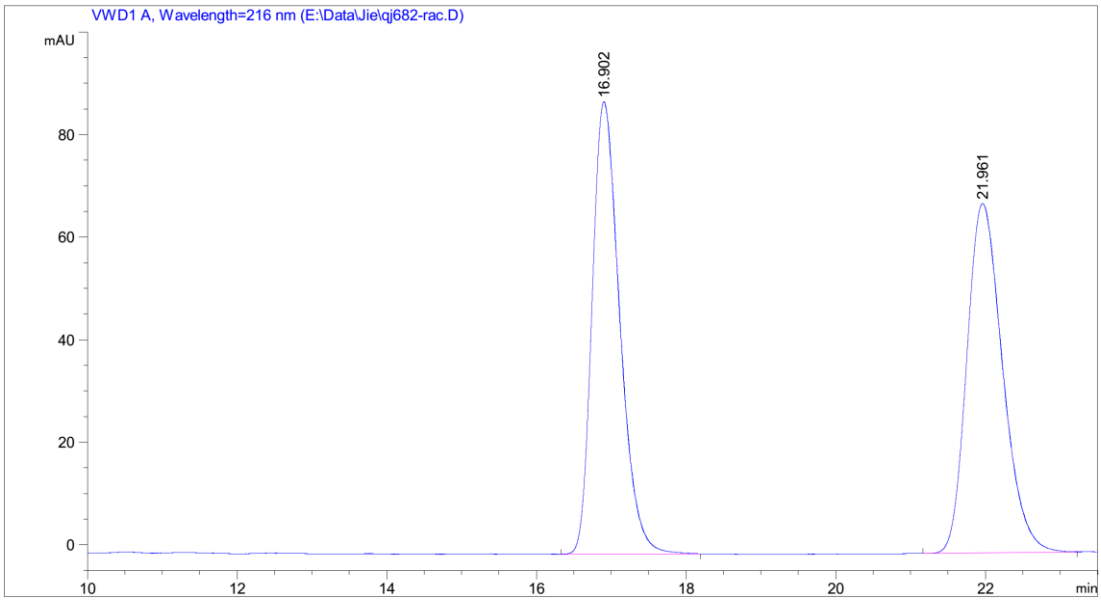

Peak #	RetTime [min]	Type	Width [min]	Area [mAU*s]	Height [mAU]	Area %
1	16.902	BB	0.3686	2253.96802	88.20301	49.9873
2	21.961	BB	0.4037	2255.11328	68.12812	50.0127

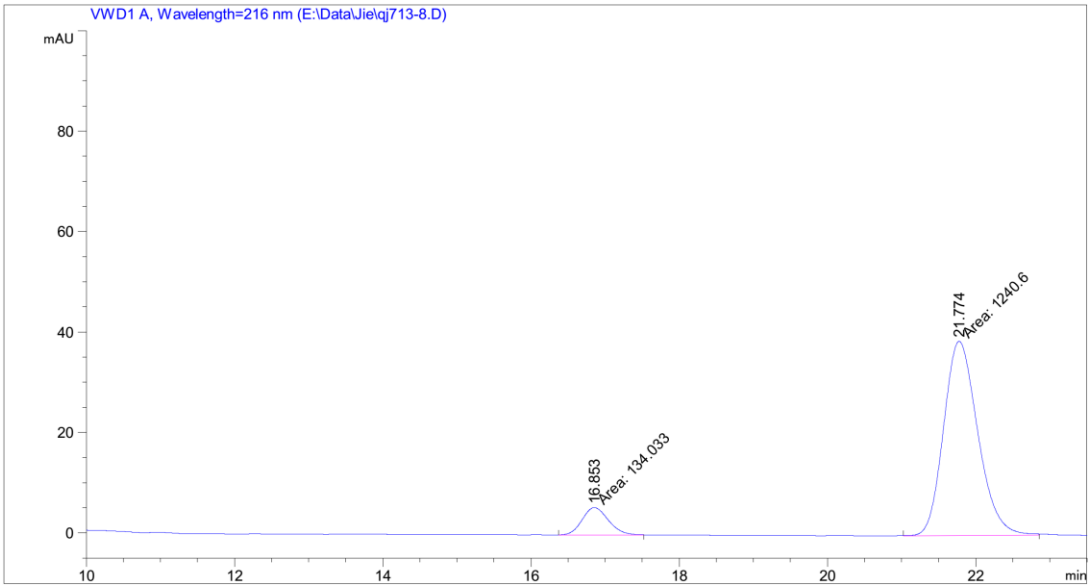

Peak #	RetTime [min]	Type	Width [min]	Area [mAU*s]	Height [mAU]	Area %
1	16.853	MM	0.4095	134.03323	5.45492	9.7504
2	21.774	MM	0.5347	1240.60425	38.66625	90.2496

Figure 44. HPLC traces of *rac*-**5a** and (*R*)-**5a** (81% ee).

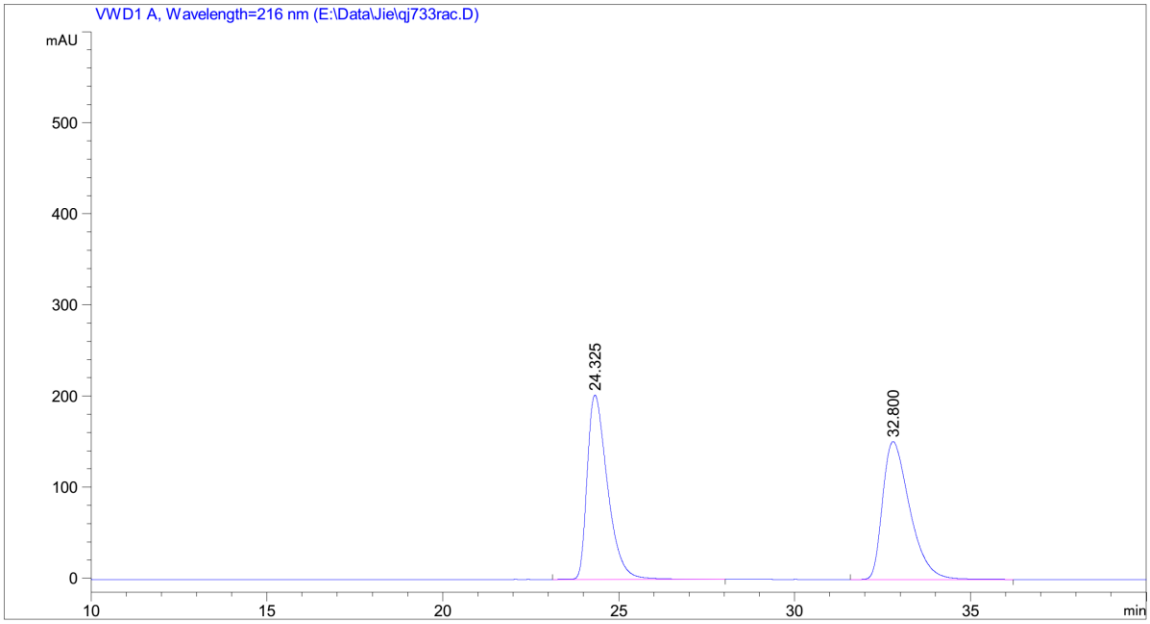

Peak #	RetTime [min]	Type	Width [min]	Area [mAU*s]	Height [mAU]	Area %
1	24.325	BB	0.6135	8127.91943	202.40256	50.0533
2	32.800	BB	0.8263	8110.59766	151.33147	49.9467

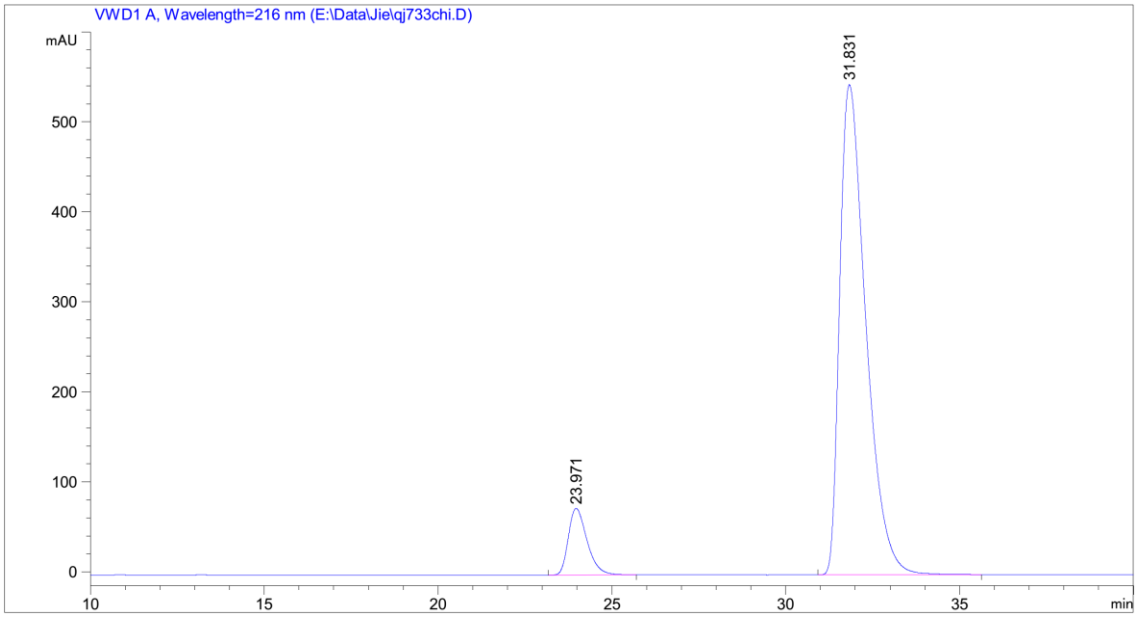

Peak #	RetTime [min]	Type	Width [min]	Area [mAU*s]	Height [mAU]	Area %
1	23.971	BB	0.5752	2765.02979	73.96222	8.8728
2	31.831	BB	0.7904	2.83980e4	544.58356	91.1272

Figure 45. HPLC traces of *rac*-**5b** and (*R*)-**5b** (82% ee).

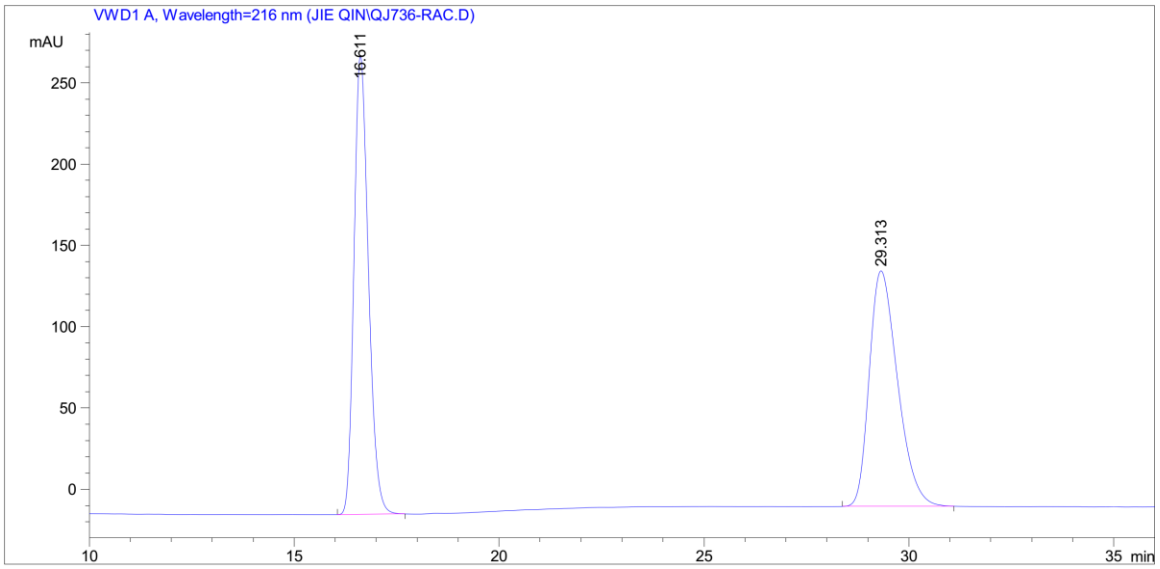

Peak #	RetTime [min]	Type	Width [min]	Area mAU *s	Height [mAU]	Area %
1	16.611	BB	0.3810	6931.88672	282.44757	49.8841
2	29.313	BB	0.7440	6964.10791	144.95572	50.1159

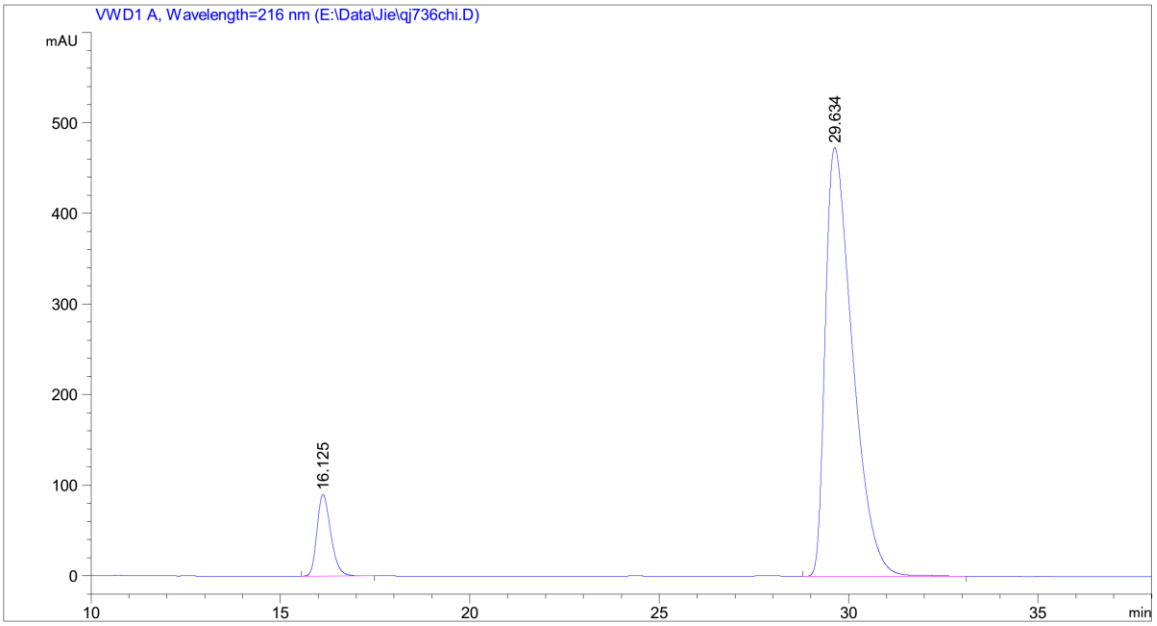

Peak #	RetTime [min]	Type	Width [min]	Area [mAU*s]	Height [mAU]	Area %
1	16.125	BB	0.3903	2278.91650	90.04118	8.7634
2	29.634	BB	0.7616	2.37261e4	473.48325	91.2366

Figure 46. HPLC traces of *rac*-**5c** and (*R*)-**5c** (82% ee).

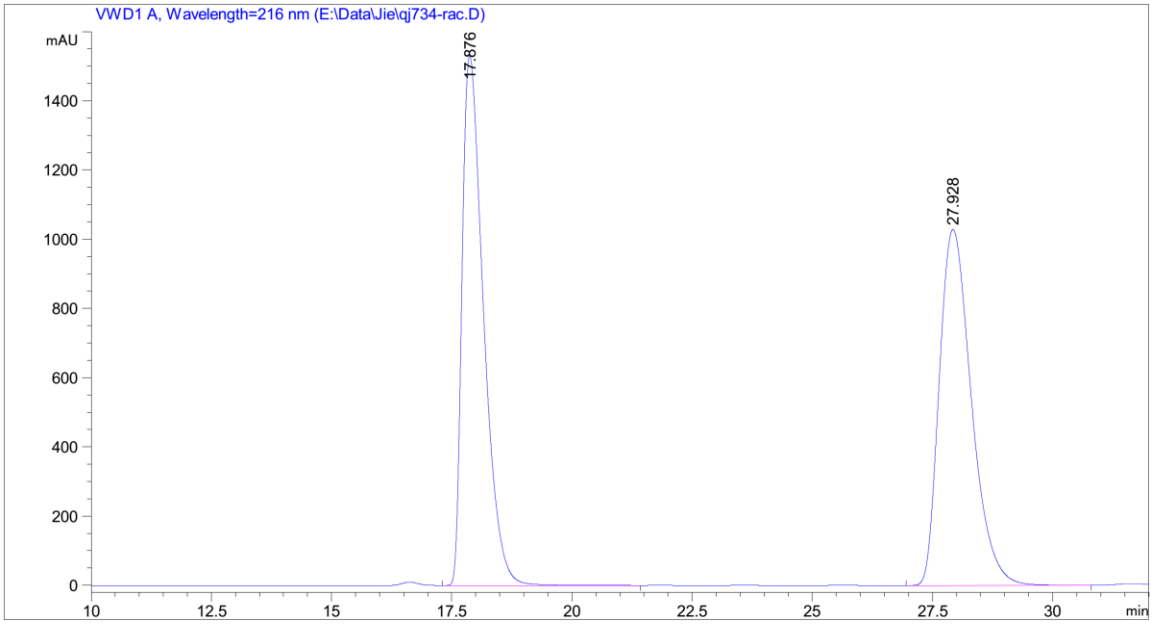

Peak #	RetTime [min]	Type	Width [min]	Area [mAU*s]	Height [mAU]	Area %
1	17.876	BB	0.4746	4.73216e4	1531.18079	49.8008
2	27.928	BB	0.7199	4.77002e4	1028.78650	50.1992

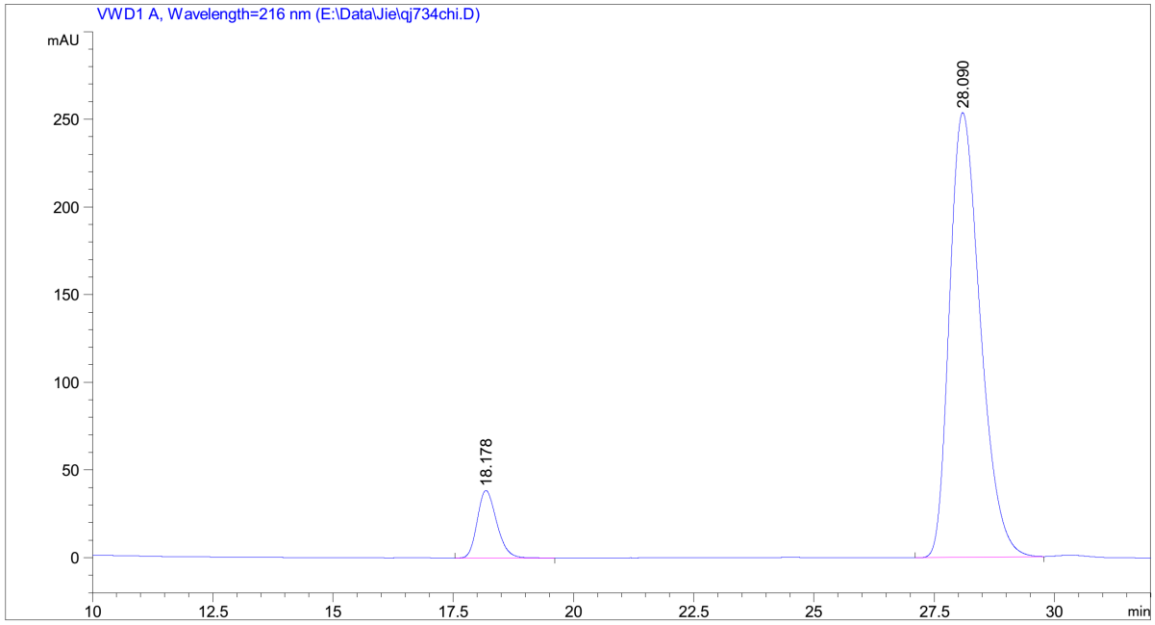

Peak #	RetTime [min]	Type	Width [min]	Area [mAU*s]	Height [mAU]	Area %
1	18.178	BB	0.4330	1084.16211	38.56817	8.7319
2	28.090	BB	0.6922	1.13320e4	253.63615	91.2681

Figure 47. HPLC traces of *rac*-**5d** and (*R*)-**5d** (82% ee).

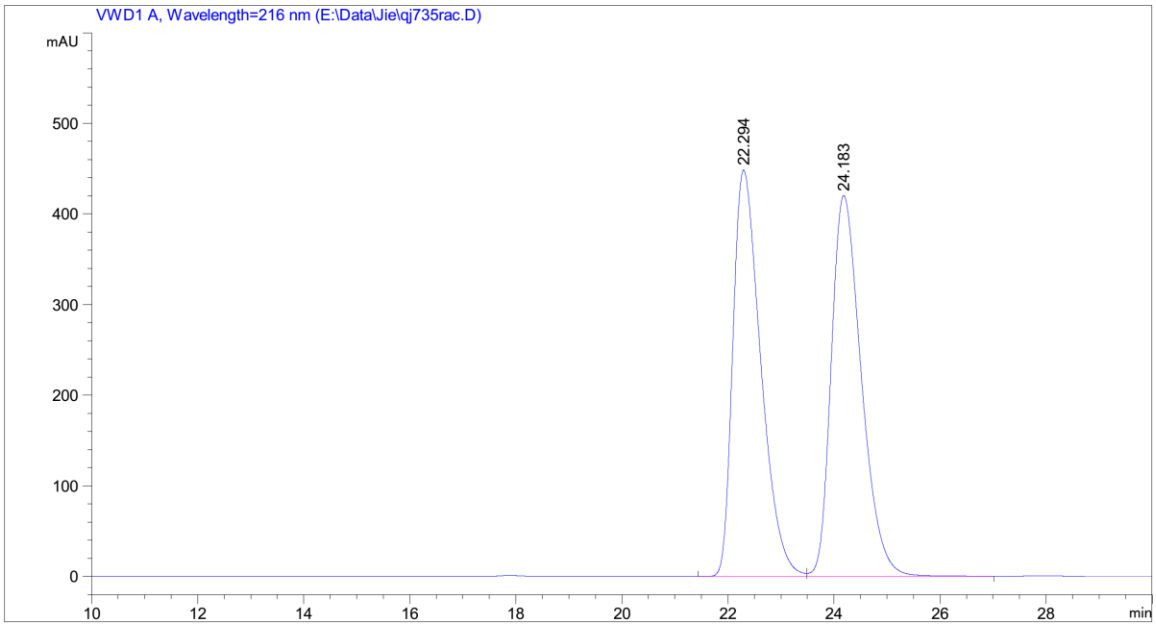

Peak #	RetTime [min]	Type	Width [min]	Area [mAU*s]	Height [mAU]	Area %
1	22.294	BV	0.5631	1.63837e4	448.59079	49.7477
2	24.183	VB	0.6064	1.65499e4	420.33170	50.2523

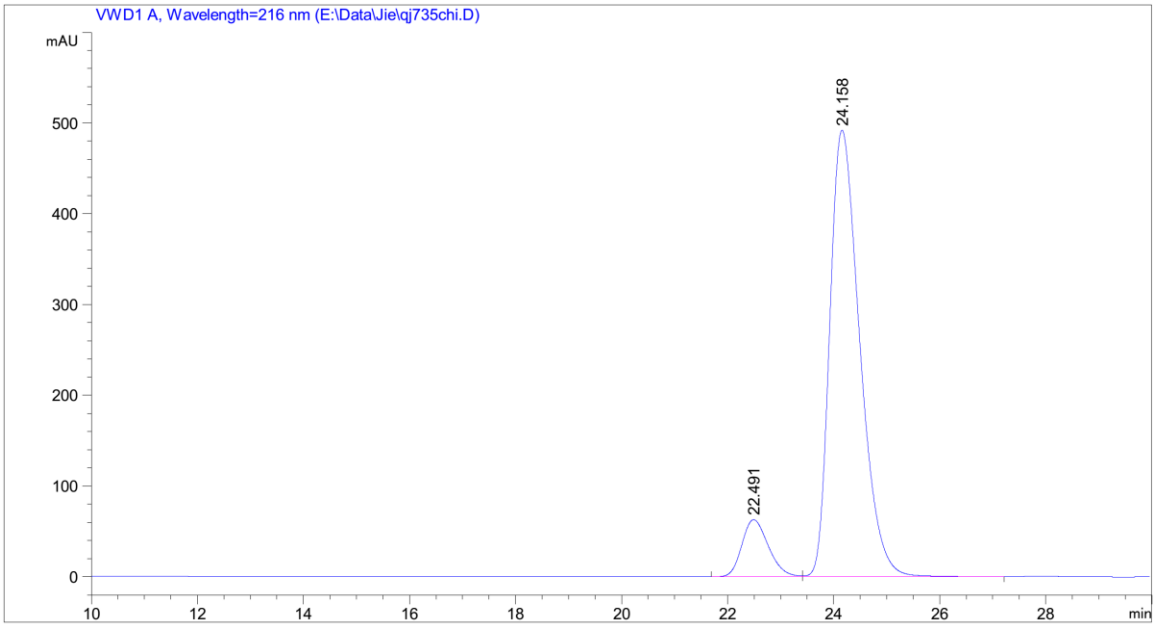

Peak #	RetTime [min]	Type	Width [min]	Area [mAU*s]	Height [mAU]	Area %
1	22.491	BV	0.5365	2176.70972	62.77989	10.1378
2	24.158	VB	0.6044	1.92946e4	492.17136	89.8622

Figure 48. HPLC traces of *rac*-**5e** and (*R*)-**5e** (80% ee).

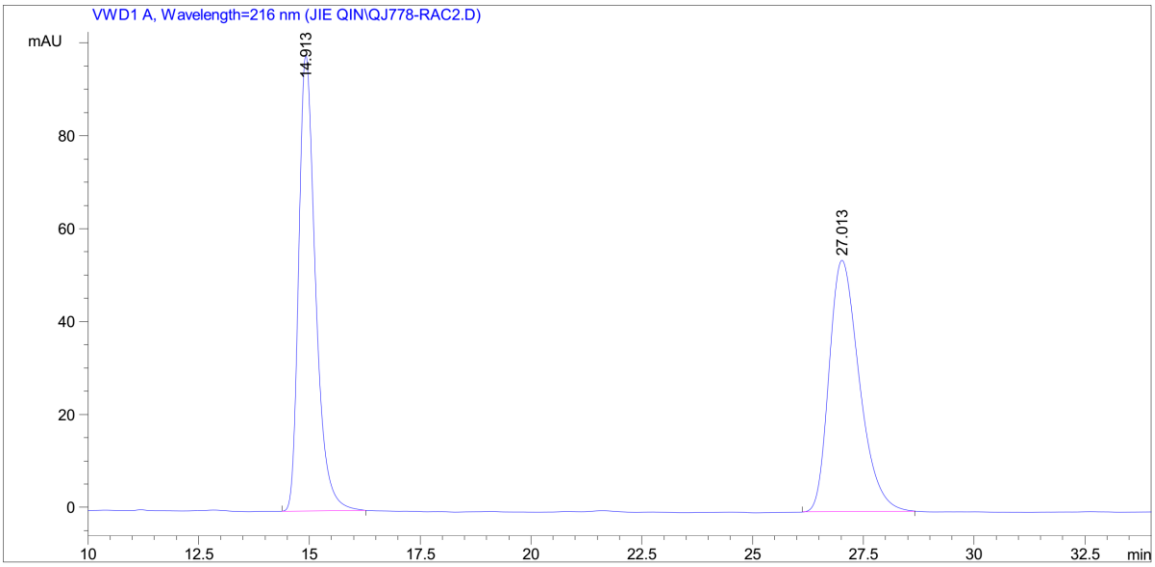

Peak #	RetTime [min]	Type	Width [min]	Area mAU *s	Height [mAU]	Area %
1	14.913	BB	0.4014	2583.75562	98.25952	50.1244
2	27.013	BB	0.7342	2570.93335	54.17445	49.8756

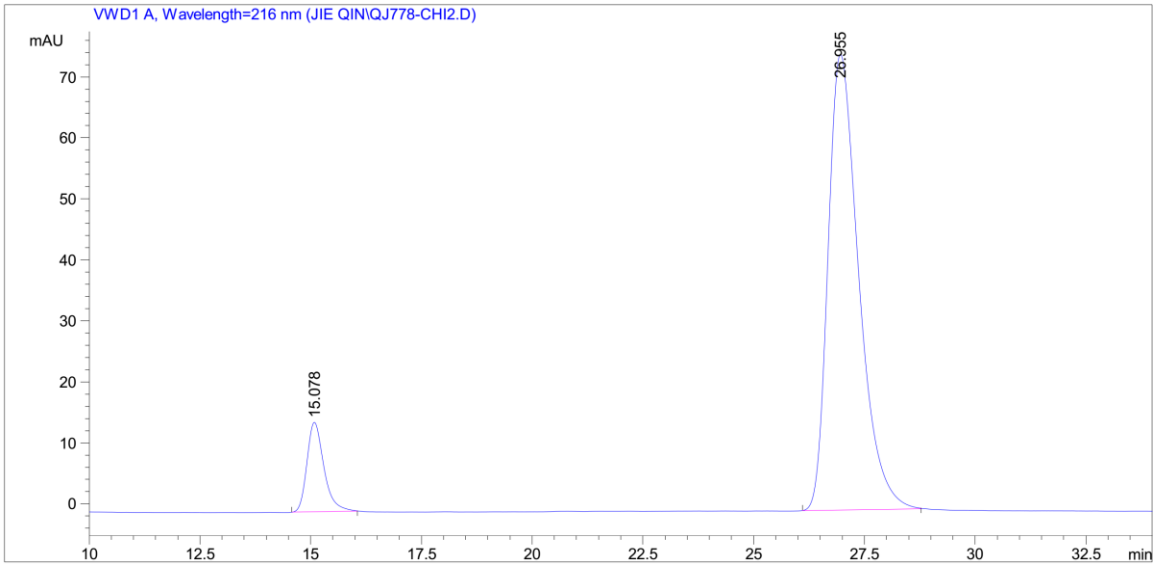

Peak #	RetTime [min]	Type	Width [min]	Area mAU *s	Height [mAU]	Area %
1	15.078	BB	0.4073	394.30521	14.71220	9.8723
2	26.955	BB	0.7368	3599.75610	74.72305	90.1277

Figure 49. HPLC traces of *rac*-**5f** and (*R*)-**5f** (80% ee).

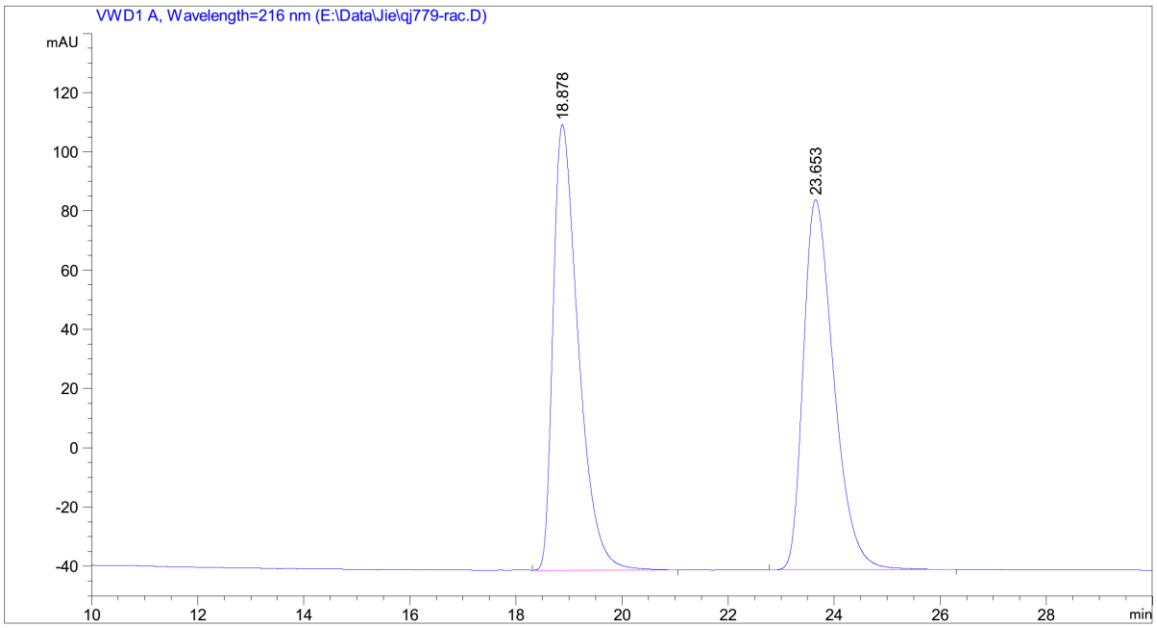

Peak #	RetTime [min]	Type	Width [min]	Area [mAU*s]	Height [mAU]	Area %
1	18.878	BB	0.5020	4964.95117	150.46060	49.8533
2	23.653	BB	0.6150	4994.17969	125.03427	50.1467

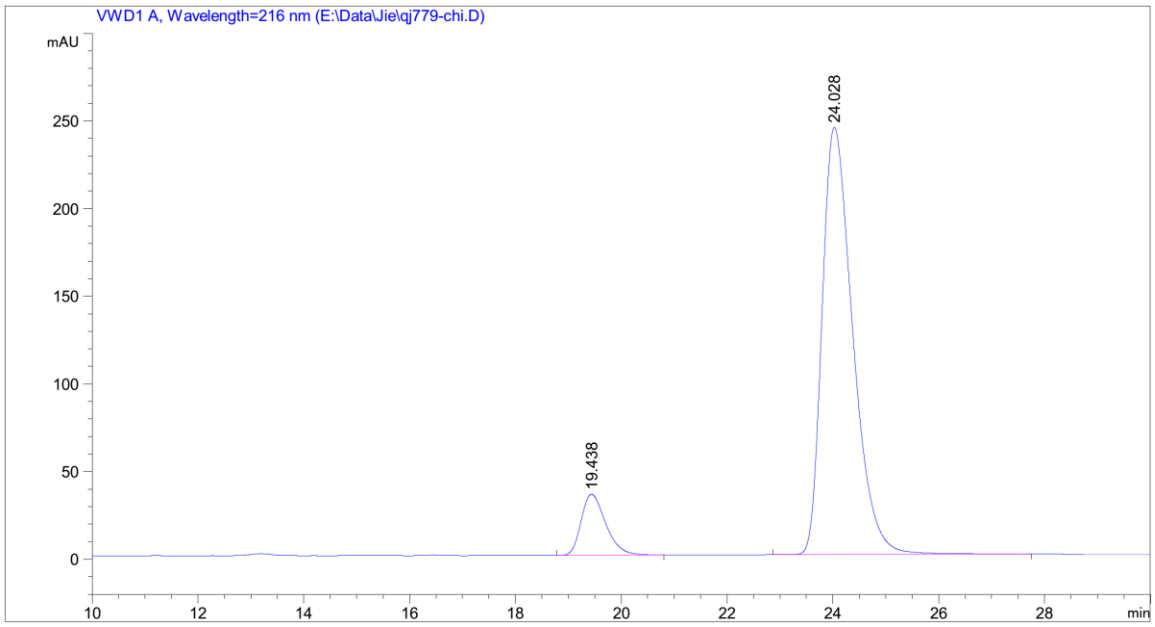

Peak #	RetTime [min]	Type	Width [min]	Area [mAU*s]	Height [mAU]	Area %
1	19.438	BB	0.4960	1126.59924	34.86368	10.2958
2	24.028	BB	0.6198	9815.74023	243.76091	89.7042

Figure 50. HPLC traces of *rac*-**5g** and (*R*)-**5g** (80% ee).

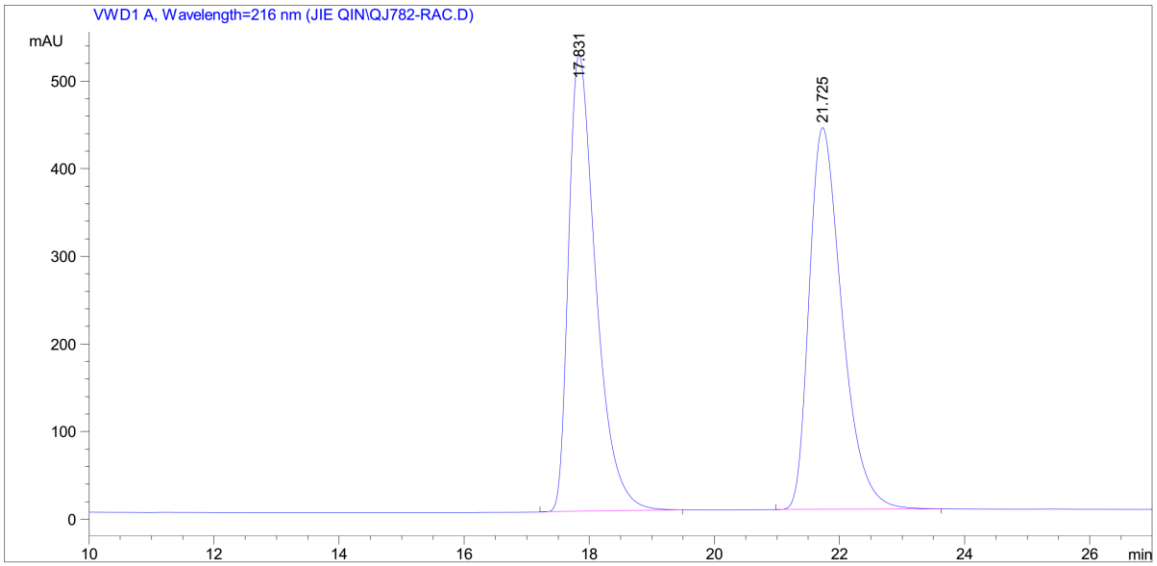

Peak #	RetTime [min]	Type	Width [min]	Area mAU *s	Height [mAU]	Area %
1	17.831	BB	0.4638	1.58437e4	521.28827	49.8893
2	21.725	BB	0.5629	1.59140e4	435.83536	50.1107

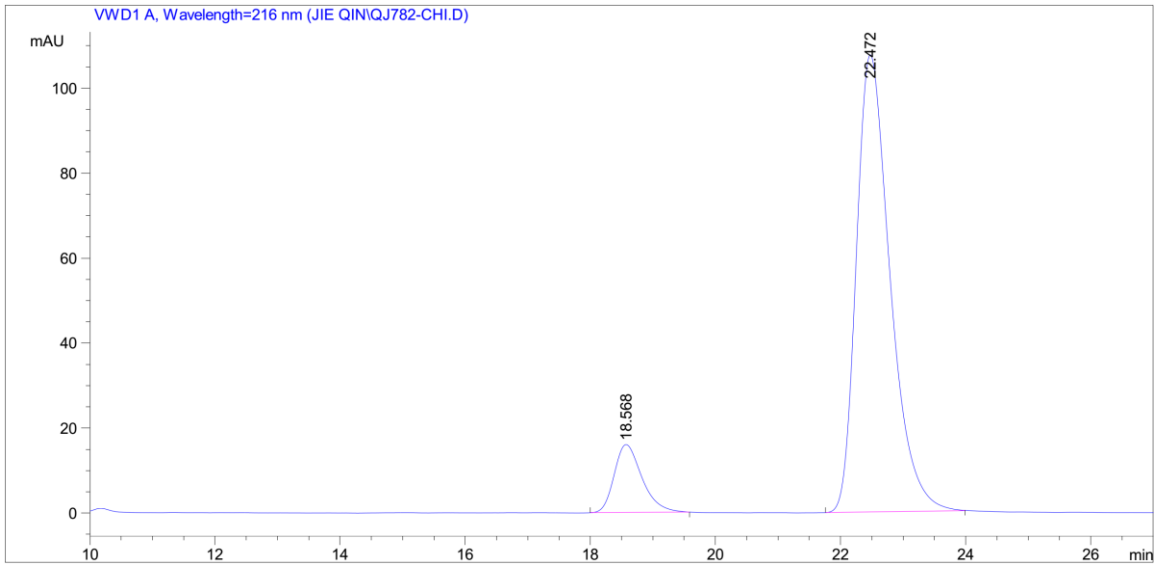

Peak #	RetTime [min]	Type	Width [min]	Area mAU *s	Height [mAU]	Area %
1	18.568	BB	0.4709	497.28134	16.04039	10.9847
2	22.472	BB	0.5737	4029.73828	107.61485	89.0153

Figure 51. HPLC traces of *rac*-**5h** and (*R*)-**5h** (78% ee).

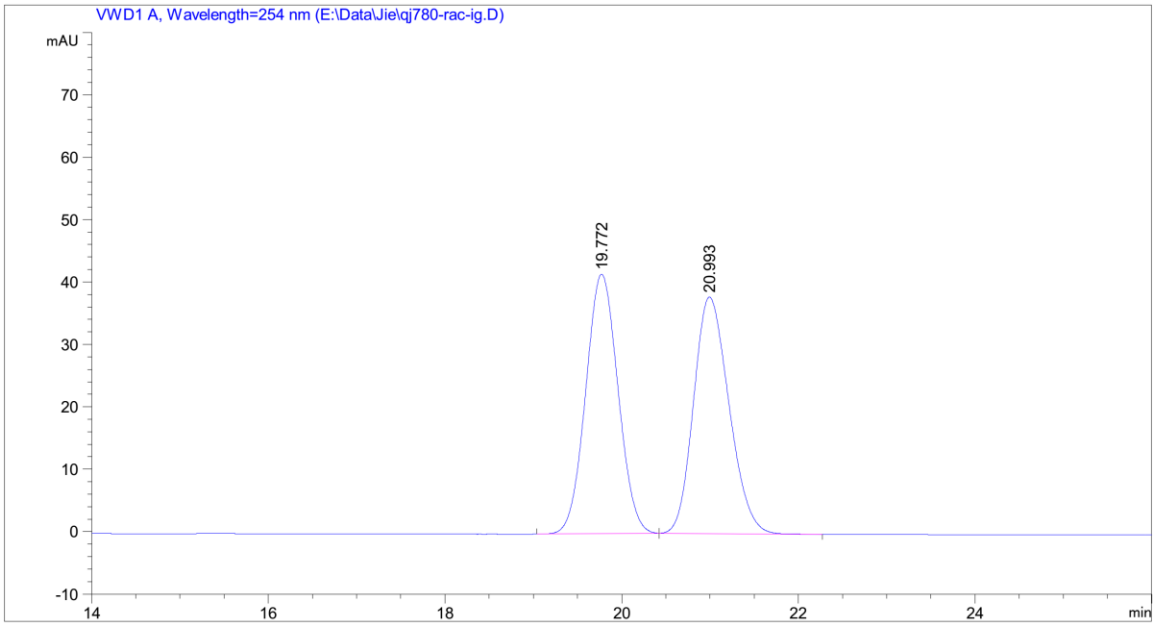

Peak #	RetTime [min]	Type	Width [min]	Area [mAU*s]	Height [mAU]	Area %
1	19.772	BB	0.3973	1055.58276	41.56600	50.0254
2	20.993	BB	0.4337	1054.51074	37.89093	49.9746

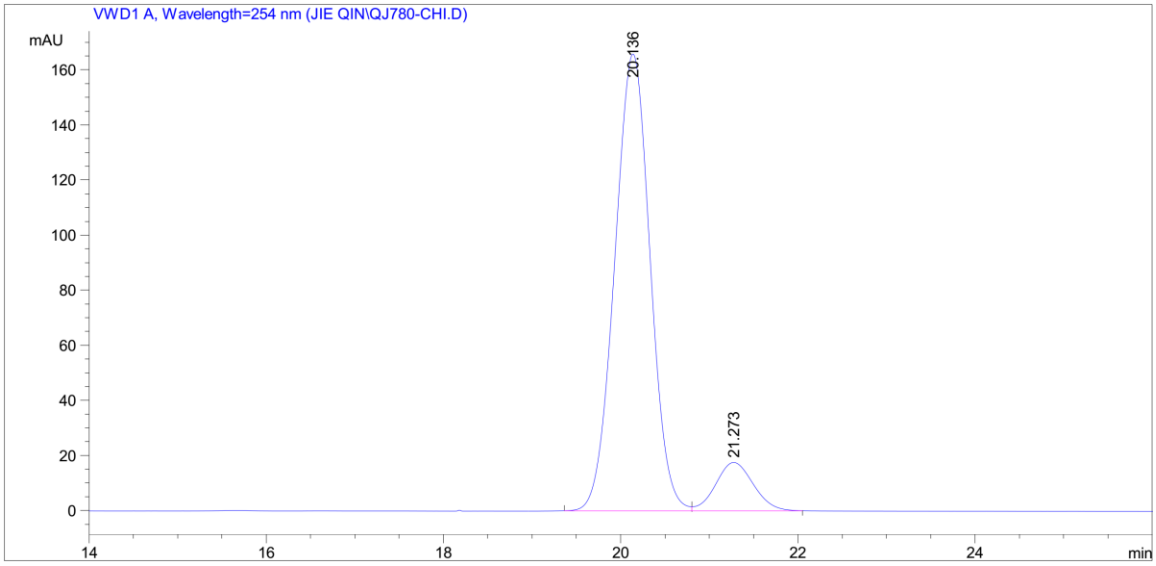

Peak #	RetTime [min]	Type	Width [min]	Area mAU *s	Height [mAU]	Area %
1	20.136	BV	0.4330	4604.32764	165.90079	89.8519
2	21.273	VB	0.4614	520.02307	17.58763	10.1481

Figure 52. HPLC traces of *rac*-**5i** and (*R*)-**5i** (80% ee).

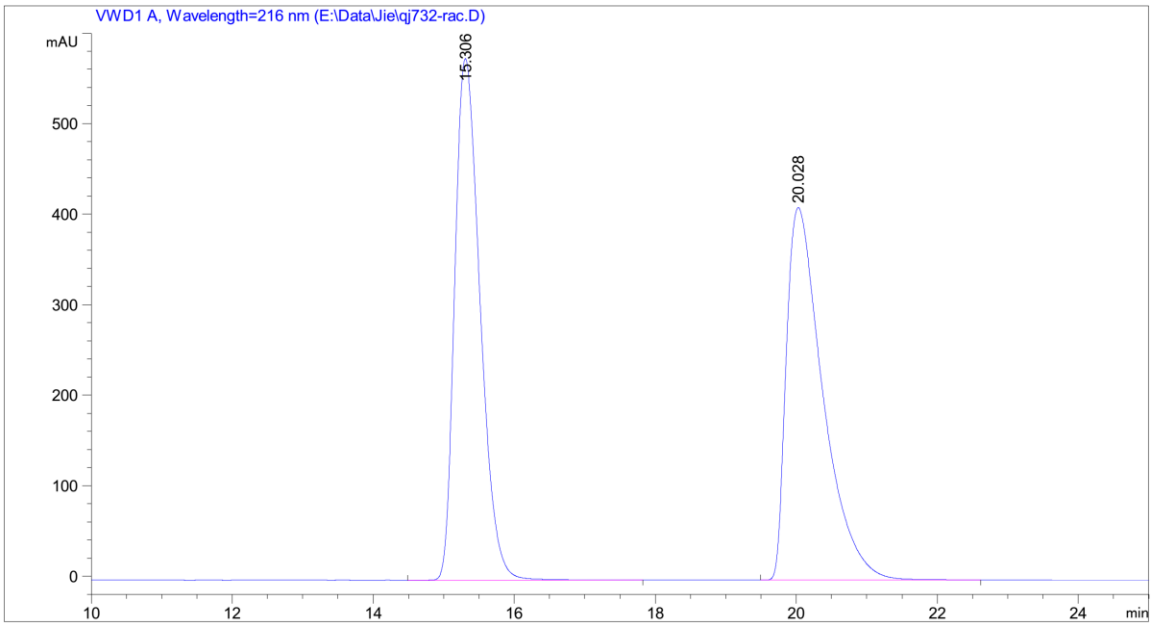

Peak #	RetTime [min]	Type	Width [min]	Area [mAU*s]	Height [mAU]	Area %
1	15.306	BB	0.3906	1.43573e4	576.30640	49.2152
2	20.028	BB	0.5449	1.48152e4	411.61276	50.7848

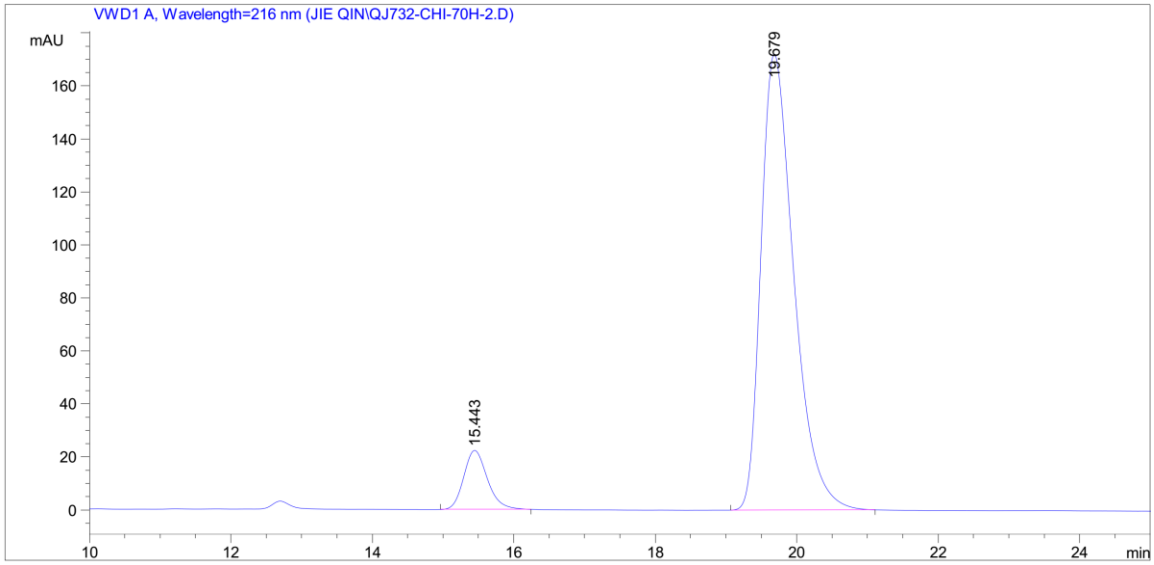

Peak #	RetTime [min]	Type	Width [min]	Area mAU *s	Height [mAU]	Area %
1	15.443	BB	0.3600	521.42291	22.31083	8.5873
2	19.679	BB	0.4958	5550.63135	172.05229	91.4127

Figure 53. HPLC traces of *rac*-**5j** and (*R*)-**5j** (82% ee).

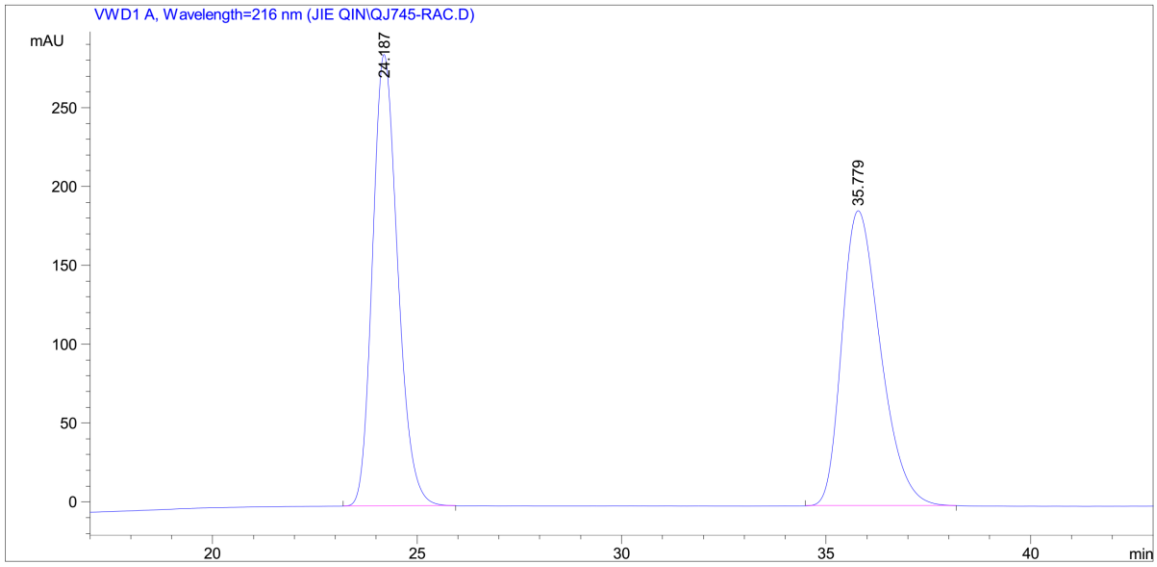

Peak #	RetTime [min]	Type	Width [min]	Area mAU *s	Height [mAU]	Area %
1	24.187	BB	0.6616	1.22711e4	286.32678	49.9597
2	35.779	BB	1.0108	1.22909e4	187.14998	50.0403

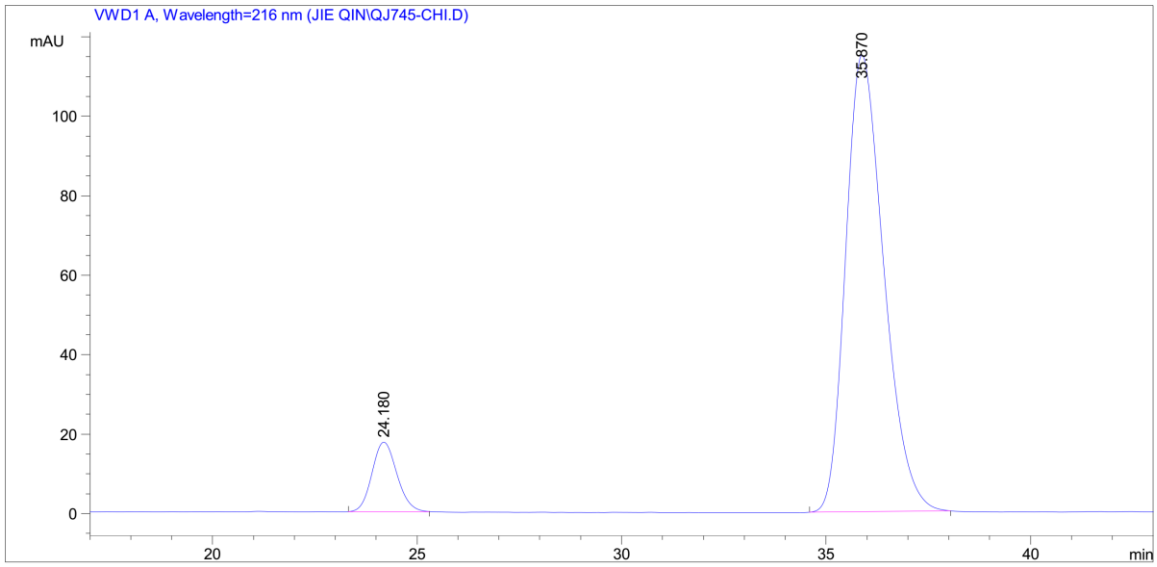

Peak #	RetTime [min]	Type	Width [min]	Area mAU *s	Height [mAU]	Area %
1	24.180	BB	0.6580	743.47540	17.52391	9.0495
2	35.870	BB	1.0026	7472.17334	115.00774	90.9505

Figure 54. HPLC traces of *rac*-**5k** and (*R*)-**5k** (82% ee).

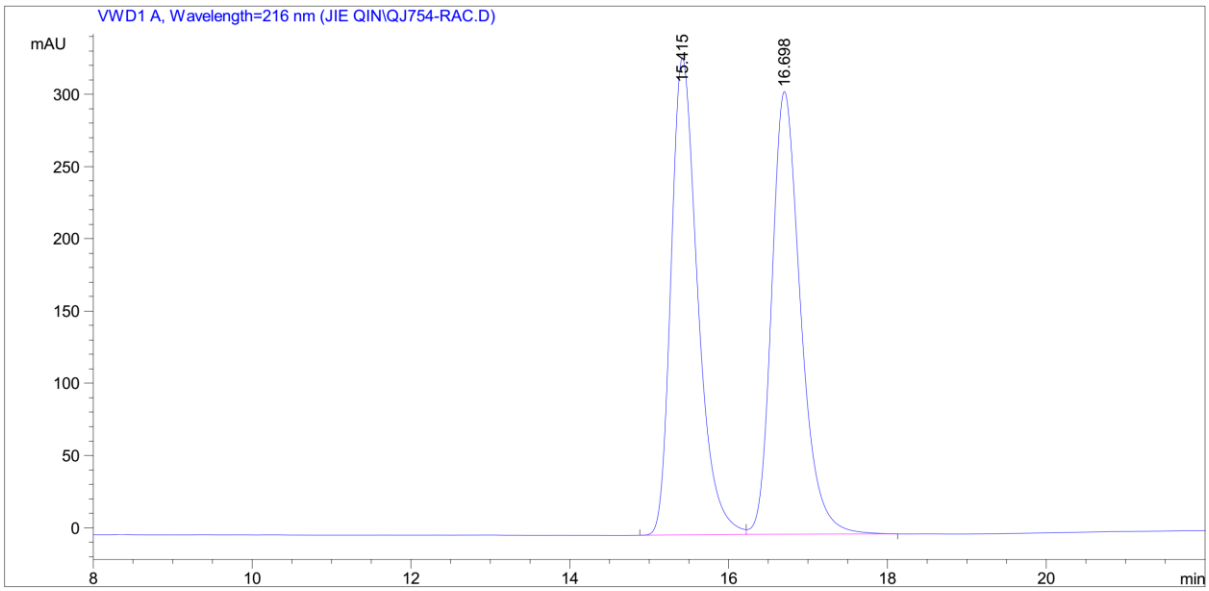

Peak #	RetTime [min]	Type	Width [min]	Area mAU *s	Height [mAU]	Area %
1	15.415	BV	0.3574	7686.66309	330.31906	49.7673
2	16.698	VB	0.3869	7758.54346	306.68829	50.2327

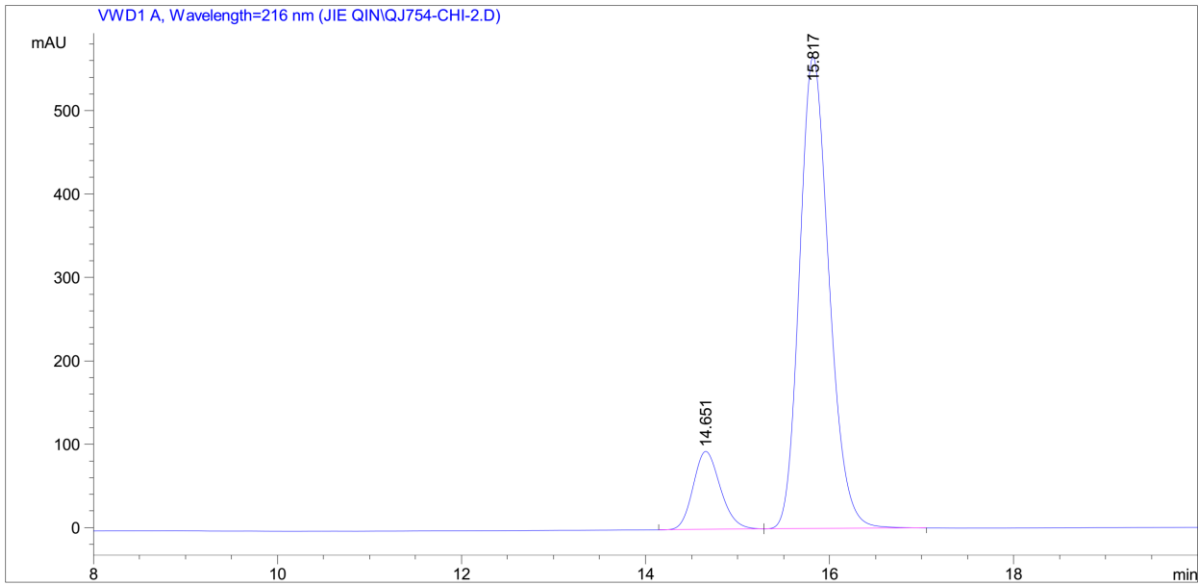

Peak #	RetTime [min]	Type	Width [min]	Area mAU *s	Height [mAU]	Area %
1	14.651	BV	0.3190	1930.42651	93.67418	13.2491
2	15.817	VB	0.3436	1.26398e4	565.83331	86.7509

Figure 55. HPLC traces of *rac*-**5l** and (*R*)-**5l** (74% ee).

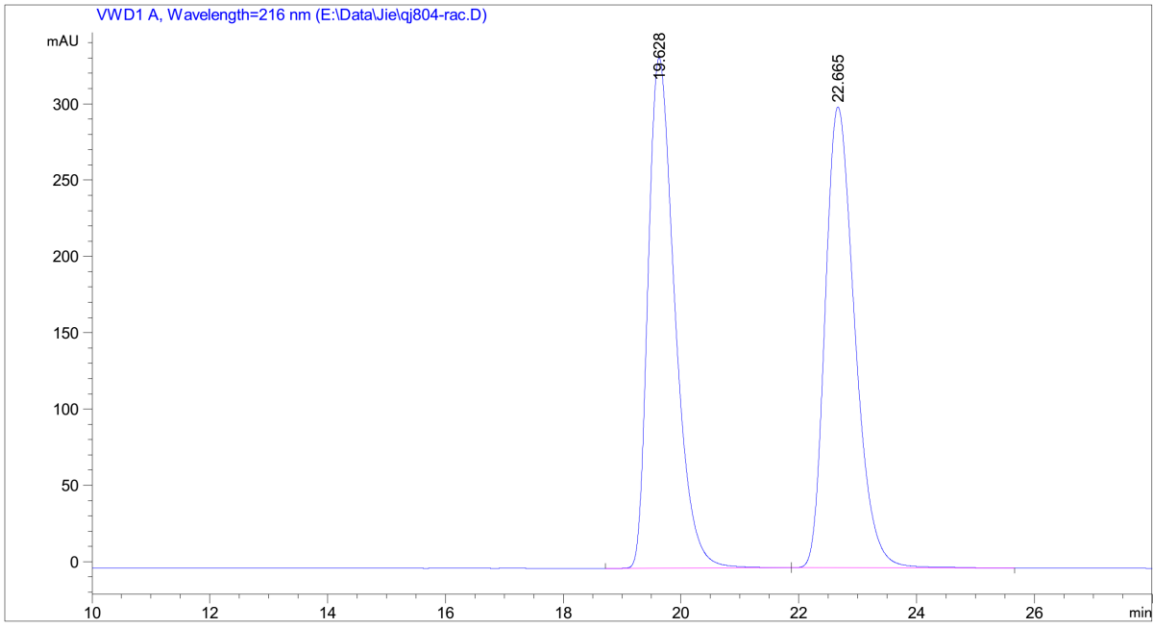

Peak #	RetTime [min]	Type	Width [min]	Area [mAU*s]	Height [mAU]	Area %
1	19.628	BB	0.4851	1.05238e4	334.42444	49.9646
2	22.665	BB	0.5401	1.05387e4	302.00287	50.0354

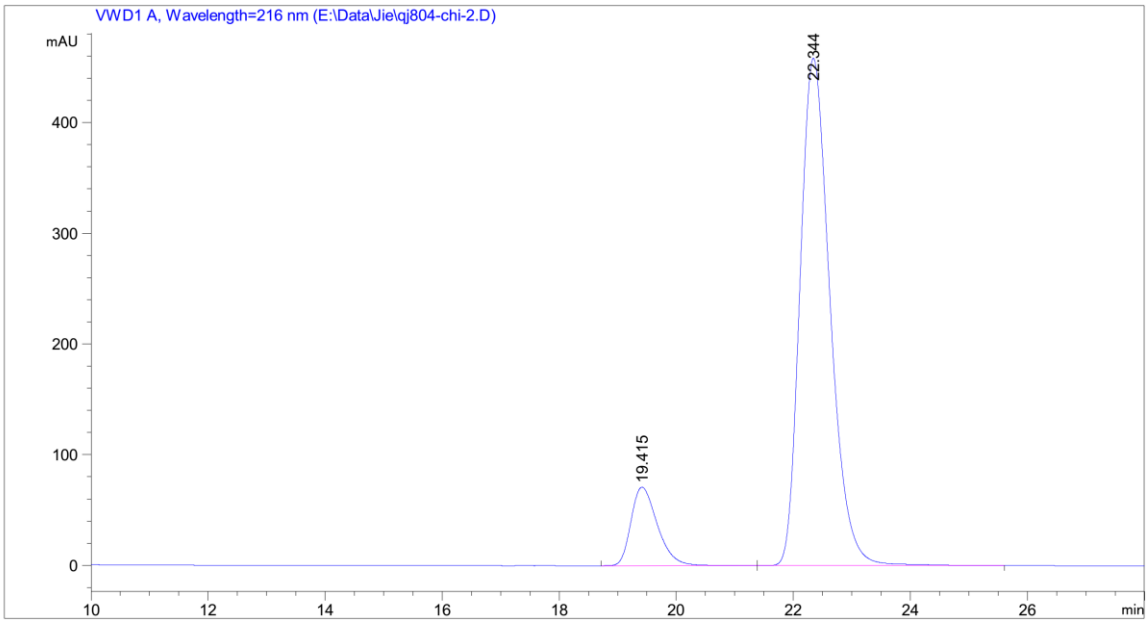

Peak #	RetTime [min]	Type	Width [min]	Area [mAU*s]	Height [mAU]	Area %
1	19.415	BB	0.4843	2227.83838	70.95590	12.0467
2	22.344	BB	0.5510	1.62654e4	458.40186	87.9533

Figure 56. HPLC traces of *rac*-**5m** and (*R*)-**5m** (76% ee).

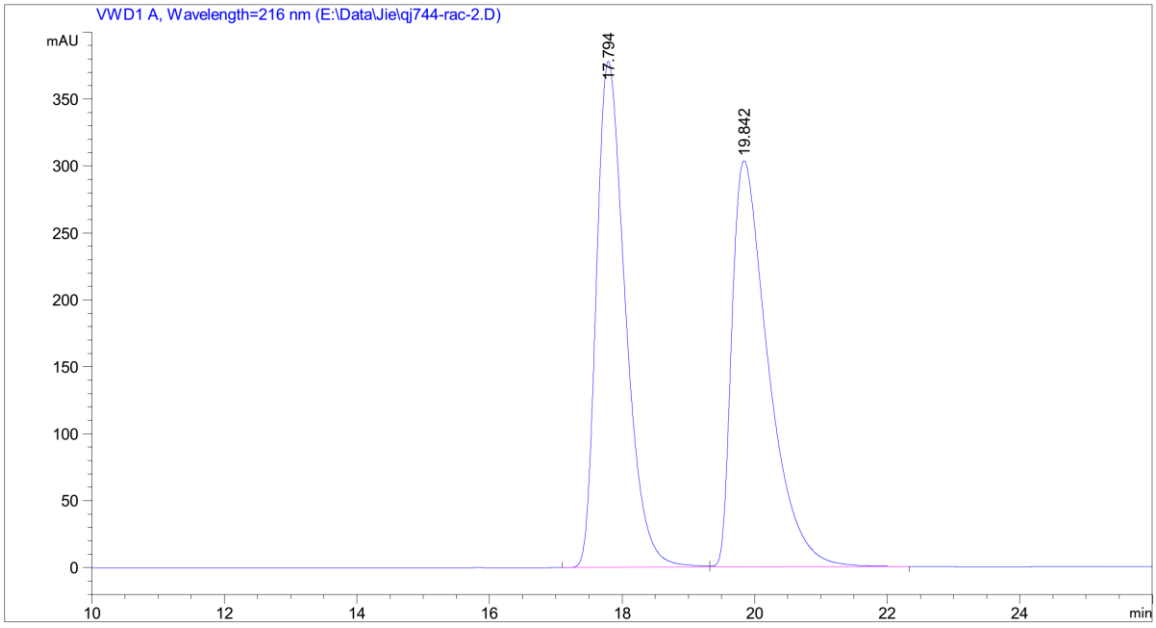

Peak #	RetTime [min]	Type	Width [min]	Area [mAU*s]	Height [mAU]	Area %
1	17.794	BV	0.4681	1.14755e4	378.06802	49.8756
2	19.842	VB	0.5733	1.15328e4	303.50049	50.1244

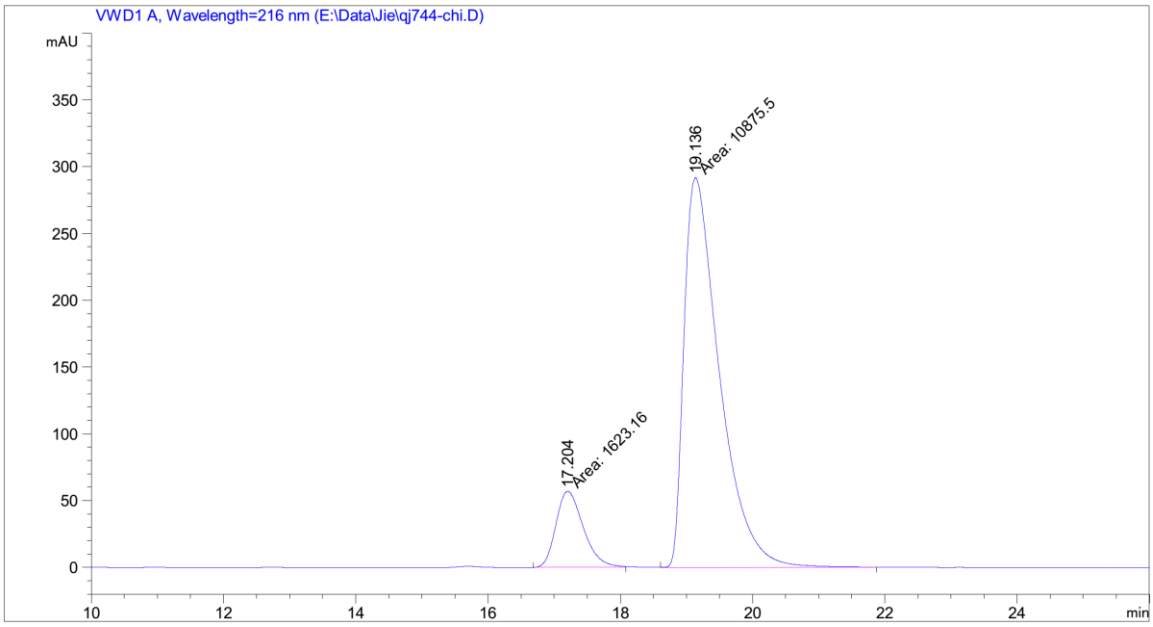

Peak #	RetTime [min]	Type	Width [min]	Area [mAU*s]	Height [mAU]	Area %
1	17.204	MM	0.4767	1623.15625	56.75089	12.9867
2	19.136	MM	0.6211	1.08755e4	291.82983	87.0133

Figure 57. HPLC traces of *rac*-**5n** and (*R*)-**5n** (74% ee).

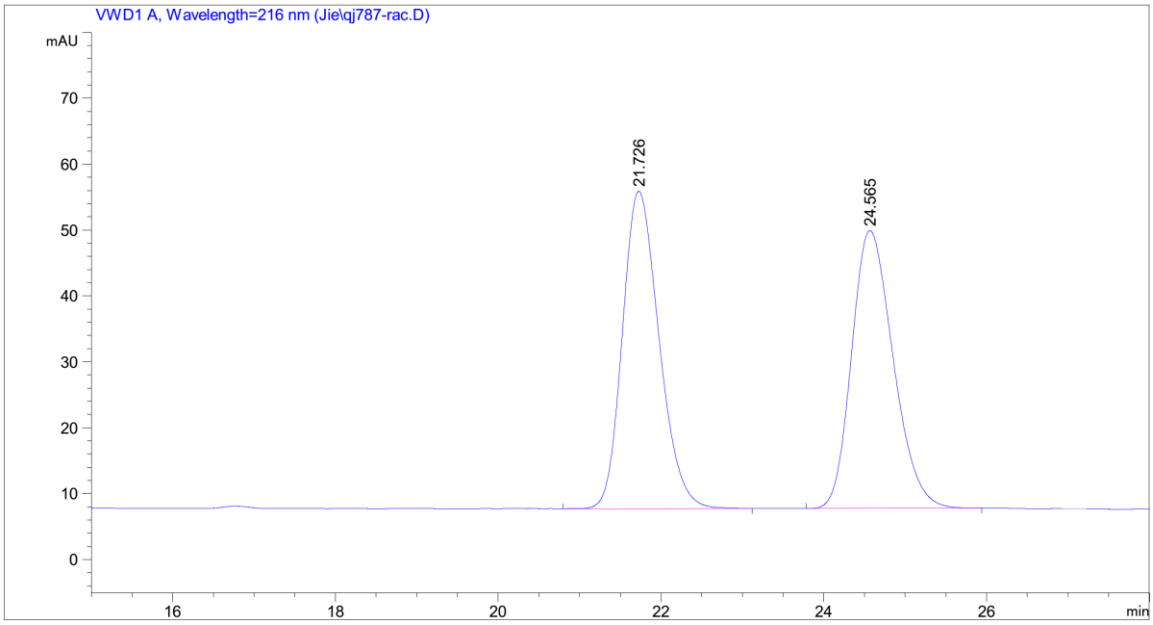

Peak #	RetTime [min]	Type	Width [min]	Area [mAU*s]	Height [mAU]	Area %
1	21.726	BB	0.4849	1505.76990	48.14754	50.2170
2	24.565	BB	0.5522	1492.75549	42.14451	49.7830

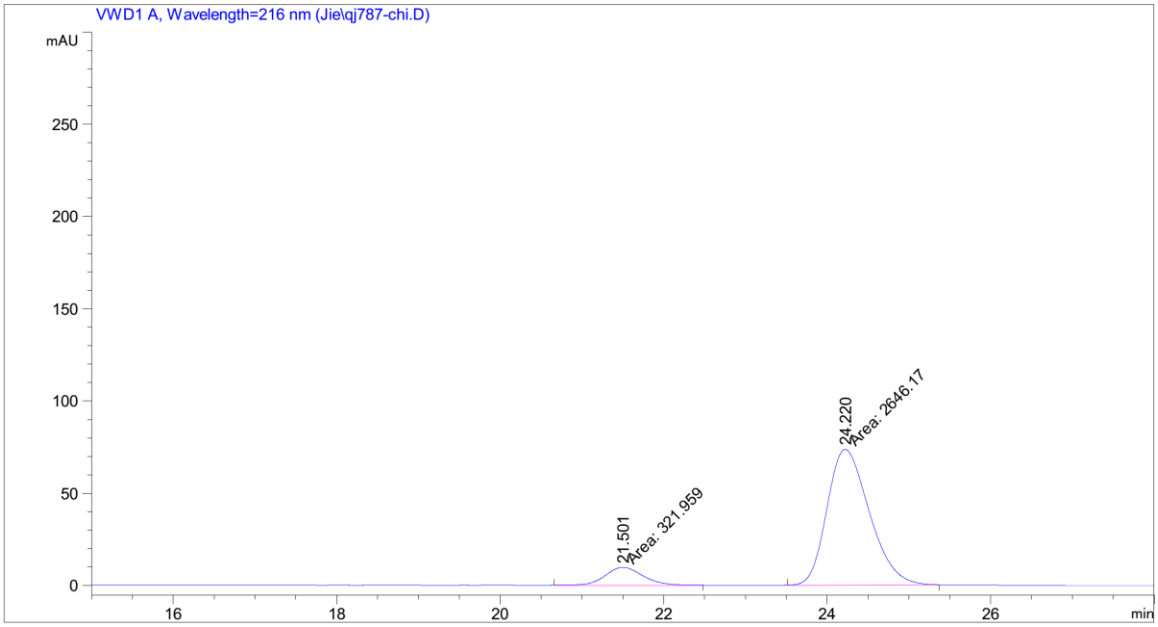

Peak #	RetTime [min]	Type	Width [min]	Area [mAU*s]	Height [mAU]	Area %
1	21.501	MM	0.5486	321.95914	9.78142	10.8472
2	24.220	MM	0.5998	2646.16846	73.52359	89.1528

Figure 58. HPLC traces of *rac*-**5o** and (*R*)-**5o** (78% ee).

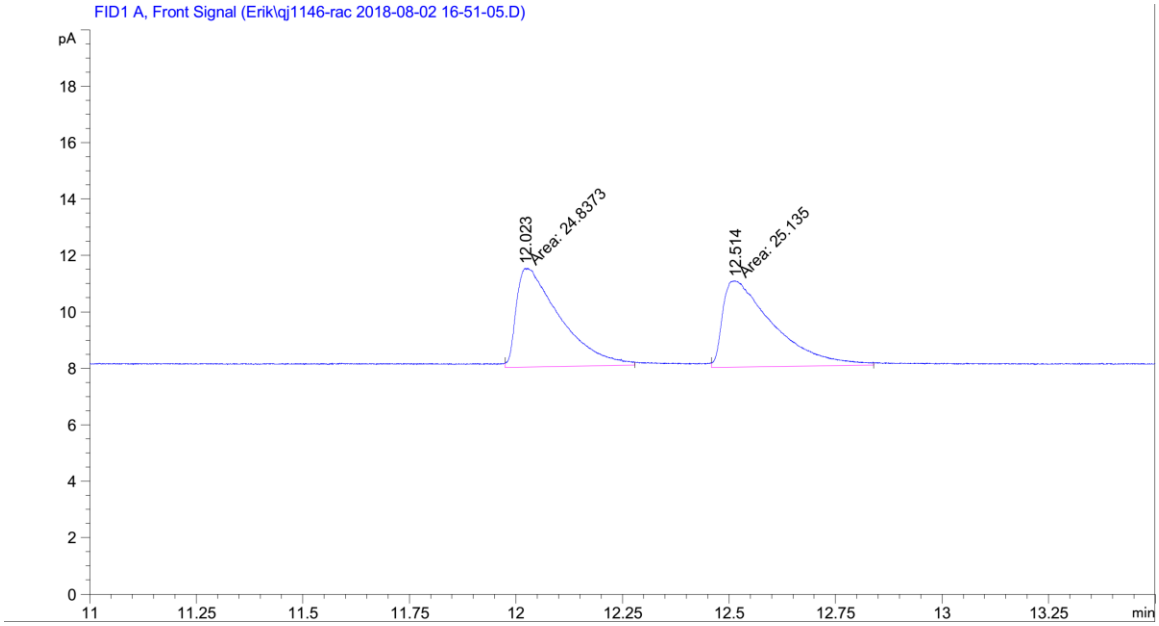

Peak #	RetTime [min]	Type	Width [min]	Area [pA*s]	Height [pA]	Area %
1	12.023	MM	0.1184	24.83726	3.49682	49.70210
2	12.514	MM	0.1376	25.13499	3.04488	50.29790

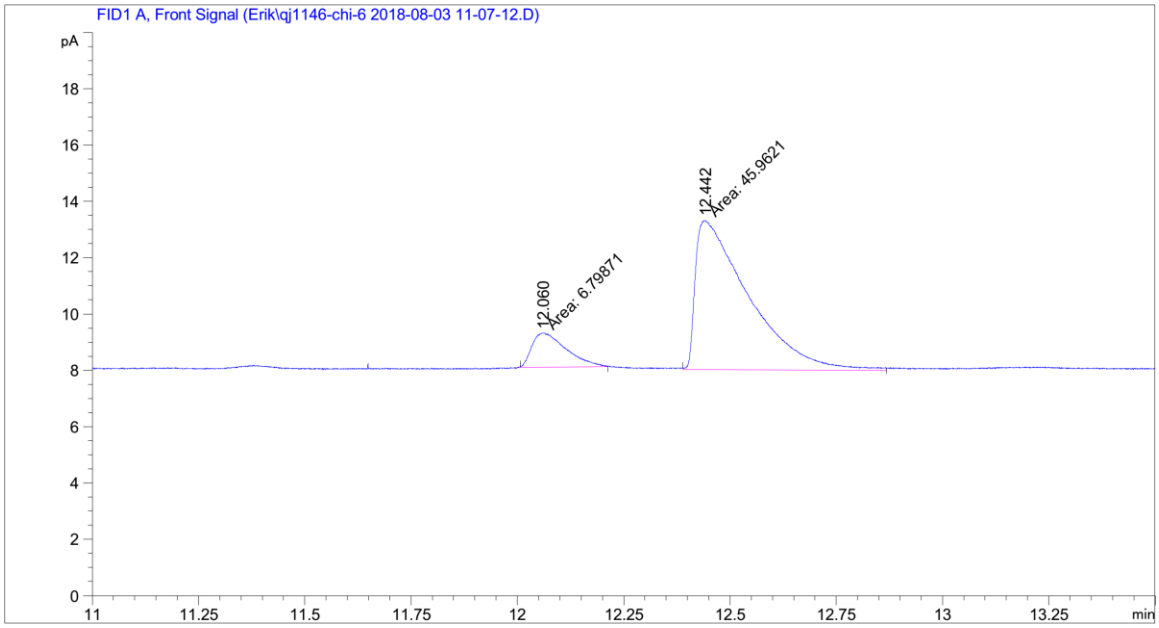

Peak #	RetTime [min]	Type	Width [min]	Area [pA*s]	Height [pA]	Area %
1	12.060	MM	0.0931	6.79871	1.21773	12.88592
2	12.442	MM	0.1444	45.96206	5.30444	87.11408

Figure 59. GC traces of *rac*-**5p** and (*S*)-**5p** (74% ee).

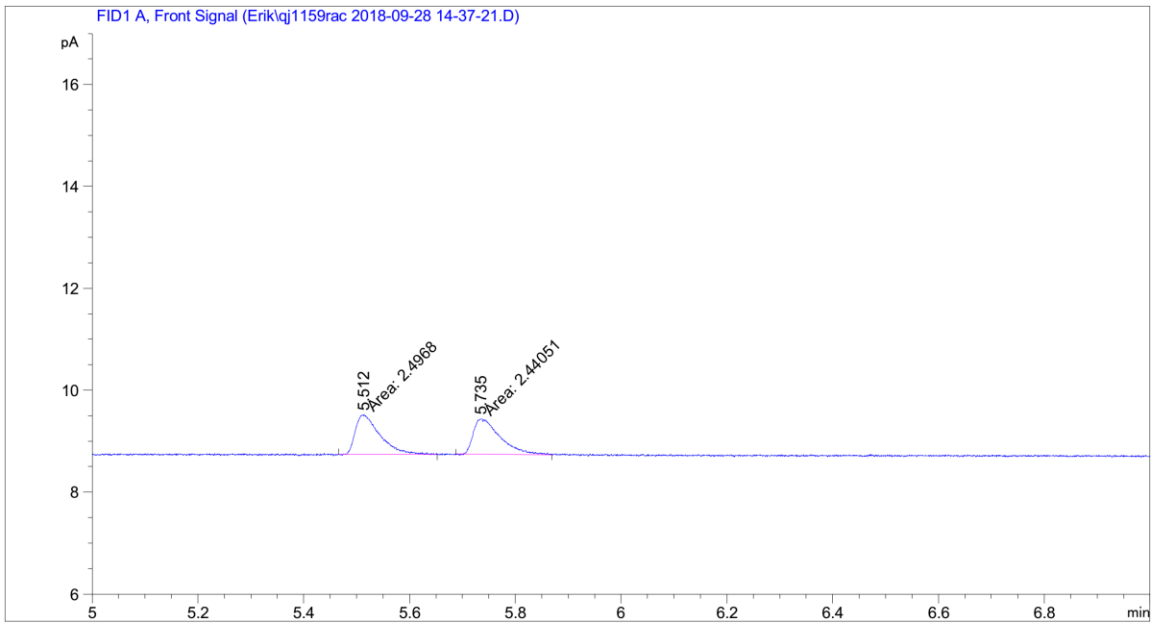

Peak #	RetTime [min]	Type	Width [min]	Area [pA*s]	Height [pA]	Area %
1	5.512	MM	0.0534	2.49680	7.78652e-1	50.57004
2	5.735	MM	0.0592	2.44051	6.87526e-1	49.42996

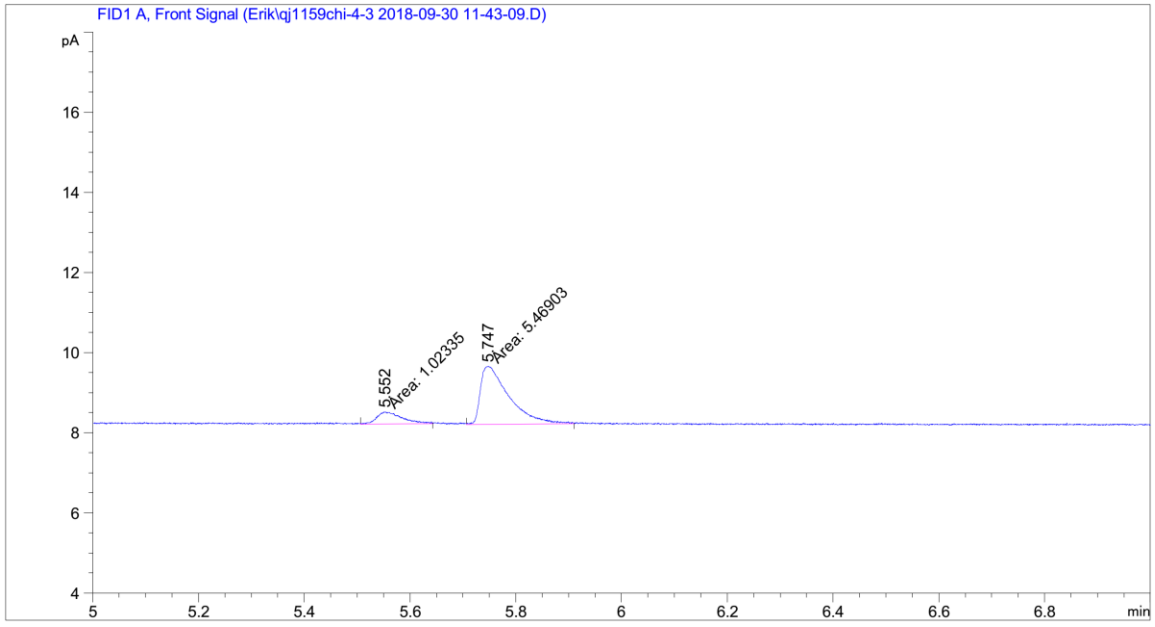

Peak #	RetTime [min]	Type	Width [min]	Area [pA*s]	Height [pA]	Area %
1	5.552	MM	0.0563	1.02335	3.02821e-1	15.76230
2	5.747	MM	0.0631	5.46903	1.44486	84.23770

Figure 60. GC traces of *rac*-**5q** and (*S*)-**5q** (68% ee).

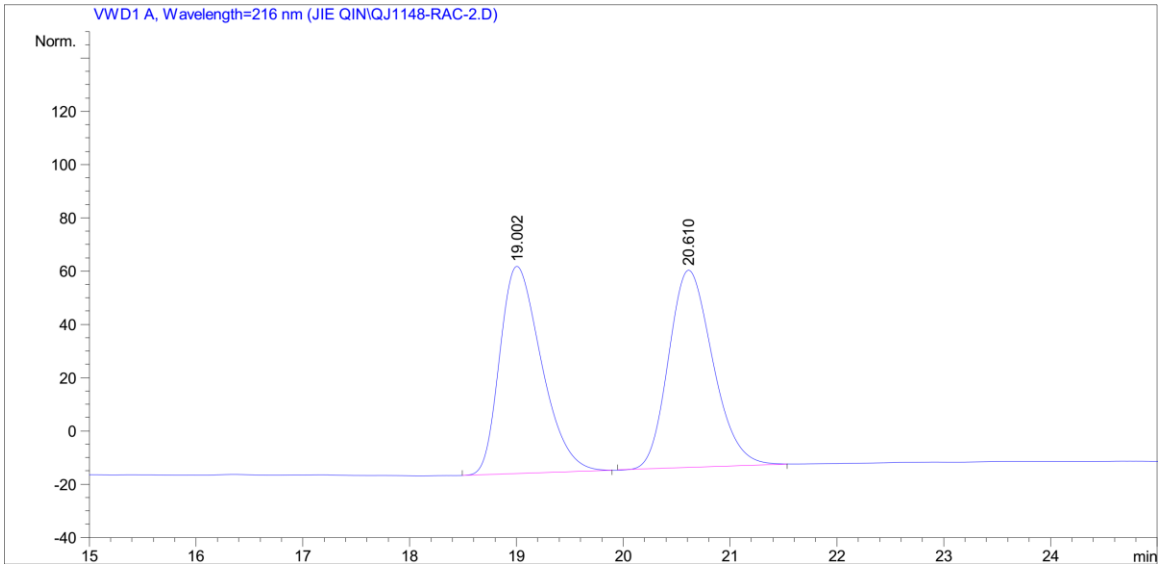

Peak #	RetTime [min]	Sig	Type	Area mAU *s	Height [mAU]	Area %
1	19.002	1	BB	2113.56787	77.83148	49.6552
2	20.610	1	BB	2142.91943	74.19716	50.3448

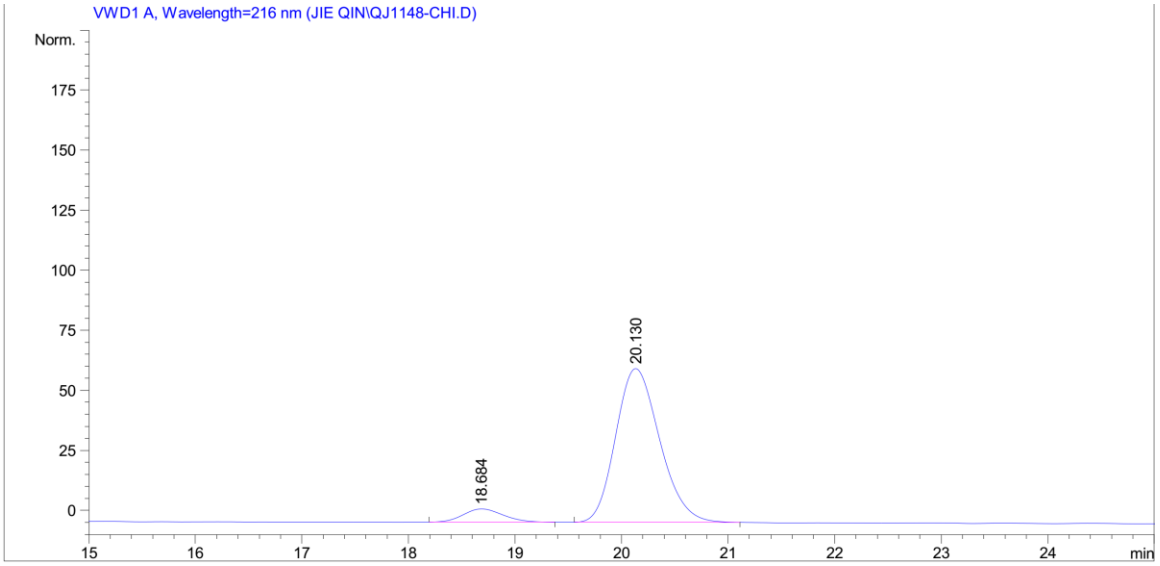

Peak #	RetTime [min]	Sig	Type	Area mAU *s	Height [mAU]	Area %
1	18.684	1	BB	147.23328	5.56465	7.4051
2	20.130	1	BB	1841.04663	64.02782	92.5949

Figure 61. HPLC traces of *rac*-**5r** and (*S*)-**5r** (86% ee).

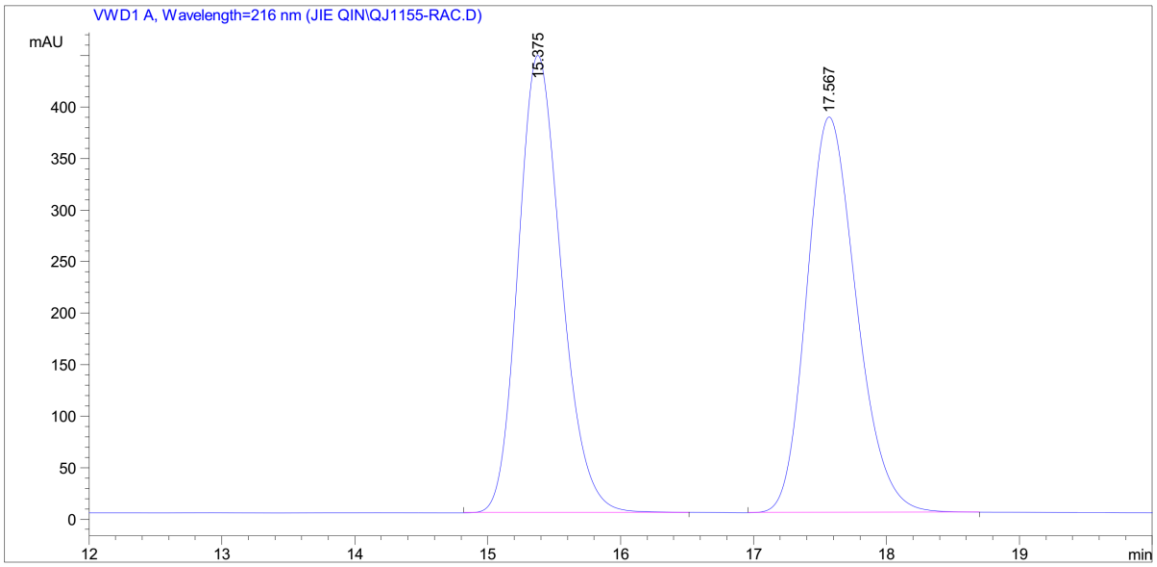

Peak #	RetTime [min]	Type	Width [min]	Area mAU *s	Height [mAU]	Area %
1	15.375	BB	0.3472	9997.63281	443.83414	49.9786
2	17.567	BB	0.4031	1.00062e4	383.83374	50.0214

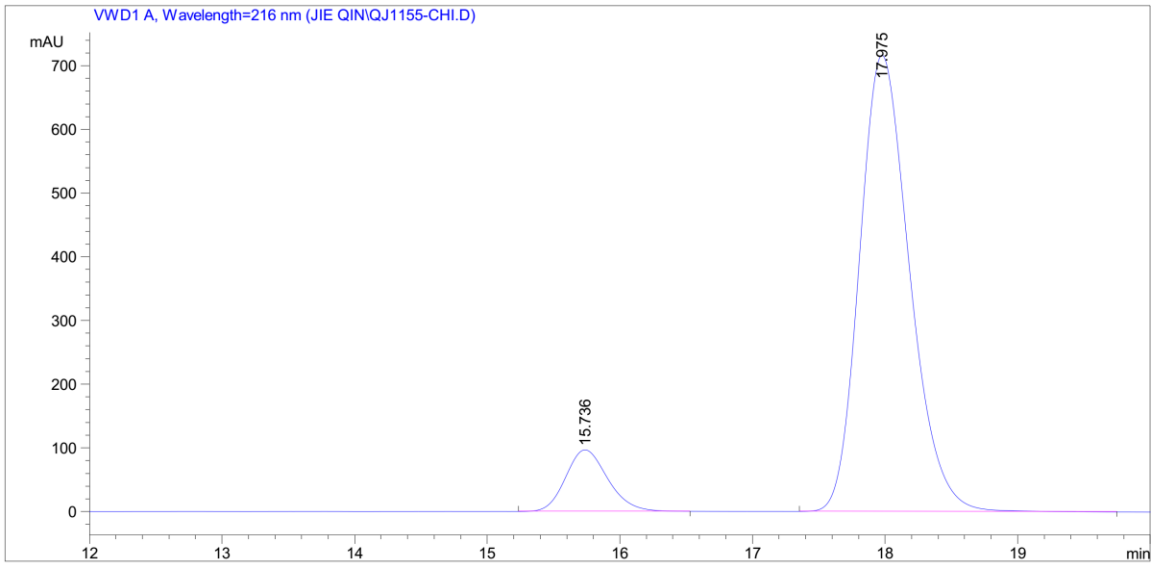

Peak #	RetTime [min]	Type	Width [min]	Area mAU *s	Height [mAU]	Area %
1	15.736	BB	0.3410	2139.73267	96.75069	10.2261
2	17.975	BB	0.4049	1.87844e4	716.45001	89.7739

Figure 62. HPLC traces of *rac*-**5s** and (*S*)-**5s** (80% ee).

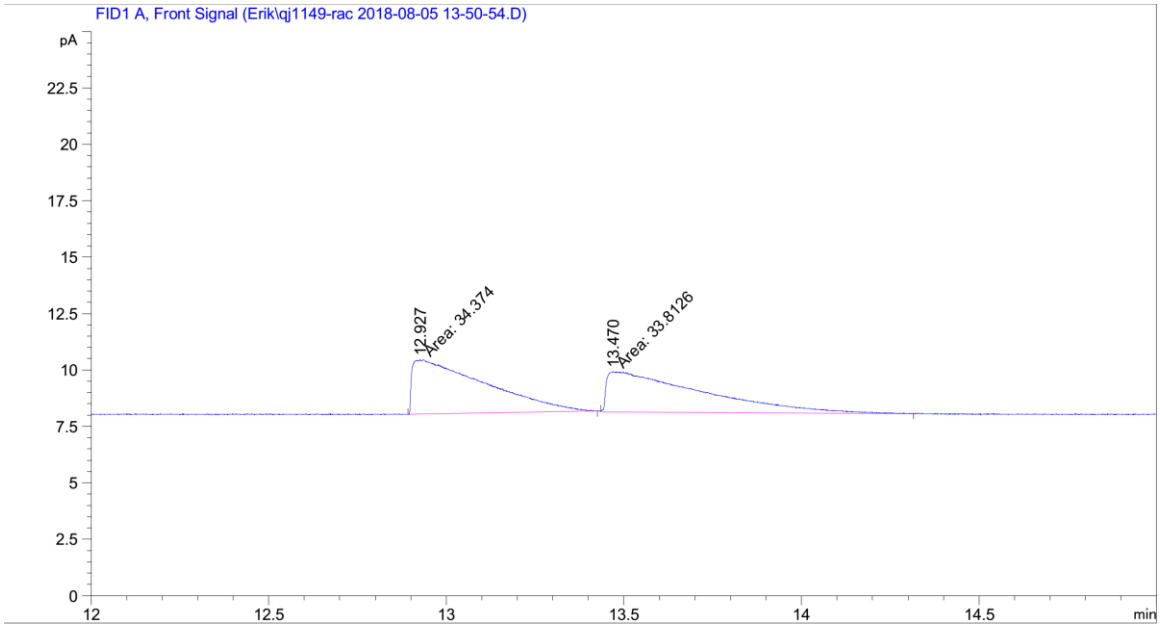

Peak #	RetTime [min]	Type	Width [min]	Area [pA*s]	Height [pA]	Area %
1	12.927	MM	0.2376	34.37403	2.41155	50.41172
2	13.470	MM	0.3134	33.81255	1.79829	49.58828

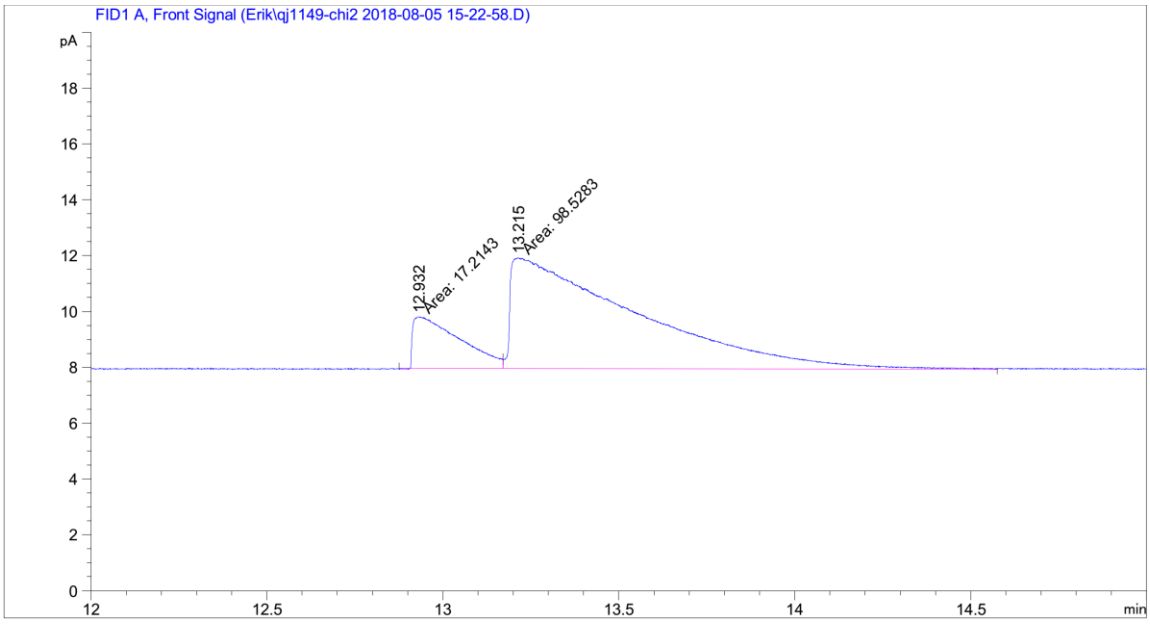

Peak #	RetTime [min]	Type	Width [min]	Area [pA*s]	Height [pA]	Area %
1	12.932	MF	0.1553	17.21426	1.84702	14.87289
2	13.215	FM	0.4136	98.52827	3.96998	85.12711

Figure 63. GC traces of *rac*-**5t** and (*R*)-**5t** (70% ee).

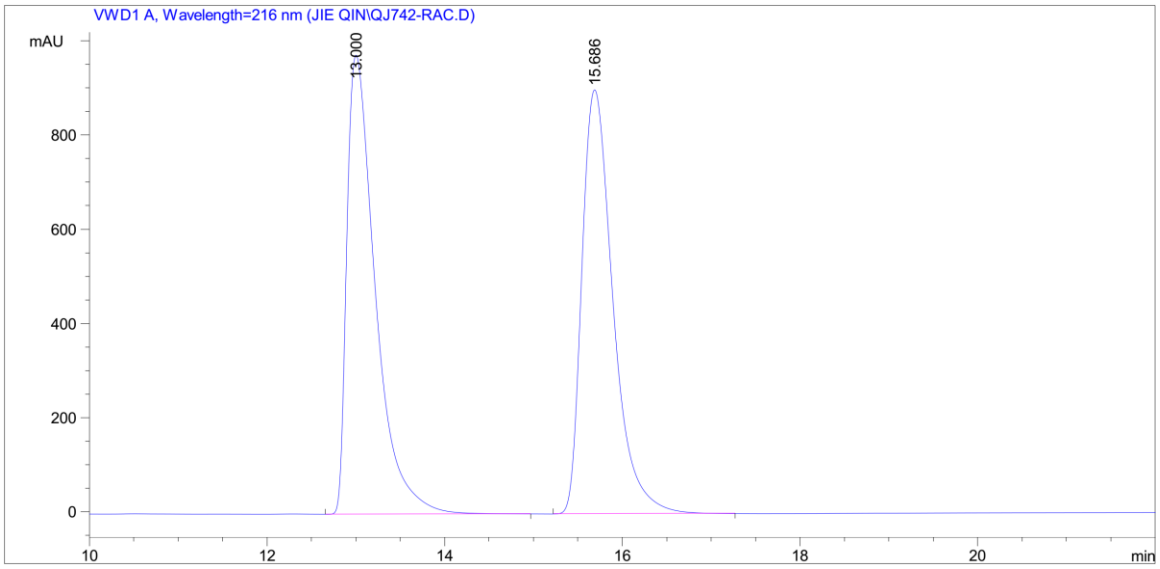

Peak #	RetTime [min]	Type	Width [min]	Area mAU *s	Height [mAU]	Area %
1	13.000	VB	0.3383	2.16866e4	974.21307	49.7660
2	15.686	BB	0.3770	2.18906e4	899.98163	50.2340

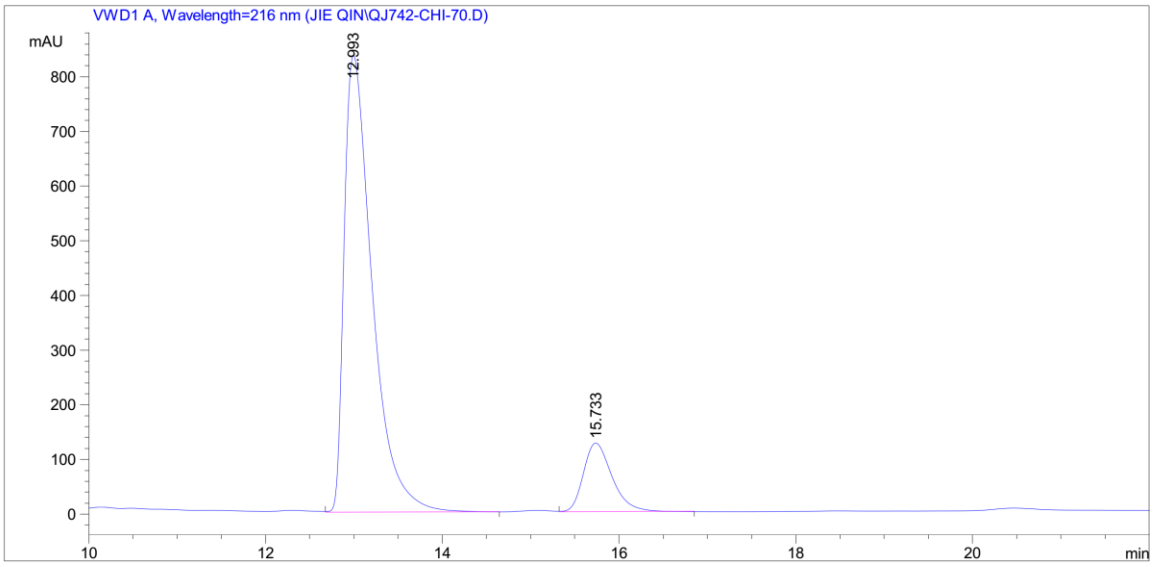

Peak #	RetTime [min]	Type	Width [min]	Area mAU *s	Height [mAU]	Area %
1	12.993	VB	0.3352	1.83901e4	836.34723	86.5957
2	15.733	VB	0.3469	2846.62378	125.86226	13.4043

Figure 64. HPLC traces of *rac*-**5v** and (*R*)-**5v** (74% ee).

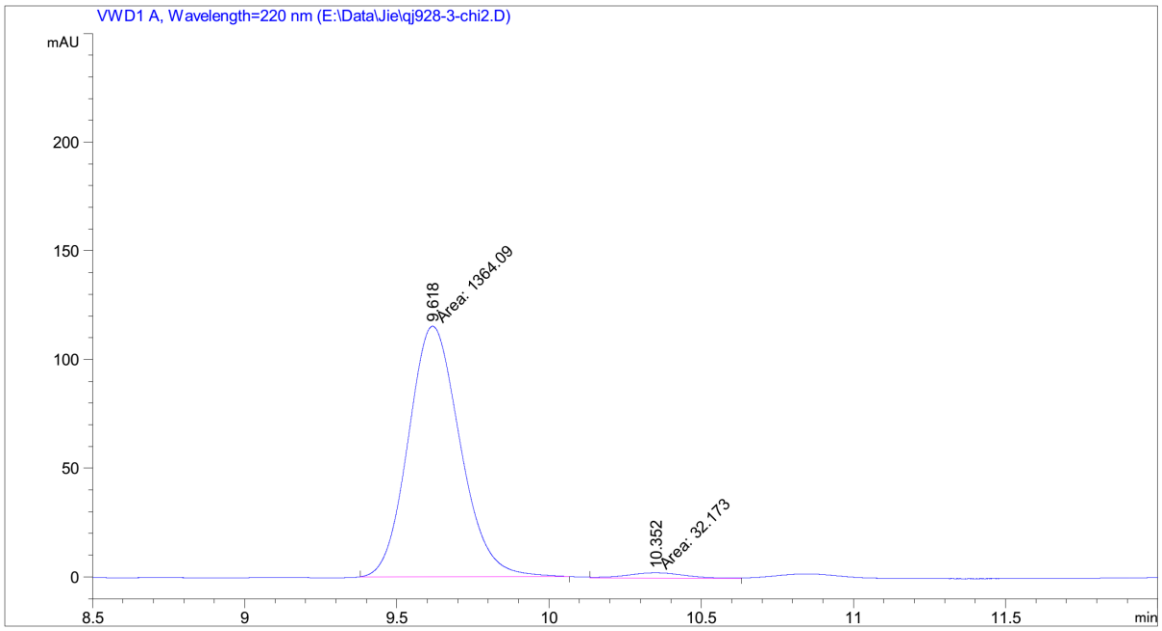

Peak #	RetTime [min]	Type	Width [min]	Area [mAU*s]	Height [mAU]	Area %
1	9.618	MM	0.1972	1364.09302	115.28564	97.6958
2	10.352	FM	0.2169	32.17296	2.47202	2.3042

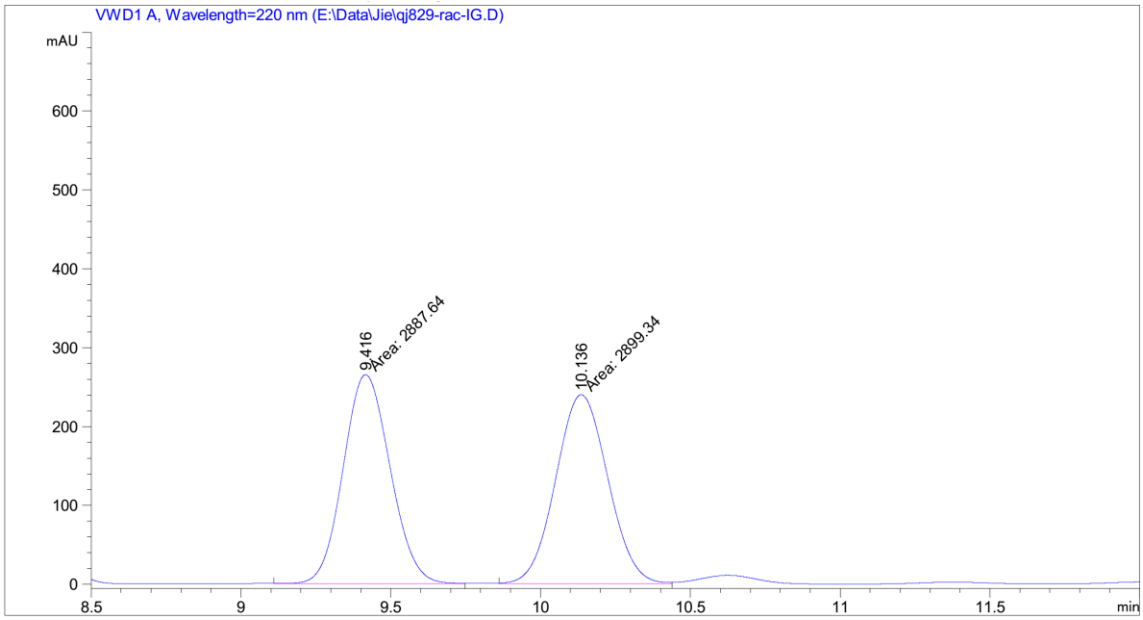

Peak #	RetTime [min]	Type	Width [min]	Area [mAU*s]	Height [mAU]	Area %
1	9.416	MM	0.1817	2887.63867	264.92700	49.8989
2	10.136	MM	0.2017	2899.34351	239.57364	50.1011

Figure 65. HPLC traces of (*R*)-**10a** (95% ee) and *rac*-**10a**.

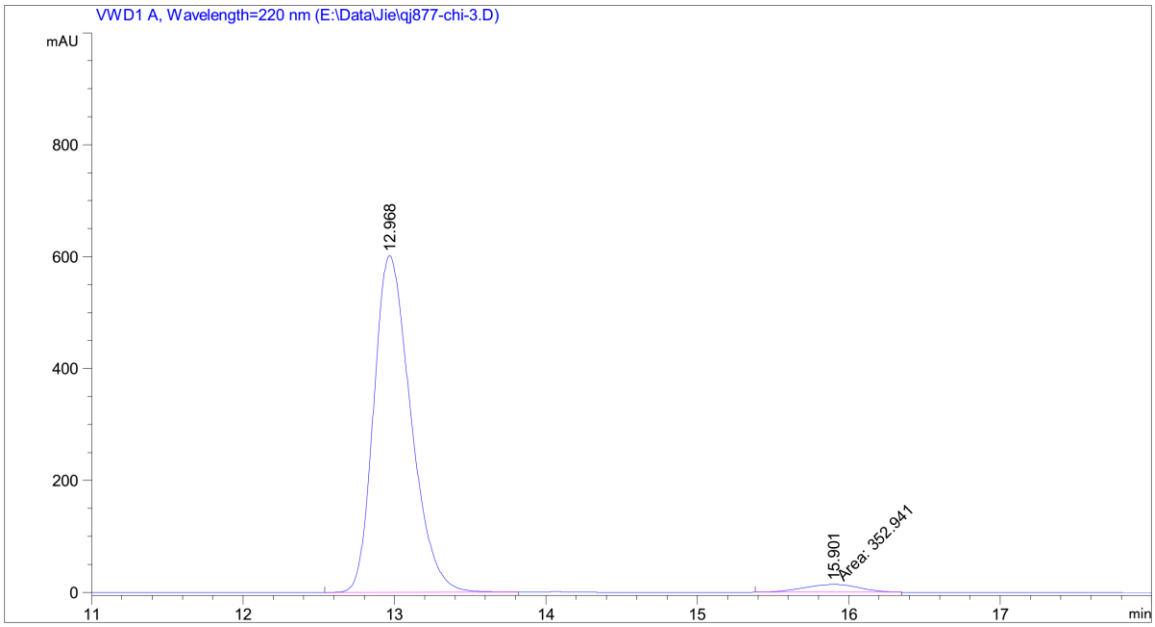

Peak #	RetTime [min]	Type	Width [min]	Area [mAU*s]	Height [mAU]	Area %
1	12.968	BB	0.2609	1.02045e4	601.63641	96.6569
2	15.901	MM	0.4217	352.94107	13.94751	3.3431

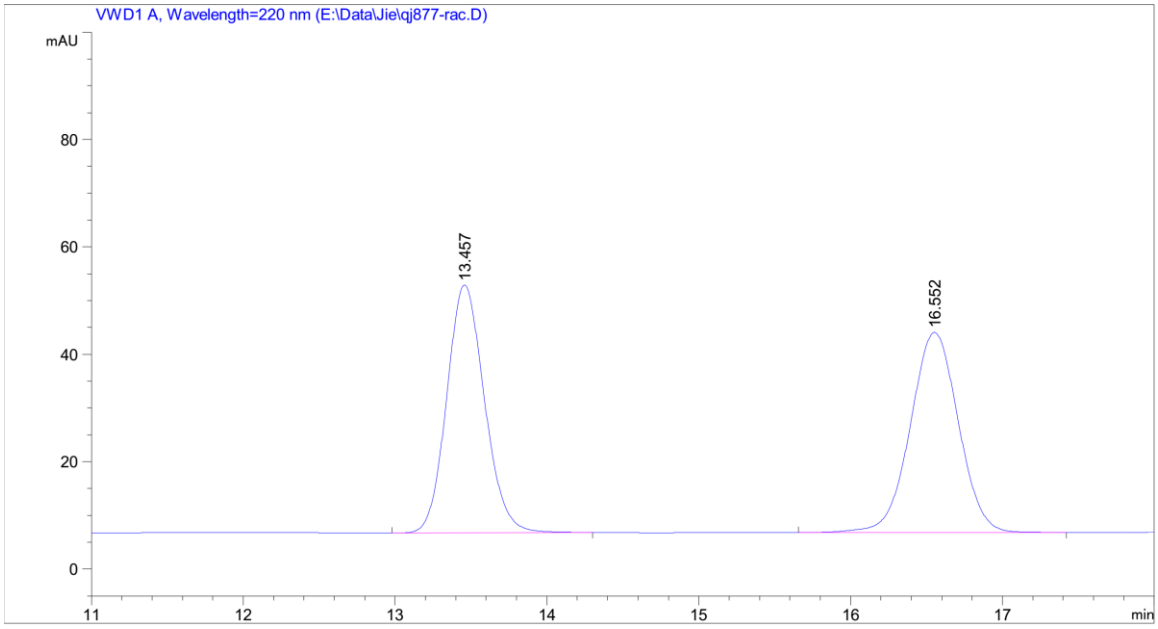

Peak #	RetTime [min]	Type	Width [min]	Area [mAU*s]	Height [mAU]	Area %
1	13.457	BB	0.2676	796.96674	46.11806	49.3249
2	16.552	BB	0.3413	818.78143	37.26893	50.6751

Figure 66. HPLC traces of (*R*)-**10b** (93% ee) and *rac*-**10b**.

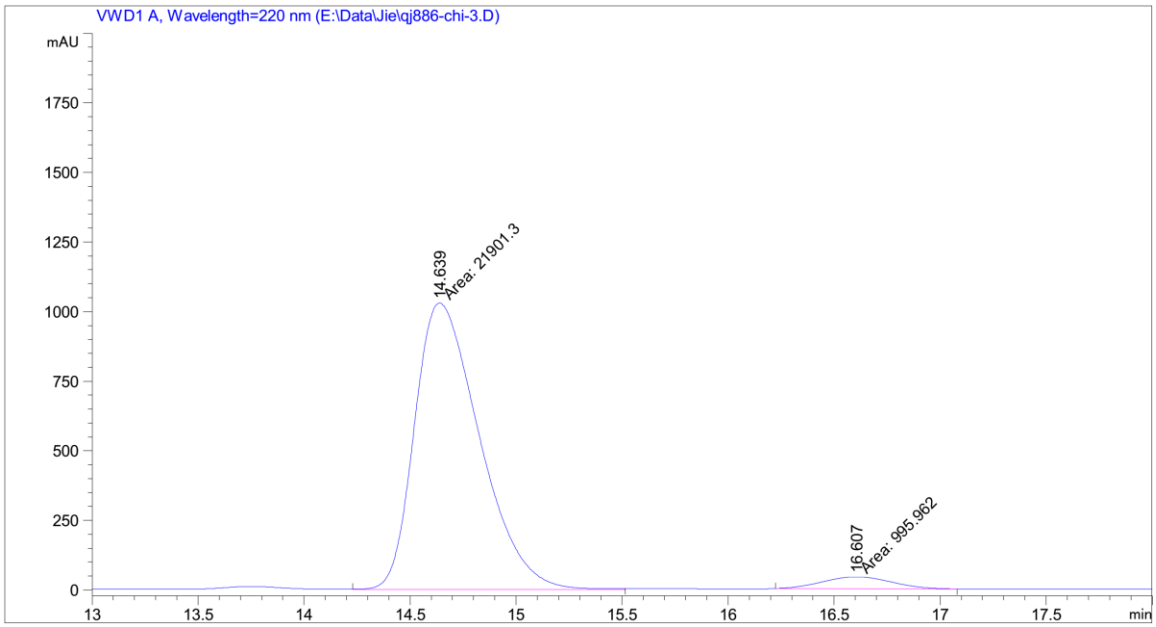

Peak #	RetTime [min]	Type	Width [min]	Area [mAU*s]	Height [mAU]	Area %
1	14.639	MM	0.3546	2.19013e4	1029.29187	95.6503
2	16.607	MM	0.3819	995.96216	43.47071	4.3497

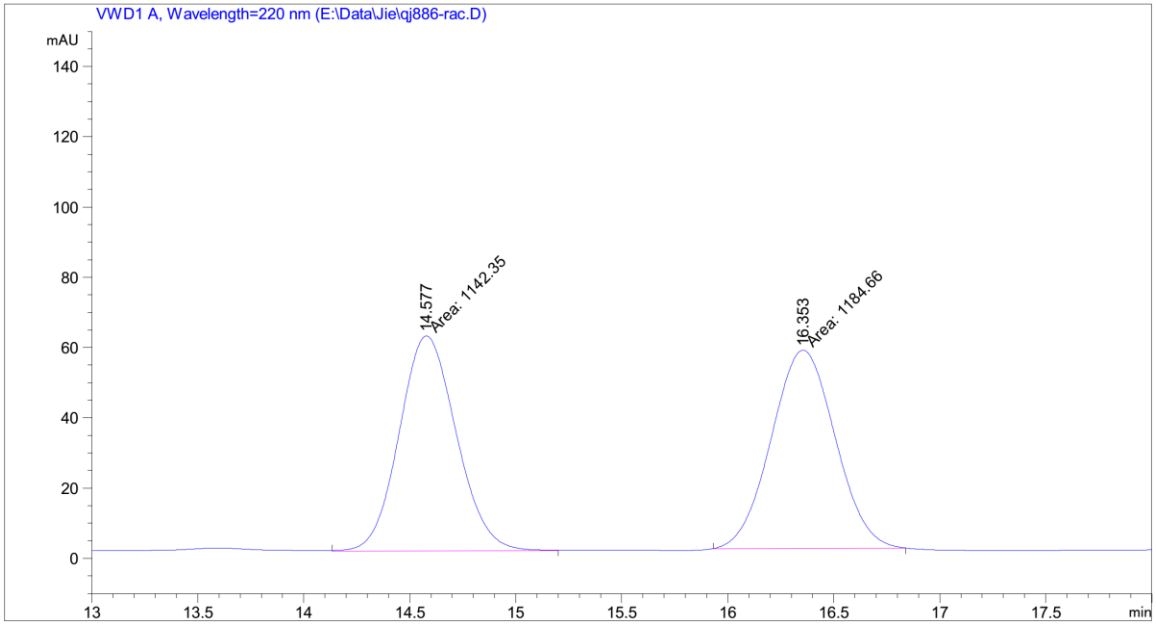

Peak #	RetTime [min]	Type	Width [min]	Area [mAU*s]	Height [mAU]	Area %
1	14.577	MM	0.3115	1142.35010	61.11277	49.0908
2	16.353	MM	0.3498	1184.66309	56.44348	50.9092

Figure 67. HPLC traces of (*R*)-**10c** (91% ee) and *rac*-**10c**.

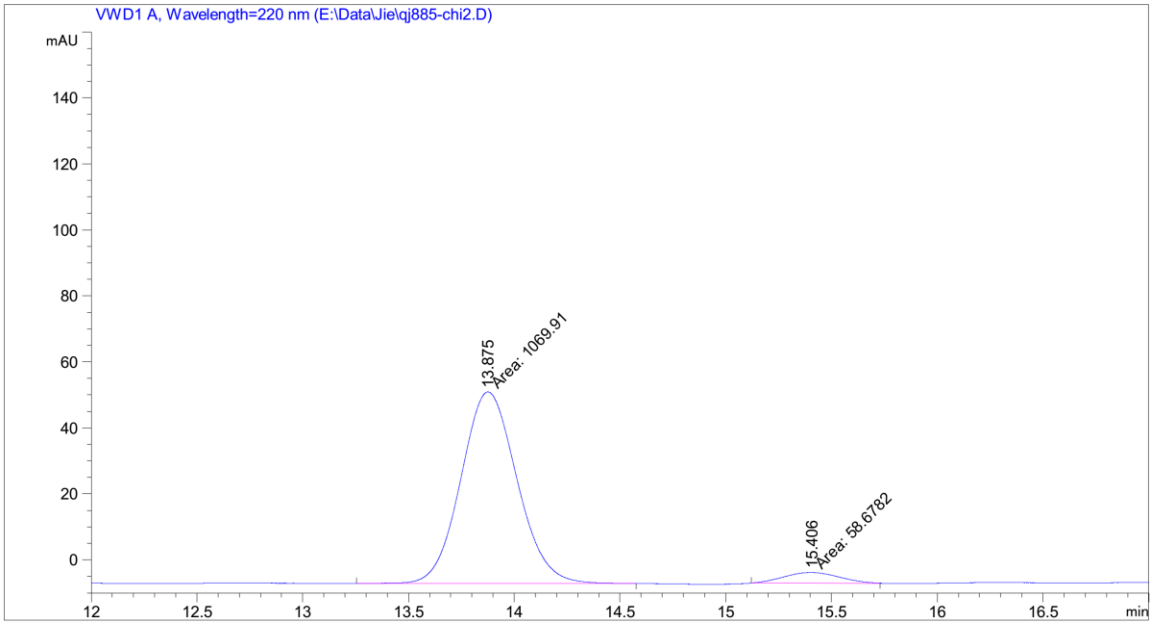

Peak #	RetTime [min]	Type	Width [min]	Area [mAU*s]	Height [mAU]	Area %
1	13.875	MM	0.3072	1069.90588	58.04494	94.8007
2	15.406	MM	0.2997	58.67817	3.26290	5.1993

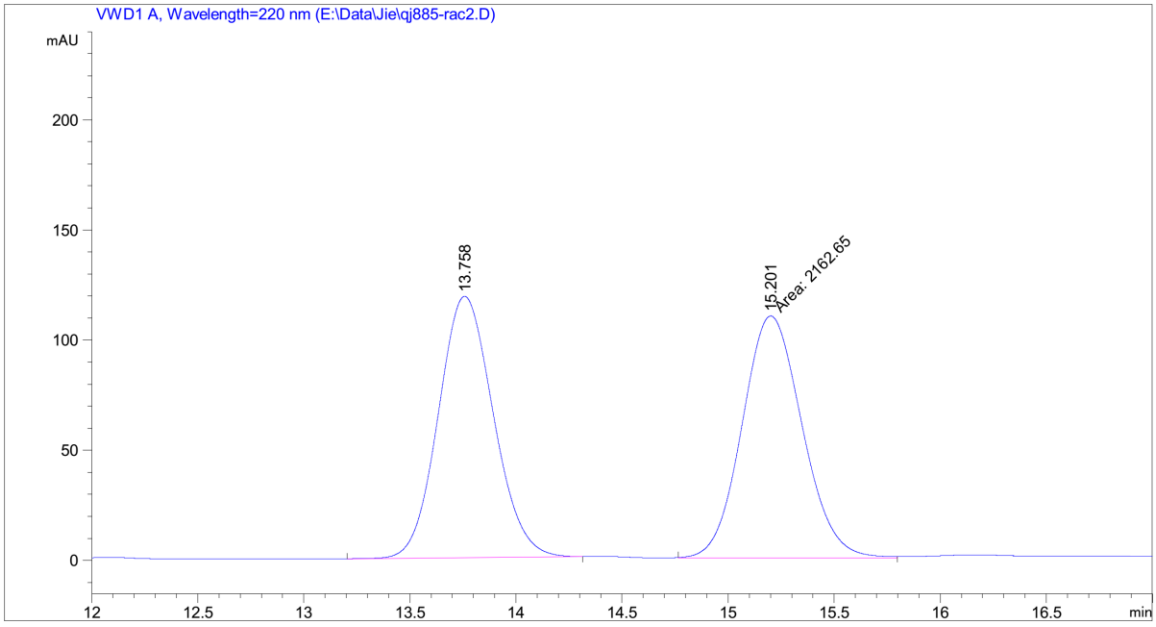

Peak #	RetTime [min]	Type	Width [min]	Area [mAU*s]	Height [mAU]	Area %
1	13.758	BB	0.2782	2136.78296	118.58102	49.6992
2	15.201	MM	0.3281	2162.65063	109.86678	50.3008

Figure 68. HPLC traces of (*R*)-**10d** (90% ee) and *rac*-**10d**.

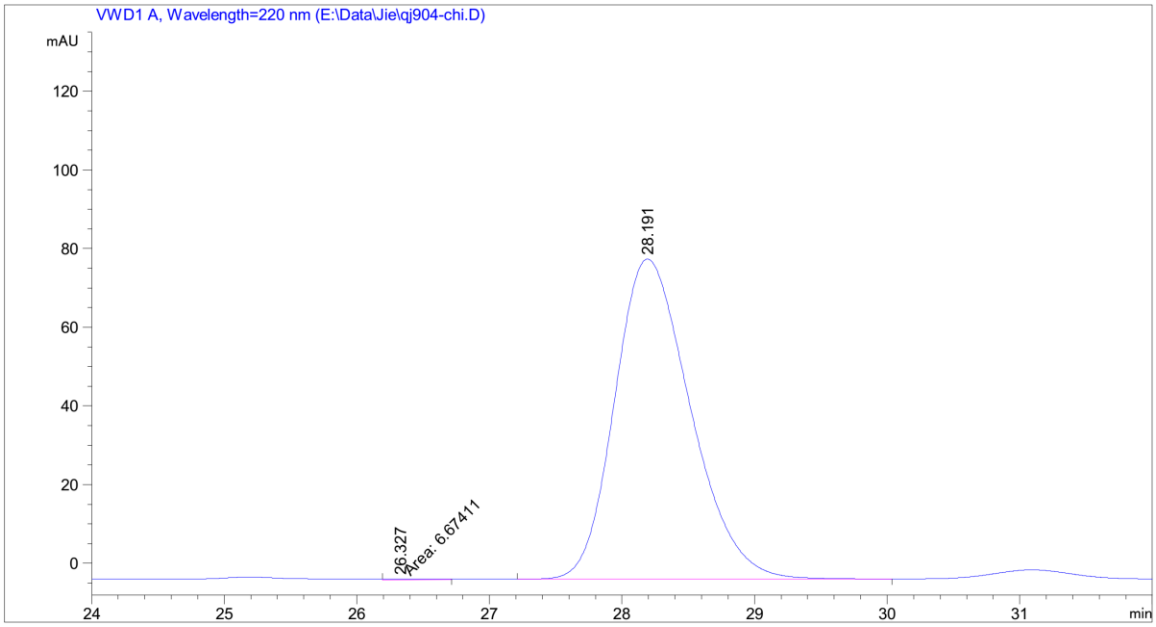

Peak #	RetTime [min]	Type	Width [min]	Area [mAU*s]	Height [mAU]	Area %
1	26.327	MM	0.3133	6.67411	2.56401e-1	0.2064
2	28.191	BB	0.6138	3226.77783	81.34184	99.7936

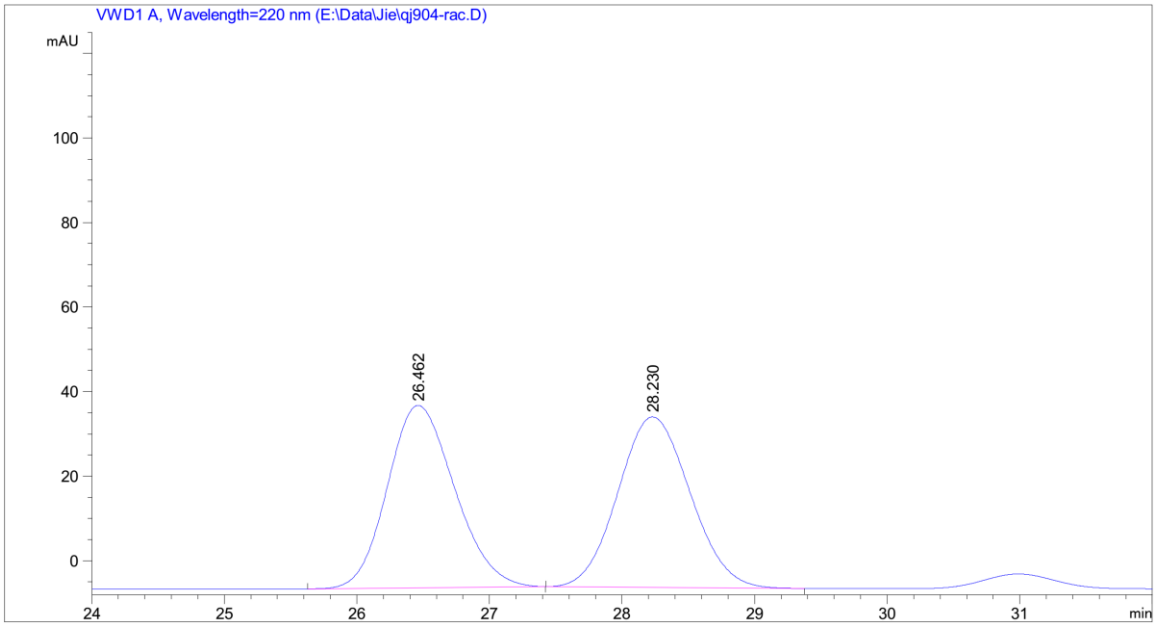

Peak #	RetTime [min]	Type	Width [min]	Area [mAU*s]	Height [mAU]	Area %
1	26.462	BB	0.5455	1518.40918	43.15740	49.8762
2	28.230	BB	0.5905	1525.94580	40.32146	50.1238

Figure 69. HPLC traces of (*R*)-**10e** (99% ee) and *rac*-**10e**.

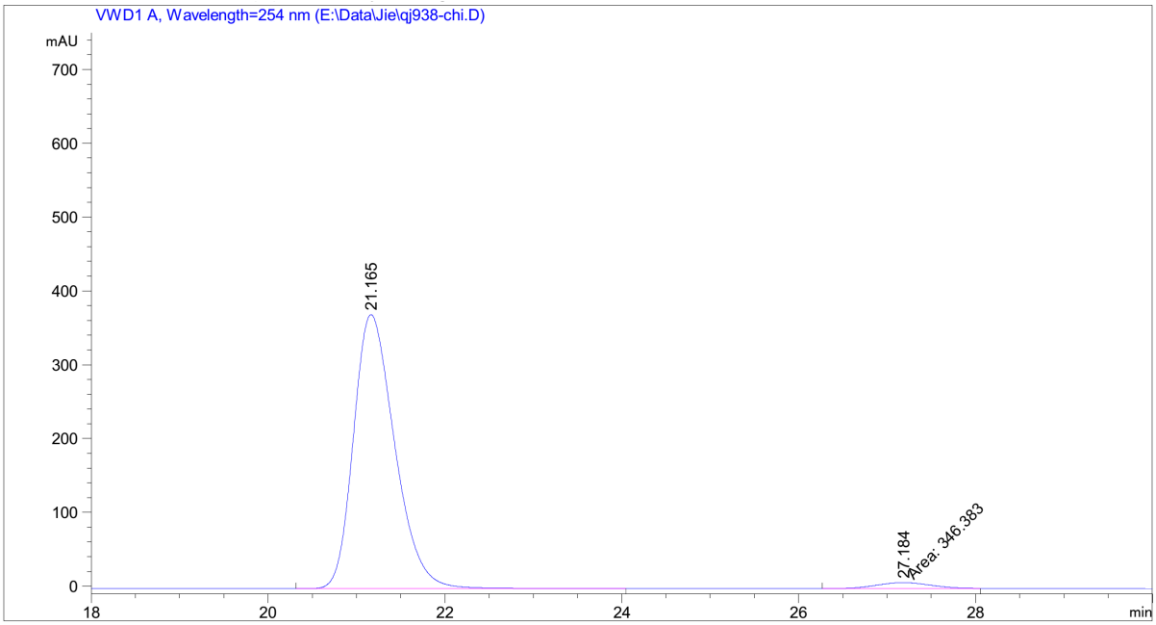

Peak #	RetTime [min]	Type	Width [min]	Area [mAU*s]	Height [mAU]	Area %
1	21.165	BB	0.4997	1.20178e4	371.21060	97.1985
2	27.184	MM	0.7162	346.38278	8.06077	2.8015

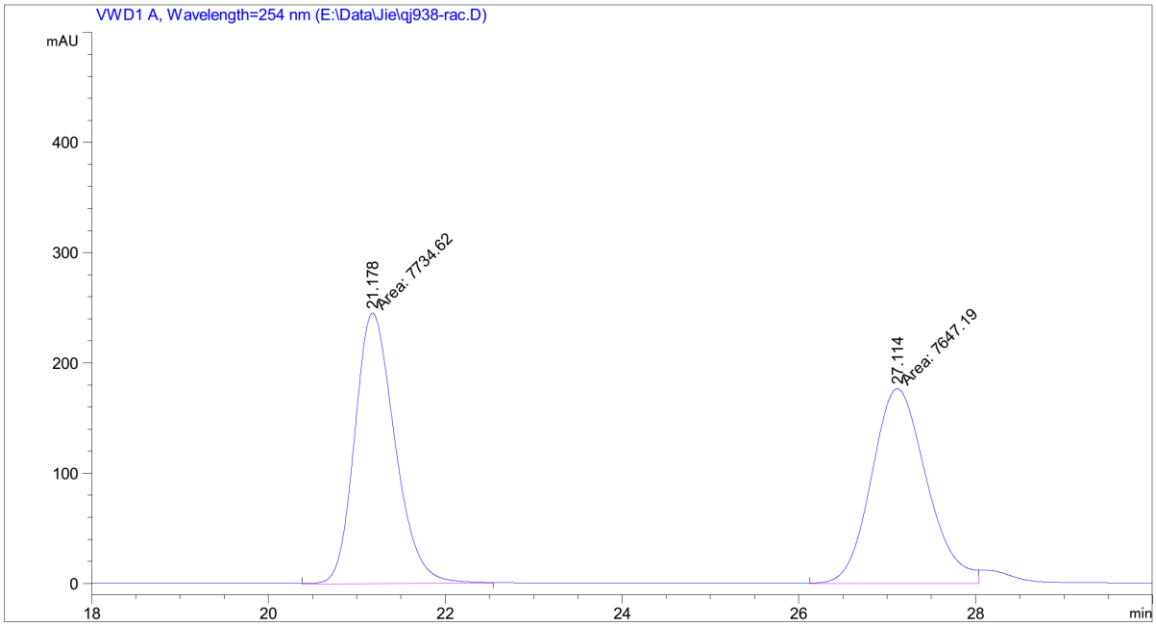

Peak #	RetTime [min]	Type	Width [min]	Area [mAU*s]	Height [mAU]	Area %
1	21.178	MM	0.5254	7734.62256	245.34273	50.2842
2	27.114	MM	0.7214	7647.19482	176.68472	49.7158

Figure 70. HPLC traces of (*R*)-**10f** (94% ee) and *rac*-**10f**.

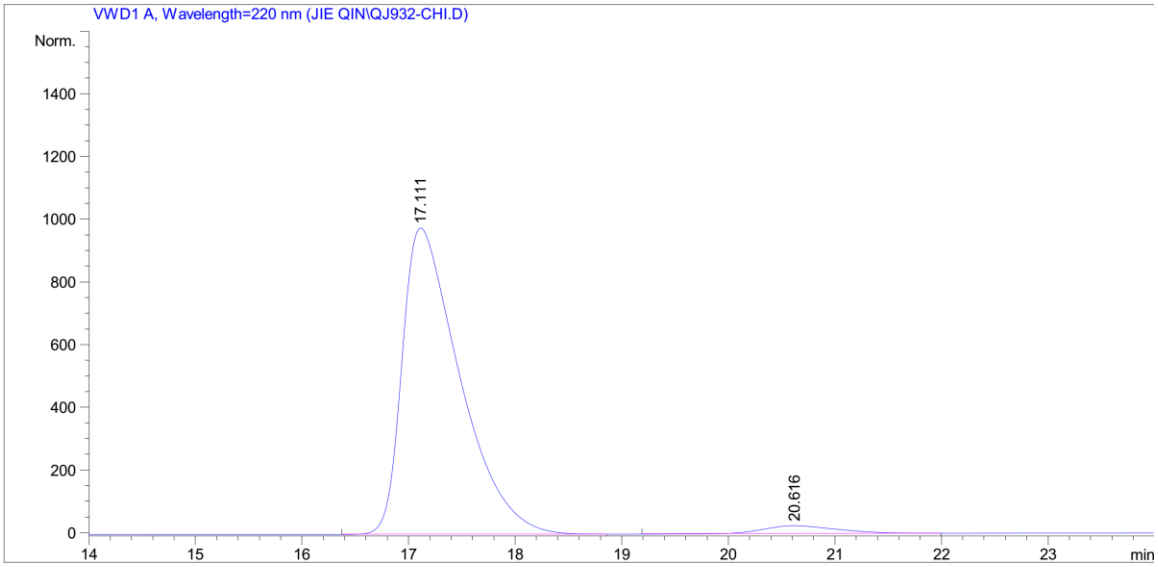

Peak #	RetTime [min]	Type	Width [min]	Area mAU *s	Height [mAU]	Area %
1	17.111	BB	0.5648	3.67111e4	977.45776	96.7770
2	20.616	BB	0.7294	1222.60083	25.38135	3.2230

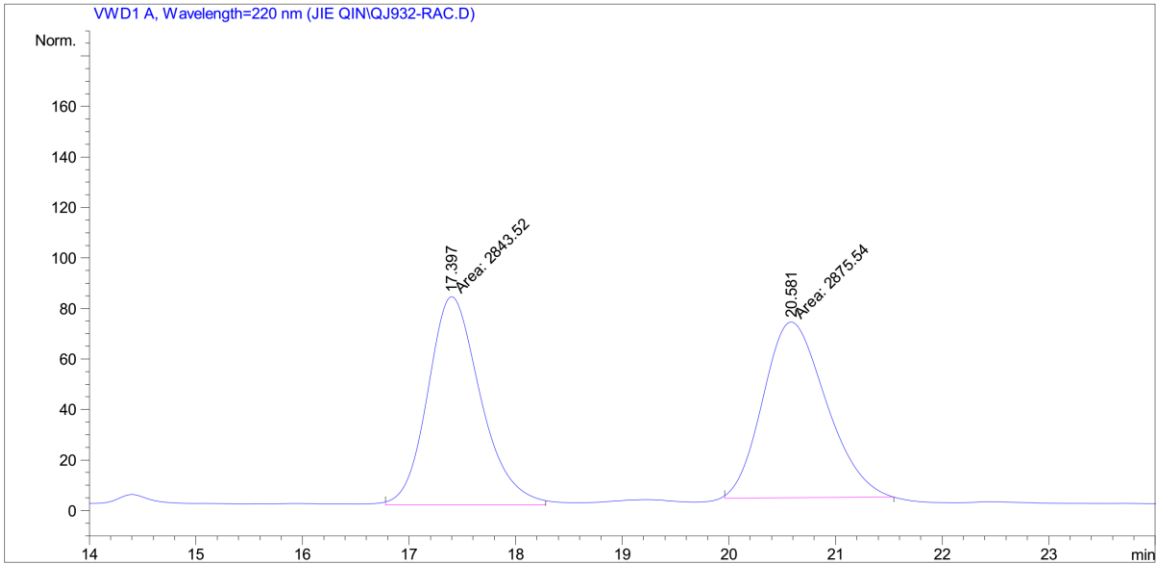

Peak #	RetTime [min]	Type	Width [min]	Area mAU *s	Height [mAU]	Area %
1	17.397	MM	0.5738	2843.51611	82.59043	49.7200
2	20.581	MM	0.6873	2875.54321	69.72562	50.2800

Figure 71. HPLC traces of (*R*)-**10g** (94% ee) and *rac*-**10g**.

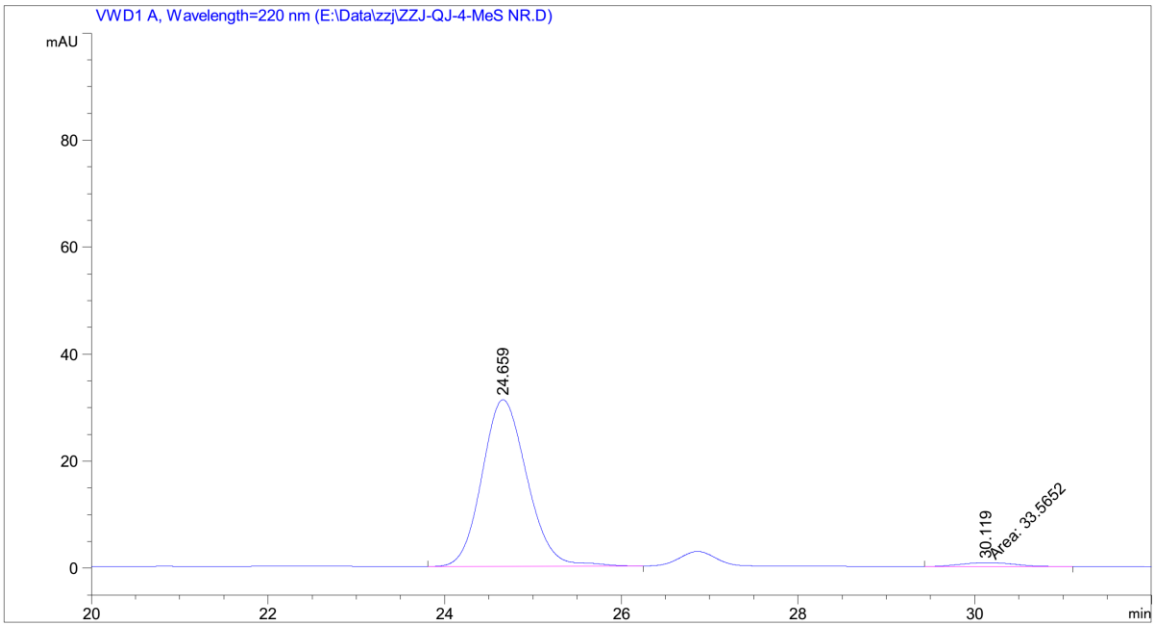

Peak #	RetTime [min]	Type	Width [min]	Area [mAU*s]	Height [mAU]	Area %
1	24.659	BB	0.5484	1100.83630	31.13904	97.0412
2	30.119	MM	0.7357	33.56524	7.60398e-1	2.9588

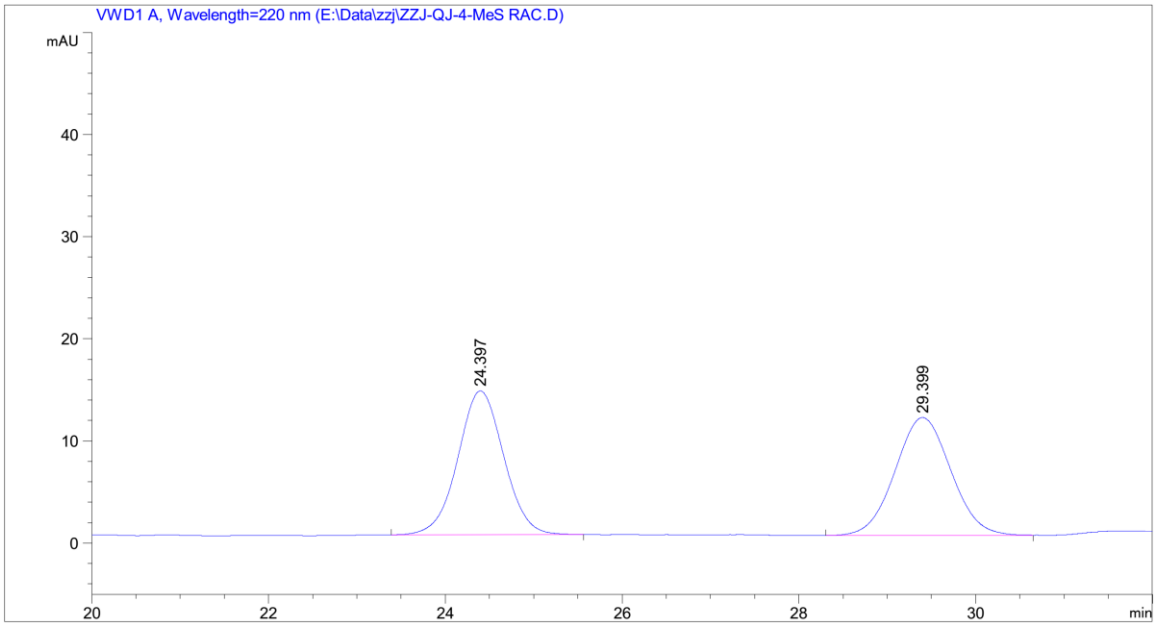

Peak #	RetTime [min]	Type	Width [min]	Area [mAU*s]	Height [mAU]	Area %
1	24.397	BB	0.5555	507.35306	14.07712	50.0605
2	29.399	BB	0.6648	506.12677	11.53792	49.9395

Figure 72. HPLC traces of (*R*)-**10h** (94% ee) and *rac*-**10h**.

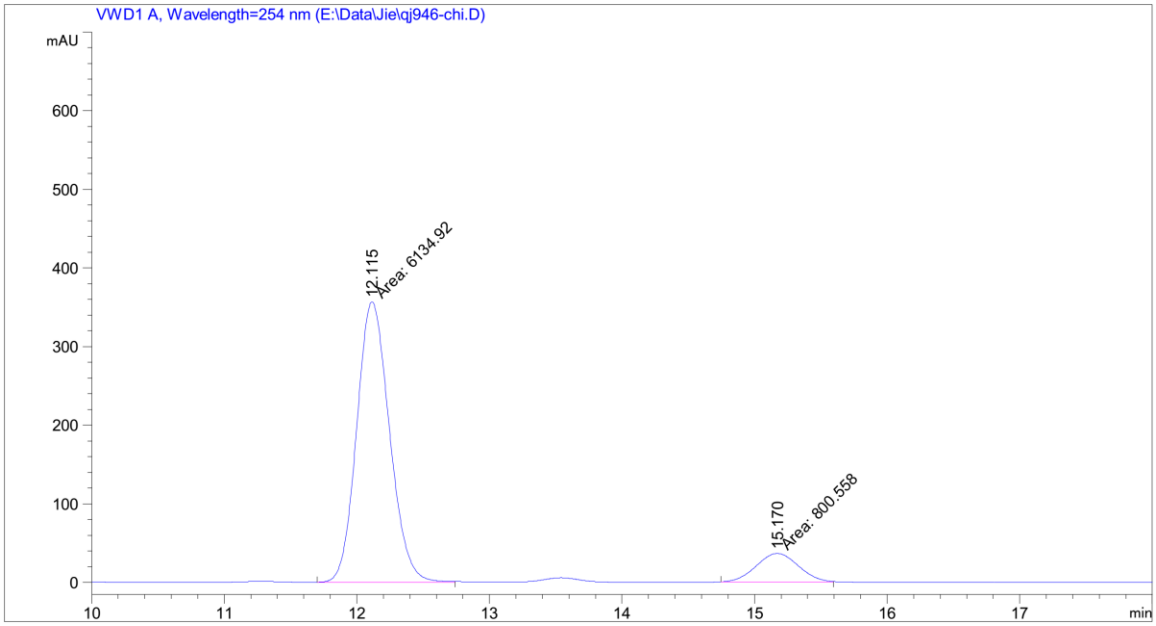

Peak #	RetTime [min]	Type	Width [min]	Area [mAU*s]	Height [mAU]	Area %
1	12.115	MM	0.2867	6134.92188	356.67624	88.4571
2	15.170	MM	0.3683	800.55774	36.23181	11.5429

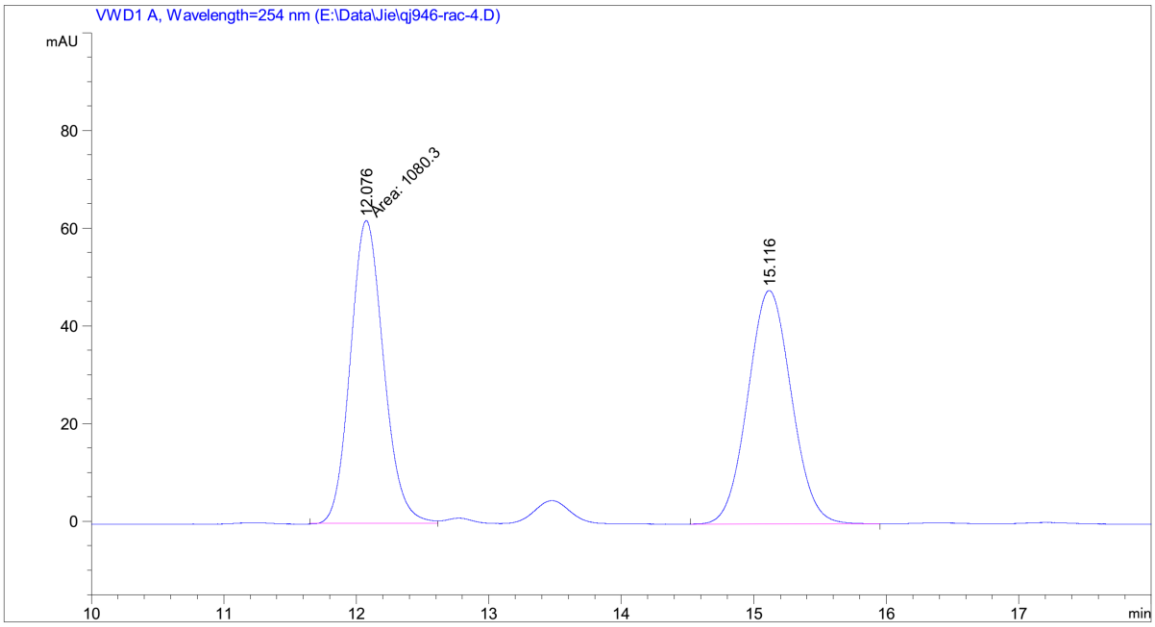

Peak #	RetTime [min]	Type	Width [min]	Area [mAU*s]	Height [mAU]	Area %
1	12.076	MM	0.2906	1080.30493	61.96456	49.6443
2	15.116	BV R	0.2985	1095.78503	47.79735	50.3557

Figure 73. HPLC traces of (*R*)-**10i** (77% ee) and *rac*-**10i**.

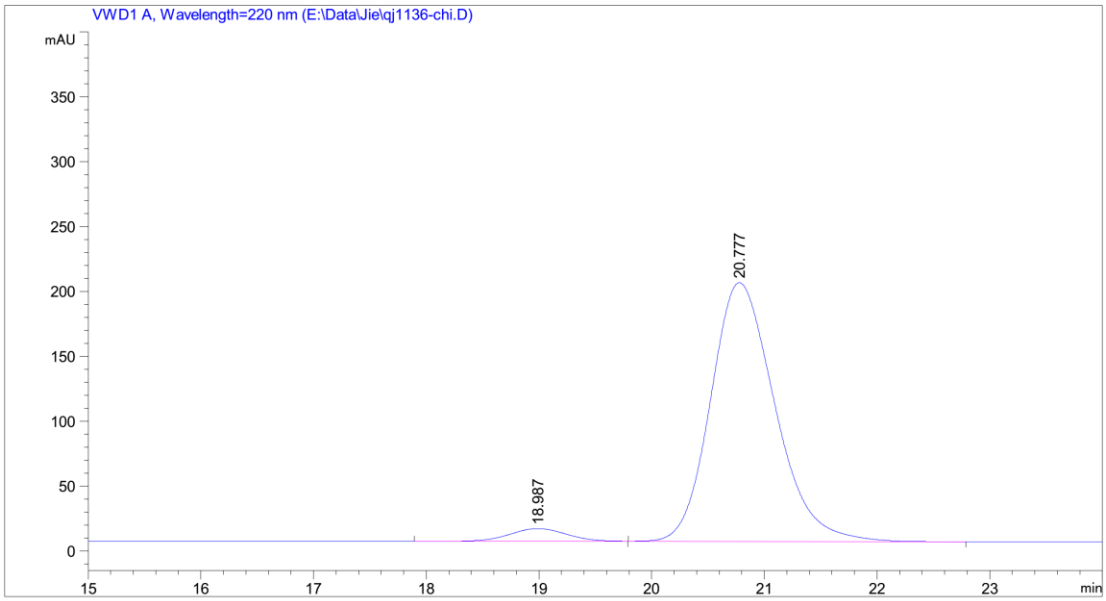

Peak #	RetTime [min]	Type	Width [min]	Area [mAU*s]	Height [mAU]	Area %
1	18.987	BB	0.5443	343.52750	9.76914	4.1771
2	20.777	BB	0.6124	7880.53027	199.24559	95.8229

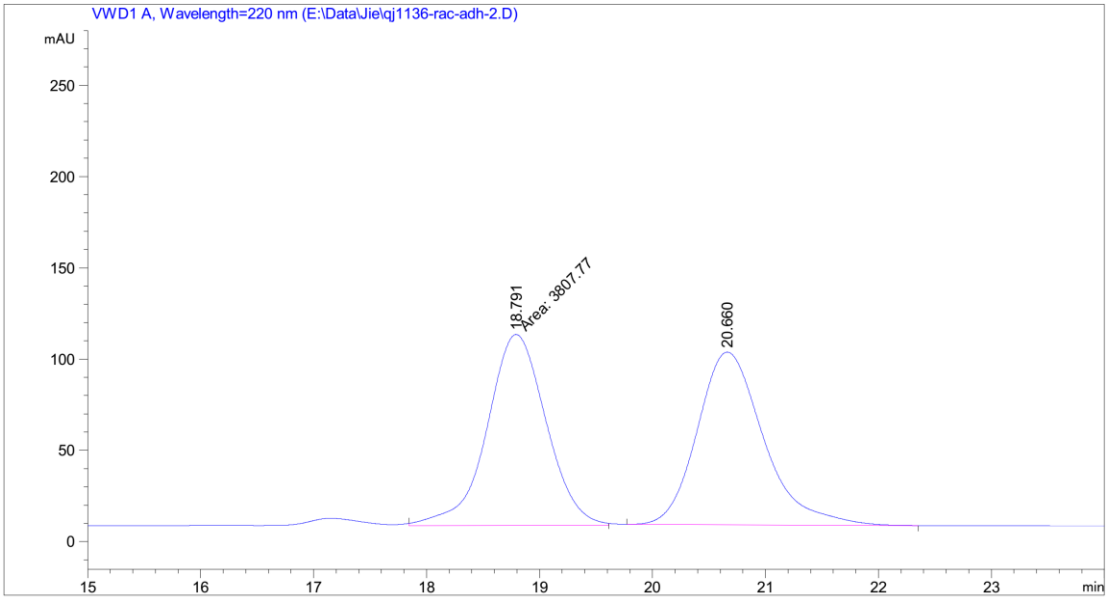

Peak #	RetTime [min]	Type	Width [min]	Area [mAU*s]	Height [mAU]	Area %
1	18.791	MM	0.6067	3807.77417	104.60165	49.6930
2	20.660	BB	0.6235	3854.82568	94.57472	50.3070

Figure 74. HPLC traces of (*R*)-**10j** (92% ee) and *rac*-**10j**.

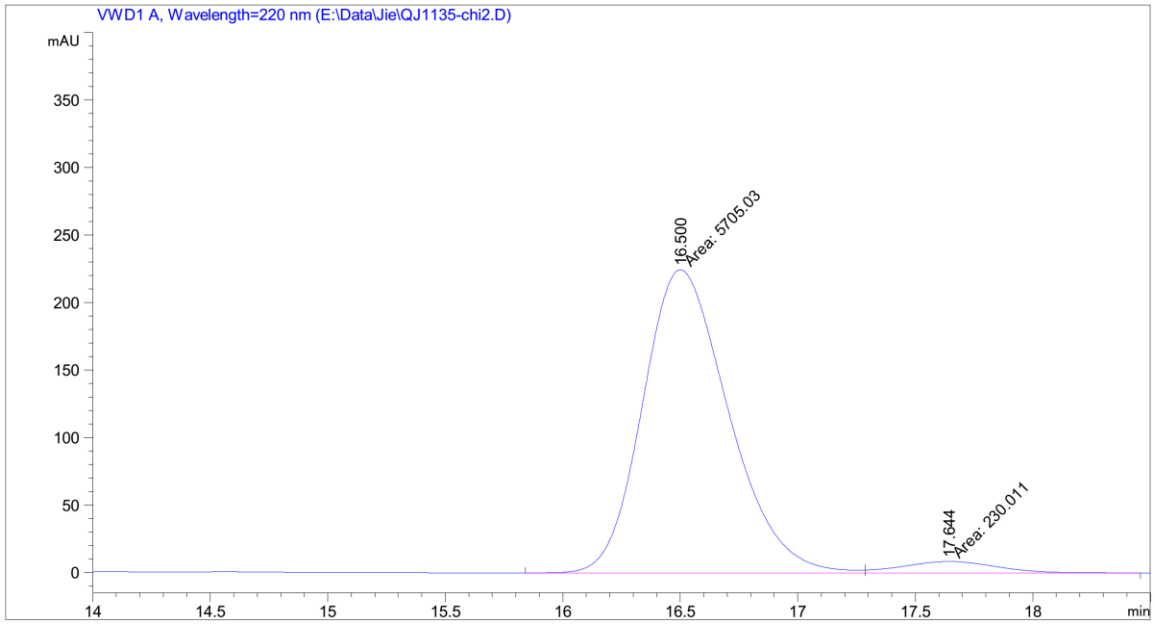

Peak #	RetTime [min]	Type	Width [min]	Area [mAU*s]	Height [mAU]	Area %
1	16.500	MF	0.4235	5705.02832	224.51117	96.1245
2	17.644	FM	0.4562	230.01082	8.40332	3.8755

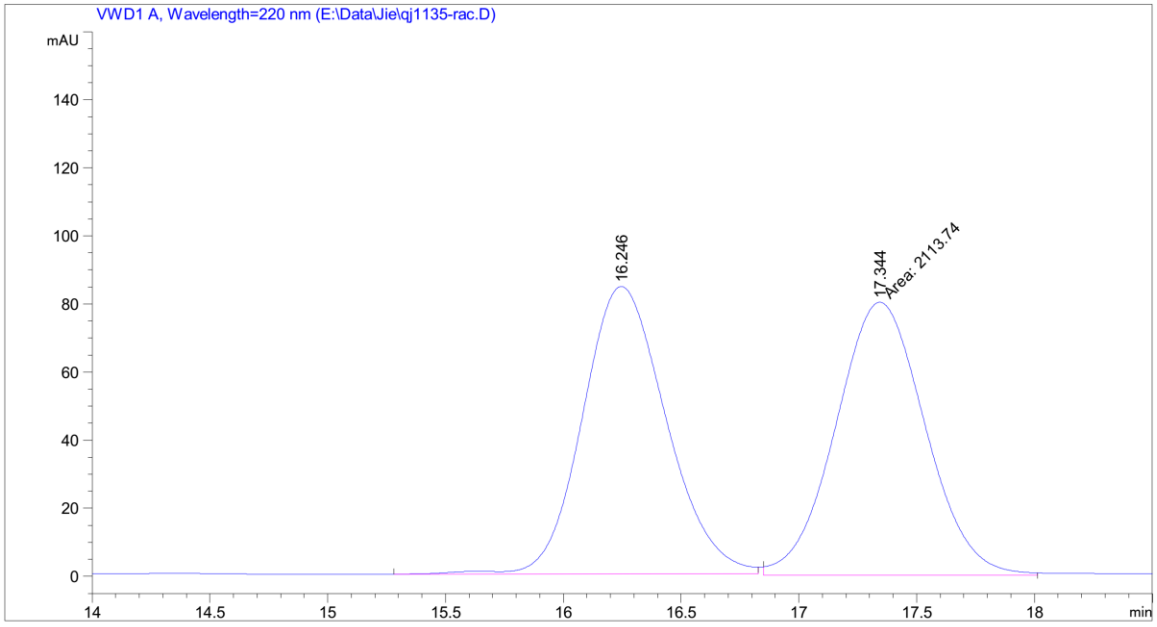

Peak #	RetTime [min]	Type	Width [min]	Area [mAU*s]	Height [mAU]	Area %
1	16.246	VV R	0.3818	2083.41479	84.45715	49.6388
2	17.344	MM	0.4392	2113.73535	80.20770	50.3612

Figure 75. HPLC traces of (*R*)-**10k** (92% ee) and *rac*-**10k**.

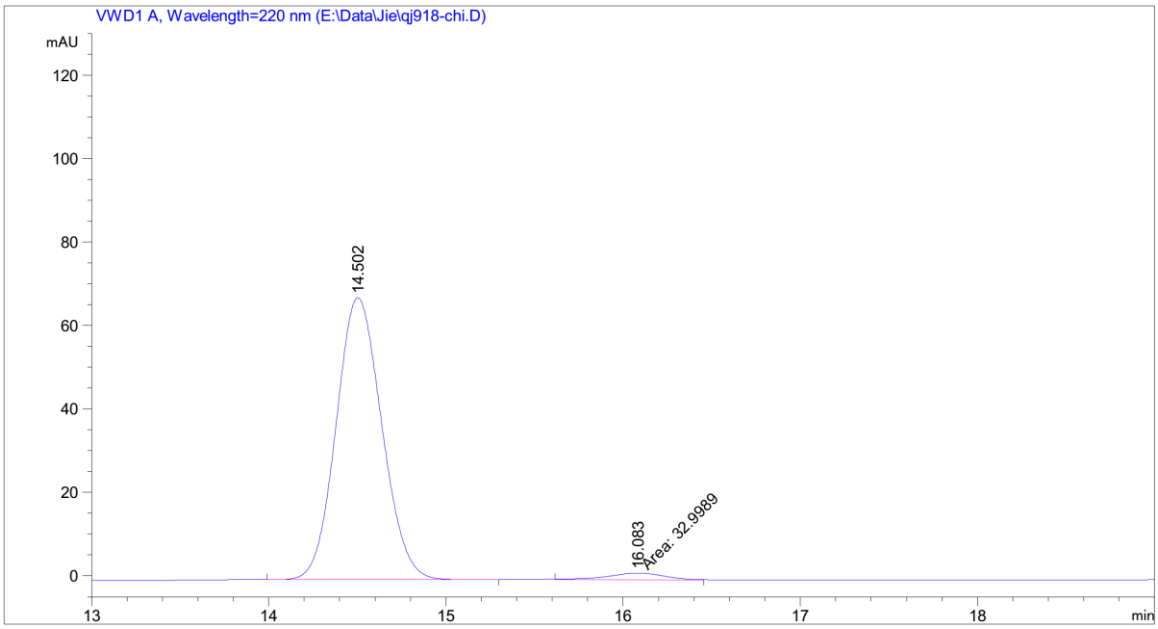

Peak #	RetTime [min]	Type	Width [min]	Area [mAU*s]	Height [mAU]	Area %
1	14.502	BB	0.2786	1208.03149	67.56878	97.3410
2	16.083	MM	0.3531	32.99894	1.55759	2.6590

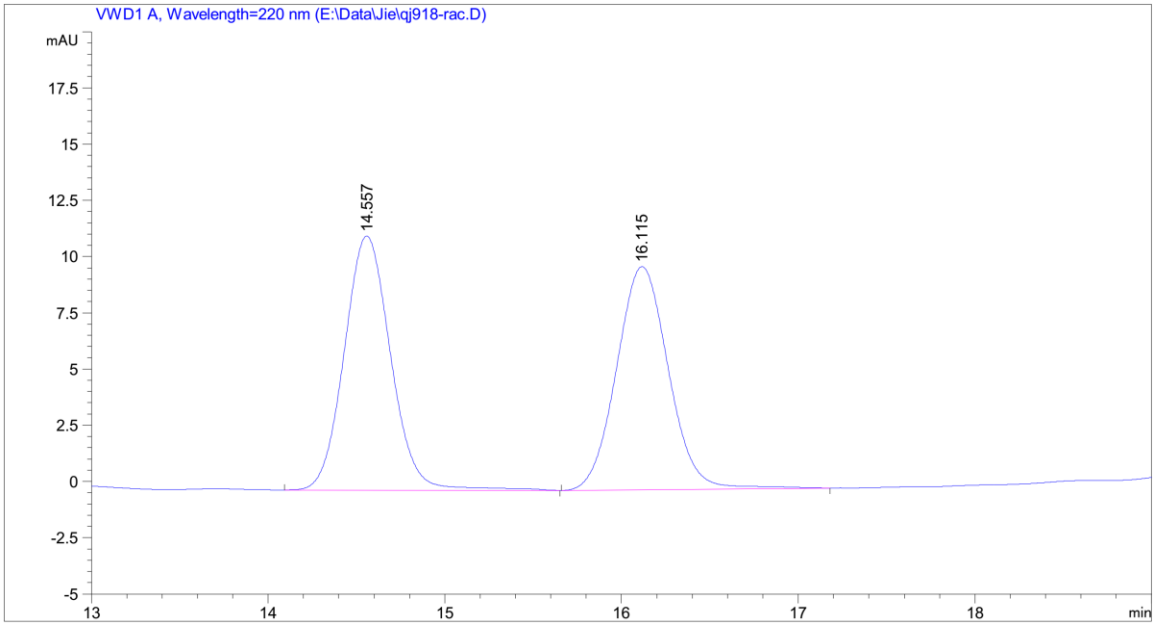

Peak #	RetTime [min]	Type	Width [min]	Area [mAU*s]	Height [mAU]	Area %
1	14.557	BB	0.2822	206.53418	11.30165	50.5179
2	16.115	BB	0.3170	202.29922	9.91856	49.4821

Figure 76. HPLC traces of (*R*)-**10l** (94% ee) and *rac*-**10l**.

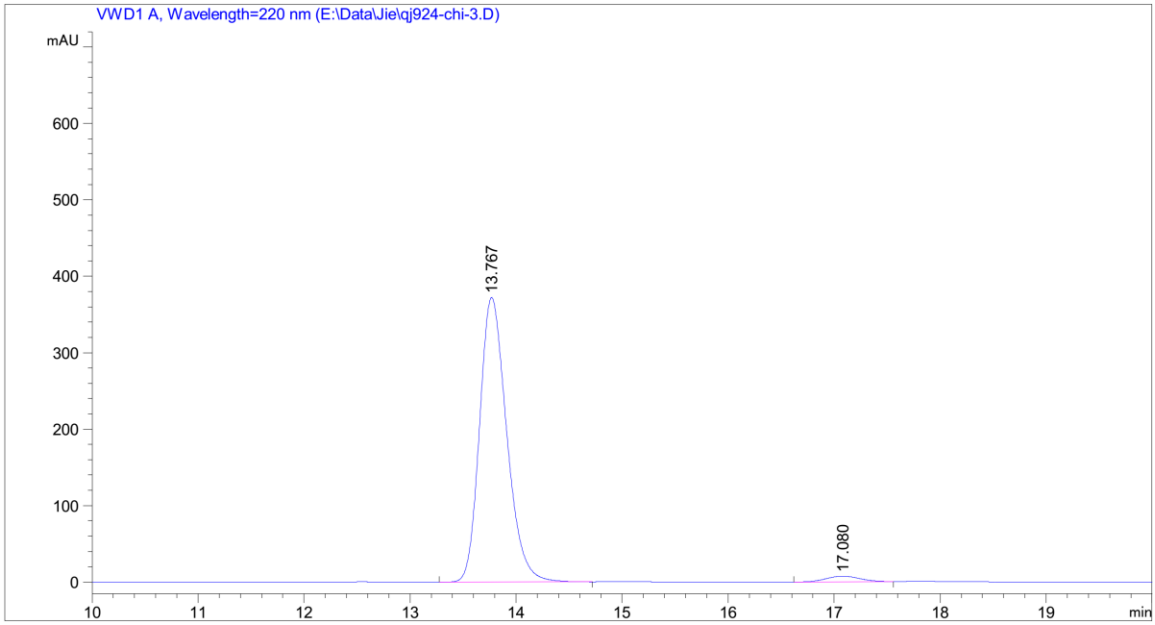

Peak #	RetTime [min]	Type	Width [min]	Area [mAU*s]	Height [mAU]	Area %
1	13.767	BB	0.2743	6613.68018	372.13562	97.6261
2	17.080	BB	0.3414	160.81754	7.37404	2.3739

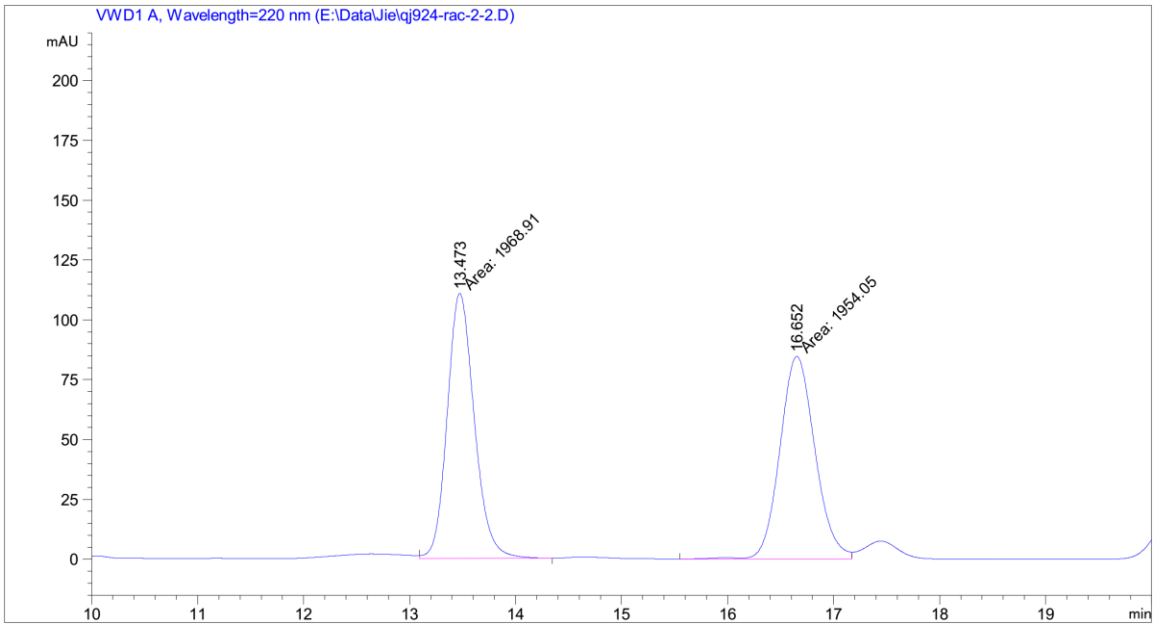

Peak #	RetTime [min]	Type	Width [min]	Area [mAU*s]	Height [mAU]	Area %
1	13.473	FM	0.2962	1968.90845	110.79773	50.1894
2	16.652	MF	0.3845	1954.05029	84.69544	49.8106

Figure 77. HPLC traces of (*R*)-**10m** (95% ee) and *rac*-**10m**.

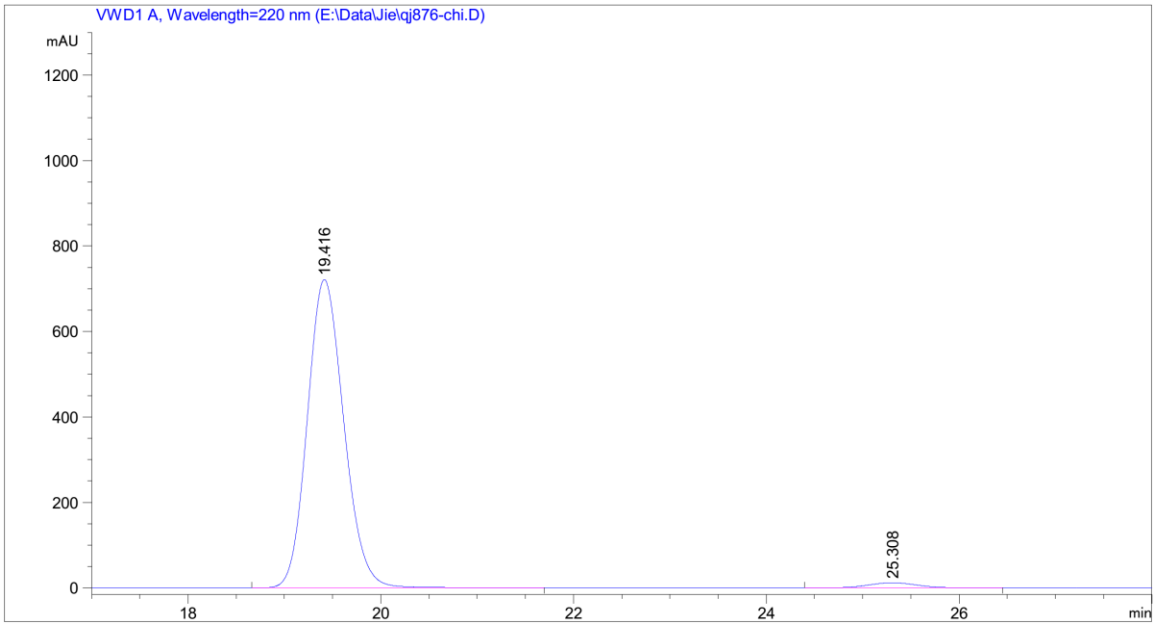

Peak #	RetTime [min]	Type	Width [min]	Area [mAU*s]	Height [mAU]	Area %
1	19.416	BB	0.4075	1.89535e4	721.33209	97.8572
2	25.308	BB	0.5448	415.03195	11.90378	2.1428

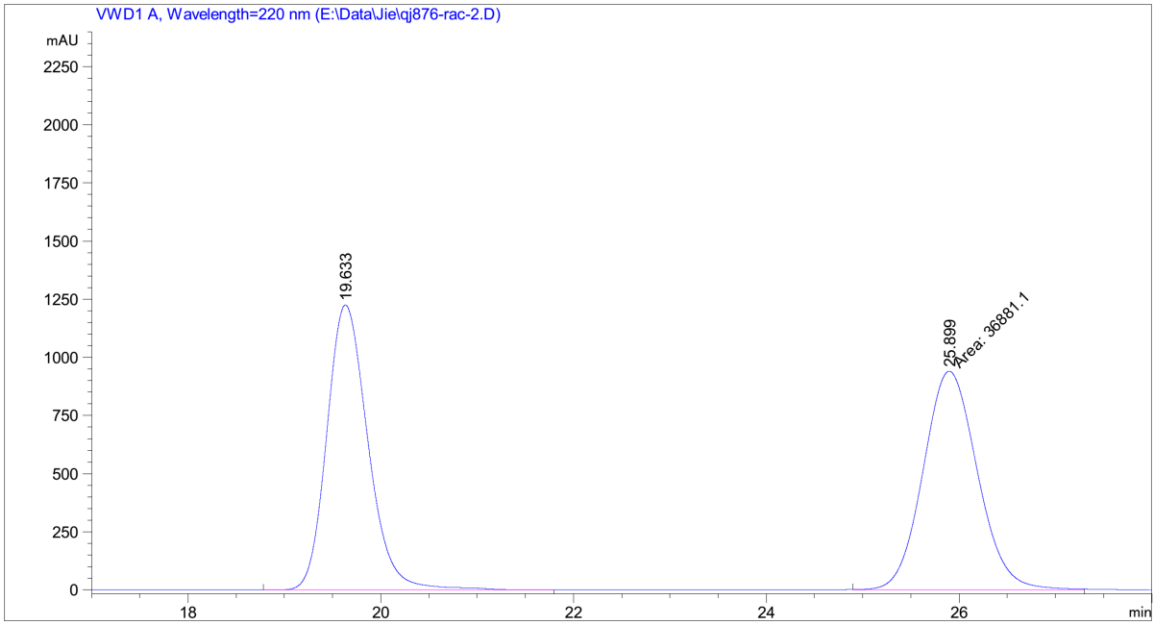

Peak #	RetTime [min]	Type	Width [min]	Area [mAU*s]	Height [mAU]	Area %
1	19.633	BB	0.4426	3.63884e4	1224.80042	49.6638
2	25.899	MM	0.6536	3.68811e4	940.40747	50.3362

Figure 78. HPLC traces of (*R*)-**10n** (96% ee) and *rac*-**10n**.

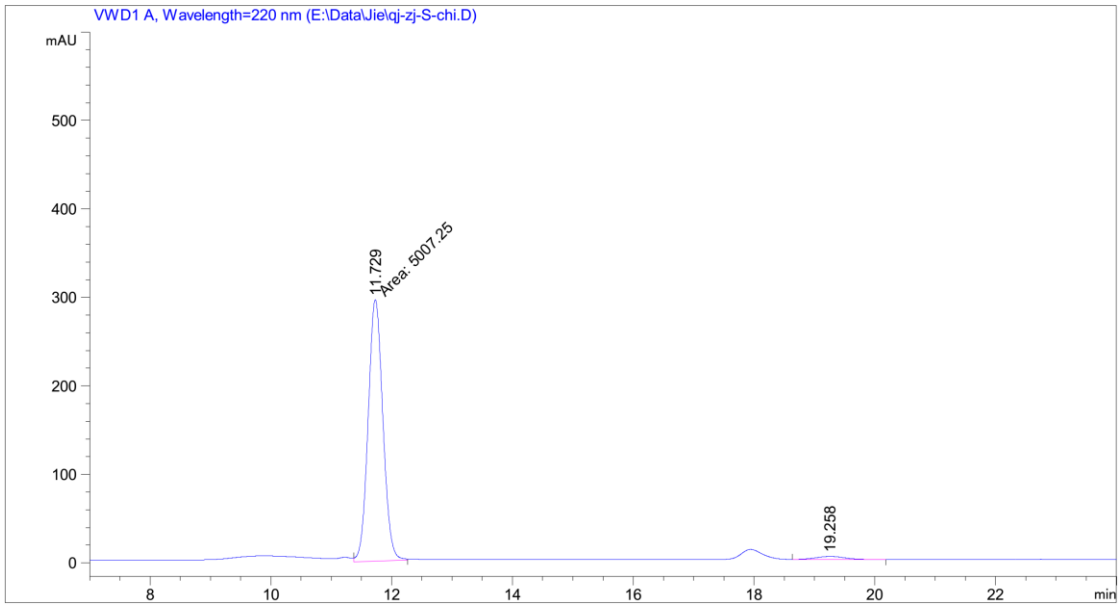

Peak #	RetTime [min]	Type	Width [min]	Area [mAU*s]	Height [mAU]	Area %
1	11.729	MM	0.2824	5007.25049	295.54510	97.7925
2	19.258	BB	0.4965	113.02968	3.44784	2.2075

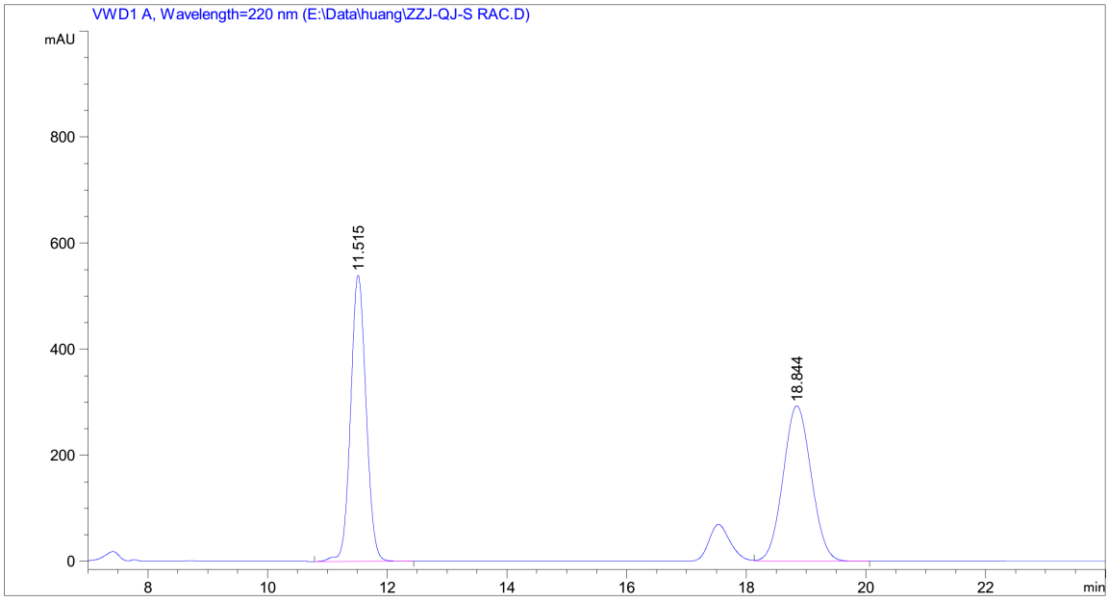

Peak #	RetTime [min]	Type	Width [min]	Area [mAU*s]	Height [mAU]	Area %
1	11.515	BB	0.2780	9667.61914	539.56299	50.2106
2	18.844	VB	0.5107	9586.52051	293.02689	49.7894

Figure 79. HPLC traces of (*R*)-**10o** (95% ee) and *rac*-**10o**.

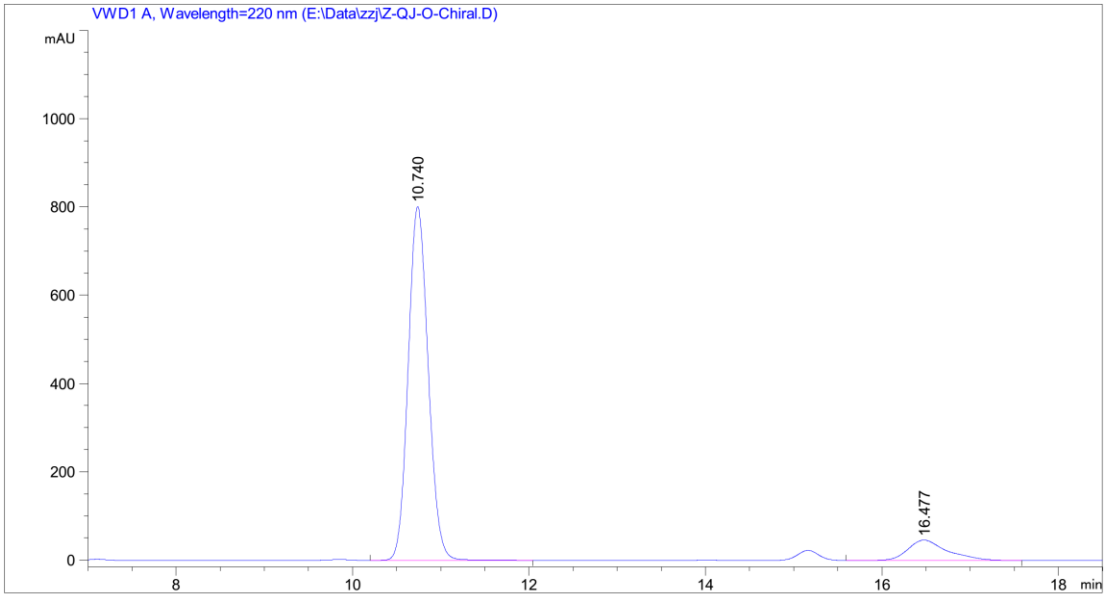

Peak #	RetTime [min]	Type	Width [min]	Area [mAU*s]	Height [mAU]	Area %
1	10.740	BB	0.2447	1.26154e4	801.02917	89.9780
2	16.477	BB	0.4504	1405.13440	45.87313	10.0220

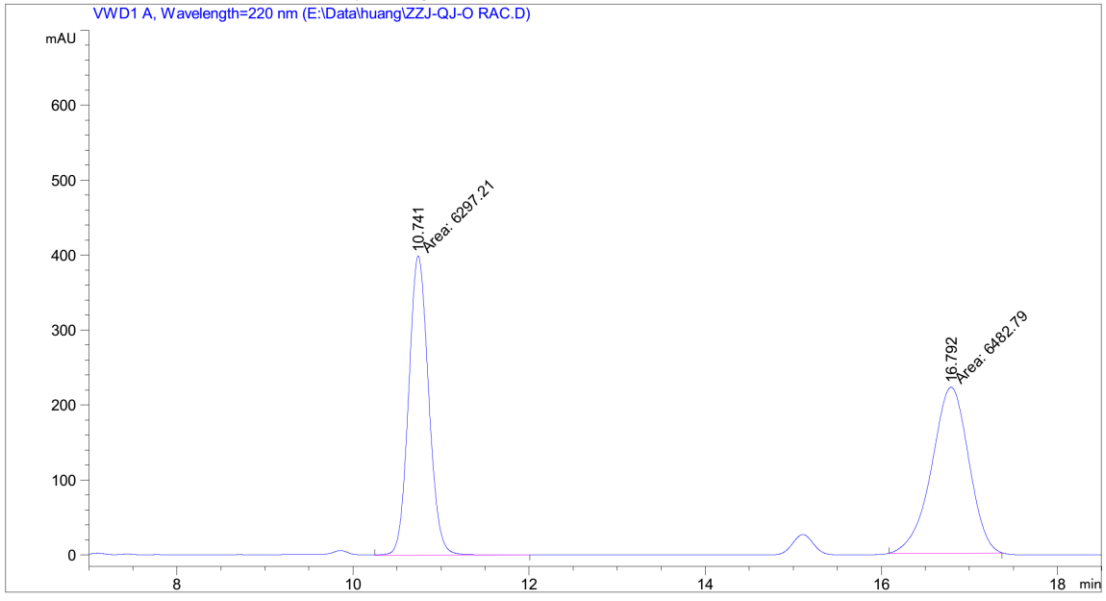

Peak #	RetTime [min]	Type	Width [min]	Area [mAU*s]	Height [mAU]	Area %
1	10.741	MM	0.2630	6297.20996	399.04593	49.2740
2	16.792	MM	0.4880	6482.78760	221.40756	50.7260

Figure 80. HPLC traces of (*R*)-**10p** (80% ee) and *rac*-**10p**.

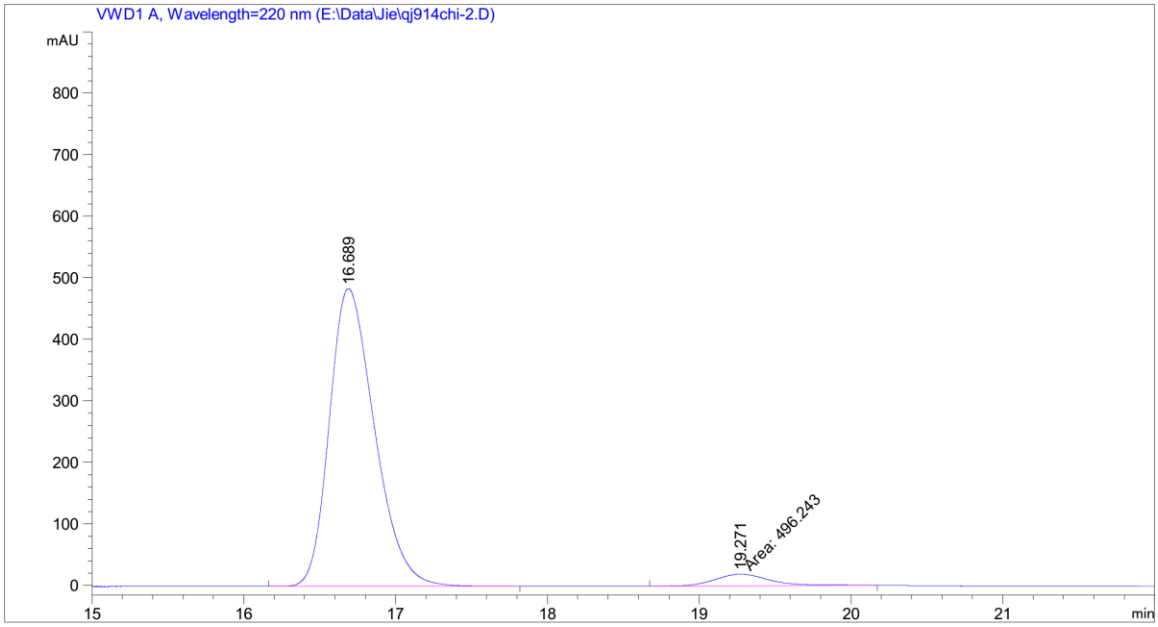

Peak #	RetTime [min]	Type	Width [min]	Area [mAU*s]	Height [mAU]	Area %
1	16.689	BB	0.3106	1.00031e4	484.07761	95.2736
2	19.271	MM	0.4314	496.24261	19.17272	4.7264

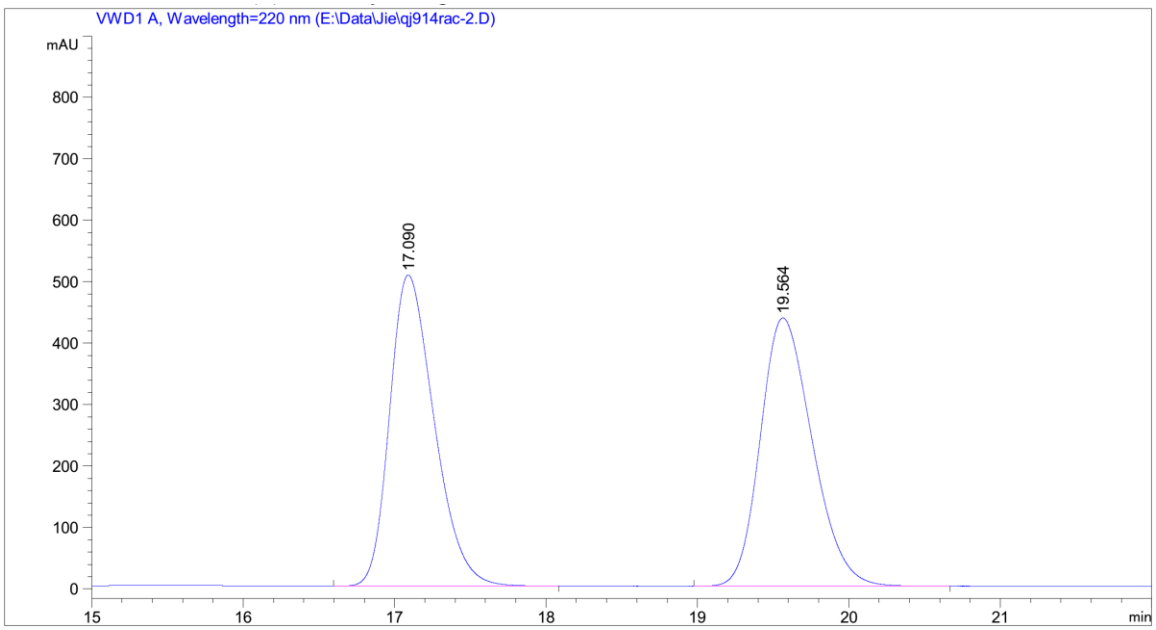

Peak #	RetTime [min]	Type	Width [min]	Area [mAU*s]	Height [mAU]	Area %
1	17.090	BB	0.3093	1.03377e4	506.11337	49.8696
2	19.564	BV R	0.3608	1.03918e4	436.44617	50.1304

Figure 81. HPLC traces of (*R*)-**10q** (90% ee) and *rac*-**10q**.

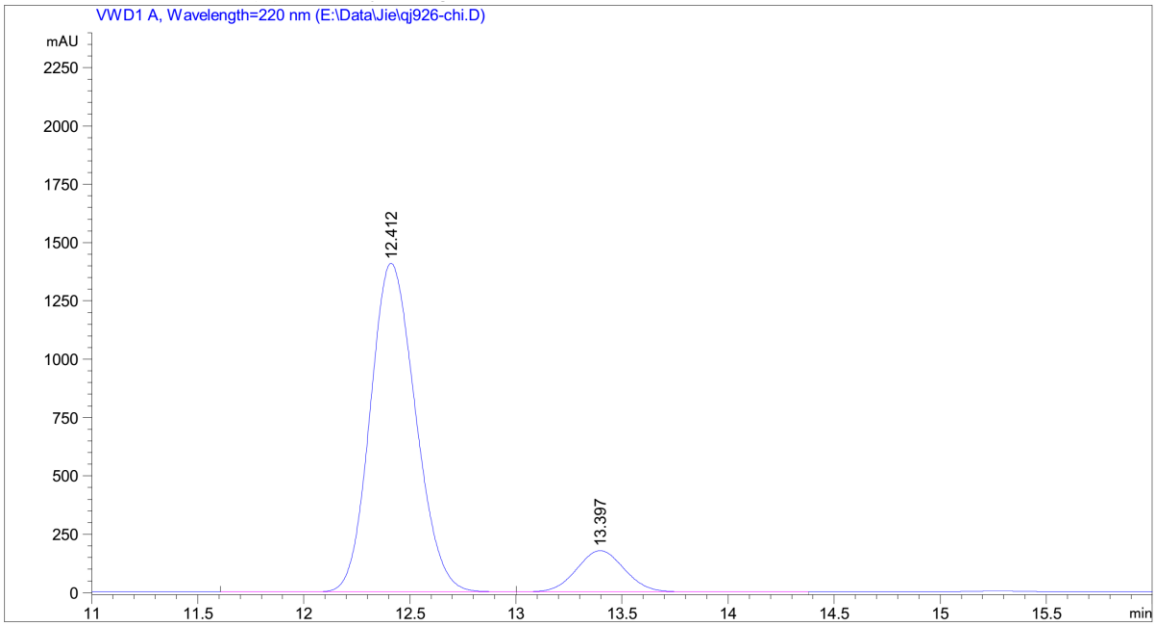

Peak #	RetTime [min]	Type	Width [min]	Area [mAU*s]	Height [mAU]	Area %
1	12.412	VV R	0.2307	2.08463e4	1408.37366	88.2370
2	13.397	VB	0.2443	2779.04565	176.86533	11.7630

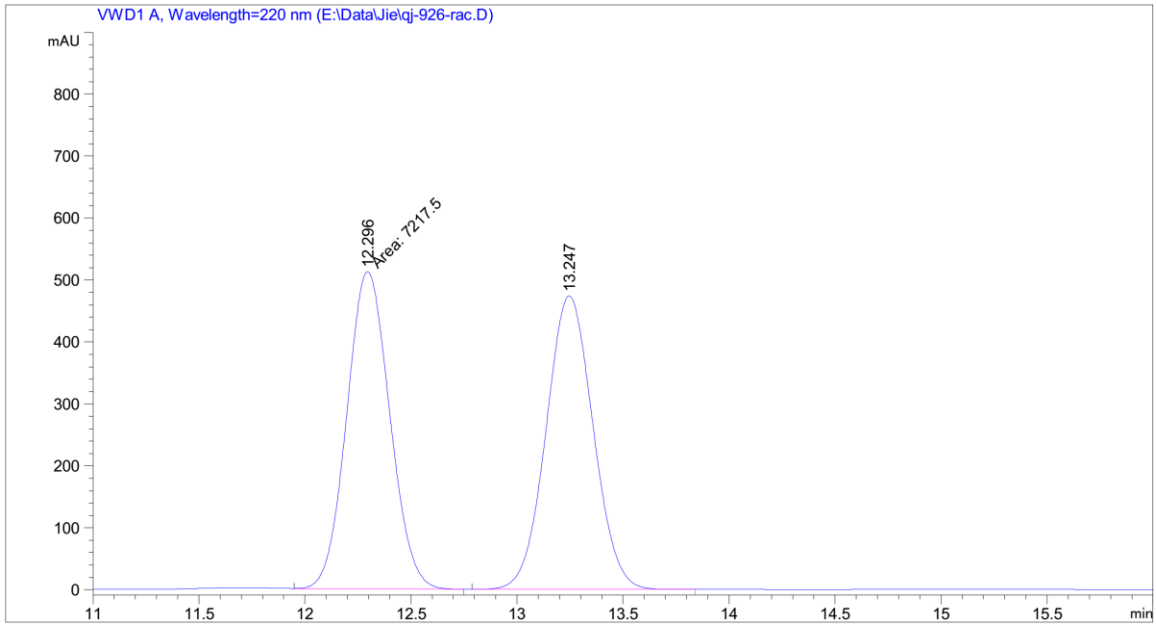

Peak #	RetTime [min]	Type	Width [min]	Area [mAU*s]	Height [mAU]	Area %
1	12.296	MM	0.2347	7217.50146	512.54224	49.7257
2	13.247	BB	0.2408	7297.13525	473.59531	50.2743

Figure 82. HPLC traces of (*R*)-**10r** (76% ee) and *rac*-**10r**.

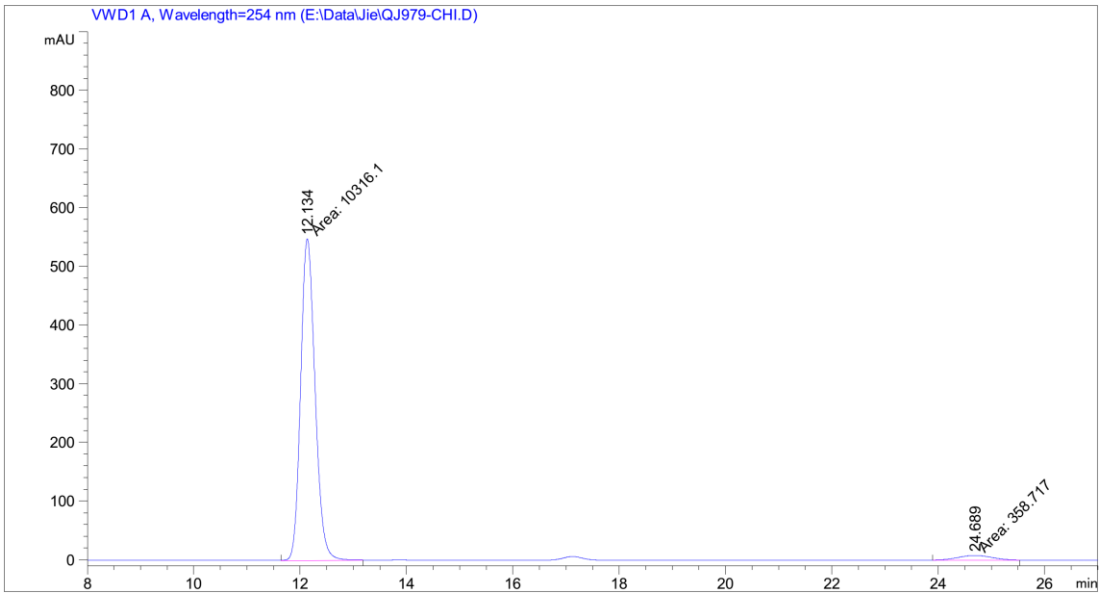

Peak #	RetTime [min]	Type	Width [min]	Area [mAU*s]	Height [mAU]	Area %
1	12.134	MM	0.3137	1.03161e4	548.12122	96.6396
2	24.689	MM	0.7442	358.71725	8.03370	3.3604

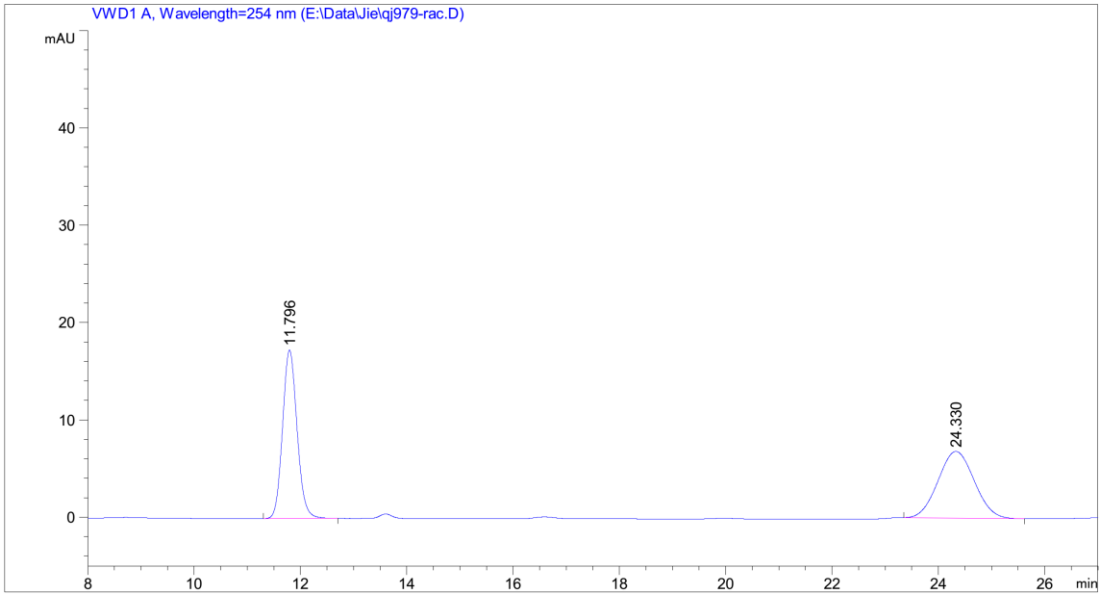

Peak #	RetTime [min]	Type	Width [min]	Area [mAU*s]	Height [mAU]	Area %
1	11.796	BB	0.2921	328.03656	17.30936	50.3076
2	24.330	BB	0.7260	324.02560	6.84878	49.6924

Figure 83. HPLC traces of (*R*)-**10s** (93% ee) and *rac*-**10s**.

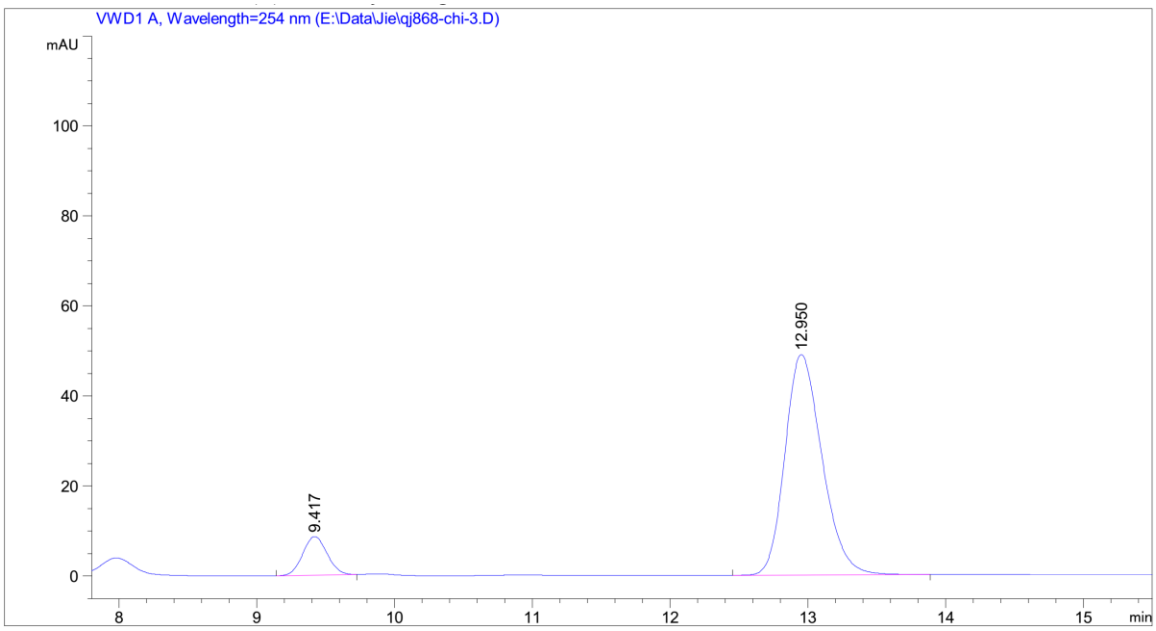

Peak #	RetTime [min]	Type	Width [min]	Area [mAU*s]	Height [mAU]	Area %
1	9.417	BB	0.1911	105.57629	8.60605	10.3254
2	12.950	BB	0.2884	916.91394	48.98840	89.6746

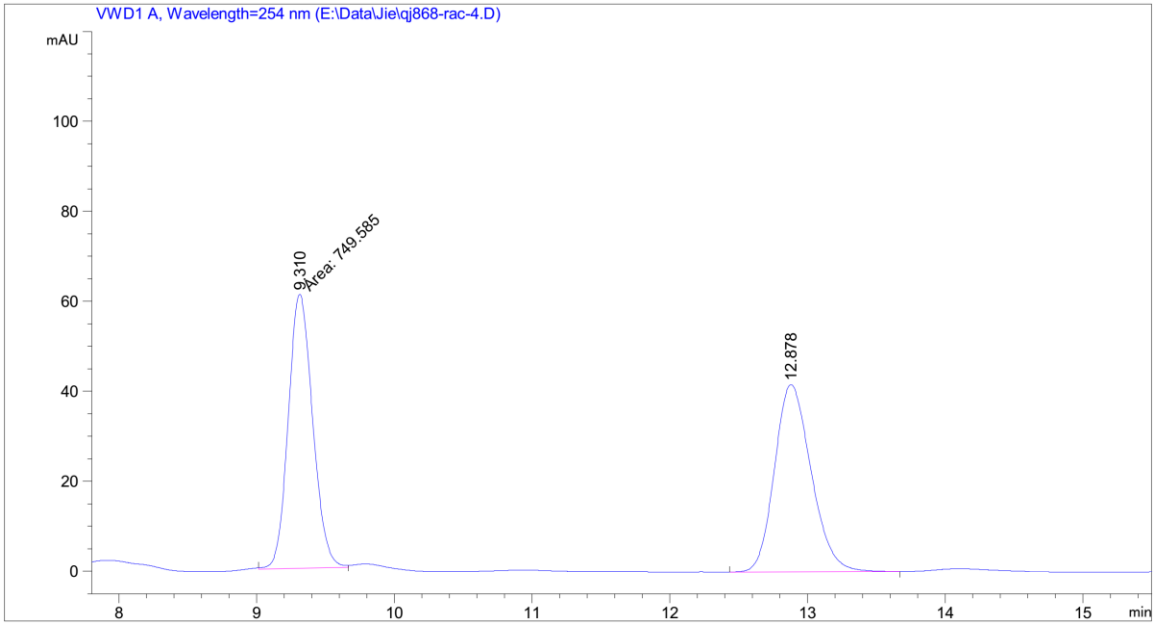

Peak #	RetTime [min]	Type	Width [min]	Area [mAU*s]	Height [mAU]	Area %
1	9.310	MM	0.2051	749.58496	60.90788	49.3562
2	12.878	BB	0.2867	769.14081	41.60713	50.6438

Figure 84. HPLC traces of (*S*)-**10t** (80% ee) and *rac*-**10t**.

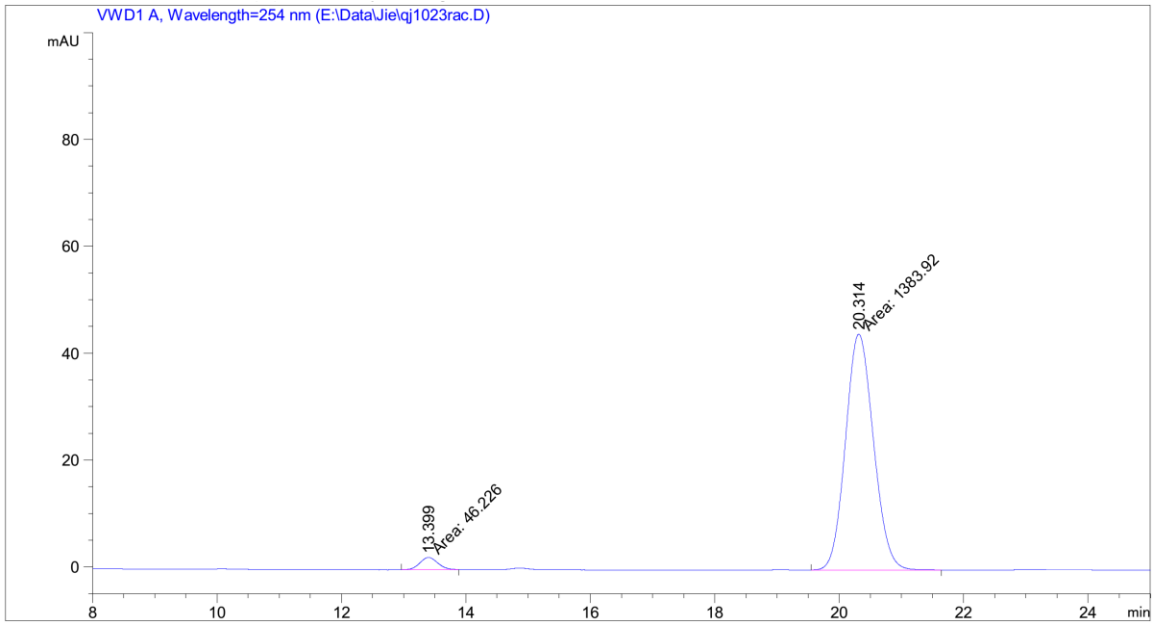

Peak #	RetTime [min]	Type	Width [min]	Area [mAU*s]	Height [mAU]	Area %
1	13.399	MM	0.3360	46.22596	2.29278	3.2322
2	20.314	MM	0.5221	1383.92383	44.18117	96.7678

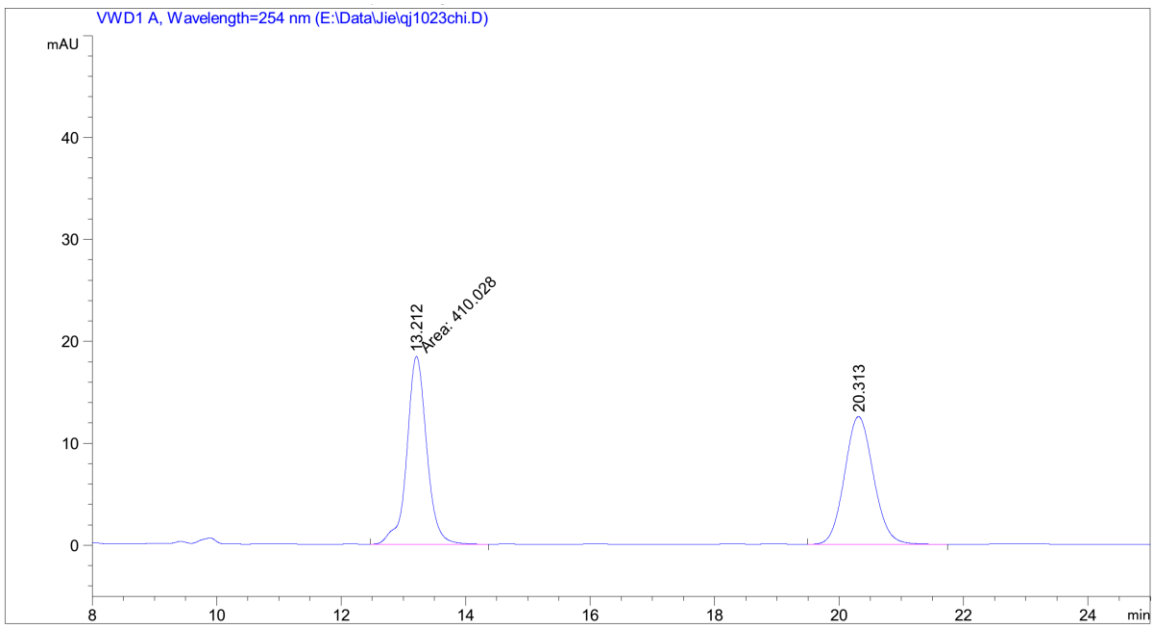

Peak #	RetTime [min]	Type	Width [min]	Area [mAU*s]	Height [mAU]	Area %
1	13.212	MM	0.3706	410.02771	18.43762	50.3430
2	20.313	BB	0.4996	404.44016	12.52828	49.6570

Figure 85. HPLC traces of (*S*)-**10u** (94% ee) and *rac*-**10u**.

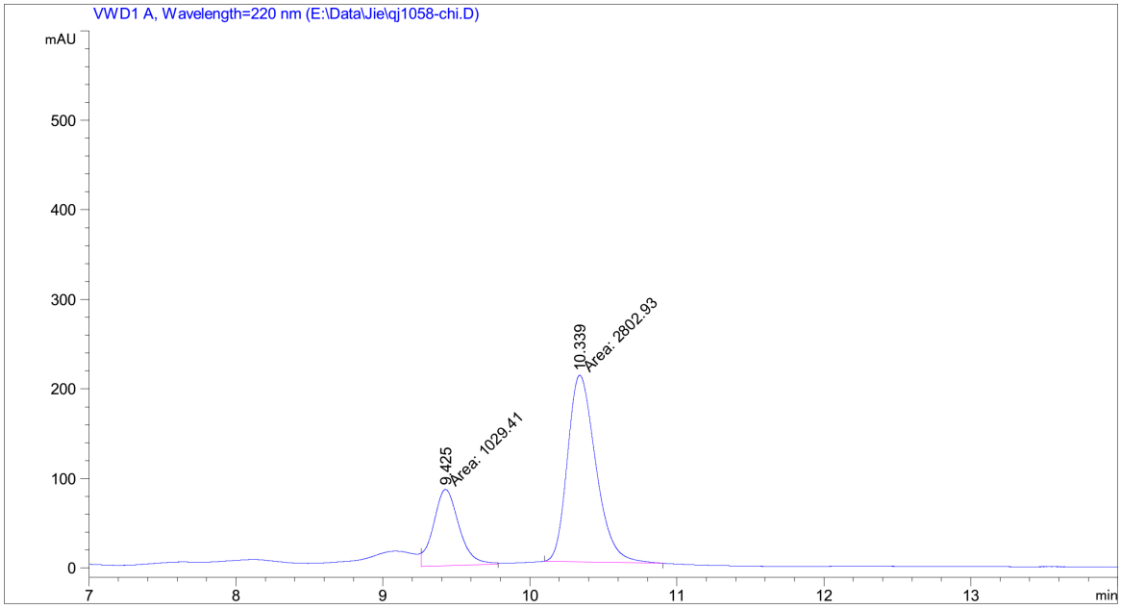

Peak #	RetTime [min]	Type	Width [min]	Area [mAU*s]	Height [mAU]	Area %
1	9.425	MM	0.2016	1029.40930	85.08244	26.8611
2	10.339	MM	0.2241	2802.93433	208.50403	73.1389

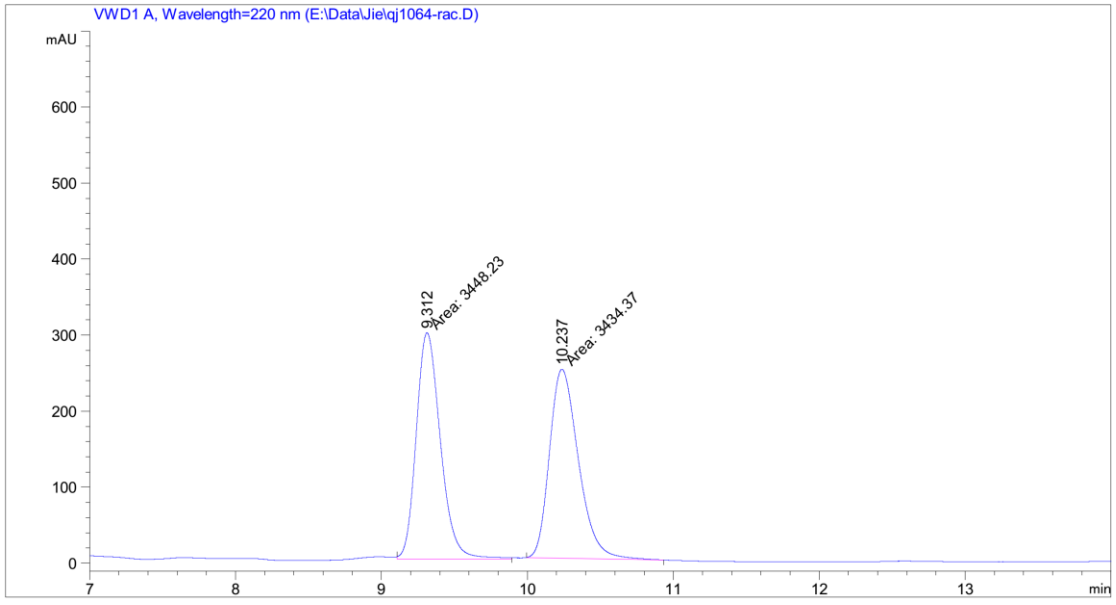

Peak #	RetTime [min]	Type	Width [min]	Area [mAU*s]	Height [mAU]	Area %
1	9.312	MM	0.1930	3448.22876	297.80496	50.1007
2	10.237	MM	0.2302	3434.37402	248.70056	49.8993

Figure 86. HPLC traces of (*R*)-**10y** (46% ee) and *rac*-**10y**.

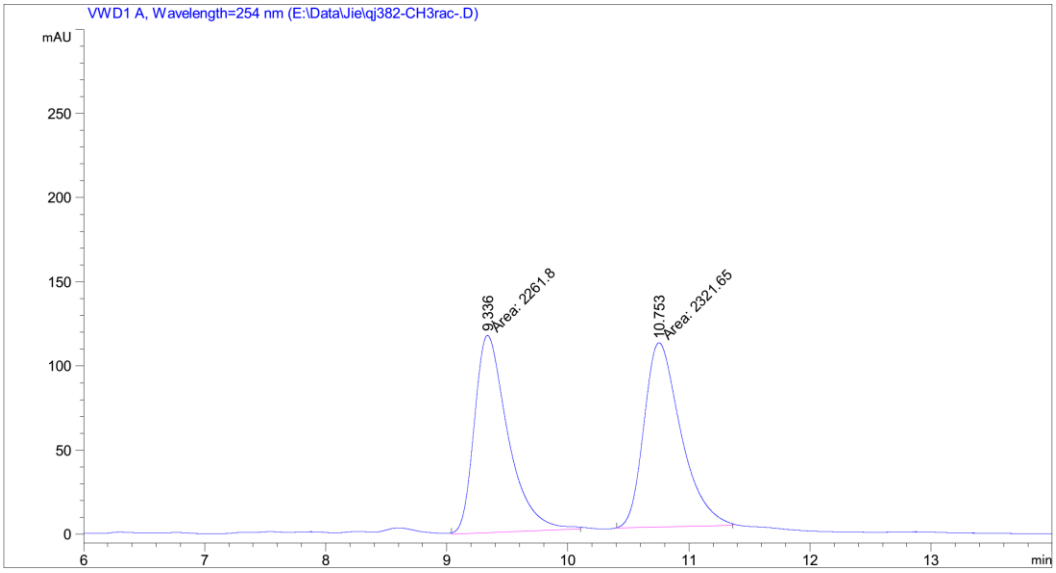

Peak #	RetTime [min]	Type	Width [min]	Area [mAU*s]	Height [mAU]	Area %
1	9.336	MM	0.3217	2261.80469	117.16328	49.3471
2	10.753	MM	0.3532	2321.65283	109.54808	50.6529

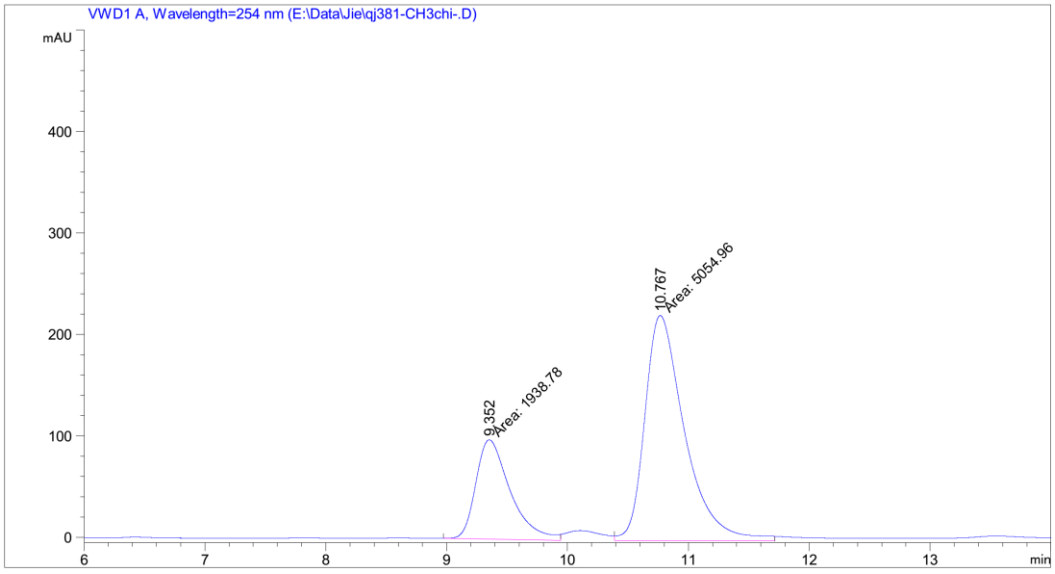

Peak #	RetTime [min]	Type	Width [min]	Area [mAU*s]	Height [mAU]	Area %
1	9.352	MM	0.3302	1938.78003	97.86170	27.7217
2	10.767	MM	0.3804	5054.95947	221.46736	72.2783

Figure 87. HPLC traces of *rac*-**15a** and (2*R*, 3*R*)-**15a** (45% ee).

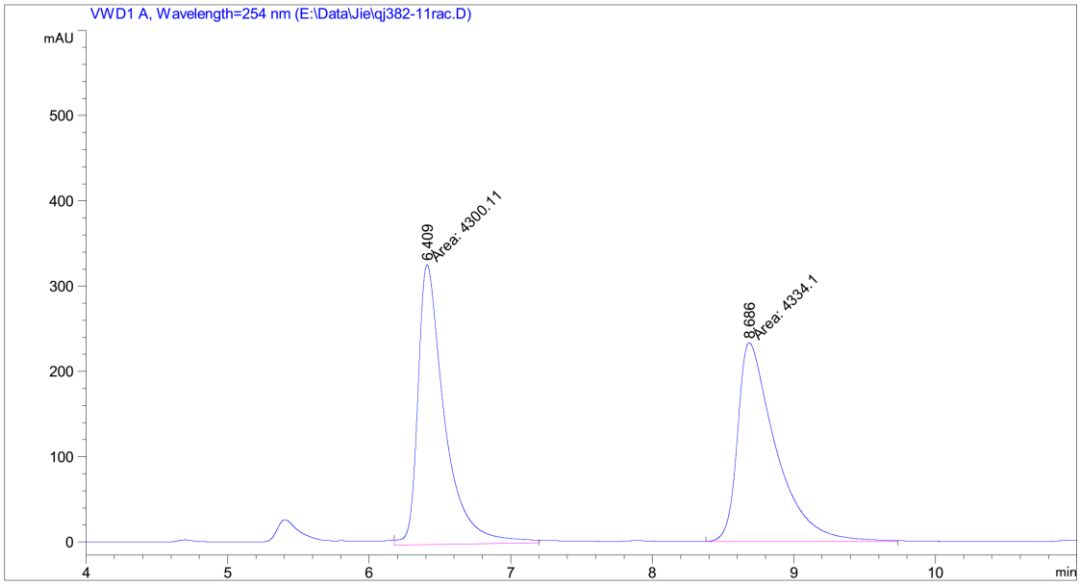

Peak #	RetTime [min]	Type	Width [min]	Area [mAU*s]	Height [mAU]	Area %
1	6.409	MM	0.2184	4300.10645	328.17801	49.8031
2	8.686	MM	0.3103	4334.10400	232.80276	50.1969

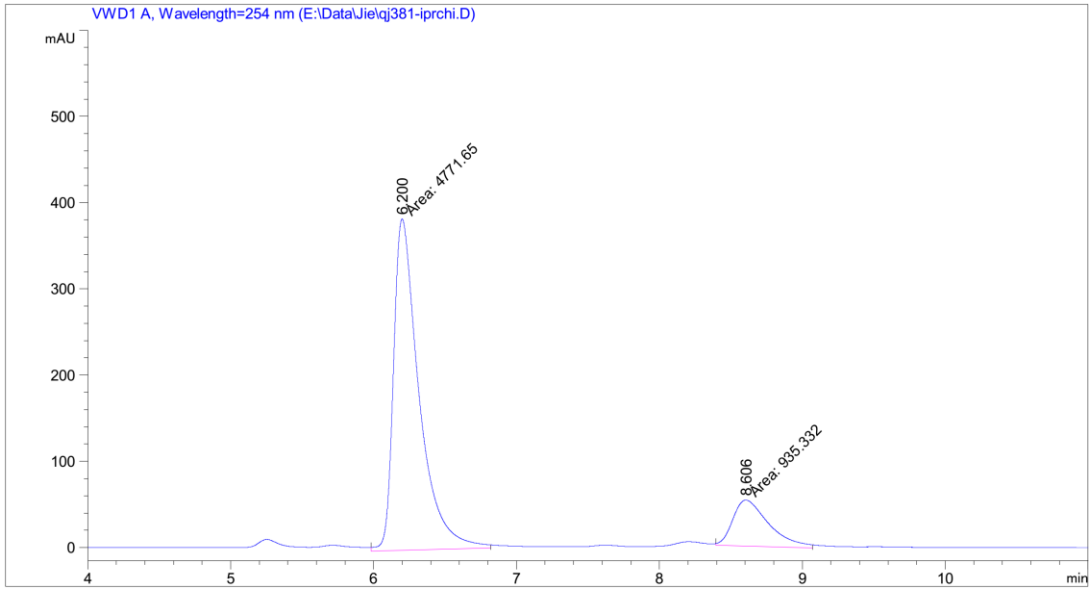

Peak #	RetTime [min]	Type	Width [min]	Area [mAU*s]	Height [mAU]	Area %
1	6.200	MM	0.2070	4771.65479	384.17831	83.6108
2	8.606	MM	0.2926	935.33173	53.27085	16.3892

Figure 88. HPLC traces of *rac*-**15b** and (2*R*, 3*R*)-**15b** (67% ee).

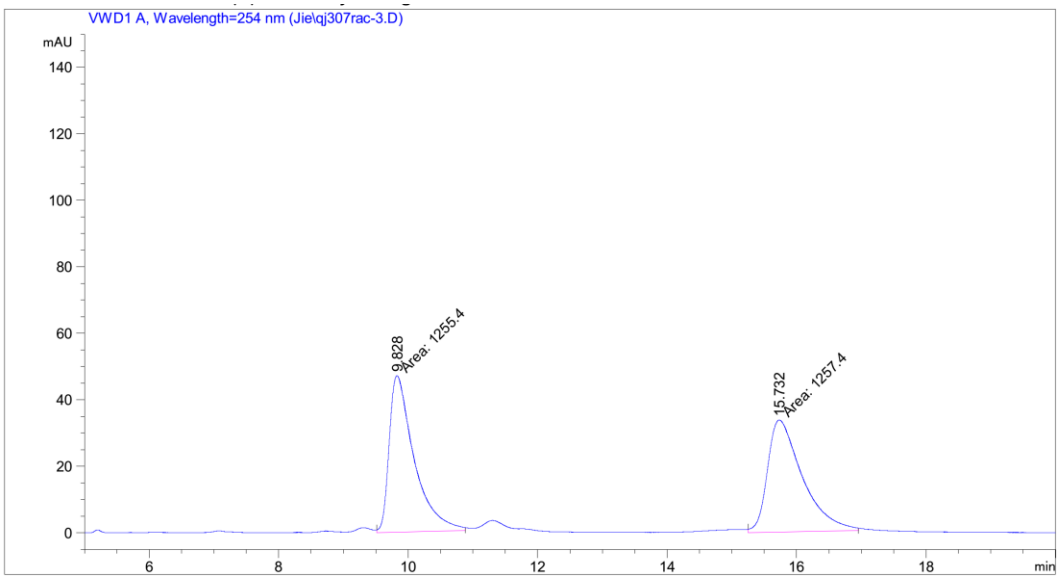

Peak #	RetTime [min]	Type	Width [min]	Area [mAU*s]	Height [mAU]	Area %
1	9.828	MM	0.4446	1255.40112	47.06250	49.9602
2	15.732	MM	0.6226	1257.40039	33.66254	50.0398

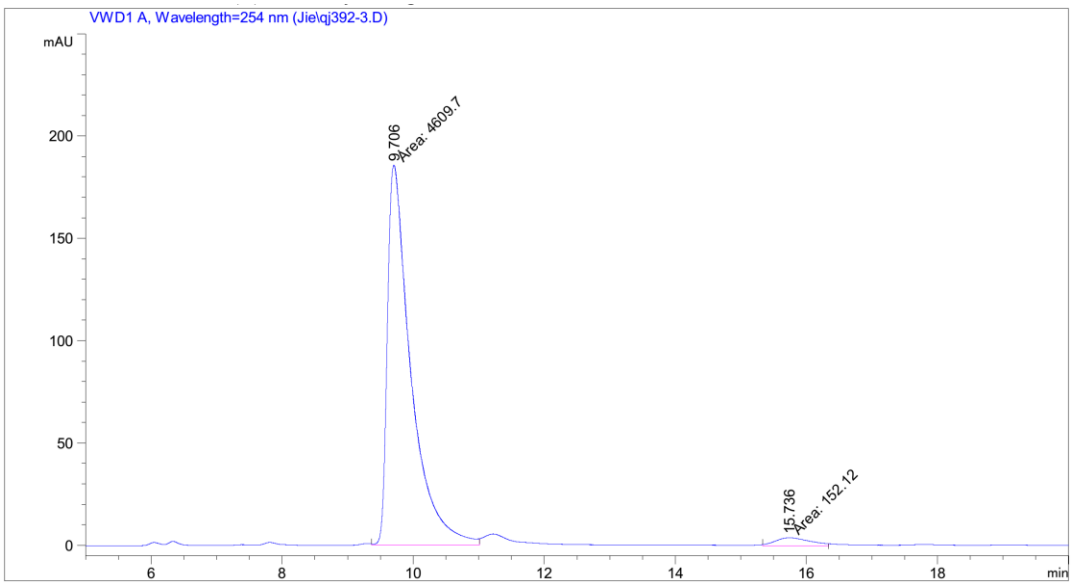

Peak #	RetTime [min]	Type	Width [min]	Area [mAU*s]	Height [mAU]	Area %
1	9.706	MM	0.4136	4609.69971	185.76880	96.8054
2	15.736	MM	0.6267	152.11977	4.04572	3.1946

Figure 89. HPLC traces of *rac*-**15c** and (2*R*, 3*R*)-**15c** (94% ee).

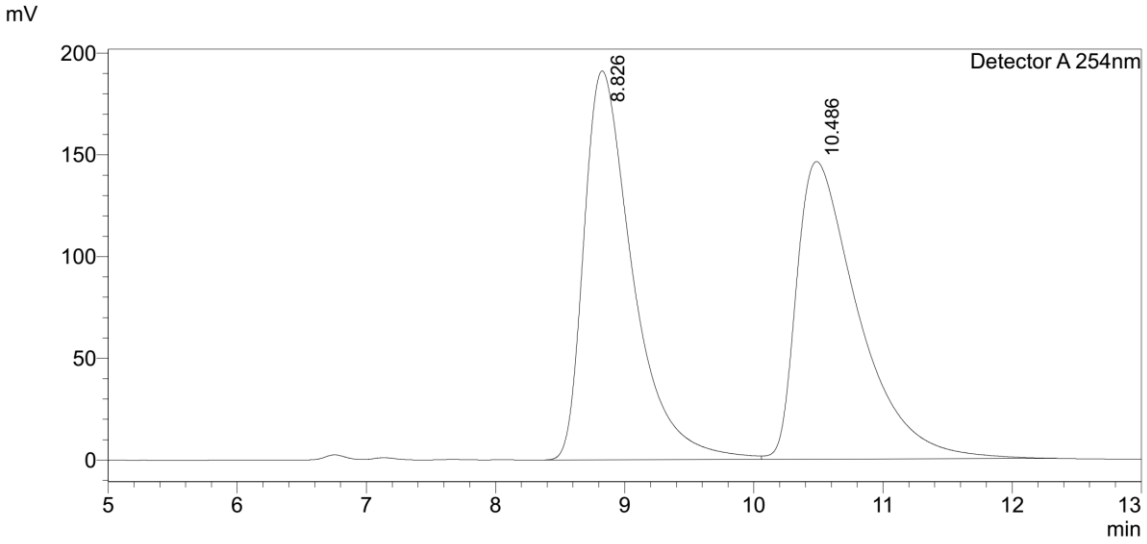

<Peak Table>

Detector A 254nm

Peak#	Ret. Time	USP Width	Area	Height	Area%
1	8.826	0.653	5011031	191060	50.716
2	10.486	0.836	4869528	146251	49.284
Total			9880558	337311	100.000

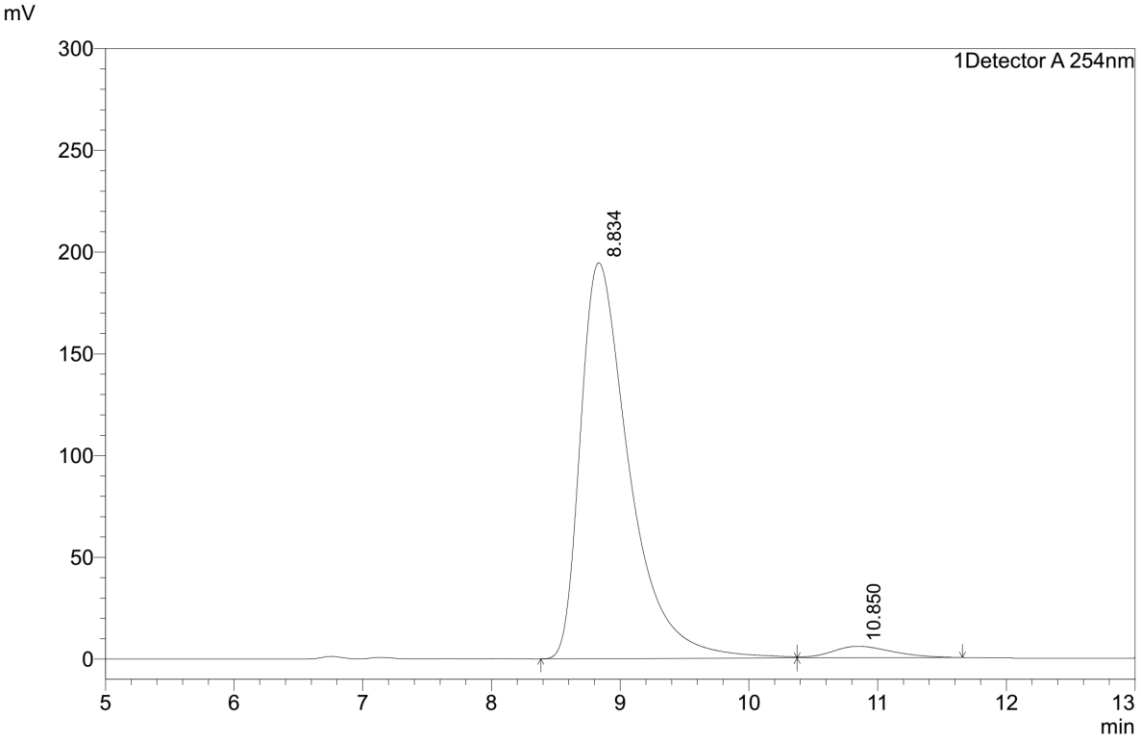

<Peak Table>

Detector A 254nm

Peak#	Ret. Time	USP Width	Area	Height	Area%
1	8.834	0.656	5141148	194560	96.476
2	10.850	0.867	187789	5702	3.524
Total			5328937	200262	100.000

Figure 90. HPLC traces of *rac*-**15d** and (2*R*, 3*R*)-**15d** (93% ee).

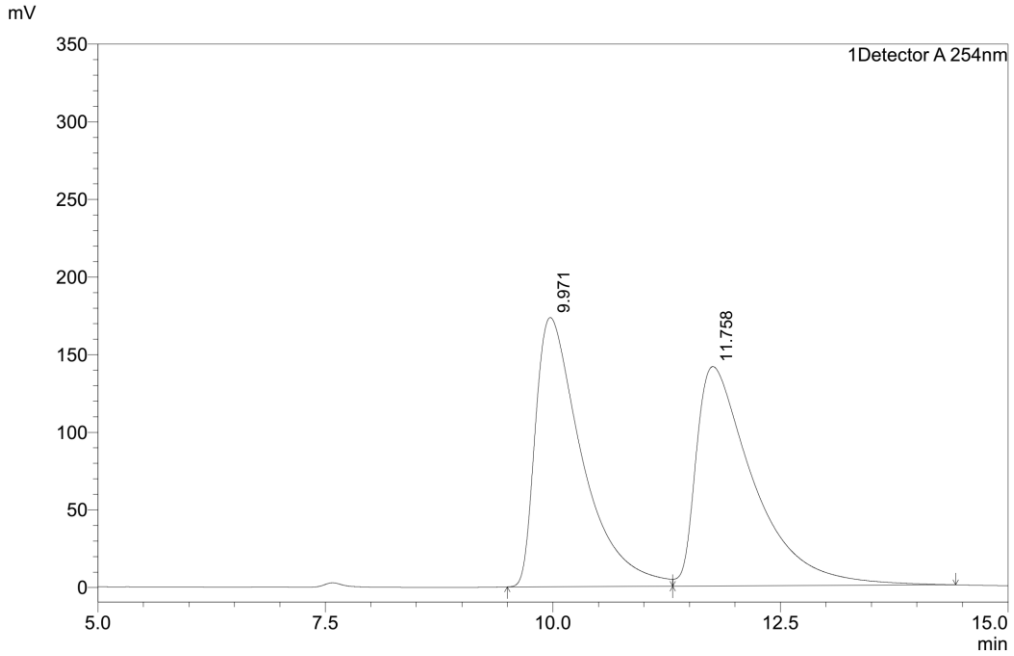

<Peak Table>

Detector A 254nm

Peak#	Ret. Time	USP Width	Area	Height	Area%
1	9.971	0.883	6175221	173341	49.805
2	11.758	1.077	6223511	141294	50.195
Total			12398732	314635	100.000

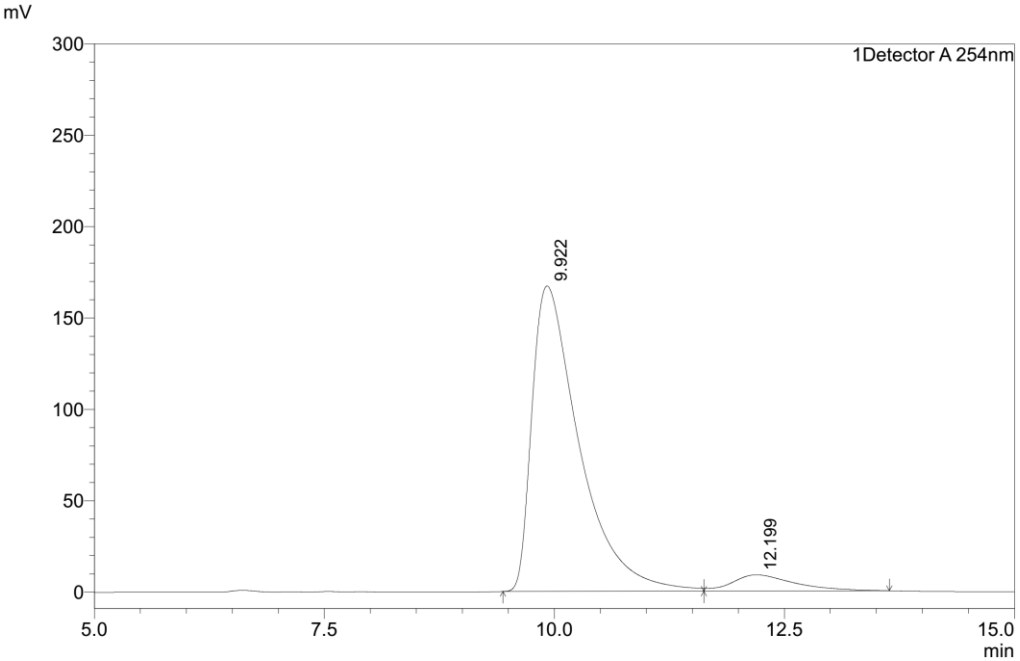

<Peak Table>

Detector A 254nm

Peak#	Ret. Time	USP Width	Area	Height	Area%
1	9.922	0.884	5978829	167153	93.460
2	12.199	1.206	418395	8860	6.540
Total			6397224	176013	100.000

Figure 91. HPLC traces of *rac*-**15e** and (2*R*, 3*R*)-**15e** (87% ee).

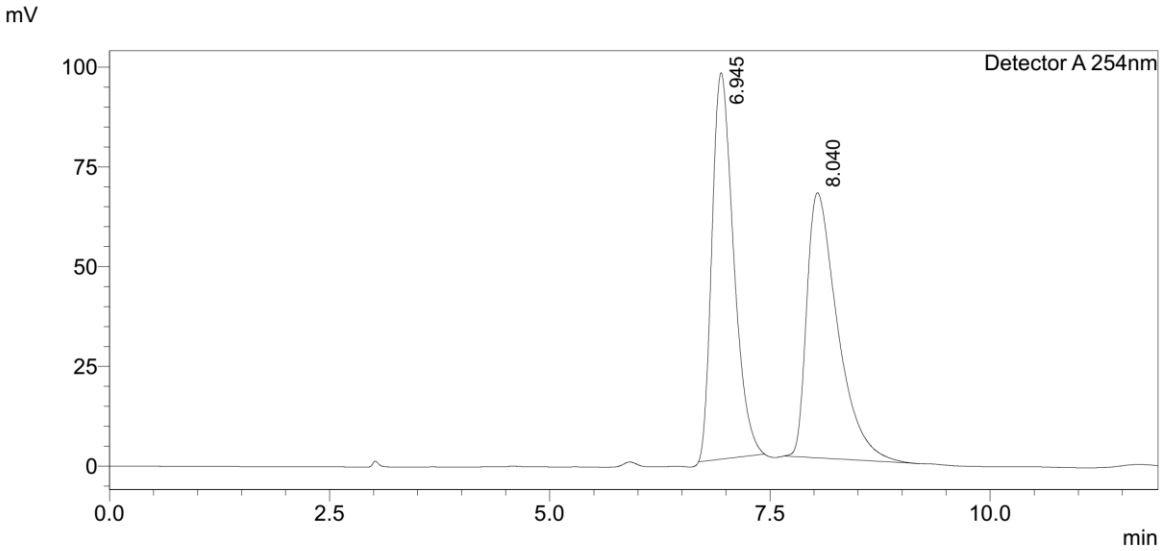

<Peak Table>

Detector A 254nm

Peak#	Ret. Time	USP Width	Area	Height	Area%
1	6.945	0.449	1655418	96822	50.608
2	8.040	0.619	1615647	66426	49.392
Total			3271065	163249	100.000

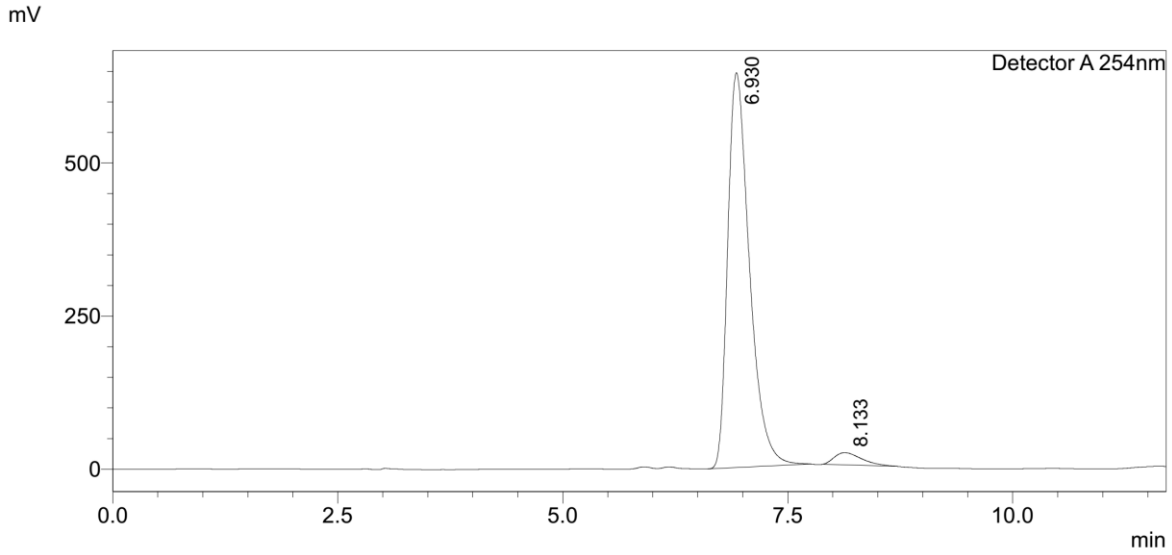

<Peak Table>

Detector A 254nm

Peak#	Ret. Time	USP Width	Area	Height	Area%
1	6.930	0.432	10848984	645075	96.232
2	8.133	0.562	424749	19972	3.768
Total			11273733	665047	100.000

Figure 92. HPLC traces of *rac*-**15g** and (2*R*, 3*R*)-**15g** (92% ee).

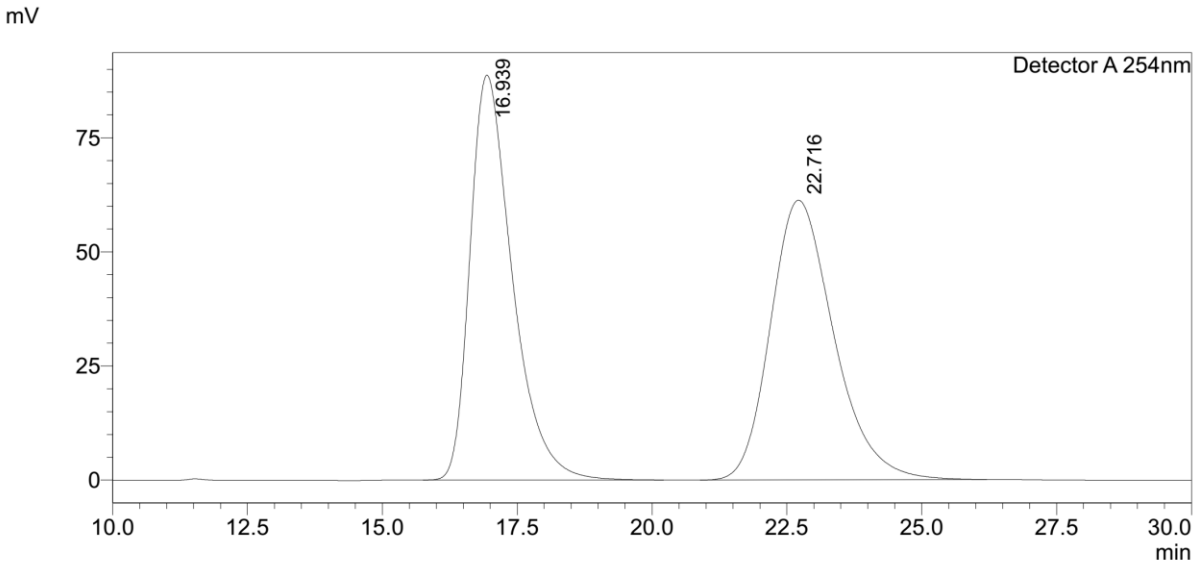

<Peak Table>

Detector A 254nm

Peak#	Ret. Time	USP Width	Area	Height	Area%
1	16.939	1.396	4841215	88696	49.143
2	22.716	2.118	5009977	61259	50.857
Total			9851192	149955	100.000

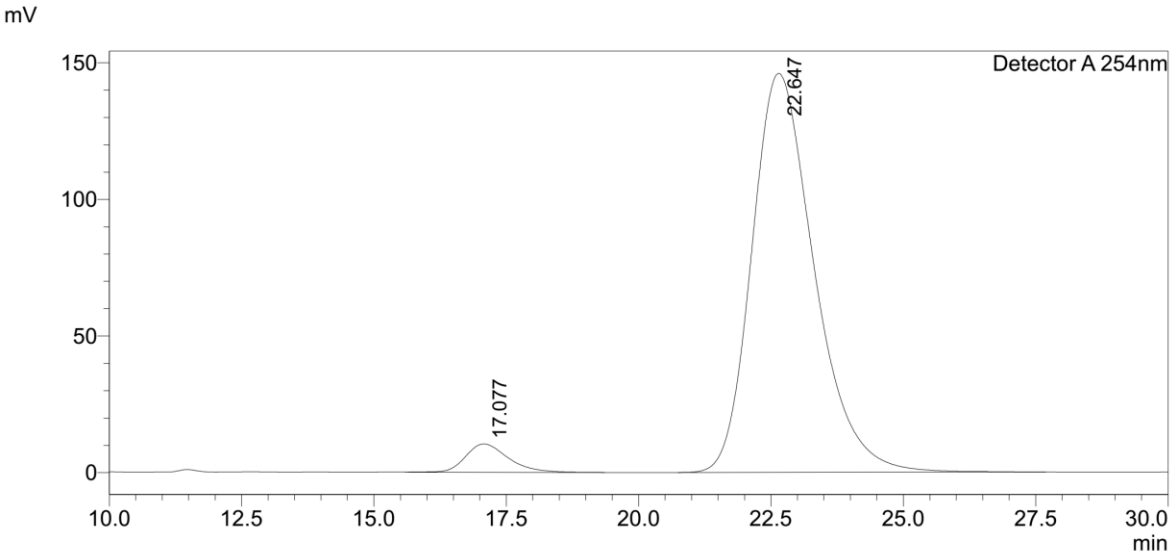

<Peak Table>

Detector A 254nm

Peak#	Ret. Time	USP Width	Area	Height	Area%
1	17.077	1.436	581663	10385	4.641
2	22.647	2.112	11950185	145994	95.359
Total			12531848	156380	100.000

Figure 93. HPLC traces of *rac*-**15h** and (2*R*, 3*R*)-**15h** (91% ee).

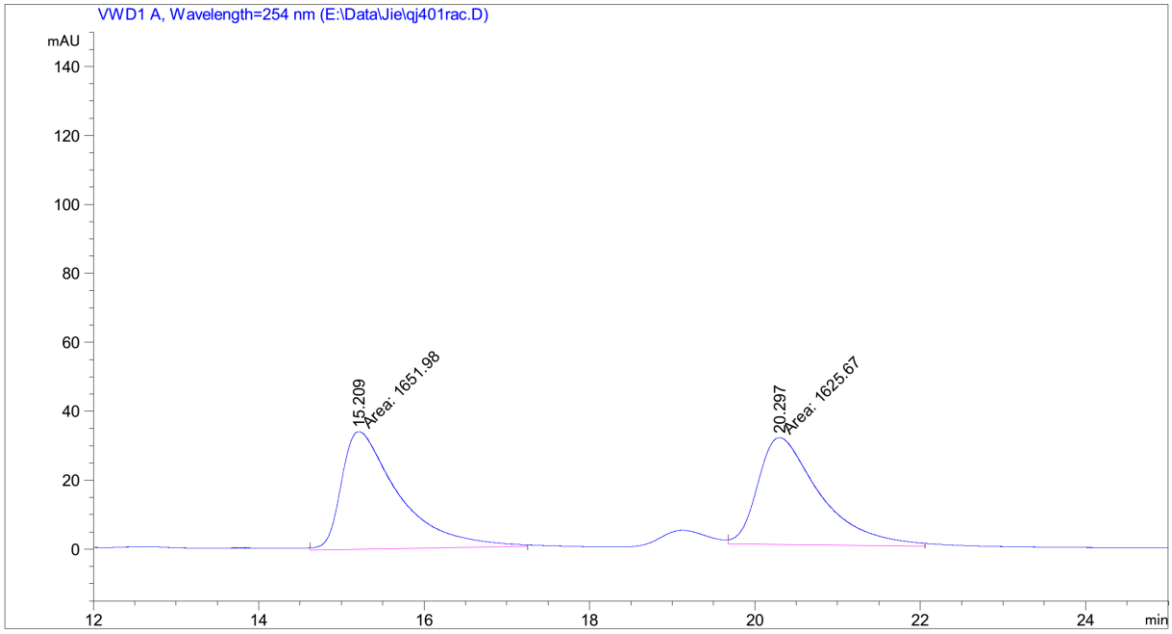

Peak #	RetTime [min]	Type	Width [min]	Area [mAU*s]	Height [mAU]	Area %
1	15.209	MM	0.8053	1651.97900	34.19169	50.4013
2	20.297	MM	0.8722	1625.67285	31.06529	49.5987

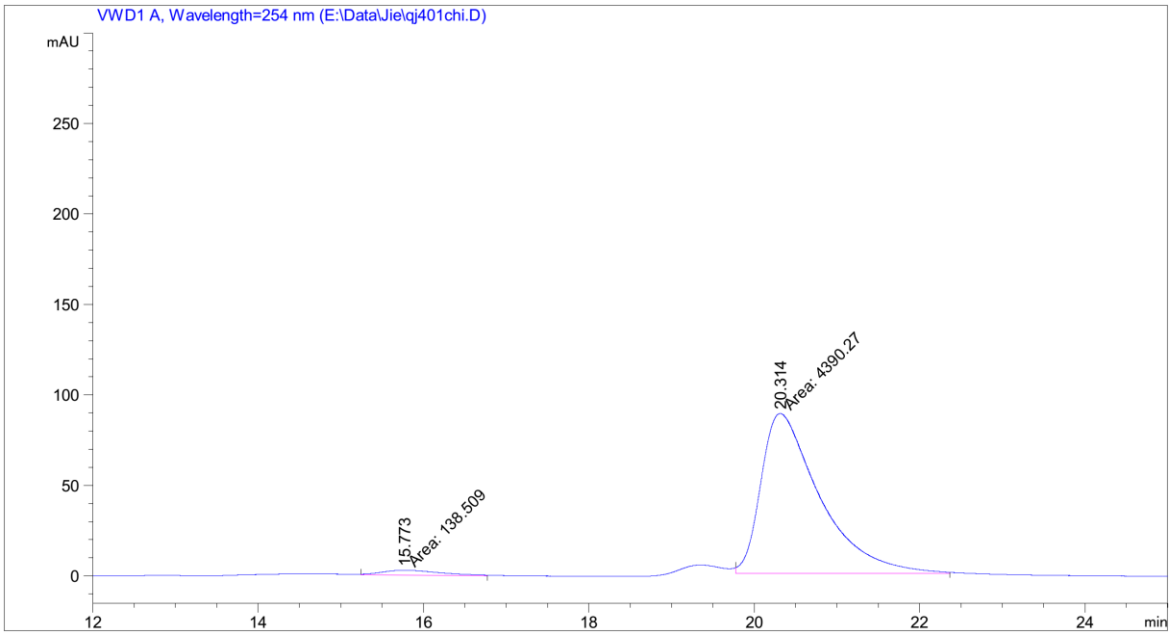

Peak #	RetTime [min]	Type	Width [min]	Area [mAU*s]	Height [mAU]	Area %
1	15.773	MM	0.8329	138.50861	2.77168	3.0584
2	20.314	MM	0.8274	4390.26660	88.43251	96.9416

Figure 94. HPLC traces of *rac*-**15i** and (2*R*, 3*R*)-**15i** (94% ee).

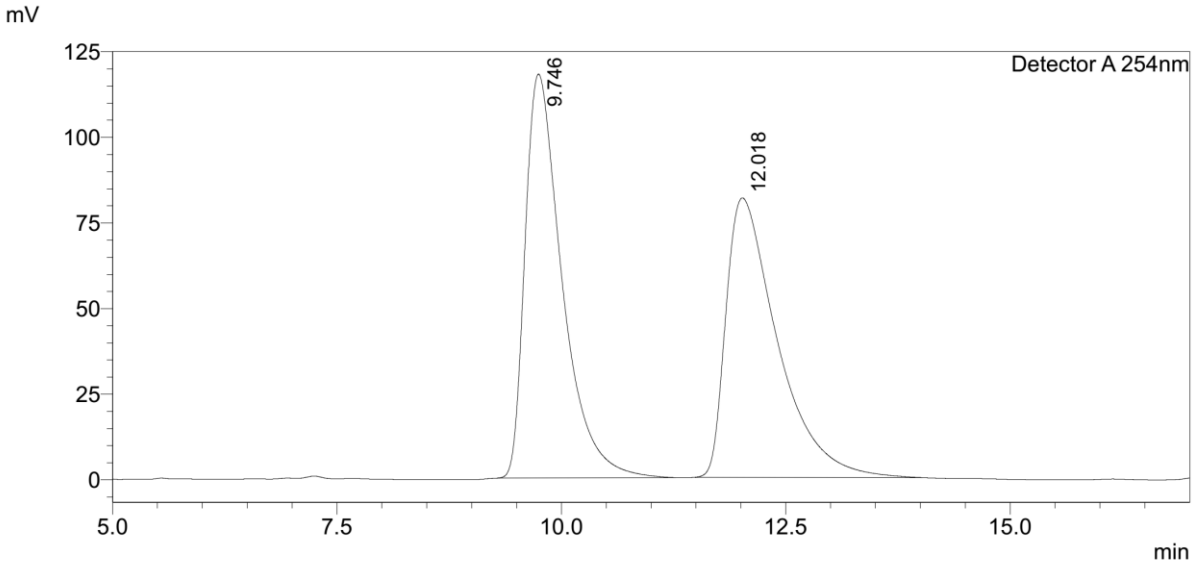

<Peak Table>

Detector A 254nm

Peak#	Ret. Time	USP Width	Area	Height	Area%
1	9.746	0.720	3380007	117927	50.981
2	12.018	1.002	3249914	81576	49.019
Total			6629921	199502	100.000

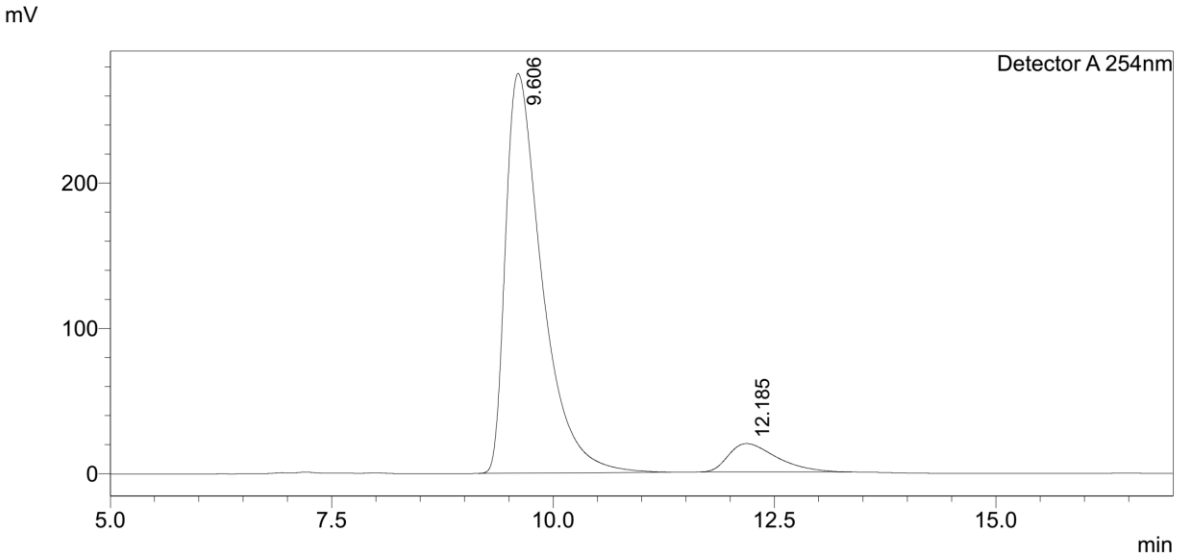

<Peak Table>

Detector A 254nm

Peak#	Ret. Time	USP Width	Area	Height	Area%
1	9.606	0.716	7868085	275018	91.394
2	12.185	0.990	740900	19561	8.606
Total			8608985	294579	100.000

Figure 95. HPLC traces of *rac*-**15j** and (2*R*, 3*R*)-**15j** (82% ee).

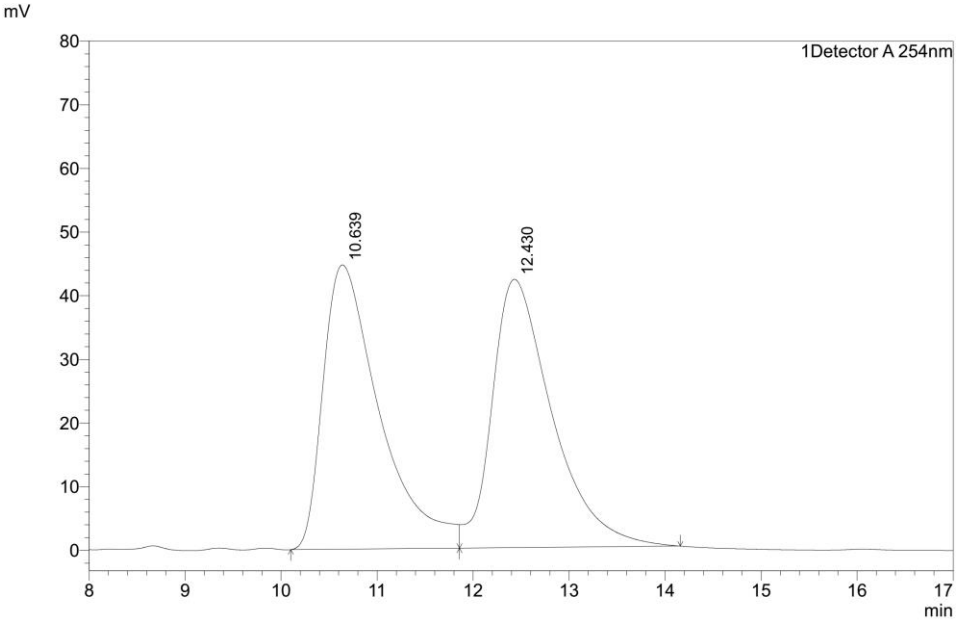

<Peak Table>

Detector A 254nm

Peak#	Ret. Time	USP Width	Area	Height	Area%
1	10.639	1.012	1824813	44660	49.908
2	12.430	1.090	1831560	42151	50.092
Total			3656373	86812	100.000

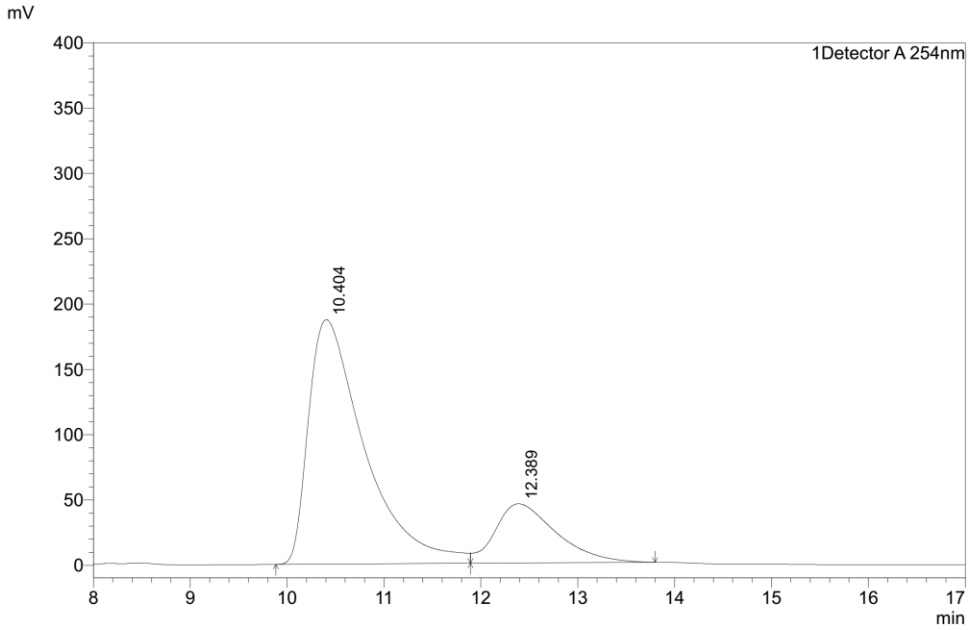

<Peak Table>

Detector A 254nm

Peak#	Ret. Time	USP Width	Area	Height	Area%
1	10.404	0.986	7507683	187071	79.148
2	12.389	1.124	1977989	45335	20.852
Total			9485671	232406	100.000

Figure 96. HPLC traces of *rac*-**15k** and (2*R*, 3*R*)-**15k** (58% ee).

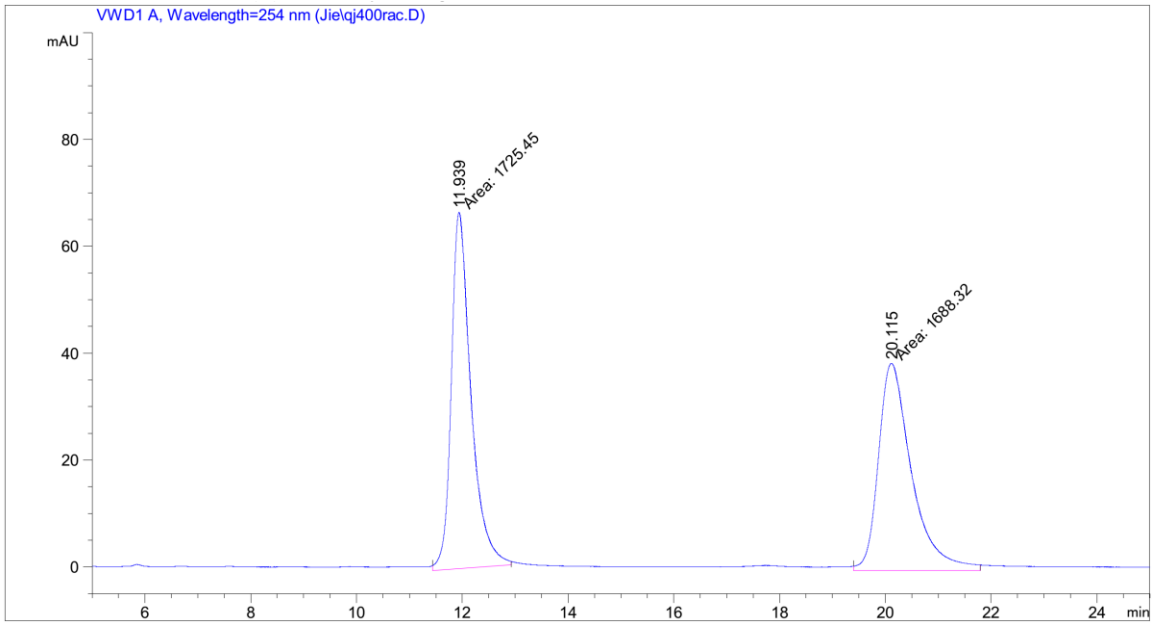

Peak #	RetTime [min]	Type	Width [min]	Area [mAU*s]	Height [mAU]	Area %
1	11.939	MM	0.4315	1725.44641	66.64944	50.5438
2	20.115	MM	0.7262	1688.31555	38.74963	49.4562

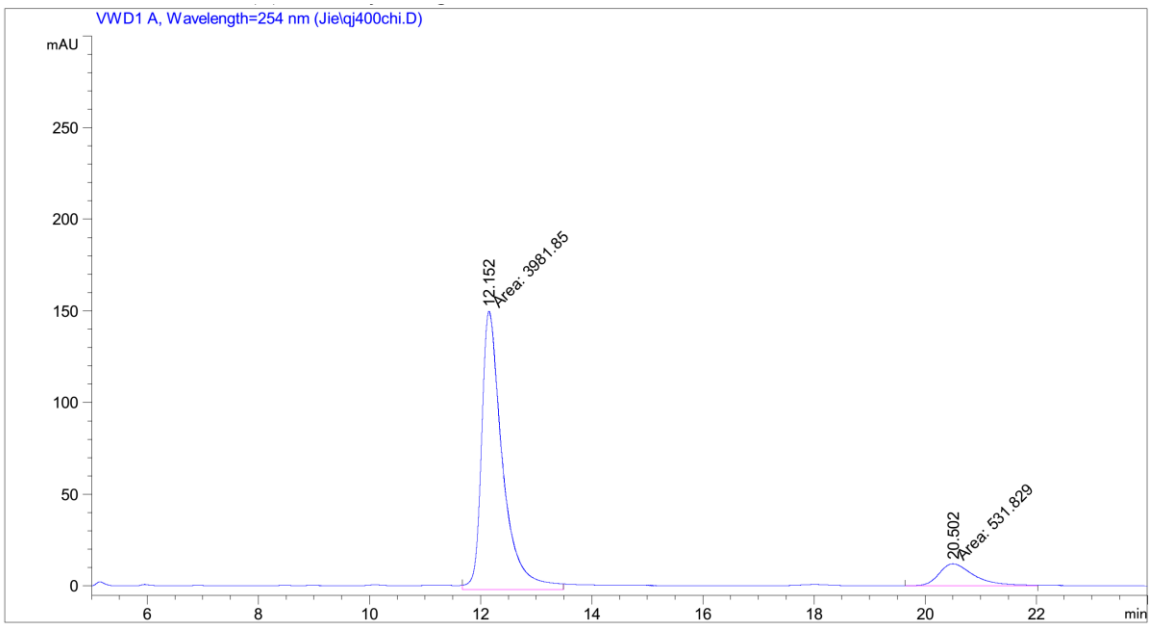

Peak #	RetTime [min]	Type	Width [min]	Area [mAU*s]	Height [mAU]	Area %
1	12.152	MM	0.4373	3981.84863	151.75200	88.2174
2	20.502	MM	0.7381	531.82904	12.00823	11.7826

Figure 97. HPLC traces of *rac*-**15l** and (2*R*, 3*R*)-**15l** (75% ee).

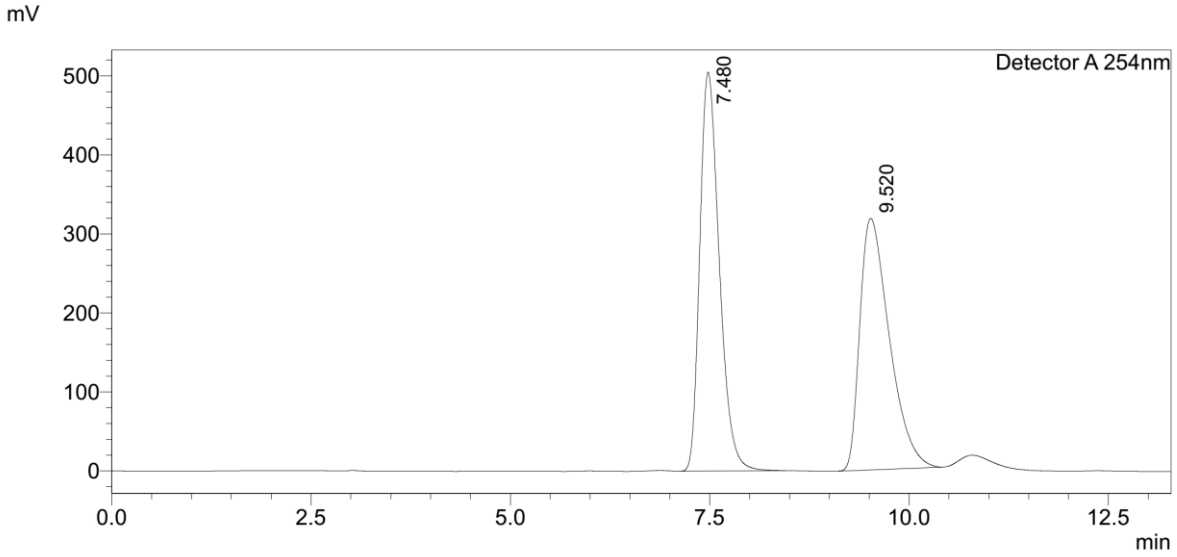

<Peak Table>

Detector A 254nm

Peak#	Ret. Time	USP Width	Area	Height	Area%
1	7.480	0.443	8589131	504596	51.174
2	9.520	0.675	8194942	318177	48.826
Total			16784073	822773	100.000

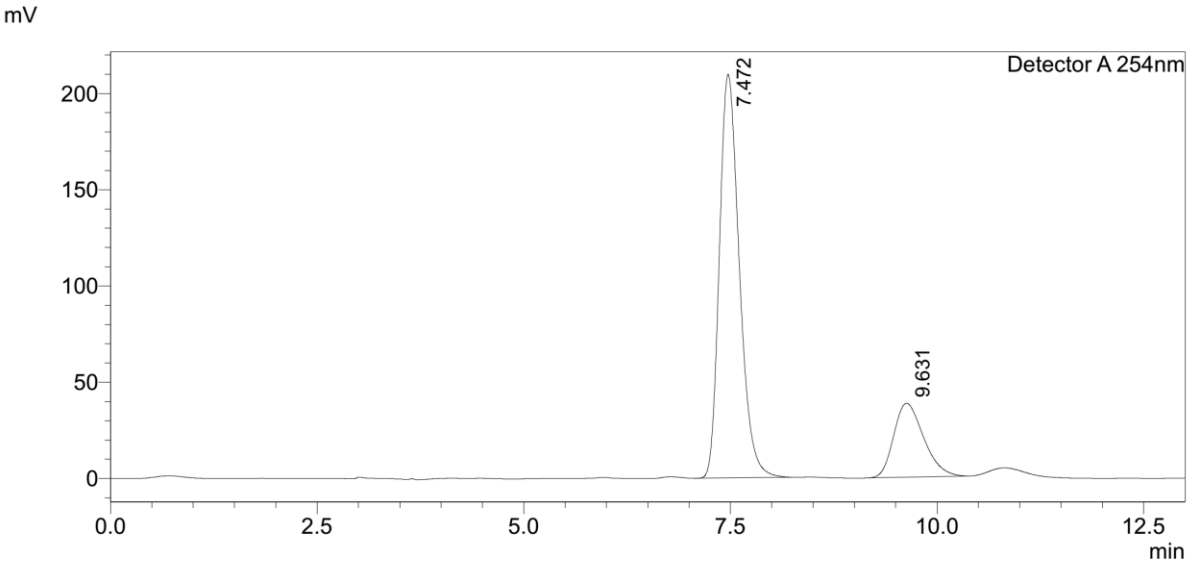

<Peak Table>

Detector A 254nm

Peak#	Ret. Time	USP Width	Area	Height	Area%
1	7.472	0.437	3523212	209589	78.469
2	9.631	0.663	966706	38368	21.531
Total			4489918	247957	100.000

Figure 98. HPLC traces of *rac*-**15m** and (2*R*, 3*R*)-**15m** (57% ee).

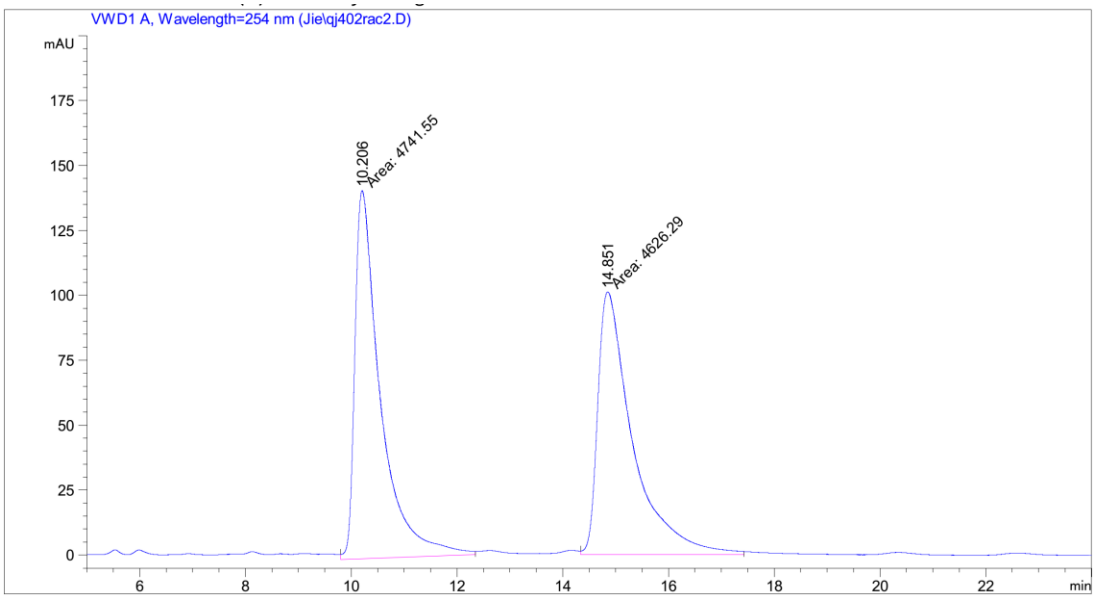

Peak #	RetTime [min]	Type	Width [min]	Area [mAU*s]	Height [mAU]	Area %
1	10.206	MM	0.5576	4741.55371	141.73466	50.6152
2	14.851	MM	0.7619	4626.28564	101.19656	49.3848

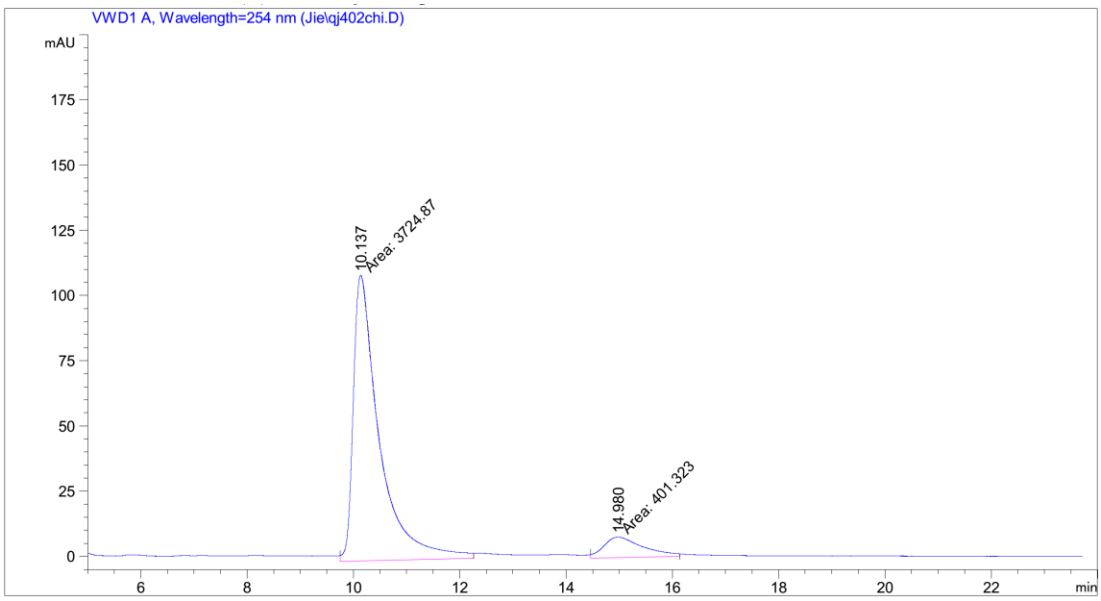

Peak #	RetTime [min]	Type	Width [min]	Area [mAU*s]	Height [mAU]	Area %
1	10.137	MM	0.5669	3724.87305	109.51054	90.2738
2	14.980	MM	0.8550	401.32254	7.82270	9.7262

Figure 99. HPLC traces of *rac*-**15n** and (2*R*, 3*R*)-**15n** (80% ee).

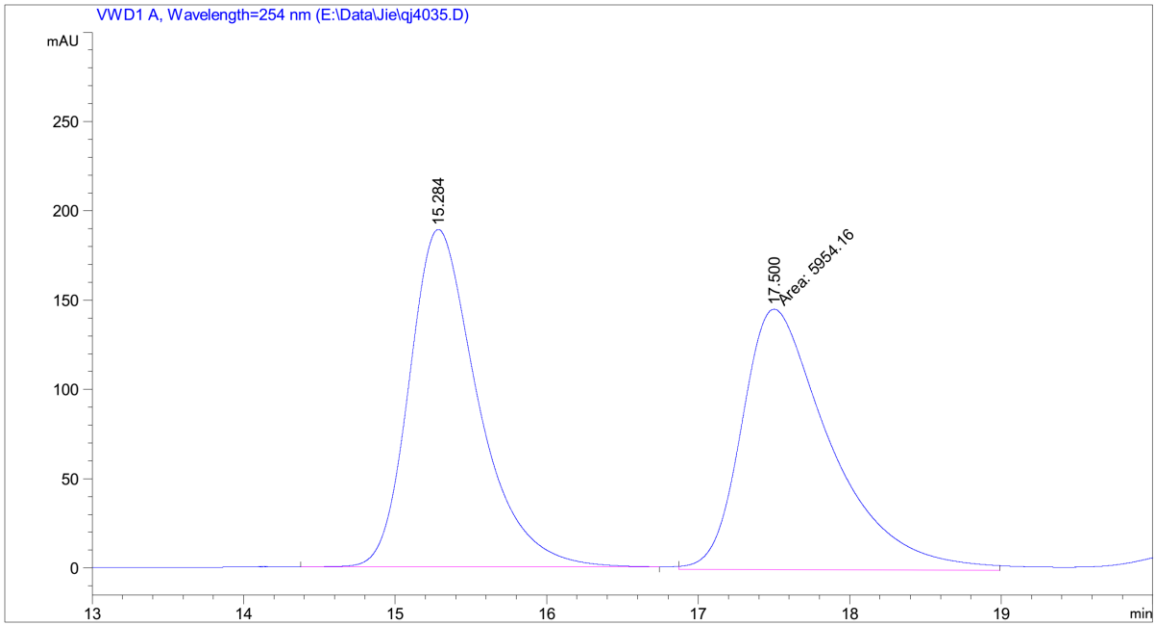

Peak #	RetTime [min]	Type	Width [min]	Area [mAU*s]	Height [mAU]	Area %
1	15.284	VB R	0.4527	5939.17041	188.93298	49.9370
2	17.500	MM	0.6804	5954.15869	145.85545	50.0630

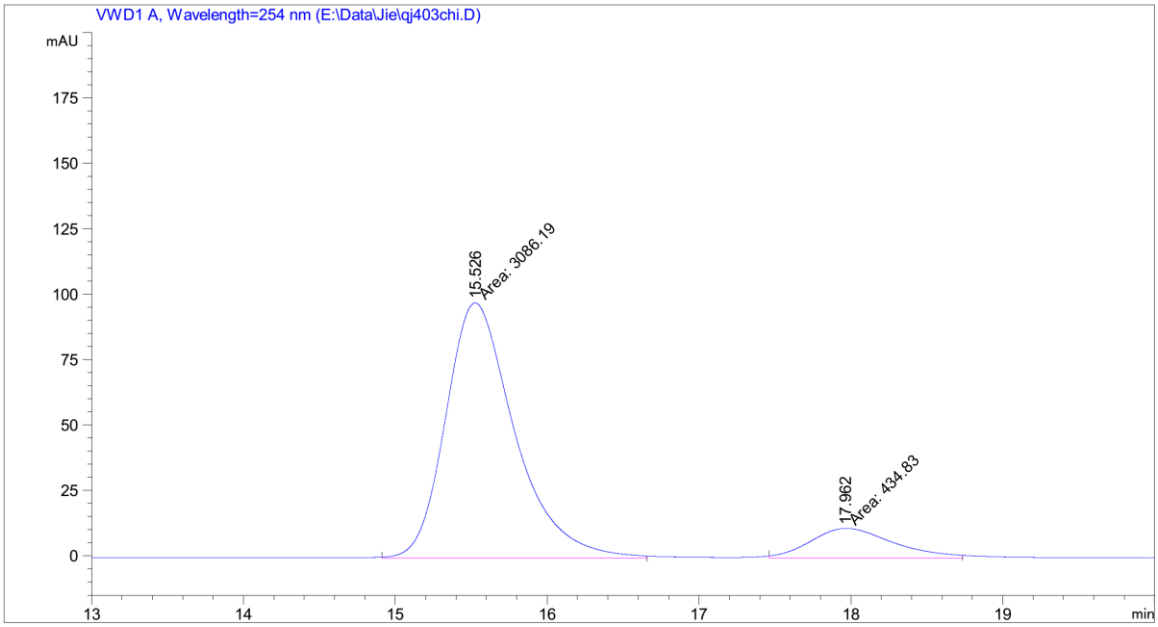

Peak #	RetTime [min]	Type	Width [min]	Area [mAU*s]	Height [mAU]	Area %
1	15.526	MM	0.5275	3086.19043	97.50414	87.6504
2	17.962	MM	0.6354	434.83047	11.40511	12.3496

Figure 100. HPLC traces of *rac*-**15o** and (2*R*, 3*R*)-**15o** (75% ee).

Statement

gemäß § 10, Abs. 1 der Promotionsordnung der mathematisch-naturwissenschaftlichen Fachbereiche und des Medizinischen Fachbereichs für seine mathematisch-naturwissenschaftlichen Fächer der Philipps-Universität Marburg vom 15.07.2009

Ich erkläre, dass eine Promotion noch an keiner anderen Hochschule als der Philipps-Universität Marburg, Fachbereich Chemie, versucht wurde und versichere, dass ich meine vorgelegte Dissertation

New Catalytic Properties of Chiral-at-Metal Complexes and a Cyclometalated Ru Complex

selbst und ohne fremde Hilfe verfasst, nicht andere als die in ihr angegebenen Quellen oder Hilfsmittl benutzt, alle vollständig oder sinngemäß übernommenen Zitate als solche gekennzeichnet sowie die Dissertation in der vorliegenden oder ähnlichen Form noch bei keiner anderen in- oder ausländischen Hochschule anlässlich eines Promotionsgesuchs oder zu anderen Prüfungszwecken eingereicht habe.

Jie Qin
Marburg, den 13.02.2019